Borehole water level response to barometric pressure as an indicator of groundwater vulnerability

Mahmoud Mohamed El Araby Mohamed Hussein

Submitted in accordance with the requirements for the degree of
Doctor of Philosophy

The University of Leeds
School of Earth and Environment

November 2012

The candidate confirms that the work submitted is his own and that appropriate credit has been given where reference has been made to the work of others.

Acknowledgements

First and foremost, I am grateful to Allah the Almighty for His immense blessings and help throughout my PhD studies. I would like to thank my wonderful parents Mohamed El Araby and Nihad Attia for their love and kind support. I would like to express my sincere appreciation and also dedicate this thesis to my wife Reham El Masri who has always stood by me and who dedicated years of her life to support me and our children Jana and Shahd.

It is with immense gratitude that I acknowledge the support and help of my supervisors Dr. Noelle Odling and Dr. Roger Clark who I consider it an honor to work with and who have been a continuous source of guidance and support throughout this research project. I would like to express my sincere and special gratitude to my main supervisor Dr. Noelle Odling for her patient guidance and continuous advice and I have to admit that I have been very lucky to have a supervisor who really cared about my work and who responded promptly to my queries.

I would like to thank my research support group Dr. Jared West (School of Earth and Environment, University of Leeds), Mr. Rolf Farrell (Environment Agency, UK), Mr. Mark Morton (Yorkshire Water ltd) and Mr. Gerd Cachandt (ARUP) for their help and guidance throughout this research project.

I also thank Mr. Rolf Farrell and Mr. James Senior from (Environment Agency, UK) for their help in accessing monitoring boreholes and for providing water level data and boreholes logs, lithology and completion details.

Many thanks to Prof. Jurgen Neuberg (University of Leeds) and Prof. Olivier Bour (University of Rennes 1) for being my thesis examiners and for providing valuable suggestions and corrections.

I acknowledge funding support from the EU Marie Curie Initial Training Network ‘IMVUL’ (PITN-GA-2008-212298). I would also like to thank all other IMVUL fellows and partners for their input and interesting discussions.

Abstract

The response of borehole water levels to barometric pressure is a function of the confining layer and aquifer properties. This study aims to use this response as an aid towards quantitative assessment of groundwater vulnerability, applying the techniques to the confined/semi-confined part of the Chalk Aquifer in East Yorkshire, UK. Time series analysis techniques are applied to data collected from twelve monitoring boreholes to characterize and remove components contributing to the borehole water level signal other than barometric pressure, such as recharge and Earth tides. Barometric response functions are estimated using the cross-spectral deconvolution-averaging technique performed with up to five overlapping frequency bands. A theoretical model was then fitted to the observed barometric response functions in order to obtain estimates of aquifer and confining layer properties. Derived ranges for pneumatic and hydraulic diffusivities of the confining layer vary over four orders of magnitudes (0.9 to 128.0 m^2/day and 10.0 to 5.0×10^4 m^2/day respectively) indicating that the aquifer is nowhere purely confined. Discrepancies between estimates of aquifer transmissivity derived from the barometric response function and pumping tests have been explored using slug tests and results suggest that aquifer model transmissivity are highly sensitive to borehole construction. A simple flow model, constructed to test the potential impact of confining layer heterogeneity on the barometric response function, shows that while high frequencies reflect the immediate vicinity of the borehole, low frequencies detect confining layer properties up to some 500 meters distant from the borehole. A ‘characteristic time scale’ is introduced as a function of derived properties of the confining layer and is used as a quantitative measure of the degree of aquifer confinement. It is concluded that barometric response functions are sensitive to confining layer properties and thus can provide a useful tool for the assessment of aquifer vulnerability.

Table of contents

List of tables

Tables in main text:

Tables in appendices:

List of figures

Figures in main text:

Figures in appendices:

List of abbreviations

ASL	above sea level
BGS	British Geological Survey
BRF	barometric response function
DFT	Discrete Fourier Transform
et al.	et alii/alia, and other people
etc.	et cetera
EA	UK Environment Agency
FFT	Fast Fourier Transform
G.S.	ground surface
IDFT	Inverse Discrete Fourier Transform
W.T.	water table

A list of symbols is provided in Appendix A.

CHAPTER 1: INTRODUCTION

1.1. The study area: the East Yorkshire Chalk Aquifer

The Chalk Aquifer is the principle source of groundwater in the UK supplying more than 50% of the groundwater abstraction for domestic and industrial needs. The East Yorkshire Chalk is classified as part of the "Northern Province Chalk" that is typically harder than and has lower porosity than the "Southern Province Chalk". The study area is shown in Figures 1.1 and 1.2 and comprised the confined/semi-confined Chalk Aquifer in East Yorkshire. Land use in East Yorkshire is dominated by arable farming and the increasing nitrate concentration in groundwater from agricultural fertilizers is a growing problem [*Wellings and Cooper*, 1983]. The fourteen major abstractions located in this aquifer, cause a lowering of groundwater heads which increases the likelihood of groundwater contamination by downward migration of pollutants from ground surface. This is linked to observed increased levels of nitrate in abstracted groundwater, which in some cases has exceeded the drinking water limit. The chalk is a dual porosity aquifer where contaminants may transport rapidly in fractures but are also able to diffuse into the matrix. This makes complete clean-up complicated if not impossible due to contaminant retention in the matrix [*Hartmann et al.*, 2007; *Foster*, 1993]. Part of the aquifer in East Yorkshire is covered by a wide range of glacial sediments ranging from clay-rich sediments to sands and gravels (see Figure 1.2) which vary in thickness from less than 10 m to around 50 m. It has generally been assumed that this cover represents a protective layer for the aquifer against contamination. However the detailed local structure within the glacial deposits is not well known and the available data do not provide sufficient information on the continuity of permeable layers, which is key for aquifer vulnerability assessment [*Kilner et al.*, 2005].

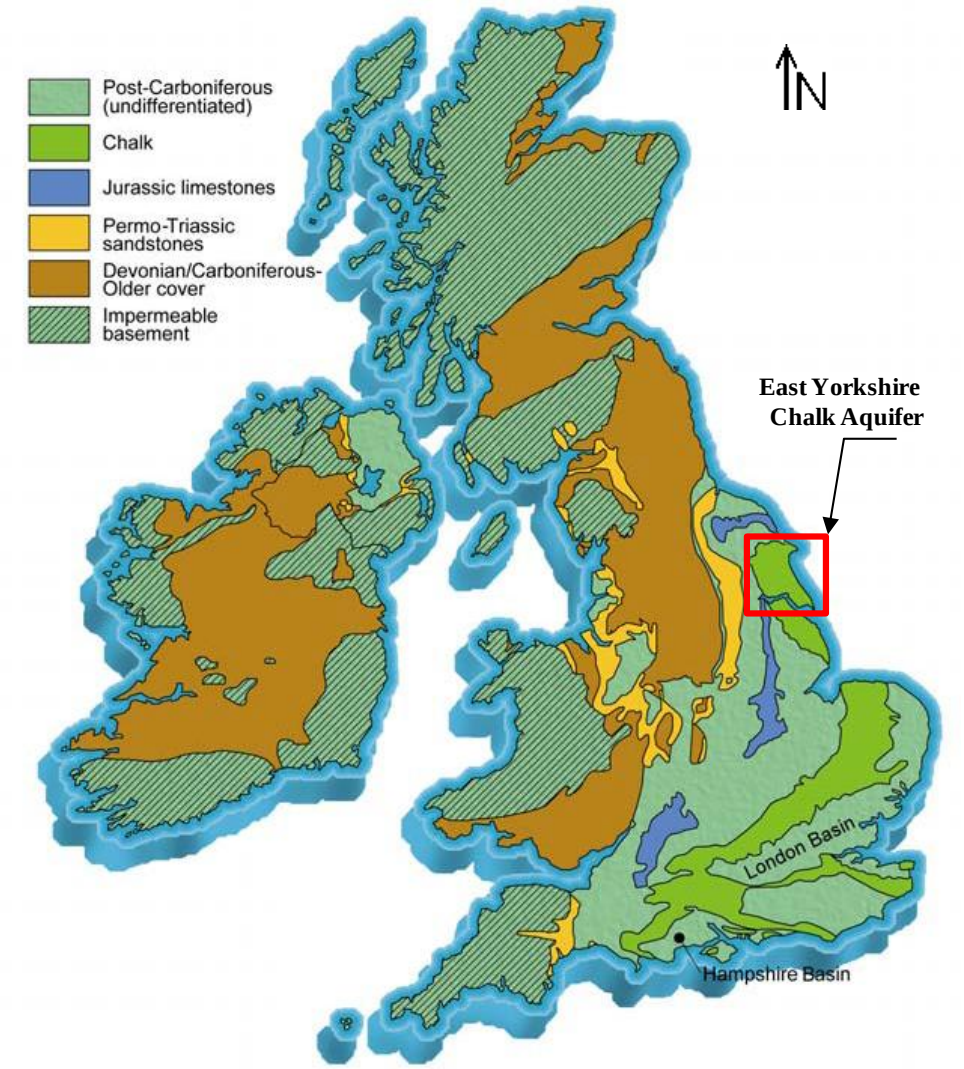

Figure 1.1. Geological map of the UK and Ireland showing the outcrop of the Chalk and the location of the study area in East Yorkshire after [*Dowing*, 1998].

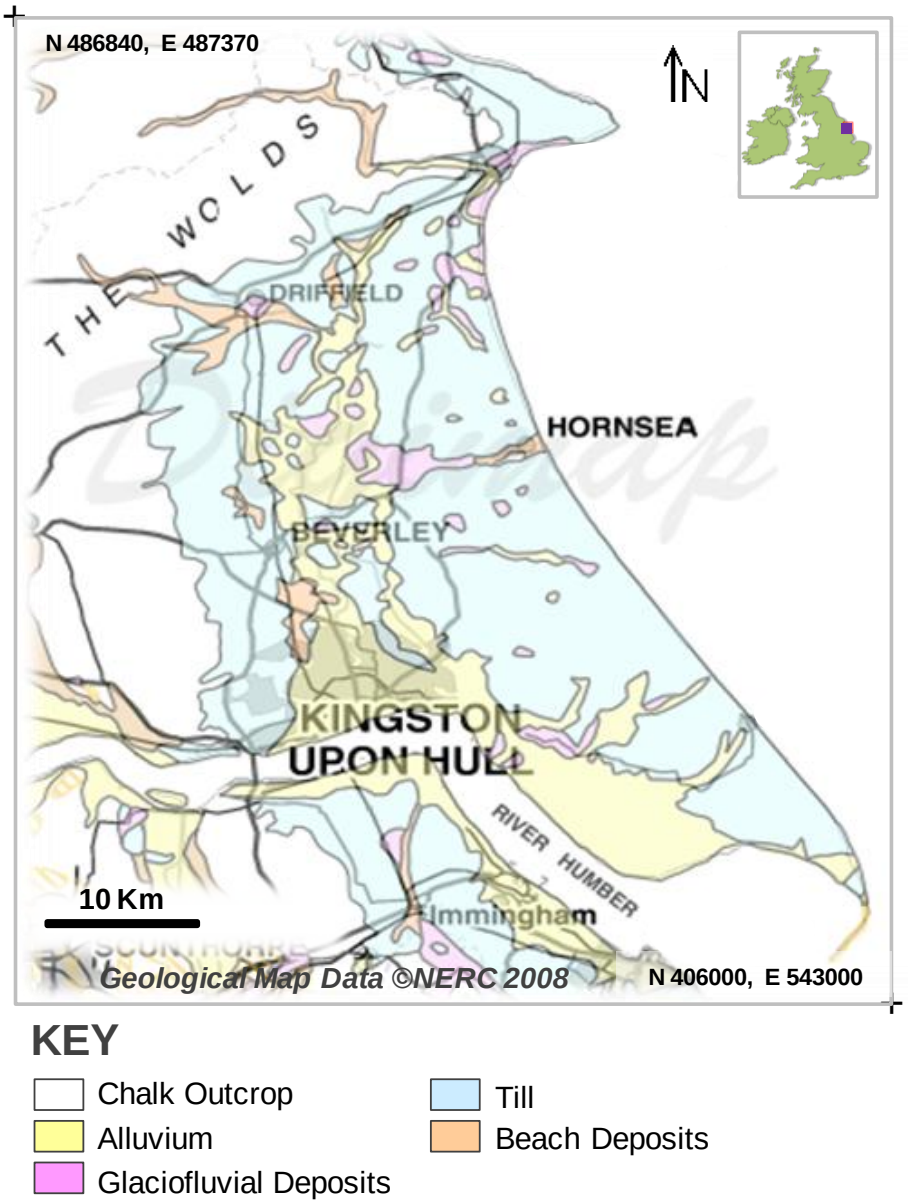

Figure 1.2. Geology map of East Yorkshire showing the outcrop of the Chalk Aquifer and superficial deposits [*Edina-Digimap "Geological Map Data © NERC 2008"*].

1.2. Borehole water level response to barometric pressure

Borehole water levels fluctuate in response to barometric pressure. The extent of response is a function of properties of the aquifer, confining layer and borehole design. While purely confined aquifers respond to changes in barometric pressure, purely unconfined aquifers show no response. However purely confined aquifers are rarely found in nature and most confined aquifers are in fact semi-confined, i.e. the confining layer has some permeability. In confined and semi-confined aquifers there is an inverse relationship between changes in barometric pressure and corresponding changes in the borehole water level. In purely confined aquifers, where confining layer has zero permeability, this relationship can be characterized by a constant called the static barometric efficiency [*Jacob*, 1940]. However, in semi-confined aquifers this relationship is a function of barometric pressure frequency. In this case, a constant barometric efficiency is not adequate to describe the response and instead a "barometric response function" must be used to represent this frequency dependant relationship.

1.3. The link between barometric response functions and aquifer vulnerability

Both the barometric response function and intrinsic groundwater vulnerability are a function of the structure and properties of the confining layer and the aquifer. Hence it is possible that the barometric response function could be used to quantify the degree of the aquifer confinement and thus the potential for contaminant transport from the surface to the aquifer. A link between the barometric response function and groundwater vulnerability as has been previously suggested by *Rojstaczer*, [1988a], *Landmeyer* [1996] and *Spane* [2002] but has not been previously tested. The barometric response function can provide us with quantitative information from routine monitoring borehole data, particularly on the vertical hydraulic properties of the confining layer. Traditional aquifer testing techniques such as pumping and slug tests give predominantly horizontal hydraulic properties but it is the vertical properties that are more relevant for assessing aquifer vulnerability. This thesis presents an attempt to assess aquifer groundwater vulnerability using barometric response functions applied to the semi-confined Chalk Aquifer in East Yorkshire as a test case.

1.4. Outline of methods and approaches

In this investigation of the semi-confined Chalk Aquifer in East Yorkshire, time series of borehole water level and barometric pressure data were collected from twelve selected boreholes using automatic pressure transducers. Barometric response functions were estimated using the methods of deconvolution in the frequency domain [*Welch*, 1967] which have also been used by a number of previous investigators [*Rojstaczer*, 1988a; *Rojstaczer and Riley*, 1990; *Beavan et al.* 1991; *Quilty and Roeloffs*, 1991]. In order to obtain the best estimates of the barometric response function, the time series of water levels and barometric pressure have been analyzed to separate and remove contributing stresses other than barometric pressure, using techniques of time series analysis. A theoretical model of borehole water level response to barometric pressure in semi-confined aquifers [*Rojstaczer*, 1988a; *Evans, et al.*, 1991] has then been fitted to the estimated barometric response functions in order to estimate aquifer and confining layer hydraulic properties. The results have been compared to available data on local geology and used to investigate the use of this approach for assessing aquifer vulnerability.

The UK is densely populated and major aquifers in UK are heavily exploited, particularly the Chalk Aquifer. Much of the farming overlying these aquifers is arable giving rise to increasing nitrate contamination over the last 70 years. The vulnerability of these major aquifers where they are semi-confined is of concern but not well understood. However, the abundance of monitoring boreholes suggests that the above techniques for quantifying the vertical hydraulic properties of semi-confining layers could provide valuable information for assessing aquifer vulnerability. So far the approach of using the borehole water level response to barometric pressure for estimating the aquifer and confining unit hydraulic properties has been applied only in the US and Egypt. This study represents the first application of these techniques in the UK. This study was undertaken as part of the Initial Training Network IMVUL, "Towards Improvement of Groundwater Vulnerability", funded by EU Marie Curie FP7 (PITN-GA-2008-212298).

1.5. Aim and objectives

The aim of this study is to develop a methodology for assessing groundwater vulnerability of confined/semi-confined aquifers using borehole water level response to barometric pressure and to apply this methodology to the Chalk Aquifer of East Yorkshire. To achieve this aim the following objectives were considered:

1. To collect time series of water level data from a selected group of monitoring boreholes and barometric pressure data using automatic pressure transducers.
2. To apply time series analysis to characterize and remove components other than barometric pressure which contribute to the borehole water level signals.
3. To apply the deconvolution technique to filtered water level signals to estimate barometric response functions.
4. To estimate aquifer and confining layer properties through application of theoretical response models.
5. To assess the use of the barometric response function for characterizing aquifer vulnerability for semi-confined aquifers.

1.6. Thesis layout

This thesis is composed of eleven chapters and six appendices.

Chapter 1 gives an overview of the project, study area, aim and objectives and the thesis layout.

Chapter 2 comprises a literature review on the principles of borehole water level response to barometric pressure and Earth and ocean tides, and an introduction to the barometric response function and groundwater vulnerability.

Chapter 3 comprises an overview of previous modeling of borehole water level response to barometric pressure from the literature.

Chapter 4 summarizes the hydrogeology of the East Yorkshire Chalk Aquifer.

Chapter 5 describes data collection, analysis of borehole water level signal components, and pre-processing of borehole water level and barometric pressure signals.

Chapter 6 explains the methods used to estimate short-term and long-term barometric efficiency and the deconvolution techniques used to estimate the barometric response function.

Chapter 7 describes the theoretical model for borehole water level response to barometric pressure, with sensitivity to model parameters and technique of fitting theoretical models to estimated barometric response functions to determine aquifer and confining layer properties.

Chapter 8 presents the resulting barometric response functions and best fit confining layer and aquifer parameters for all selected boreholes.

Chapter 9 describes further investigations on the impact of heterogeneity of confining layer and borehole construction on the barometric response function.

Chapter 10 discusses the key results of this study and presents a measure of intrinsic aquifer vulnerability that utilizes information gained from barometric response functions.

Chapter 11 summarizes the main conclusions of this study and gives recommendations for further work.

Appendix A provides a list of symbols.

Appendix B describes the *SC* (Separate Component) Matlab code, developed to analyze, separate and remove components in the water level signal other than barometric pressure, and how to use it.

Appendix C describes the *BE* (Barometric Efficiency) Matlab code, developed to estimate short-term and long-term barometric efficiencies, and how to use it.

Appendix D describes the *RF* (Response Function) Matlab code, developed to estimate the barometric response function using the deconvolution technique, and how to use it.

Appendix E describes the *Automatic_Fitting* Matlab code, developed to fit the theoretical response model to estimated barometric response functions using a hybrid automatic search algorithm, and how to use it.

Appendix F describes the *Manual_Fitting* Matlab code, developed to explore the sensitivity of the best fit to variations in derived parameters, and how to use it.

CHAPTER 2: BOREHOLE WATER LEVELS, BAROMETRIC PRESSURE, EARTH AND OCEAN TIDES AND GROUNDWATER VULNERABILITY

2.1. Introduction

Borehole water levels are known to fluctuate in response to barometric pressure. Fluctuations in barometric pressure are mainly periodic fluctuations (diurnal and semi-diurnal) caused by atmospheric tides and aperiodic fluctuations due to longer term movement of higher and lower pressure air masses over the ground surface. Boreholes water levels are also known to respond to ocean tides and Earth tides [*Maréchal et. al.*, 2002] where loading pressure on an aquifer oscillates in response to periodic tidal forces causing periodic oscillations in boreholes water levels [*Merritt*, 2004].

Water levels in boreholes tapping entirely confined aquifers are known to fluctuate in response to barometric pressure changes, while in entirely unconfined aquifers no response is observed. Entirely confined and unconfined aquifers are end members and most aquifers are in fact semi-confined where either the confining unit is not entirely impermeable, or semi-unconfined where the unsaturated zone is relatively thick or has low permeability. *Jacob* [1940] related the ratio of water level changes in boreholes tapping entirely confined aquifers to the corresponding barometric pressure changes by a constant called the *static barometric efficiency*. However, representing the borehole water level response to barometric pressure by a single constant (barometric efficiency) is not appropriate in semi-confined and semi-unconfined aquifers. In reality this response is often lagged or delayed due to borehole storage or skin effects [*Furbish*, 1991] or where the aquifer is semi-confined [*Rojstaczer*, 1988a] or semi-unconfined [*Weeks*, 1979]. In these cases the borehole-aquifer system response can be described by the *barometric response function* which represents the response of the borehole-aquifer system to the full range of frequencies in barometric pressure signal.

2.2. Mechanisms of borehole water level response to barometric pressure change

2.2.1. Purely unconfined aquifers

In the ideal unconfined aquifer case, Figure 2.1, the barometric pressure loading stress acting on the ground surface is transmitted instantaneously and totally through the unsaturated zone thickness to the water table, and is totally borne by the aquifer pore water pressure. At the same time the same stress is totally transmitted to the borehole water surface resulting in pressure head balance between the borehole water pressure and the aquifer pore water pressure. Thus there is no change in the borehole water level and no response to barometric pressure changes [*Weeks*, 1979; *Batu*, 1998].

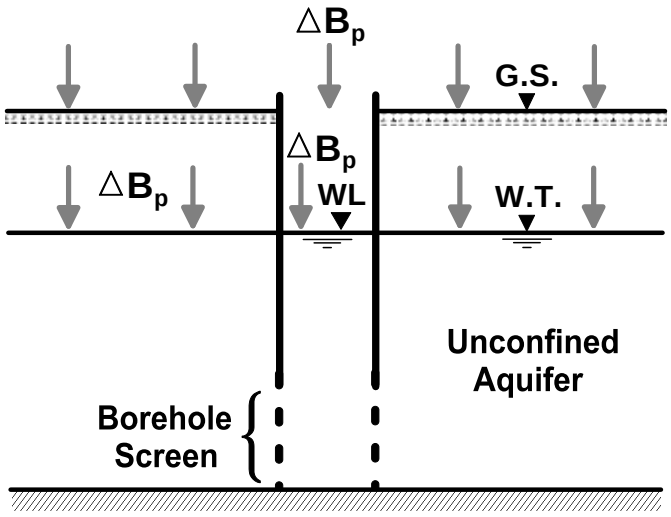

Figure 2.1. Purely unconfined aquifer response mechanism to barometric pressure, after *Batu* [1998]. ΔB_p is the barometric pressure change, ΔWL is the change in borehole water level, W.T. is the water table and G.S. is the ground surface.

2.2.2. Purely confined aquifers

In case of an entirely confined aquifer, Figure 2.2, the confining layer is a rigid non-permeable layer which does not absorb any of the barometric pressure loading stress acting on the ground surface. Consequently a step increase in barometric pressure is instantaneously and fully transmitted to the interface between the confining layer and the aquifer. This stress is then distributed between the aquifer skeleton (ΔP_k) and the

aquifer pore water pressure (ΔP_w) [*Batu*, 1998]. The more rigid the aquifer skeleton, the greater the proportion of stress borne by the aquifer skeleton, and thus the smaller the stress borne by the pore waters. Thus, barometric pressure stress at the Earth's surface is partially transmitted to the aquifer pore water pressure but is transmitted in total to the water surface in the borehole. This results in a pressure head imbalance between the borehole water pressure and the aquifer pore water pressure causing a corresponding decrease in the borehole water level. Thus, a step increase in barometric pressure causes a step decrease in borehole water level and vice versa. Therefore, a plot of water level will show a mirror image to barometric pressure changes.

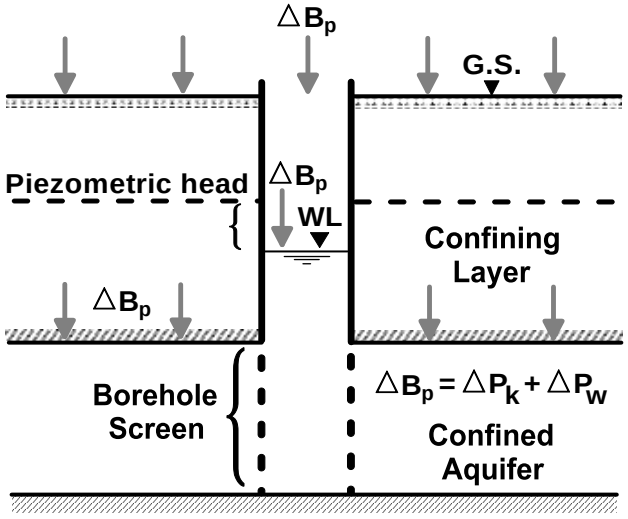

Figure 2.2. Purely confined aquifer response mechanism to barometric pressure, after *Batu* [1998]. ΔB_p is the barometric pressure change, ΔWL is the change in borehole water level, G.S. is the ground surface, ΔP_k is the part of stress borne by the aquifer skeleton and ΔP_w is the part of stress borne by the aquifer pore water pressure.

Borehole water level fluctuations induced by barometric pressure changes under confined conditions are thus a constant fraction of the barometric pressure changes and in phase with them [*Weeks,* 1979]. This constant fraction was first termed *barometric efficiency*, BE, by *Jacob* [1940] and is defined as the ratio of water level changes ΔWL in boreholes tapping confined aquifers to the corresponding barometric pressure changes, ΔB_p, for a given time interval Δt:

$$BE = -\Delta WL/\Delta B_p\ , \tag{2.1}$$

where: ΔB_p is expressed in the same units as ΔWL.

Barometric efficiency, BE, is also a function of the aquifer porosity, n, aquifer compressibility, β_f, and water compressibility, β_w, [*Jacob,* 1940; *Batu,* 1998; *Price,* 2009]:

$$BE = n \cdot \beta_w/(\beta_f + n \cdot \beta_w)\ . \tag{2.2}$$

Thus, confined aquifers with very low compressibility β_f (rigid) have a barometric efficiency close to unity or 100 % [*Rasmussen and Crawford*, 1997; *Acworth and Brain,* 2008; *Price,* 2009]. The ratio between the aquifer pore pressure change and the atmospheric pressure change is termed the aquifer loading efficiency, ε. The summation of loading efficiency and barometric efficiency for confined aquifers is unity, that is *(BE+ ε)* =1 [*Rasmussen and Crawford*, 1997; *Acworth and Brain*, 2008; *Price*, 2009].

2.2.3. Semi-confined aquifers

In the semi-confined aquifers, the aquifer is overlain by a semi-permeable confining unit which does not transmit the whole of the barometric stress from the ground surface to the interface between confining layer and aquifer, as in the confined aquifer case. Also, a change in the aquifer pore pressure as a response to a step change in barometric pressure will slowly depressurize to reach equilibrium (zero change) by groundwater flow between the water table and the semi-permeable confining unit. This process requires a finite period of time to occur, and thus the response is in general a function of frequency of the barometric changes.

The response mechanism of a borehole-aquifer system tapping a semi-confined aquifer is governed by the geometry and properties of the confining layer and aquifer, and the borehole design [*Rojstaczer*,1988a]. Due to a step change in barometric pressure, four pressure imbalances instantaneously occur [*Rojstaczer*,1988a], see Figure 2.3. These are:

1) Pressure imbalance between the Earth's surface and the water table inducing vertical air flow through the unsaturated zone.

2) Pressure imbalance between the water table and the confining layer inducing vertical groundwater flow within the saturated confining unit.

3) Pressure imbalance between the confining layer and the aquifer inducing vertical groundwater flow between the aquifer and confining unit.

4) Pressure imbalance between the aquifer and the borehole inducing lateral or radial groundwater flow to (or from) the borehole.

Rojstaczer [1988a] developed an analytical model for the borehole water level response to barometric pressure under semi-confined conditions. Conceptually his model is composed of two layers, a confining layer and an underlying aquifer layer. He assumes that the loading efficiencies (elastic properties and porosities) of the confining unit (ε') and the aquifer (ε) are equal. As a result imbalances 2 and 3 are combined and the four imbalances above are reduced to three. Based on this assumption he described the borehole water level response to a step increase in barometric pressure (ΔB_p) in four phases shown in Figure 2.3.

In phase (1), borehole water level drops due to water flow out of the borehole into the aquifer driven by the pressure imbalance between the borehole water pressure and the aquifer pore water pressure.

In phase (2), the drop in borehole water level reaches $(1-\varepsilon)\,\Delta B_p/\rho g$, where ρ is the density of water and g is the acceleration due to gravity, i.e. the remaining borehole pressure is ($\varepsilon\,\Delta B_p/\rho g$), at which it is in equilibrium with the undrained response of the

aquifer. Under these undrained conditions, no flow occurs between aquifer and confining layer and a plateau of equilibrium is temporarily established. At this plateau the aquifer pore pressure bears a proportion ($\varepsilon.\Delta B_p/\rho g$) of the full step change in pressure $\Delta B_p/\rho g$. The time length of this plateau is governed by the time needed for groundwater flow from the aquifer to the water table to start depressurize the aquifer pressure. Thus, the less permeable the confining layer, the wider is this plateau and vice versa.

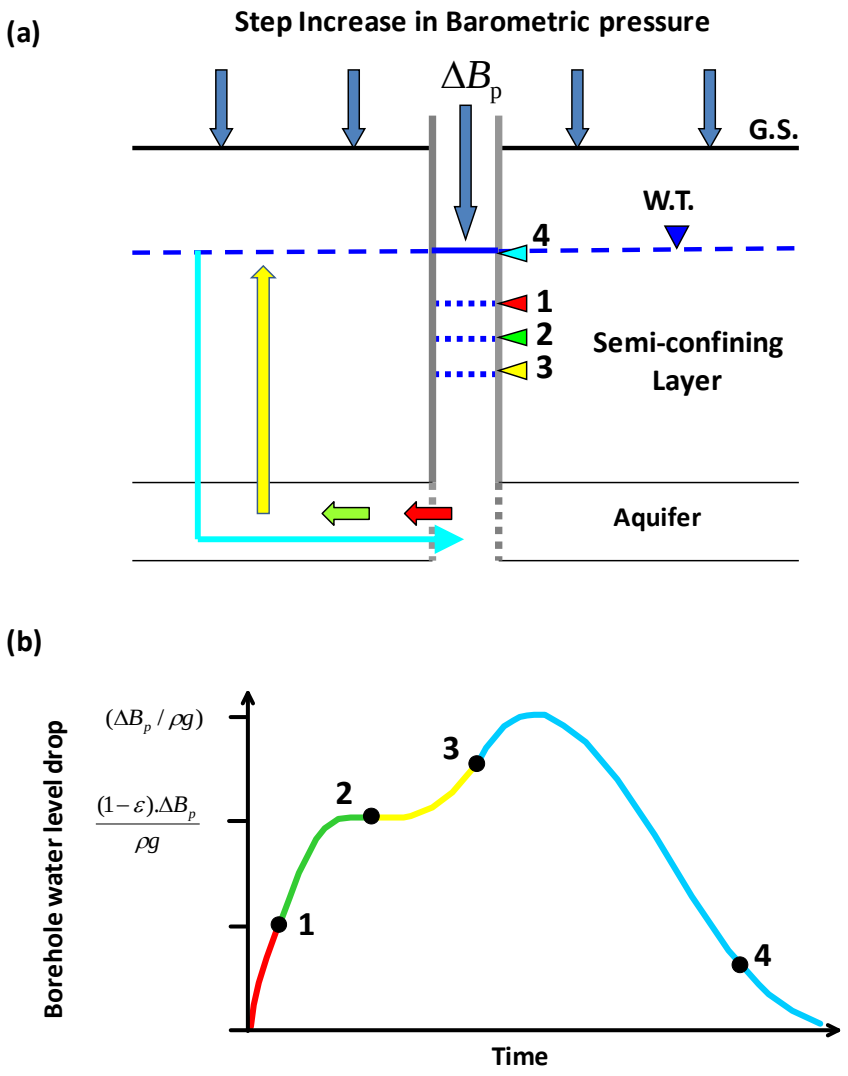

Figure 2.3. Four response phases of borehole water level to a step increase in barometric pressure, ΔB_p, under semi-confined conditions, after [*Rojstaczer*, 1988a]. (a) Cross section of water level response to barometric pressure. (b) Idealized response of water level versus time.

In phase (3), if the unsaturated zone is thick and/or has low permeability, pressure at the water table will take a considerable time period to build up due to the slow propagation of the air pressure pulse through the unsaturated zone. During this time period, the confining layer and the aquifer gradually depressurize through vertical groundwater flow to the water table inducing a further drop in borehole water level. Thus the total drop is ($\Delta B_p/\rho g$) which is the full step increase in barometric pressure. During this phase, the barometric pressure infiltration through the unsaturated zone gradually increases the air pressure at the water table.

In phase (4), the air pressure has reached the water table, and a new pressure imbalance is produced between the water table and the aquifer. This induces groundwater flow to the aquifer, causing an increase in the aquifer pressure and consequently a corresponding rise in the borehole water level until it reaches its original level.

2.2.4. Semi-unconfined aquifers

As described above (section 2.2.1) water levels in boreholes tapping purely unconfined aquifers do not respond to barometric pressure variations. However *Weeks* [1979] showed that where the unsaturated zone is thick or of low permeability (semi-unconfined) water levels may fluctuate in response to barometric pressure changes and the borehole-aquifer system may have a significant barometric efficiency. This response is governed by the pneumatic diffusivity of the unsaturated zone which can be considered as a lumped parameter that includes both properties of the unsaturated zone materials and properties of the soil gas. The vertical pneumatic diffusivity represents the unsaturated zone resistance to the propagation of air through it.

A plot of water levels versus the corresponding barometric pressure for a borehole tapping a semi-unconfined aquifer can be similar to the same plot for a semi-confined aquifer but the response mechanism is somewhat different [*Rojstaczer and Riley*, 1990; *Spane*, 2002]. In contrast to the semi-confined aquifer case, in semi-unconfined aquifers, the access of pore pressure to the water table which is a free surface

minimizes pore pressure changes due to grain-to-grain transmission of surface load [*Butler et al.*, 2011].

Rasmussen and Crawford [1997] described the semi-unconfined aquifer response to a step increase in barometric pressure, shown in Figure 2.4a, b, c and d. Two points (P1 and P2) shown in Figure 2.4a, are used to illustrate the response process. Figure 2.4b shows the instantaneous step increase in borehole pressure (ΔB_p) at time zero (t_0). A specific period of time (time lag= t_d-t_0) is needed for the pressure pulse to diffuse from the ground surface to the water table to reach the aquifer pore water pressure which will then pressurize gradually with time to reach ΔB_p. As pore pressure is increasing the borehole water level returns gradually to its original level as shown in Figure 2.4c. Thus, the total head (water pressure plus barometric pressure) at both points 1 and 2 will stay in equilibrium at all times and will gradually increase to reach ΔB_p, Figure 2.4d.

Water levels in unconfined aquifers may respond to barometric pressure changes due to the presence of air bubbles or pockets below the water table or within the capillary fringe [*Price*, 2009]. *Peck* [1960], *Turk* [1975] and *Evans et al.* [1991b] also noted that the presence of entrapped air pockets below the water table can cause water levels in boreholes tapping shallow unconfined aquifers to respond to barometric pressure variations. In case of fine textured soils, this may happen when a specific thickness of the unsaturated zone just below the ground surface becomes nearly saturated (due to rainfall recharge event) forming a ‘saturated front’ which will gradually infiltrate downwards causing an amount of air to be entrapped and compressed between this front and the water table or capillary fringe [*Healy and Cook,* 2002]. The change in volume of these air bubbles attenuates and absorbs part of the barometric pressure changes from being transmitted to the aquifer pore pressure.

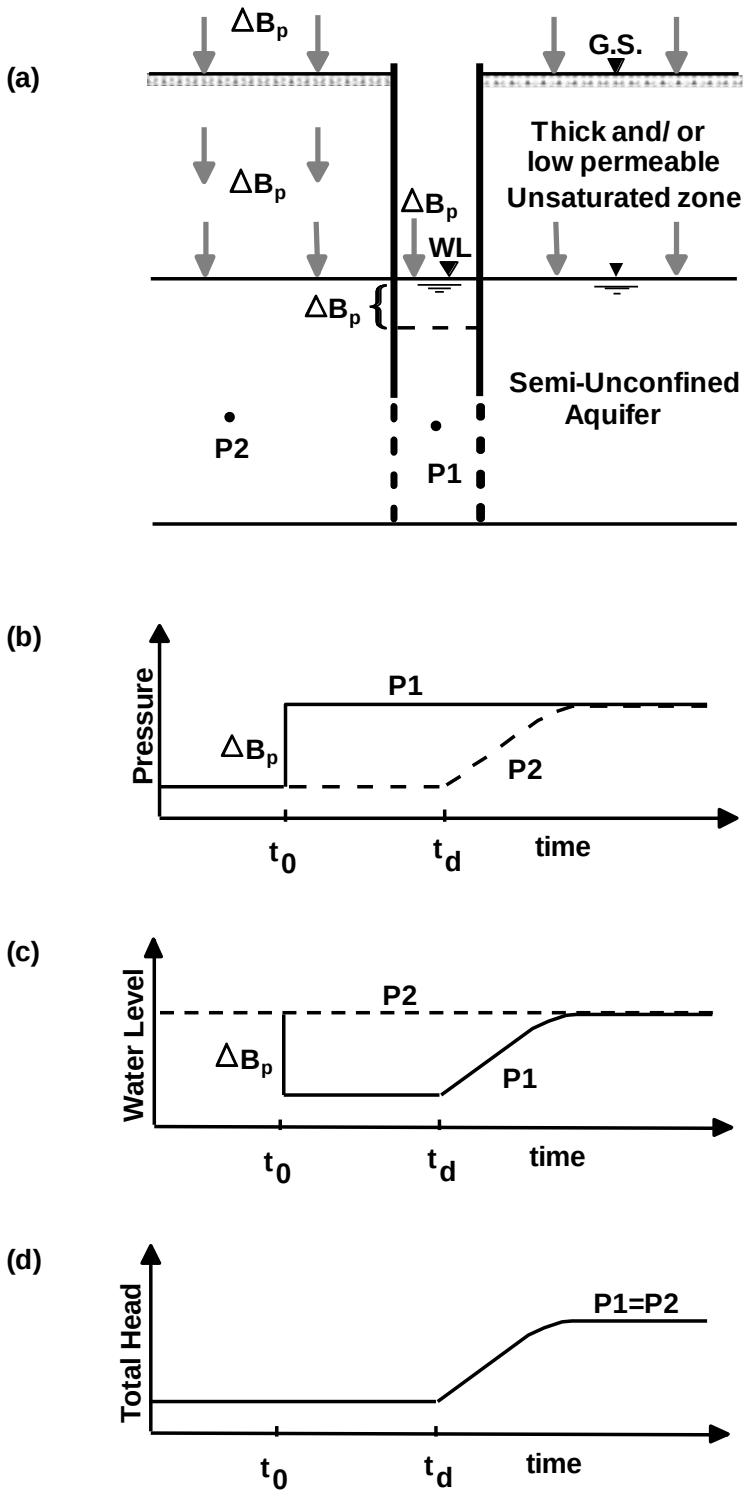

Figure 2.4. Semi-unconfined aquifer response to a step increase in barometric pressure after [*Rasmussen and Crawford,* 1997]. (a) Shows locations of two illustrative points P1 and P2, (b) shows pressure head (P), (c) shows water levels (WL) and (d) shows the total head (Ht). WL and B_p are expressed in equivalent head units.

Hare and Morse [1997] concluded that barometrically induced changes in water levels of boreholes tapping an unconfined aquifer could be also caused by man-made features (e.g., buildings, parking lots...etc) if they have a sufficient areal extend to confine the aquifer. They conducted a field study of two boreholes tapping an unconfined sandy aquifer. The first borehole is located inside a contaminant experiment isolation system (cut-off wall) where the aquifer is covered by about 1.5 m of confining layer and the second borehole is located about 12 m outside the cut-off wall. A comparison of the two boreholes records, showed that the water levels in first borehole show a confined behavior and respond to barometric pressure fluctuations with a barometric efficiency of about 94%, while the second borehole shows no response.

2.3. Estimation of static confined barometric efficiency

Rasmussen and Crawford [1997] described the use of the least-squares regression method to calculate the long-term, $\propto_L$, and short-term, $\propto_S$, barometric efficiencies. The long-term barometric efficiency, $\propto_L$, represents the borehole water level response to low frequency fluctuations of barometric pressure, whereas, the short-term barometric efficiency, $\propto_S$, represents the borehole water level response to rapid high frequency fluctuations of barometric pressure. Long-term ($\propto_L$) and short-term ($\propto_S$) barometric efficiencies are given by [*Rasmussen and Crawford*, 1997]:

$$\Delta WL = -\propto_L \ \Delta B_p \ , \tag{2.3}$$

$$\Delta WL = -\propto_S \ \Delta B_p \ , \tag{2.4}$$

where: ΔWL and ΔB_p are changes in water levels and barometric pressure over time interval Δt.

Rasmussen and Crawford [1997] show the relationship between $\propto_L$ and $\propto_S$ for confined aquifers. Where there is negligible borehole storage or skin effects $\propto_L$ should equal $\propto_S$ and where there is significant borehole storage or skin effects $\propto_L$ should be larger than $\propto_S$. For semi-confined aquifers $\propto_L$ should be smaller than $\propto_S$.

Barometric efficiency is readily determined if the borehole water level is fluctuating solely in response to barometric pressure changes [*Rasmussen and Crawford*, 1997]. However, borehole water levels in confined aquifers may fluctuate due to stresses other than barometric pressure. In this case estimating the barometric efficiency using the ordinary least-squares regression method is not accurate if the form of any underlying interference is not known [*Davis and Rasmussen*, 1993]. *Clark* [1967] proposed a method for estimating barometric efficiency without the need to identify the underlying trend of other influences. Estimation of the barometric efficiency using this method is obtained by calculating the summation of the first differences of the water level divided by the summation of the first differences of the corresponding barometric pressure record as shown in Equation 2.5:

$$BE = \sum \Delta WL \,/\, \sum \left|\Delta B_p\right| . \qquad (2.5)$$

Here ΔWL is given a positive sign for water level rise and ΔBp is given a positive sign for barometric pressure decrease. To calculate $\sum \Delta WL$ the following rules are applied; (1) if ΔB_p is zero, ΔWL is omitted from the $\sum \Delta WL$ calculations, (2) if ΔB_p and ΔWL have like signs, add ΔWL, (3) if ΔB_p and ΔWL have unlike signs, subtract ΔWL. $\sum \left|\Delta B_p\right|$ is the summation of the absolute values of ΔB_p. Then the cumulative summations of both $\sum \Delta WL$ and $\sum \left|\Delta B_p\right|$ for a time series are plotted against each other and the slope of a plot gives the estimated barometric efficiency. Estimating the barometric efficiency using Clark's Method is the same conceptually as estimating the short term barometric efficiency, $\propto_S$, using the ordinary least-squares regression method but with an added procedure for eliminating any underlying unknown trend.

It is assumed when using Clark's Method that the water levels fluctuations and the corresponding barometric pressure fluctuations are linearly related (instantaneous response), i.e. the aquifer is purely confined. In case of non-instantaneous response (semi-confined aquifer) part of the response will be attributed to an apparent trend which can lead to an error in the barometric efficiency estimation [*Davis and Rasmussen*, 1993]. Estimated barometric efficiency values using the Clark's method

tend to be too low when high quality water level data are not available or when data sets are affected by strong trend or noise [*Merritt*, 2004].

Gonthier [2007] proposed a graphical method for calculating barometric efficiency. Water level and barometric pressure data should be recorded at short time intervals (15 minutes intervals were used in his applications). A plot of water level on (Y-axis) versus barometric pressure on (X-axis) shows a curved line which describes a series of overlapping ellipses, which are formed due to influences other than barometric pressure that contribute to borehole water level. The barometric efficiency is then considered to be the slope of the major axis of selected elliptical loops.

All the above mentioned methods for calculating the barometric efficiency are convenient if the borehole water level response to barometric pressure perturbations is instantaneous, i.e. when the aquifer is purely confined. In reality the response of the borehole water level is often lagged or delayed due to borehole storage or skin effects [*Furbish*, 1991] or where the aquifer is semi-confined [*Rojstaczer*, 1988a] or semi-unconfined [*Weeks*, 1979]. Under these circumstances it is important to estimate the barometric response function which represents the borehole-aquifer system response to the full range of frequencies in the barometric pressure signal.

2.4. The barometric response function (BRF)

Generally the main approach for estimating the time and frequency dependent response of the borehole-aquifer system to barometric pressure perturbations is the mathematical deconvolution approach. Both the convolution and deconvolution approaches can be applied in either the time or frequency domains.

In the time domain convolution, Equation 2.6 [*Weeks*, 1979; *Furbish*, 1991; *Rasmussen and Crawford*, 1997; *Toll and Rasmussen*, 2007; *Rasmussen and Mote*, 2007], the output variable (changes in borehole water levels, ΔWL) is related to the

input variable (corresponding changes in the barometric pressure, ΔB_p) by the impulse barometric response function μ.

$$\Delta WL = \mu * \Delta B_p = \sum_{\tau=0}^{m} \mu(\tau)\ \Delta B_p(t-\tau), \quad (2.6)$$

where: $*$ is the convolution operator symbol and τ is the number of lags from 0 to a maximum of *m*.

In order to estimate the impulse response function from Equation (2.6) a regression deconvolution approach is solved using the least square method [*Rasmussen and Crawford*, 1997; *Spane*, 2002; *Toll and Rasmussen*, 2007; *Rasmussen and Mote*, 2007]. Then the step response function, $R(\tau)$, which is the barometric response function in the time domain, is calculated as the cumulative aggregate summation of the impulse response function, μ, Equation 2.7:

$$R(\tau) = \sum_{i=0}^{\tau} \mu(i)\ . \quad (2.7)$$

BETCO (Barometric and Earth tides correction) is free computer software introduced by *Toll and Rasmussen* [2007] based on the least squares regression deconvolution method. This utility can be used to calculate the barometric response function and to correct the water level time series for barometric pressure and Earth tides effects.

The time domain convolution summation, Equation 2.6, is theoretically equivalent to multiplication of the Discrete Fourier Transforms, DFT, in the frequency domain, Equation 2.8 [*e.g. Gubbins*, 2004]:

$$WL(f) = BRF(f)\ B_p(f), \quad (2.8)$$

Where: $WL(f)$ is the DFT of the water level time series, $BRF(f)$ is the DFT of the barometric response function and $B_p(f)$ is the DFT of the barometric pressure time series.

Deconvolution in the frequency domain can be achieved by dividing the DFT of the water levels, $WL(f)$, by the DFT of the barometric pressure, $B_p(f)$, in order to obtain the DFT of the barometric response function $BRF(f)$. This $BRF(f)$ is in the complex form and can be used to characterize the frequency-dependant relationship between the barometric pressure loading and the borehole water level response using two components; the gain or admittance component and the phase component. These are obtained by calculating the modulus and the argument of $BRF(f)$ respectively. The step response function in the time domain ($R(\tau)$) can be calculated using the Inverse Discrete Fourier Transform, IDFT, of the $BRF(f)$, however this is not straight forward analytically [*Furbish*, 1991].

The "cross-spectral deconvolution by ensemble averaging" method [*Welch*, 1967] is another approach for estimating the barometric response function that has been used by a number of previous investigators [*Rojstaczer*, 1988a; *Rojstaczer and Riley*, 1990; *Beavans et al.*, 1991; *Quilty and Roeloffs*, 1991; *Ritizi et al.*, 1991]. In this approach, the barometric response function is obtained by dividing the cross-spectrum between water levels and barometric pressure by the auto-spectrum of barometric pressure. Specifications of the cross-spectrum and the auto-spectrum estimation can be found in [*Bendat and Piersol*, 2010]. More details on the cross-spectral deconvolution approach which is used in this study are given in Chapter 6.

2.5. The Earth, ocean and atmospheric tides

Earth tides and ocean tides are caused by the gravitational pulling forces of the Moon and Sun on the Earth's crust and water bodies respectively. Because the Moon is closer to the Earth than the Sun, it's tidal effects on the Earth (the lunar tides) are stronger and more dominant than those of the Sun (the solar tides). Spring tides (the higher tides)

occur when the Moon, the Sun and the Earth are in line (the Moon is full or new). Neap tides (the lower tides) occur when the Moon and Sun are right angles to each other. The dominant periodic components of Earth tides are diurnal (~1 cycles/day) and semi-diurnal (~ 2 cycles/day). Five of these components represent 95% of the tidal potential [*Bredehoeft*, 1967], which are O_1, K_1, N_2, M_2 and S_2. Table 2.1 shows the tidal frequency and the gravitational source for these 5 components [*Merritt*, 2004].

Table 2.1. The main five Earth tidal components after *Merritt* [2004].

Component	Frequency (cycles/day)	Gravitational source
O_1	0.9295	Main Lunar diurnal
K_1	1.0027	Lunar-Solar diurnal
N_2	1.8959	Lunar semi-diurnal
M_2	1.9323	Main Lunar semi-diurnal
S_2	2.0000	Main Solar semi-diurnal

The solar radiation of the Sun causes changes to ground temperature, air temperature and air pressure at tidal periods. Variations in ground temperature cause thermoelastic deformations and variations in air pressure and temperature causes atmospheric tides [*Chapman and Lindzen*, 1970; *Agnew*, 2007] which occur primarily at diurnal (S_1, at 1 cycle/day) and semi-diurnal (S_2, at 2 cycles/day) periods. Ozone heating, and water vapor and heating from the ground are two types of heating caused by the solar radiation. The S_1 diurnal component is largely caused by water vapor and heating from the ground, causing it to be irregularly distributed. Hence, the diurnal S_1 component can significantly vary from place to place due to variations in temperature and wind. In contrast, about two-thirds of the S_2 semi-diurnal component is caused by ozone heating with the rest by water vapor and heating from the ground. For these reasons, S_2 has much more homogeneous distribution than S_1 [*Chapman and Lindzen*, 1970; *Dia and Wang*, 1999]. The lunar forces of the Moon also generate gravitational atmospheric tides. However these are much smaller by a factor of 20 than the solar atmospheric tides. In order to characterize the small contribution of lunar forces to atmospheric tides, statistical analysis over a span of decades is needed [*Volland*, 1997]. Atmospheric tides form the periodic element of variations in barometric pressure. The

movement of higher and lower pressure air masses causes the aperiodic fluctuations in barometric pressure which, occur at longer periods, are dominant and have much more energy than the periodic fluctuations [*Maréchal et. al.*, 2002].

2.6. Effects of Earth and ocean tides on borehole water levels

Boreholes water levels are known to respond to Earth and ocean tides [*Maréchal et al.*, 2002]. Aquifer loading pressure oscillates in response to periodic tidal stresses causing periodic oscillations in the boreholes water levels [*Merritt*, 2004]. The borehole water level response to Earth tides is due to [*Rojstaczer and Riley*, 1990; *Ritizi et al.*, 1991; *Kümple*, 1997; *Inkenbrandt et al.*, 2005];

(a) aquifer skeleton deformation (compression or dilatation) caused by the applied tidal stress,

(b) vertical diffusion of pressure pulse through the aquifer, and

(c) groundwater flow between the aquifer and the borehole, driven by pressure imbalance between them.

(d) direct effect of periodic tidal forces on aquifer pore waters.

Therefore, the phenomena of borehole water level response to Earth tides reflects the deformation (compression or dilatation) cycles of the aquifer rock material, where compression cycles cause a rise in borehole water level and dilatation cycles cause a drop in borehole water level [*Kümple*, 1997]. Thus, the borehole water level response to Earth tides is independent of the pneumatic diffusivity of the unsaturated zone which contributes to the response to barometric pressure. The more elastic the aquifer, the greater the deformation due to Earth tides and the larger the response in borehole water level and vice versa [*Inkenbrandt et al.*, 2005]. *Rojstaczer and Agnew* [1989] and *Rojstaczer* [1988b] defined three potential causes that can attenuate the borehole water level response to Earth tides: (a) limited hydraulic connection between the borehole and the aquifer, (b) large scale horizontal flow, and (c) vertical flow between the aquifer and the water table.

The response of borehole water levels to Earth tides may be contaminated by barometric pressure effects at the solar components. Therefore, it is recommended for Earth tides analysis that the O_1 and M_2 components (Table 2.1) are used as the main lunar components as they represent most of the Earth tides signal [*Galloway and Rojstaczer*, 1988; *Rojstaczer and Riley*, 1990; *Ritizi et al.*, 1991; *Beavan et al.*, 1991]. In confined aquifers, borehole water level changes induced by Earth tides can be up to several centimetres. A significant borehole water level response to Earth tide O_1 and M_2 components is therefore a good indicator that the aquifer is confined [*Kümple*, 1997].

WPARICET is free software created by Hans-Georg Wenzel in 1994. This software is designed to calculate the theoretical Earth tidal parameters in terms of gravity units (using longitude, latitude and elevation of a specific location) based on a 0.5°x0.5° grid template over the surface of the Earth. This software also takes into account oceanic loading effect which can reach up to 10% of the Earth tides. This program works with two different approaches. One approach assumes a purely elastic Earth model and the other assumes an inelastic Earth model [*International Center for Earth Tides*, 2009]. *TSoft* is free software, developed by *Van Camp and Vauterin* [2005], that can be used to calculate the theoretical Earth tides time series for a specific location using a set of tidal parameters calculated with *WPARICET*, or provided by the user.

2.7. Groundwater vulnerability

Groundwater contamination is a growing problem that is mainly caused by human activities such as agriculture, industry, mining and waste disposal. However, groundwater contamination can also occur due to naturally occurring activities such as mixing with another groundwater source that has a different chemistry or natural leaching from the soil [*Liu and Liptak*, 2000]. Once a contaminant is introduced to groundwater it moves and spreads as a result of different hydraulic and chemical processes which are a function of the properties of both the aquifer and the contaminant [*Liggett and Talwar*, 2009]. Clean up or remediation of a contaminated aquifer is difficult, costly and time consuming, and thus it is important to manage and

protect properly groundwater resources from future contamination [*Liggett and Talwar*, 2009]. Therefore, scientists and resource managers have recognized the need to develop effective methods for groundwater protection and to identify aquifers which are vulnerable to contamination [*United States National Research Council*, 1993].

The concept of groundwater vulnerability is "relative rather than absolute" [*United States National Research Council*, 1993], thus it is not possible to determine an absolute value for the vulnerability of an aquifer. However it is possible to assess the vulnerability of an aquifer relative to another aquifer or another part of the same aquifer [*United States National Research Council*, 1993]. Over the past 20 years, the concept of groundwater vulnerability has evolved in North America and Europe [*Frind et al.*, 2006]. Groundwater vulnerability to surface pollution is defined by the *United States National Research Council* [1993] as "the tendency or likelihood for contaminants to reach a specified position in the groundwater system after introduction at some location above the uppermost aquifer". *Boland et al.* [1999] defined groundwater vulnerability as "a measure of the significance of a pathway and receptor". *Vrba and Zoporozec* [1994] distinguished between the "specific vulnerability", as a function of both potential contaminant and hydrogeological features, and the "intrinsic vulnerability" that is a function of hydrogeological features only. Thus, "specific vulnerability" is a more general term which includes intrinsic properties of the aquifer and confining layer as well as transport properties of a specific contaminant [*Liggett and Talwar*, 2009].

There is no direct measure for groundwater vulnerability. Therefore all assessment approaches of groundwater vulnerability aim to synthesize the complex hydrogeologic factors into a form which describes the relative ease with which contaminants reach groundwater and which can be used by planners and decision makers [*Liggett and Talwar*, 2009]. The general hydrogeologic factors which contribute to groundwater vulnerability are the thicknesses and properties of unsaturated zone, saturated confining layer and aquifer, and the pattern and rate of recharge [*United States National Research Council*, 1993]. Approaches for assessment of groundwater vulnerability are categorized into overlay and index methods, process-based methods

and statistical methods [*United States National Research Council*, 1993; *Liggett and Talwar*, 2009].

Overlay and index methods, such as the DRASTIC approach [*Aller et al.*, 1985], are the most popular because they use readily available data, and are easy and inexpensive to implement. In these methods, the protection provided by layers overlying the aquifer is expressed in a semi-quantitative way in which a subjective index or score is assigned to each parameter of these layers (e.g. geology, depth to water table, recharge rate) [*Frind et al.*, 2006]. The scores of all parameters are superimposed to form one map that gives a relative indication of vulnerability over an area which is usually at a regional scale. These scores are usually categorized into a set of vulnerability levels, e.g. low, medium and high. The subjective selection of these scores in addition to the lack of dependence on the hydrogeological processes that control movement and spread of contaminants through the groundwater system impose limitations on the applicability and certainty of these methods [*United States National Research Council*, 1993; *Liggett and Talwar*, 2009]. Process-based methods are distinguished from other vulnerability assessment methods in that they involve the use of deterministic approaches, such as analytical and numerical models (e.g. SWAT, MODFLOW), to predict transient contaminant transport. These methods can be applied on either local or regional scales and require a comprehensive level of input information [*United States National Research Council*, 1993; *Liggett and Talwar*, 2009]. Statistical methods are the least used amongst other assessment methods for groundwater vulnerability; however they can be used to quantify the relationship of hydrogeological measures of vulnerability to the occurrence of contamination [*United States Environmental Protection Agency*, 1993]. These methods "involve the calculation of the probability of a particular contaminant exceeding a certain concentration" [*Liggett and Talwar*, 2009]. They require data of good quality and are usually applied in areas which have a good coverage of water quality and hydrogeological information [*United States National Research Council*, 1993].

As explained above, many useful approaches have been developed for the purpose of groundwater vulnerability assessment, all of which provide either predictive or

probability estimates of the relative ease of contaminant transport through protective layers to reach the aquifer. However, results of all these methods should be regarded with caution due to uncertainty which is inherent in vulnerability assessment. Uncertainties can be due to modeling errors (e.g. inappropriate model or inadequate level of information or data resolution) or errors in data input [*United States National Research Council*, 1993]. Intrinsic groundwater vulnerability is a function of the thicknesses and properties of the overlying confining layer. One of the main hindrances to accurate assessment of groundwater vulnerability is the scarcity of information on the properties of confining layers, particularly vertical hydraulic conductivity. The borehole water level response to barometric pressure also reflects the properties of confining layers. This opens the way to a more quantitative approach for the assessment of groundwater vulnerability which is explored in this work.

CHAPTER 3: PREVIOUS WORK ON DETERMINATION OF BAROMETRIC RESPONSE FUNCTION AND AQUIFER PARAMETERS

3.1. Introduction

The borehole water level response to barometric pressure can be categorized into four mechanisms; purely unconfined (zero response), purely confined (constant response), semi-confined and semi-unconfined (lagged responses), see Chapter 2. The barometric response function can be used as a diagnostic tool for assessing the aquifer response mechanism and the significance of the borehole storage or skin effects [*Rasmussen and Crawford*, 1997]. It can also be used to estimate or place bounds on the properties of confining layer and the aquifer [e.g. *Rojstaczer*, 1988a; *Evans et al.*, 1991b]. The barometric response function can be estimated in the time and frequency domains using the deconvolution approach (section 2.4 in Chapter 2). The time-domain barometric response function represents the amplitude and time lag relationships of borehole water level to barometric pressure. Whereas the frequency-domain barometric response function represents the amplitude and phase relationships of borehole water level response to barometric pressure at each frequency. In order to estimate the barometric response function, borehole water level responses to factors other than the barometric pressure should be removed. Major interference factors which can mask this response are; the rainfall recharge, seasonal or long term trends, Earth tides, ocean tides and pumping activities close to the borehole [*Gonthier*, 2007]. This chapter comprises a review of time-domain and frequency-domain models and applications for the barometric response function.

3.2. Theoretical time-domain response models and applications

Rasmussen and Crawford [1997] categorized aquifer response to barometric pressure change into three time-domain conceptual models for the barometric response function. These are represented by the purely confined aquifer model of *Jacob* [1940], the semi-unconfined aquifer model of *Weeks* [1979] and borehole storage or skin effects model of *Furbish* [1991]. A brief description of these theoretical models along

with corresponding shapes of barometric response functions are described in the following sections and summarized in Figure 3.1.

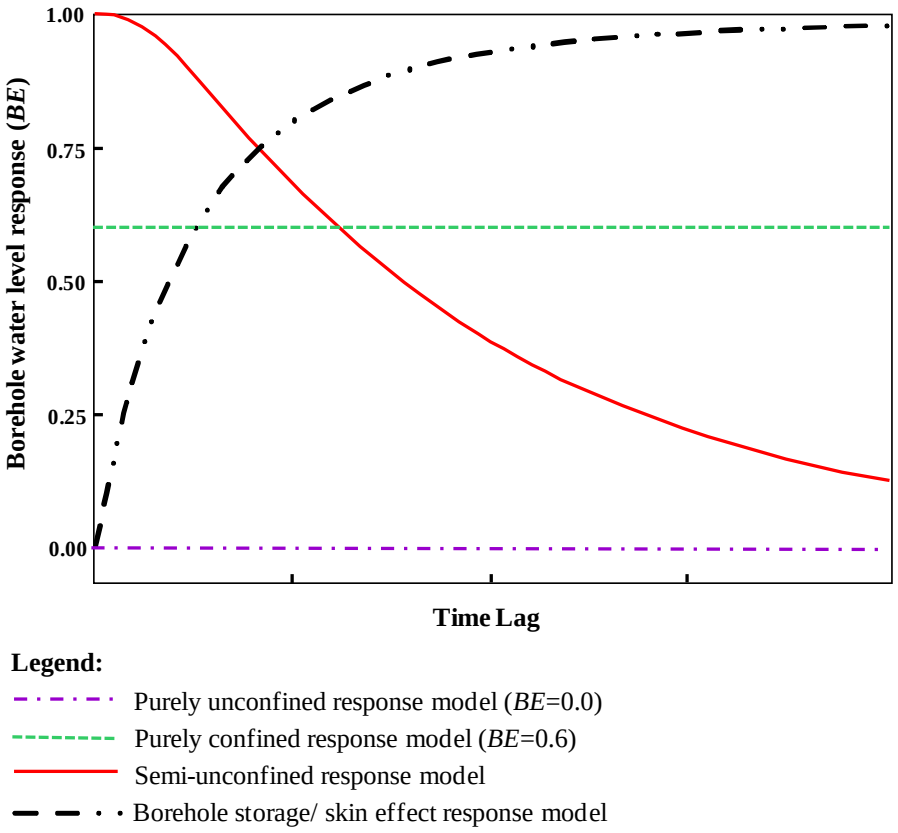

Figure 3.1. Conceptual time-domain models for barometric response function after [*Rasmussen and Crawford*, 1997].

The cases of purely confined and purely unconfined aquifer are relatively simple. The barometric response function of the purely confined aquifer can be simply represented by a constant barometric efficiency (*BE*) [*Jacob*, 1940], see sections 2.2.2 and 2.3. In this model, the aquifer responds instantaneously with no time lag at all frequencies of the barometric pressure signal and thus the response in this model is frequency independent. Therefore, the confined barometric response function in the time domain is simply a constant equal to the static confined barometric efficiency (*BE*) of the borehole-aquifer system, see Figure 3.1. In purely unconfined aquifers (section 2.2.1) borehole water levels show no response to changes in barometric pressure and thus have a barometric efficiency of zero, see Figure 3.1. *Butler et al.* [2011] reported such

a case for a borehole tapping an unconfined alluvial aquifer with unsaturated zone thickness of ~ 2 m.

3.2.1. Borehole storage or skin effect response model

Borehole screen design and the presence of low permeability skin layer surrounding it can delay (lag) flow between the borehole and the aquifer. *Furbish* [1991] explained that the effects of a series of barometric pressure step changes are similar to the effects of a series of slug tests. Thus, the known equations for slug tests can be used for estimating the borehole storage response function in the time domain.

Furbish [1991] introduced two slug tests solutions to estimate the barometric response function using time domain convolution (Equation 2.6). The first is the Cooper-Bredehoeft-Papadopulos solution [*Cooper et al.,* 1967], a precise but mathematically intensive solution [*Furbish,* 1991]. In this solution, he concluded that the response function of water level to barometric pressure is equivalent to the derivative of water level response to a slug test. The second solution is by *Hvorslev* [1951], which is an exponential approximation of Cooper-Bredehoeft-Papadopulos solution, a mathematically much simpler solution but only applicable to aquifers with small storativity. His results showed that the aquifer transmissivity plays an important role in damping and lagging the response of borehole water level to atmospheric loading and that these effects increase with increasing loading signal frequency. Similar conclusions were predicted by [*Rojstaczer*, 1988a]. In reality, the borehole storage/skin effect response model is combined with a confined, semi-confined or semi-unconfined response [*Spane,* 2002]. For borehole-aquifer systems with no skin effects, it is not expected that significant time lags due to well bore storage would be observed for aquifer transmissivity values greater than ~10 m^2/day. Larger borehole radii and lower aquifer storativities increase the time lag [*Spane,* 2002].

In summary, the borehole storage/skin effect model shows that the delay in borehole water level response is caused by the time required for water to flow between the aquifer and the borehole. This time lag is dependent of the transmissivity and

storativity of the aquifer and on the borehole design and condition. Here the barometric response function begins with a *BE* and time lag of zero which gradually increase with increasing the time lag as shown in Figure 3.1.

3.2.2. Semi-unconfined aquifer (vadoze zone) response model

Weeks [1979] used Equation 3.1 to describe gas flow through the unsaturated zone as a function of pneumatic diffusivity, D_{unsat}, depth, z, and time, t, assuming a no-flow boundary at the water table (i.e. no soil gas flows across the water table).

$$\frac{\partial^2 h}{\partial z} = \left(\frac{1}{D_{unsat}}\right)\frac{\partial h}{\partial t}, \tag{3.1}$$

where: h is the air pressure (pneumatic potential).

In *Weeks* [1979] model, he implicitly ignores the capillary fringe effects which may be important in case of shallow unconfined aquifers. His approach is to calculate the water level time series based on an assumed pneumatic diffusivity (D_{unsat}) value, and then compare this to the observed water levels time series. By trial and error a good fit between the calculated and the observed water levels time series is achieved. He applied this technique to one week of data recorded at two hour intervals for a borehole tapping an alluvial aquifer near Texas with around 38 m of unsaturated zone.

In the semi-unconfined barometric response model shown in Figures 3.1, the borehole water level responds instantaneously to changes in barometric pressure at time lag of zero, showing a 100% response (*BE*=1, i.e. the borehole water level drops an equivalent amount to the full change in barometric pressure), followed by a decrease in *BE* with increasing the time lag [*Rasmussen and Crawford*, 1997]. This is due to the time required for the air flow through the vadoze zone to reach the water table and increase the aquifer pore pressure causing the borehole water level to return back to its original level.

3.2.3. Semi-confined aquifer response model

The response of the semi-confined case is qualitatively similar to the semi-unconfined one [*Rojstaczer,* 1988a; *Rojstaczer and Riley,* 1990]. In both cases, the aquifer dissipates the change in pore pressure by flow to/from the water table causing borehole water levels to return to its original level. *Butler et al.* [2011] developed a theoretical time-domain response model for the borehole water level response to barometric pressure under semi-confined conditions. His model considers the specific hydrological situation in which the aquifer and the semi-confining unit are overlain by an unconfined aquifer. The model simulates the saturated one-dimensional vertical flow problem for a two layer system (aquitard and aquifer layers). The upper model boundary is the top of the semi-confining layer, and represents conditions in the overlying unconfined aquifer. This boundary is simulated as a constant head boundary representing step changes in the barometric pressure signal after its propagation through the unsaturated zone. The main parameter of interest in this model is the aquitard vertical diffusivity. To estimate this parameter, heads in the upper unconfined aquifer (model upper boundary) in addition to diffusivity of the aquifer should be known in advance.

Butler et al. [2011] applied this model to four boreholes located at Larned Research Site, Kansas Geological Survey. Three of these boreholes penetrate a semi-confined alluvial aquifer and one borehole penetrates an unconfined alluvial aquifer. Water level and barometric pressure data were recorded every 15 minutes during the winters of 2004 and 2008. It was assumed that borehole water levels are only affected by barometric pressure and Earth tides. *TSoft* was used to estimate the Earth tides potential at boreholes locations and time-domain barometric response functions were estimated using regression deconvolution technique solved using the ordinary least squares approach by *Rasmussen and Crawford* [1997]. The three boreholes tapping the semi-confined aquifer, although located ~ 680 m distant from each other, showed very similar responses for winter 2004. The theoretical response model was fitted to the estimated barometric response functions and an estimate of aquitard hydraulic diffusivity of 170 m^2/day obtained. *Butler et al.* [2011] showed that for boreholes tapping the semi-confined aquifer, the estimated barometric response function for winter 2004 is distinctly different from that of winter 2008 which followed a long

period of recharge, Figure 3.2. Thus under certain circumstances the barometric response function may not be a characteristic of the borehole and can vary with conditions in confining layer [*Butler et al.*, 2011]. The change in conditions is thought to have been caused by frozen soil or a perched water table or air pockets trapped below the water table [*Butler et al.*, 2011; *Peck*, 1960; *Turk*, 1975; *Evans et al.*, 1991b].

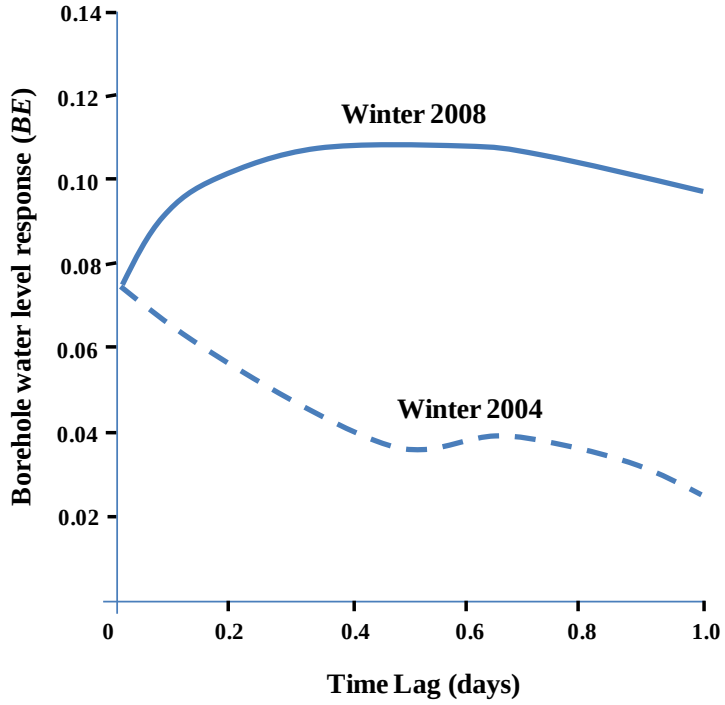

Figure 3.2. Time-domain barometric response functions for a borehole tapping a semi-confined aquifer estimated for winters of 2004 and 2008 [*Butler et al.*, 2011]. Distinctly different responses are observed for the same borehole at these two periods.

The estimated barometric response function for the borehole penetrating the unconfined aquifer is close to zero for winter 2004. However the same borehole showed a response to barometric pressure during the winter of 2008. This is an interesting result which shows that an unsaturated zone (in an alluvial aquifer) of only 2 meters depth can cause significant attenuation of the barometric pressure signal.

3.3. Theoretical frequency domain models and applications

3.3.1. Theoretical frequency domain models

Rojstaczer [1988a] developed a theoretical analytical response model for the borehole water level response to barometric pressure under semi-confined conditions. His model is composed of two layers, a semi-confining and an aquifer layer. He decoupled the problem into three separate flow problems, see section 2.2.3. These are:

1) Vertical air flow between the Earth's surface and the water table through the unsaturated zone.

2) Vertical groundwater flow between the water table and the aquifer through the confining layer.

3) Radial groundwater flow between the aquifer and the borehole with vertical leakage from the confining layer.

In his model the response is a function of the thickness and vertical pneumatic and hydraulic diffusivities of confining layer and lateral hydraulic diffusivity of the aquifer. More details about his model and equations are given in Chapter (7).

Evans et al. [1991b] also developed a theoretical analytical model for the borehole water level response to barometric pressure under semi-confined conditions. His model is similar to that of *Rojstaczer* [1988a] but with three differences. First, his model is composed of one layer divided into unsaturated and saturated zones. Second, the model allows for the possible attenuating effects of the capillary fringe on the air pressure. *Evans et al.* [1991] justified this phenomenon as attenuation of the pressure pulse by encapsulated air pockets within and below the capillary fringe. These air pockets, which are not connected to the atmosphere, are compressed and expanded as the pressure pulse propagates through the unsaturated and saturated zones causing a displacement of the water table and thus an attenuation of the observed pressure pulse. This phenomenon was also observed by *Peck* [1960] and *Turk* [1975]. Evans represents this effect using an attenuation factor applied to the pressure pulse as it infiltrates the unsaturated zone. Third, Evans considers the presence of a low

permeability skin at the interface between the borehole screen and the aquifer formation.

Rojstaczer and Riley [1990] and *Quilty and Roeloffs* [1991] developed theoretical analytical models for borehole water level response to barometric pressure similar to that of *Rojstaczer* [1988a] but for semi-unconfined aquifers. Their models consider two flow problems; air flow through the unsaturated zone and water flow to/from the water table. Thus the response is controlled by two parameters; the vertical pneumatic diffusivity of unsaturated zone and vertical hydraulic diffusivity of the aquifer. *Rojstaczer and Riley* [1990] assume that the aquifer has high lateral permeability, i.e. borehole storage effects are negligible, and that water table fluctuations due to air encapsulated in the capillary fringe are negligible.

Ritizi et al. [1991] developed a theoretical analytical model for the combined response of borehole water levels to barometric pressure and Earth tides for confined aquifers, following the work of *Rojstaczer* [1988a] and *Hsieh et al.* [1987]. This model simulates only saturated flow between the borehole and the aquifer in response to both barometric pressure and Earth tides. Thus, the response is a function of aquifer transmissivity and storativity. To apply this approach, measurements of aquifer pore pressure were collected using packers to isolate sections of the borehole from the atmospheric pressure in addition to data on water level changes in the open borehole. The authors concluded that a good estimate for the combined response function is obtained at the diurnal and semi-diurnal frequencies and at frequencies below 0.5 cycles/day at which the energy of the input barometric pressure and Earth tides signals is significant. This approach can provide better estimates of response functions but on the other hand it requires more effort and additional costs to collect the data needed [*Ritizi et al.,* 1991].

3.3.2. Applications of frequency domain models

Estimation of barometric response functions

In most applications in the literature, the "cross-spectral deconvolution by ensemble averaging" method [*Welch,* 1967] has been used to obtain the barometric response

function. In this technique, time series records of borehole water levels and barometric pressure are divided into segments and the barometric response function estimate is averaged over all segments. Error bars are calculated for each frequency based on coherence estimate and number of segments [*Beavan et al.*, 1991; *Bendat and Piersol*, 2010]. This method is explained in detail in Chapter (6).

Rojstaczer [1988a], *Galloway and Rojstaczer* [1988] and *Rojstaczer and Riley* [1990] simultaneously removed Earth tides effects from borehole water level records and estimated the barometric response function. This is done using cross-spectral deconvolution between borehole water levels and barometric pressure and between borehole water levels and Earth tide strain simultaneously. The theoretical Earth tides strain is estimated using the technique by *Harrison* [1971]. Here two response functions are estimated; the barometric response function and the water level response function to Earth tides.

Beavan et al. [1991] and *Evans et al.* [1991b] calculated theoretical Earth tides using technique by *Longman* [1959]. Earth tide and barometric pressure influences on borehole water level changes are separated using a multi-channel least squares filter, in which theoretical Earth tides and observed barometric pressure are considered as inputs and observed water levels as the desired output. Then the barometric response function was estimated using these filtered water level signals.

Analysis of observed water level records

Rojstaczer [1988a] estimated barometric response functions for three boreholes, two of them tapping a sandstone formation near Parkfield, California and a third borehole tapping a fractured basalt formation near Mammoth Lakes, California. The frequency band of the estimated barometric response functions is 0.02-2 cycles/day using record lengths of 150 days. Best fit theoretical model curves are fitted to the observed barometric response functions and estimates for static barometric efficiency, pneumatic diffusivity of unsaturated zone and hydraulic diffusivity of confining layer

are obtained for all boreholes. Only a lower bound could be estimated for aquifer transmissivity due to the limit of the barometric response function at high frequencies.

Galloway and Rojstaczer [1988] investigated the frequency response of borehole water levels to Earth tides and atmospheric loading. Data was collected at 15 minutes intervals from four deep boreholes tapping a fractured aquifer formation (rhyolitic tuffs overlying carbonate rocks) in Yucca Mountain, Nevada, U.S.A. Record lengths are 171 days for a borehole tapping the lower carbonate aquifer (1805m depth) and 57 days for three boreholes in tuffs (915 m depth). The study area climate is arid and the estimated annual recharge is very low (5 mm), i.e. there is negligible contribution from recharge. Estimated barometric response functions are in the frequency range of 0.02-2 cycles/day. Best fit model curves were determined for both the semi-confined and semi-unconfined response models by *Rojstaczer* [1988a] and *Rojstaczer and Riley* [1990]. The borehole tapping the lower carbonate aquifer showed a scattered response giving a non-unique fit. Thus, only the estimated static confined barometric efficiency and Earth tides areal strain sensitivity could be used to estimate the aquifer elastic properties. Results for the other three boreholes tapping the tuffs showed semi-unconfined responses and it was possible to estimate the pneumatic and hydraulic diffusivities of the unsaturated and saturated zones.

Rojstaczer and Riley [1990] examined a well tapping an unconfined granodiorite aquifer near Parkfield, California; with an open interval at 18-88 m (depth to water table is 18 m). Length of record used is about 150 days. The upper frequency limit for analysis is 2 cycles/day (tidal frequency limit). They imposed two thresholds, based on the coherence and power spectrum of the water level signal, to select the viable frequency range of the barometric response function. Estimates for static barometric efficiency, pneumatic diffusivity of unsaturated zone and hydraulic of the aquifer were successfully obtained.

Quilty and Roeloffs [1991] determined barometric response functions for four boreholes tapping different formations (marine sediments, sandstone and crystalline rocks) near Parkfield, California. The recorded water level and barometric pressure

time series were smoothed using hourly averages and were divided into 37 day segments for calculation of the barometric response function. Long-term trends were removed by applying high-pass Butterworth filter with cut-off frequency of 0.03 cycles/day and the analysis frequency band range is 0.03-0.8 cycles/day (below the tidal frequencies). Pneumatic diffusivity of the unsaturated zone and the hydraulic diffusivity of the aquifer were obtained for three boreholes (one of which was also examined by *Rojstaczer and Riley* [1990]) by fitting their theoretical model to observed barometric response functions. The third borehole showed a confined response where barometric response function is independent of frequency, implying negligible hydraulic conductivity for the confining layer.

Beavan et al. [1991] and *Evans et al.* [1991b] examined water level records from five boreholes tapping the Nubian Sandstone aquifer near Aswan Reservoir, Egypt. Data is collected from two deep and three shallow boreholes for a 2 year period at 0.2 hour recording intervals. This study area is ideal because it is an extremely arid region with very little recharge, the stratigraphy is relatively simple and there are no other interferences [*Evans et al.,* 1991a]. Both Earth tides and barometric pressure induced water level changes are clearly seen in the water level spectrum of the two deep boreholes, while only barometric induced water level changes were found in the 3 shallow boreholes. The method of cross-spectral deconvolution by ensemble averaging [*Welch*, 1967] has been used along with overlapping frequency bands technique (described in section 6.3.4, Chapter 6) to obtain the barometric response function. A high-pass filter is applied with a range of 0.02-0.25 cycles/day to remove energy of frequencies lower than the fundamental frequency of each segment. Gaps in water level and barometric pressure time series records were filled using linear interpolation in both signals to avoid spectral damage. They report barometric response functions over a large frequency range of 0.02-50 cycles/day due to the use of pressure transducers with high resolution. Best model curves from *Evans et al.* [1991b] theoretical model were fitted to observed barometric response functions. Estimates were obtained for the pneumatic diffusivity of the unsaturated zone, the fraction of the air pressure transmitted through the unsaturated zone, the aquifer loading efficiency, vertical and horizontal diffusivities of the aquifer and the permeability of the borehole screen skin.

In summary, during the late 80's and early 90's the barometric response function has been estimated by a number of authors using the method of cross-spectral deconvolution by ensemble averaging [*Welch*, 1967] for semi-confined and semi-unconfined aquifer cases. The frequency ranges of estimated barometric response functions is 0.02 to 2 cycles/day, although *Evans et al.* [1991b] reported estimates up to a frequency of 50 cycles/day. Before estimating the barometric response function, interferences from Earth tides were removed using cross-spectral deconvolution or a least squares filter and interferences from long term trends removed using high pass filters. Theoretical models were fitted to estimated barometric response functions and used in estimating or placing bounds on the unsaturated zone vertical pneumatic diffusivity, confining layer vertical hydraulic diffusivity and aquifer horizontal hydraulic conductivity.

CHAPTER 4: HYDROGEOLOGY OF THE EAST YORKSHIRE CHALK AQUIFER

4.1. Introduction

The study area comprises the Chalk Aquifer of East Yorkshire (Figure 4.1) and is bounded by the Yorkshire Wolds to the north-west, the North Sea to the east and the River Humber in the south. The chalk aquifer is the major groundwater source in the UK supplying more than 50% of the groundwater abstraction for domestic and industrial needs [*Smedley et al.,* 2004]. The East Yorkshire Wolds represent the unconfined aquifer in the north-west, with an elevation up to 200 m ASL [*Smedley et al.,* 2004]. On the Holderness Plain, south-east of the outcrop, the chalk aquifer is confined to semi-confined by a relatively flat cover of glacial deposits with an elevation of 2-15 m ASL.

4.2. Lithostratigraphy

The lithostratigraphy of the East Yorkshire Chalk, which is classified as part of the 'Northern Province Chalk', has been divided into three main units as shown in Table 4.1 and in the cross section Figure 4.2 which are the Lower Chalk (Hunstanton and Ferriby Chalk Formations), the Middle Chalk (Welton Chalk Formation) and the Upper Chalk (Burnham, Flamborough and Rowe Chalk Formations). The Chalk aquifer is underlain by low permeability aquicludes comprising the Speeton Clay series, Kimmeridge Clay, Oxford Clay and the Lias [*Foster and Milton,* 1976].

As shown in Figure 4.1 and Table 4.1, the confined part of the East Yorkshire Chalk aquifer is covered by a wide variety of superficial glacial deposits including boulder clay, alluvium, till, sand and gravel. The Basement Till thickness is up to 30 m at the coast and is a largely homogenous clay-rich till, whereas the Skipsea and Withernsea Tills are much more heterogeneous containing an appreciable sand and gravel content. Observations of coastal exposures show that the top 5 m of the tills are fractured and weathered, thus it is possible that an upper weathered zone of about 5 m thickness may be found inland [*Kilner et al.,* 2005]. In general, the glacial deposits are highly heterogeneous and vary in thickness from less than 10 m west of the buried cliff-line

(see Figure 4.1) and gradually increasing towards the south-east up to a thickness of 50 m. Thus in general, the aquifer is unconfined in the west and north-west Wolds, thinly confined south-east of the outcrop and west of the buried cliff-line, and confined further to the east [*Zhang and Lerner*, 2002; *Smedley et al.*, 2004].

4.3. Permeability development of East Yorkshire Chalk

The chalk was deposited and diagenesis occurred during the Cretaceous period. In the Tertiary, due to the active tectonic movements in Europe various tectonic events affected the chalk including folding (causing the chalk to dip towards the south-east), development of fractures and faults. Later joints formed due to the removal of overburden caused by uplift and erosion [*Hartmann*, 2004; *Parker* 2009]. These processes formed a pervasive fracture system within the chalk significantly enhancing the chalk permeability by providing pathways for fluid flow. In the Quaternary, East Yorkshire was above sea level and hence the chalk underwent weathering through a series of glacial and interglacial cycles. This contributed to the development of fracture permeability particularly in the upper layers of the chalk. Under the periglacial conditions, the continuous freeze-thaw process significantly contributed to fracturing in the top few meters of the chalk, and the chalk was broken up into small fragments forming chalk gravels (chalk bearings), and in some cases 'putty' chalk where the chalk is disaggregated into a soft slurry which has low hydraulic conductivity [*Hartmann*, 2004]. Under glacial conditions, glacial meltwater caused fracture enlargement by dissolution, which contributed to the development of permeability. Vertical flow through the unsaturated zone caused enlargement of vertical fractures, whereas horizontal flow at the water table generated horizontal high permeability zones [*Parker*, 2009]. Dissolution rates depend on the carbon dioxide content in groundwater. Biogenic activities in the soil zone generate high concentrations of carbon dioxide, and thus most dissolution take place close to the surface. The upper 30-60 m of the chalk has the greatest permeability and is considered to comprise the main aquifer horizon [*Parker*, 2009].

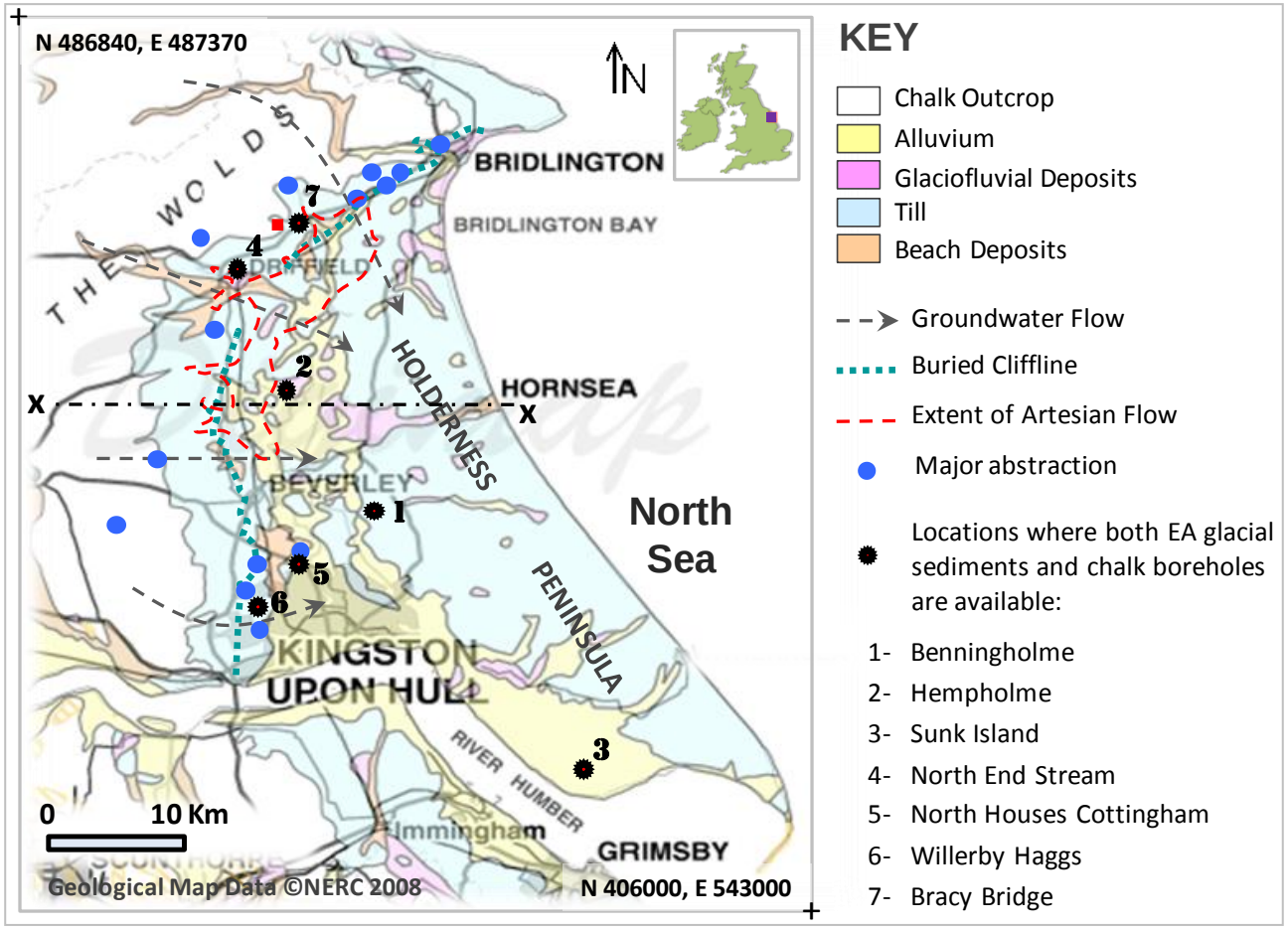

Figure 4.1. Geology map of East Yorkshire showing the outcrop of the Chalk Aquifer and superficial deposits. Also shown are major abstractions, groundwater flow directions, buried cliffline and the zone of artesian flow. After [*Edina-Digimap "Geological Map Data © NERC 2008"*; *Smedley et al.*, 2004; *Gale and Rutter*, 2006]. X-X is cross-section shown in Figure 4.2.

Table 4.1. Lithostratigraphy of East Yorkshire Chalk, adapted from *Salmon et al.* [1996], *Smedley et al.* [2004], *Gale and Rutter* [2006], *Kilner et al.* [2005].

Period	Units	Formations	Thickness (m)	Formation Features
Quaternary	Glacial Sediments	Alluvium	< 20	Highly heterogeneous glacial sediments, thickness less than 10 m in west, increasing to 55 m in east.
		Glacial Sands and Gravels	< 12	
		Withernsea Till	< 30	
		Skipsea Till	< 40	
		Chalky Gravels	< 30	
		Loess	< 1.5	
		Head	< 10	
		Shoreline deposits	< 11	
		Basement Till	< 30	
Cretaceous	Upper Chalk	Rowe	70	Chalk with flints
		Flamborough	260-280	Essentially flintless, white, well bedded marly Chalk. Softer than underlying chalks.
		Burnham	130-150	Thinly bedded, hard white chalk with tabular and discontinuous flint bands, forms the crest and plateau of the Yorkshire Wolds.
	Middle Chalk	Welton	44-53	Extremely pure, massive or thickly bedded, white chalk containing flint nodules.
	Lower Chalk	Ferriby	20-30	Grey marly chalk including gritty, ‘bioclastic’ chalks and hard cemented chalks.
		Hunstanton (Red)	Few meters	Brick-red color mainly due to iron staining.

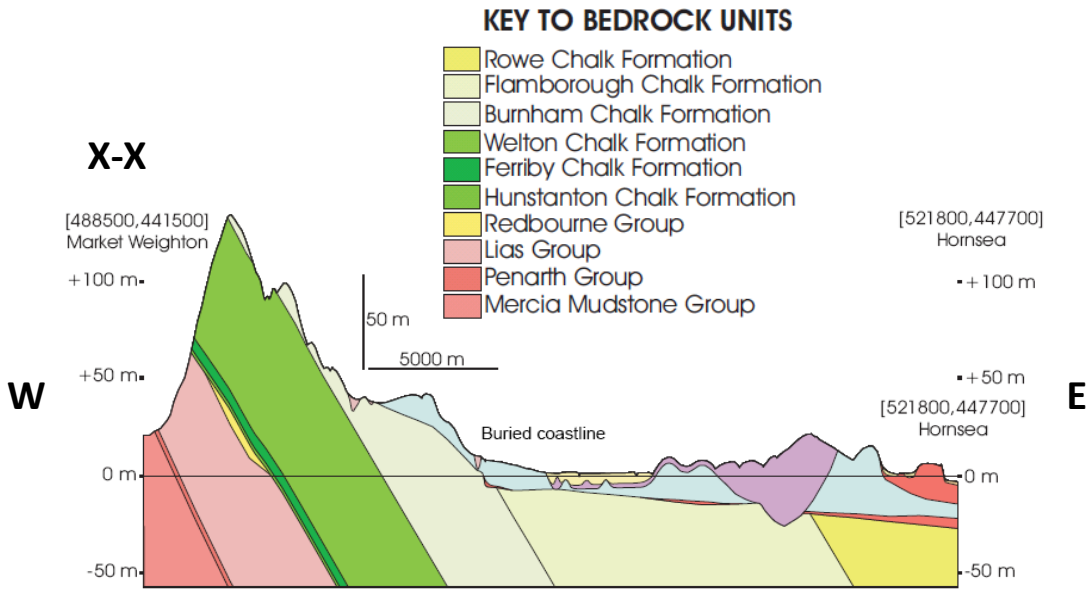

Figure 4.2. Cross-section showing the lithostratigraphy of East Yorkshire Chalk Aquifer and confining glacial sediments after *Smedley et al.* [2004]. Cross-section location X-X is shown in Figure 4.1. Note that the key is only for the bedrock geology, key for superficial deposits is provided in Figure 4.1.

4.4. Aquifer hydraulic parameters

The Chalk aquifer is a dual porosity aquifer where the matrix has high porosity but very low effective permeability because pore throats are very small (0.1-1 μm), while the fractures have low porosity but high permeability. Flow through the Chalk aquifer is primarily through the fracture networks. The average hydraulic conductivity of the chalk matrix is 10^{-4} m/day which is up to 7 orders of magnitude lower than the fracture conductivity. *Foster and Milton* [1974, 1976] and *Foster and Crease* [1975] concluded that the unconfined part of the Chalk aquifer has a moderate/high transmissivity and low specific yield. Pumping tests give transmissivity values ranges from 1000±300 m^2/day to 2200±500 m^2/day with a specific yield of 0.005 and porosity of 0.14%-0.2%. *Elliot et al.* [2001] noted transmissivities higher than 10,000 m^2/day near the buried cliff-line. Further south-east in the Holderness plain transmissivities are much lower, less than 50 m^2/day [*Smedley et al.*, 2004]. *Parker et al.* [2010] developed a new method for the interpretation of impeller flow logs to characterize vertical variations in the chalk hydraulic conductivity. They conducted impeller flow logs, pumped and ambient dilution tests for boreholes, including 5 boreholes used in this study, located in the East Yorkshire Chalk Aquifer. Their results show that the top 10 to 15 m zone of the chalk has the highest transmissivity values, with a range from 100 m^2/day (in the Holderness plain) to 5000 m^2/day (in the unconfined part). Upper Yorkshire Chalk total porosity ranges from 17.7% to 38.3% with a mean value of 24.4% [*Bell et al.*, 1999]. Storativities range from 1.5×10^{-4} to 1.0×10^{-1} with a geometric mean of 7.2×10^{-3} [*Allen et al.*, 1997].

Hartmann [2004] and *Hartmann et al.* [2007] conducted a radially-convergent tracer test at Wilfholme site which is one of sites included in this study (No.2 Figure 5.1). They injected fluorescent dyes into three boreholes M1, M2 and M3, located at 25 m from borehole P which was pumped at a rate of 330 m^3/day. All boreholes were logged using acoustic televiewer, neutron and natural Gamma ray tools to gain information about the chalk structure and frequency of fractures, bedding planes and marl bands. Results show that fractures are mostly concentrated in the upper section (37 m), and injection packer tests show that the top 5-10 m has the highest contribution to transmissivity. Results from a long term pumping test gave transmissivity in the range of 485 to 510 m^2/day and storativity in the range of 0.3×10^{-4} to 3.5×10^{-4}. Laboratory

measurements on core samples showed matrix porosities of 33% to 37% and hydraulic conductivity of 0.07×10^{-4}- 0.68×10^{-4} m/day [*Hartmann*, 2004].

The hydraulic conductivity of the sediments composing the glacial cover range from 10^{-7} to 10 m/day over seven orders of magnitudes. Table 4.2 lists hydraulic conductivities, obtained from laboratory measurements and slug tests for various types of glacial sediment [*Kilner*, 2004]. Sand and gravels show hydraulic conductivity values of about seven orders of magnitude higher than clay and till. Specific storage average values for glacial till and laminated silt and clay calculated from compressibility and porosity [*Quinn*, 2009] are 0.00025 m^{-1} and 0.0025 m^{-1} respectively.

Table 4.2. Shows hydraulic conductivity values for glacial sediments which might be found in the study area after [*Kilner*, 2004].

Source	Material (sample depth)	Hydraulic conductivity (m/day)
Fetter, 1998	Clay	$10^{-7} – 10^{-3}$
	Silt, Sandy silts, Clayey sands, Till	$10^{-3} – 10^{-1}$
	Silty sands, Fine sands	$10^{-2} – 10$
	Well sorted sands, Glacial outwash	$10 – 10^{2}$
Boland and Klinck, 1998 (Cottingham, East Yorkshire)	Till and Gravel (0 - 4m)	10^{-3}
	Sandy clay (4 - 6m)	10^{-5}
	Chalky rubble (6 – 7.4m)	10^{-2}
Kilner, 2004 (Cottingham and Dunswell, East Yorkshire)	Fine sand, Sand and Gravel (0.62 -1.6m)	$10^{-2} – 10^{-3}$
	Alluvial clay (1.5 – 1.8m)	$10^{-3} – 10^{-5}$
	Skipsea Till (2.95 – 4.16m)	$10^{-5} – 10^{-6}$
	Stiff brown clay (1.5 – 1.8m)	10^{-5}

4.5. Recharge, discharge and groundwater flow

The average annual rainfall varies from 630 mm in the Holderness plain to 870 mm on the Wolds where the topography is higher [*Foster and Milton*, 1976]. The potential evapotranspiration average is 425 mm/year. The main period of recharge occurs in the months October to March through the unsaturated zone of the unconfined aquifer (Yorkshire Wolds) and is about 300 mm/year [*Smedley et al.*, 2004]. Consequently the regional groundwater flow direction is south-east towards the lower lying areas of the confined aquifer to the east as shown in Figure 4.3.

Discharge occurs through abstraction wells, natural springs and to the North Sea. Springs, located throughout zone of artesian over flow of 3-5 km width, (see Figure 4.1), feed streams and river channels which flow into the River Hull, shown in Figure 4.3. Drain systems feeds into main drains from which water is pumped into River Hull or discharged to the North Sea [*Gale and Rutter*, 2006; *Parker*, 2009]. The furthest southern stream gauge point on the River Hull is at Hempholme Lock (TA 079 499, Figure 4.3), at which the average daily flow (period from 1989 to 2007) is 350,000 m^3/day [*Parker*, 2009]. The Gypsey Race is a main stream located in the north of the aquifer, see Figure 4.3, with an average daily discharge (period from 1981 to 2008) of 20,000 m^3/day gauged at Boynton (TA 136 677, Figure 4.3) [*Parker*, 2009].

The total groundwater abstraction distributed over the aquifer (major abstractions are shown in Figure 4.1) represents around 14% of the total aquifer recharge with estimated total abstraction of 105 Ml/day and a total licensed abstraction of about 300 Ml/day [*Gale and Rutter*, 2006]. Springs which partially feed the River Hull have been showing decreasing discharge due to heavy groundwater abstraction. Pumping of groundwater in the area north of Hull (e.g. Cotingham) has caused a lower of groundwater levels, as shown in Figure 4.3, resulting in cessation of many springs in the area [*Elliot et al.*, 2001; *Smedley et. al.*, 2004].

The UK Environment Agency (EA) has a network of monitoring boreholes in the Chalk Aquifer in East Yorkshire consisting of about 100 boreholes, 45 of which are located in the confined part of the aquifer. The EA collects monthly water level data for all boreholes (hand dipped), and 14 boreholes are auto monitored at 15 minutes to 1

hour intervals with a recording precision to the nearest centimetre. Auto monitored boreholes are concentrated in the unconfined part and near the confined edge of the aquifer. These data were used to plot 27 monthly contour maps of groundwater heads for the period from November 2005 to January 2008 to study the groundwater flow behaviour across the aquifer through the seasons. Two of these maps are shown in Figure 4.3 to illustrate groundwater heads for a typical summer (July 2006) and for a typical winter (January 2008). This illustrates that recharge occurs mainly in the unconfined part with a steep head gradient west to the confined edge. The regional direction of groundwater flow is towards the south-east with contour lines parallel to the confined edge. Groundwater heads range between -2.5 m ASL north of Hull (due to heavy groundwater abstraction) to 100 m ASL in the Yorkshire Wolds.

The EA has a network of 16 shallow monitoring boreholes which penetrate the glacial sediments layer confining the Chalk Aquifer. At seven of these boreholes, EA chalk boreholes also exist, see Figure 4.1. EA monthly head records (m ASL) for the period 1995-2012 from both glacial sediments and chalk boreholes were plotted to explore the head gradient (recharge/discharge) across the aquifer, see illustrative examples in Figure 4.4. The boreholes at Benningholme, North Houses Cottingham and Willerby Haggs, located in the eastern part of the confined aquifer and near major abstractions between Beverley and Hull, showed continuous recharge (downwards gradient) from glacial sediments to the aquifer (Figure 4.4a). In contrast, the boreholes at Hempholme and Bracy Bridge, located near the artesian flow zone (Figure 4.1) showed continuous discharge (upwards gradient) from the aquifer to the glacial sediments, see Figure 4.4b. The boreholes at Sunk Island showed a varying recharge/discharge pattern which changes with seasons, with recharge occurring during winter and discharge occurring during summer, Figure 4.4c. The North End stream boreholes showed a neutral pattern with no distinct recharge or discharge compared with other locations. This suggests that over much of the confined aquifer, east and south to the zone of artesian flow, head gradients are either continuously downwards or vary with the seasons with downwards head gradients. Since rainfall is highest in winter, this implies that much of the confined part of the aquifer is potentially vulnerable to contaminants from the surface.

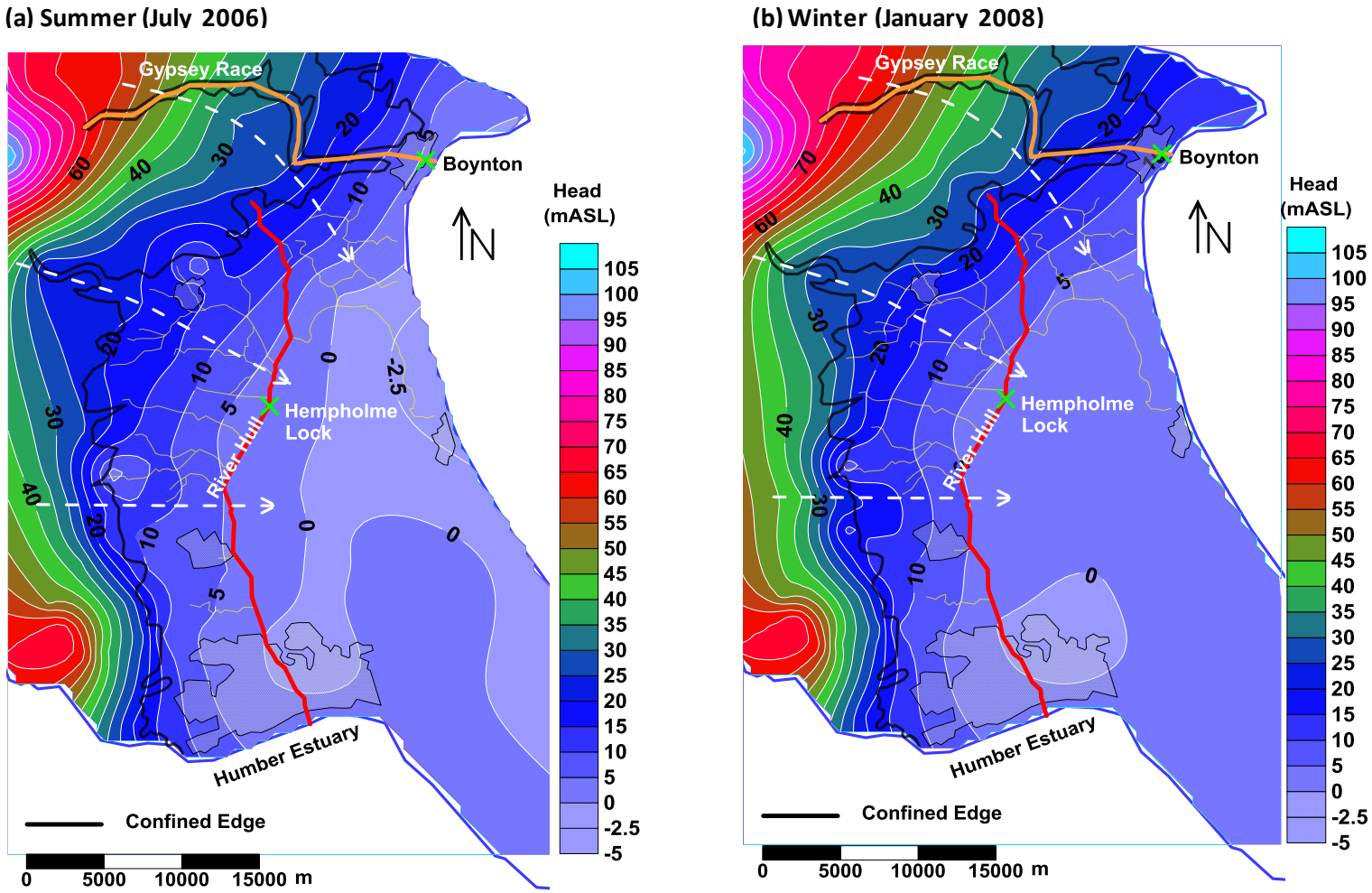

Figure 4.3. Groundwater heads contour map of East Yorkshire aquifer using EA monthly records. Recharge occurs through the unconfined part and groundwater heads ranges between -2.5 m to 100 m ASL. (a) Typical summer (July 2006). (b) Typical winter (January 2008).

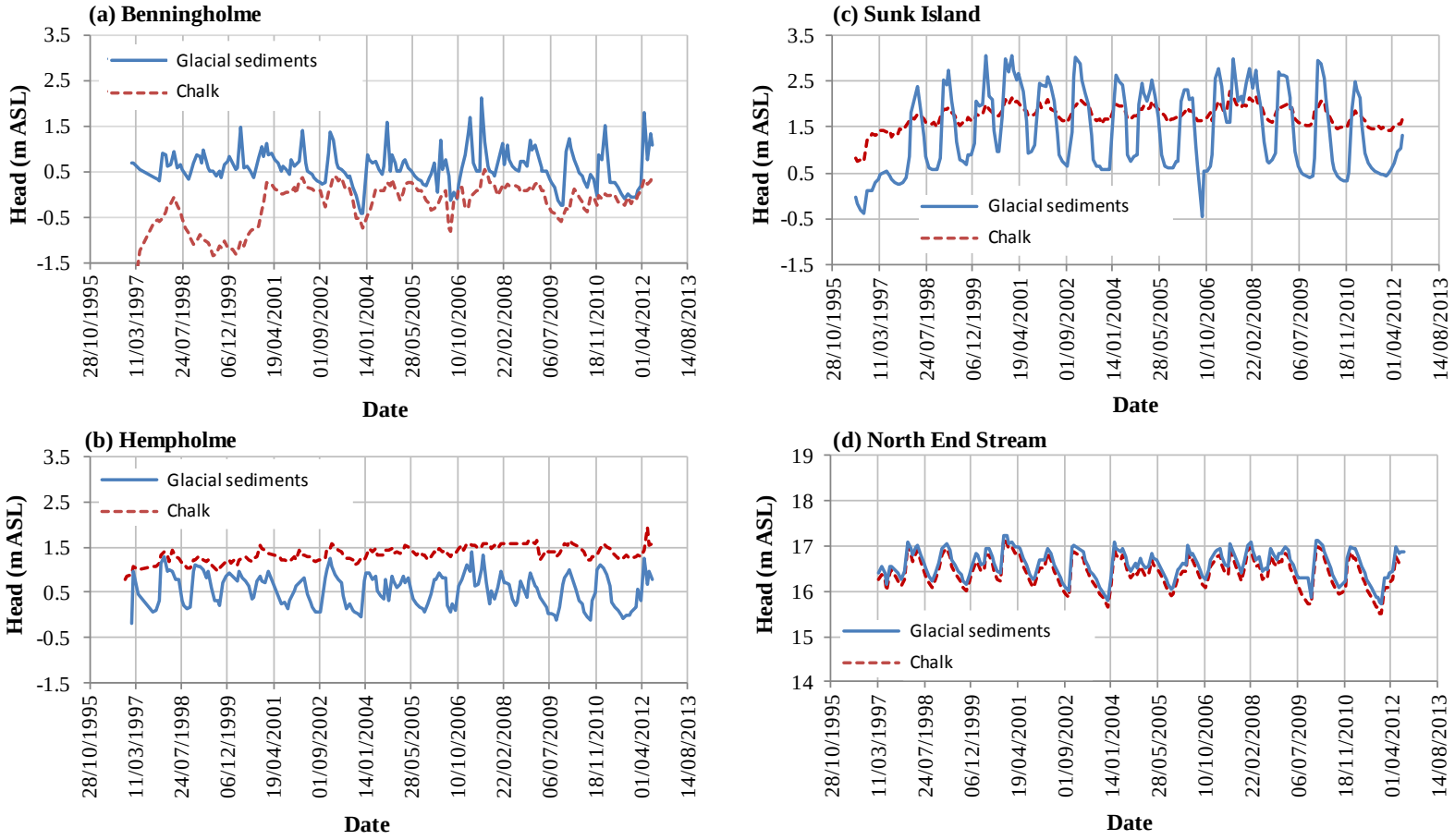

Figure 4.4. Illustrative head records (m ASL, provided by EA) at four locations where EA boreholes in both glacial sediments and chalk are found. (a) The Benningholme location shows continuous downward head gradient, (b) Hempholme location shows continuous upward head gradient, (c) Sunk Island location shows varying upward and downward gradient with seasons, and (d) North End Stream shows a nearly neutral head gradient.

4.6. Land use and aquifer vulnerability

The land use in East Yorkshire is dominated by arable farming and increasing nitrate concentrations in groundwater is a growing problem [*Wellings and Cooper*, 1983] in many of the fourteen major abstractions located along the confined edge of the aquifer (Figure 4.1). Due to the fractured and dual porosity nature of the Chalk aquifer, complete clean-up is complicated because of rapid lateral transport in fractures and retention in the Chalk matrix [*Hartmann et al.*, 2007; *Foster*, 1993].

The intrinsic vulnerability of the confined/semi-confined part of this aquifer is a function of the nature and thickness of overlying confining layer (glacial sediments cover), depth to water table and characteristics of aquifer material [*UK Environment Agency*, 1998; *Frind et al.*, 2006]. In general, the higher the clay content in the glacial sediments, the more protective they are to the aquifer. However the presence of high permeability sediments (sand and gravels) may provide preferential pathways for contaminants from the ground surface to the aquifer. The local structure of the glacial deposits is not well known in detail (except at coastal cliffs and inland quarries) and can vary over only a few meters. Superficial deposits maps for Quaternary glacial sediments and the BGS Lithoframe Viewer [*BGS © NERC*, 2008. All Rights Reserved] are based on sparse borehole logs and cannot provide detailed local information about lithology and continuity of permeable layers which are key information for aquifer vulnerability assessment [*Kilner et al.*, 2005]. Previously it has been assumed within the Groundwater Protection Policy that the study area is generally well protected by the glacial sediments where they are 5 m or more thick [*UK Environment Agency*, 1998]. This assumption has been replaced in April 2010 with the new aquifer designation system that is in line with the EU Water Framework Directive (WFD) [*© Environment Agency and database right*, 2012]. This new system classifies aquifer vulnerability into five zones (Figure 4.5). The most vulnerable zone is the unconfined part of the aquifer 'Major Aquifer High', followed by the area located between the confined edge and buried cliff-line 'Major Aquifer Intermediate', where the glacial sediments cover is less than 10 m. The aquifer area east to the buried cliff-line that is covered by glacial till is assumed to be fully protected 'Major aquifer Low'. Whereas the areas covered by glaciofluvial and alluvium deposits are considered to be high and intermediate vulnerable zones respectively, Figure 4.5.

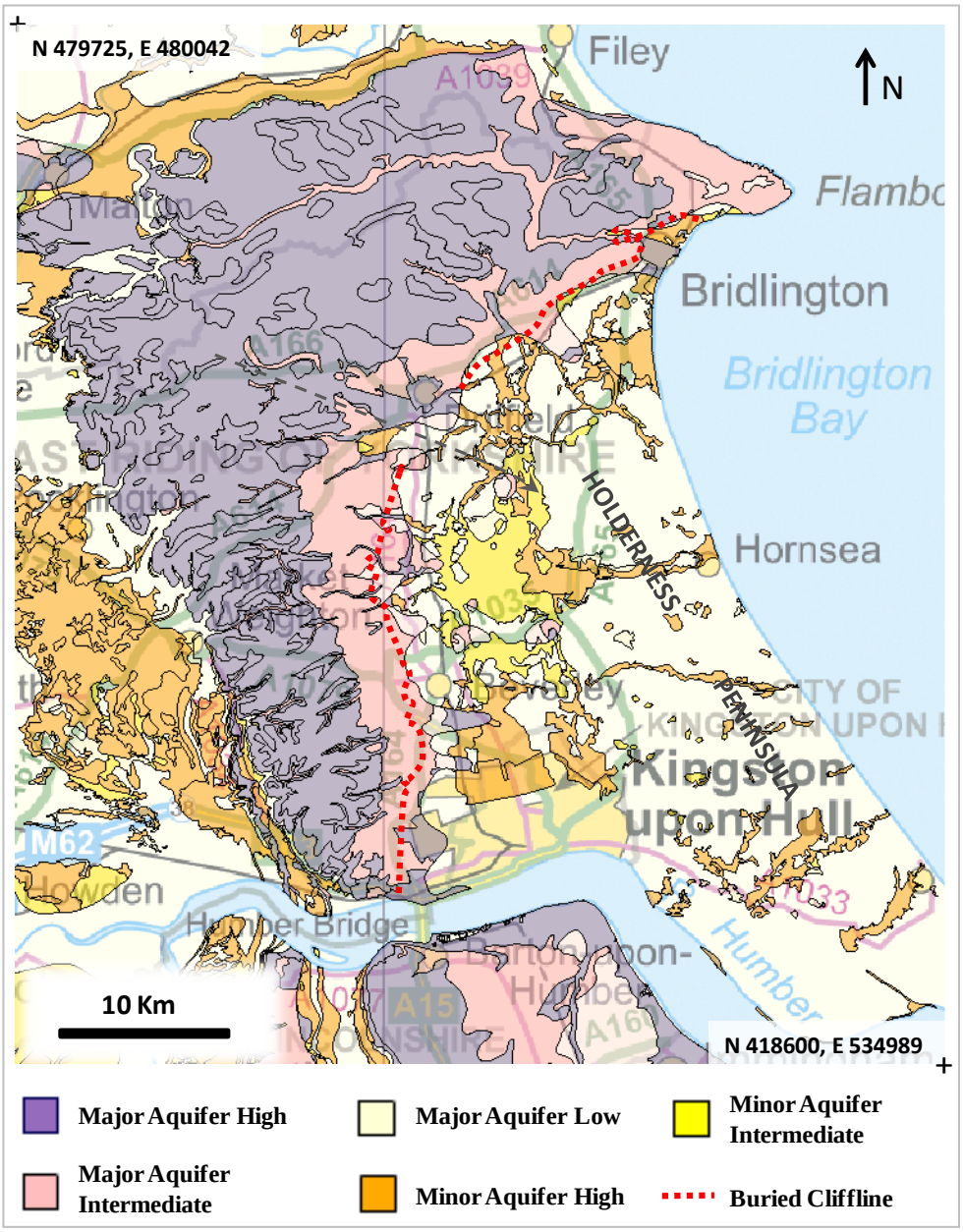

Figure 4.5. Designation map for groundwater vulnerability [© *Environment Agency and database right 2012. © Ordnance Survey Crown copyright. All rights reserved*].

Kilner et al. [2005] investigated the vulnerability of the Chalk Aquifer to transport of contaminants through the glacial sediments using the geophysical techniques resistivity and electromagnetic induction at two source protection zones locations around major abstractions at Cottingham (TA 049 340) and Dunswell (TA 065 357). Their study characterized the glacial deposits covering the chalk, and explored the suitability of these geophysical techniques for the purpose of aquifer vulnerability assessment. Borehole logs showed glacial sediments of 5 to 10 m thick overlying the chalk, largely comprised of glacial till with a series of small discontinuous channels of sands and gravels inferring that the aquifer is relatively well protected. The electromagnetic induction technique provided useful information about large scale lateral variations in lithology. Results showed that vulnerability to pollution may be underestimated by electric resistivity surveys if a conductive (clay) layer overlies more resistive layers (sand), because the interface between the two layers is smeared and the conductive layer masks the resistive layer. However, the use of the resistivity imaging coupled with a good level of geological information (borehole and trench logs) allowed the characterization of high permeability pathways (sands and gravels) within the confining layer. Coupling these geophysical techniques with an appropriate level of geological investigation was found to result in a more detailed model for the glacial deposits than is possible using boreholes records alone, thus improving assessment of aquifer vulnerability. However, geophysical surveys are time consuming and expensive to carry out over the whole aquifer. They are useful for specific local studies, e.g. close to specific abstraction stations.

CHAPTER 5: DATA COLLECTION AND IDENTIFICATION OF COMPONENTS IN WATER LEVEL SIGNALS

5.1. Data collection

The UK Environment Agency (EA) maintains a network of about 100 monitoring boreholes distributed over the Chalk Aquifer in East Yorkshire. About 45 of these are located in the confined part of the aquifer. Twelve of these monitoring boreholes were selected and instrumented for collection of time series data. The locations of these boreholes are shown in Figure 5.1 (boreholes numbers 1 to 10), where three of them are located at the same site (Wilfholme, number 2).

5.1.1. Pre-existing data

The EA provided manual monthly water level data for 45 boreholes located in the confined aquifer for the period 1996-2008. The EA also provided automatically recorded water level data (at 15-30 minutes intervals) for the period of September 2008 to December 2009 for seven boreholes located in the unconfined aquifer near the confined edge (Figure 5.1 and numbers 11-17). Data from these unconfined boreholes are discussed in detail in section 5.2.2 where they were used to characterize the recharge signal.

The EA provided borehole lithology logs and completion details for all selected monitoring boreholes except Wilfholme and Sunk Island. Site lithology data and completion details for three boreholes at Wilfholme were obtained from [*Hartmann*, 2004]. BGS provided borehole information for the Sunk Island borehole. The EA also provided geological cross sections from the BGS Lithoframe Viewer [*BGS © NERC*, 2008. *All Rights Reserved*] at all boreholes locations except Sunk Island borehole (not covered by the model). These cross sections (discussed in Chapter 10) are used in combination with superficial deposits maps, obtained from EDINA Geology Digimap [*Geological map data © NERC*, 2011] as a guide to the glacial sediment cover in the area. Water level data from two shallow boreholes, penetrating the glacial sediments cover only, at Benningholme and Sunk Island sites were collected during field visits. The EA provided water level data for a shallow borehole at Bracy Bridge.

Pumping tests data for Benningholme, Wilfholme, Sunk Island and Thornholme Moor boreholes were obtained from *Hartmann* [2004], *Straughton* [2008] and *Parker* [2010]. *Parker* [2010] conducted Impeller flow logs at Benningholme, Wilfholme and Thornholme Moor boreholes and dilution tests at Benningholme, Wilfholme, Sunk Island and West Newton Farm boreholes. These data are discussed with results of present study in Chapter 9.

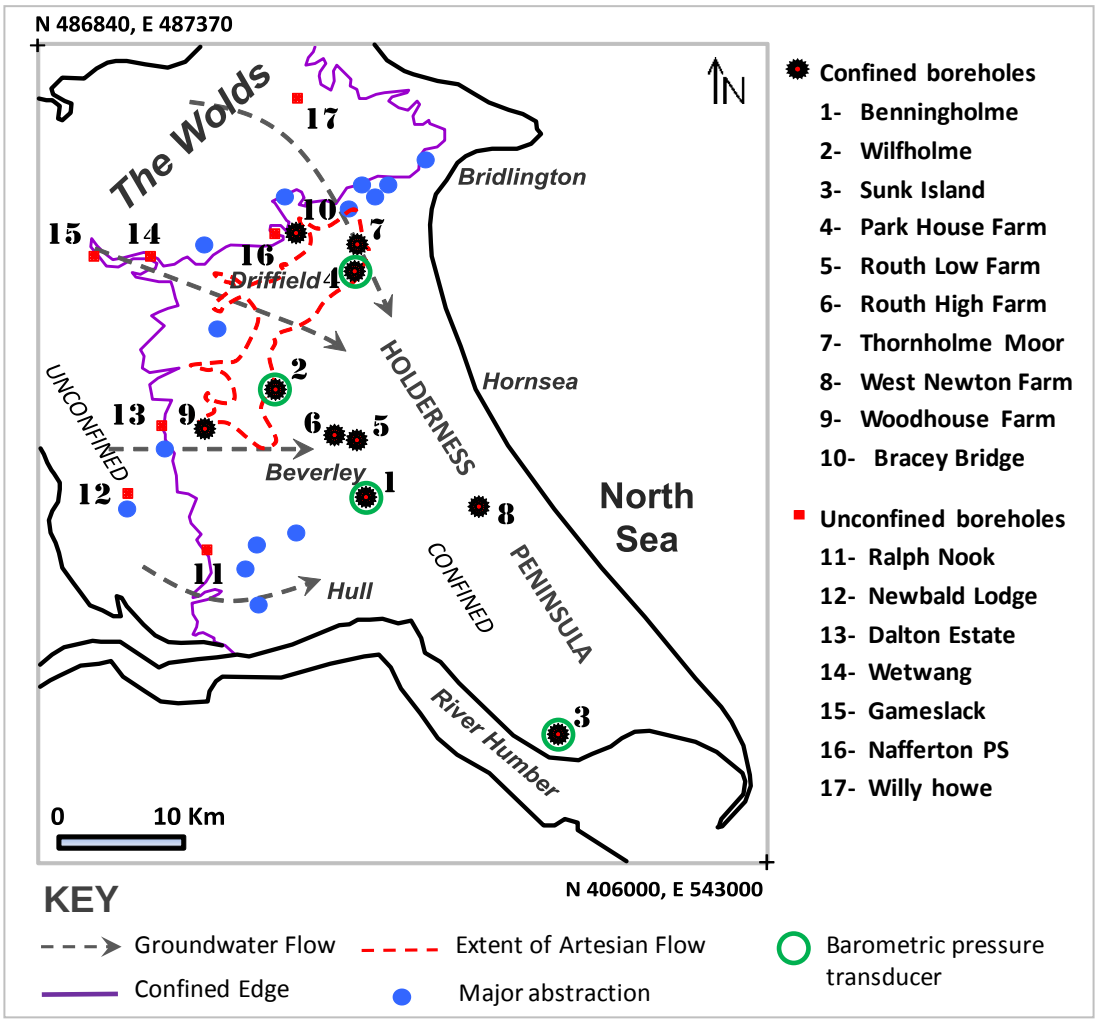

Figure 5.1. Shows locations of monitoring boreholes and major abstractions.

5.1.2. Selection of monitoring boreholes

Twelve monitoring boreholes at 10 locations were selected based on the following criteria. Firstly, boreholes were chosen to represent the variety of glacial superficial

deposits confining the aquifer in order to investigate different degrees of confinement. Secondly, the EA monthly records were used to check the continuity of water level records in order to avoid boreholes which are periodically dry. Thirdly, the EA monthly head records and data provided by Yorkshire Water on locations and pumping rates of 14 major abstractions were used to avoid boreholes which are severely affected by pumping. Fourthly, field inspection of potential boreholes was carried out to check the suitability of boreholes for the monitoring purposes. Boreholes were selected to be easily accessible, secure and suitable for instrumentation installation. Figure 5.2 shows various designs of the casing head works for all selected monitoring boreholes. Three of the selected monitoring boreholes, located at Wilfholme landing (location 2 in Figure 5.1), are located 45 m apart and form a 'huddle test' and were used to compare results from boreholes in close proximity.

5.1.3. Monitoring boreholes completion and lithology

A summary of monitoring boreholes coordinates, depths and completion details are listed in Table 5.1. The depth of boreholes ranges from 18.9 m to 78.8 m, and top casing inner diameter ranges from 5.0 cm to 20.5 cm. At most boreholes, plain casing is installed through the glacial sediments cover and the soft weathered chalk and the rest of the borehole is open to the aquifer. At Routh Low Farm, Routh High Farm and West Newton Farm (boreholes number 5, 6 and 8 respectively) slotted casing is used through the chalk. The depth of plain casing at Woodhouse farm borehole is not known. Plastic casings are used at all boreholes except Thornholme Moor and Woodhouse Farm where a steel casing is used.

Thickness of glacial sediments cover at the selected monitoring boreholes (Table 5.1) ranges from 4.4 m at Woodhouse Farm borehole to 38.1 m at West Newton Farm located at about 3.3 km and 22.5 km respectively east of the confined edge. Figures 5.3 and 5.4 show the lithology logs for the chosen boreholes. These show that at each site the glacial sediments are highly heterogeneous on the scale of meters with compositions ranging from clay rich materials (e.g. boulder clay, brown clay and strong dark clay) to sand and gravels.

Figure 5.2. Design of casing head works for 10 boreholes instrumented in this case study. The top of casing of M1 borehole is similar to those of M2 and M3 boreholes located at the Wilfholme site.

Table 5.1. Details about thickness of glacial sediments and completion details for selected boreholes.

Borehole			Easting	Northing	Top of casing level (ASL)	Total depth (m)	Glacial sediments thickness (m)	Plain casing depth (m)	Casing inner diameter (cm)
1	Benningholme		512481	438936	2.5	78.8	16.2	23.0	19.7
2	Wilfholme	M1	566136	447172	1.5	74.0	11.0	26.2	16.5
		M2			1.1	74.0	13.0	26.2	20.5
		M3			1.3	74.0	10.0	22.6	16.5
3	Sunk Island		526739	418909	3.0	51.9	34.2	34.2	9.7
4	Park House Farm		511503	458265	7.5	39.6	20.4	30.5	20.0
5	Routh Low Farm		510362	443665	2.0	18.9*	13.5	13.5	5.0
6	Routh High Farm		509400	444100	3.0	18.9	13.5	13.5	5.0
7	Thornholme Moor		511700	460600	13.5	50.0	19.0	28.0	20.5
8	West Newton Farm		520475	437860	10.0	67.1	38.1	48.8	9.6
9	Woodhouse Farm		499960	444130	18.0	30.5*	4.4	Not known	10.0
10	Bracy Bridge		507800	462200	18.5	25.0	9.5	20.0	10.0

* From EA records. However, depths measured at field at the time of study were 16.9 m (Routh Low Farm) and 9.66 m (Woodhouse Farm) so these boreholes may have partially collapsed.

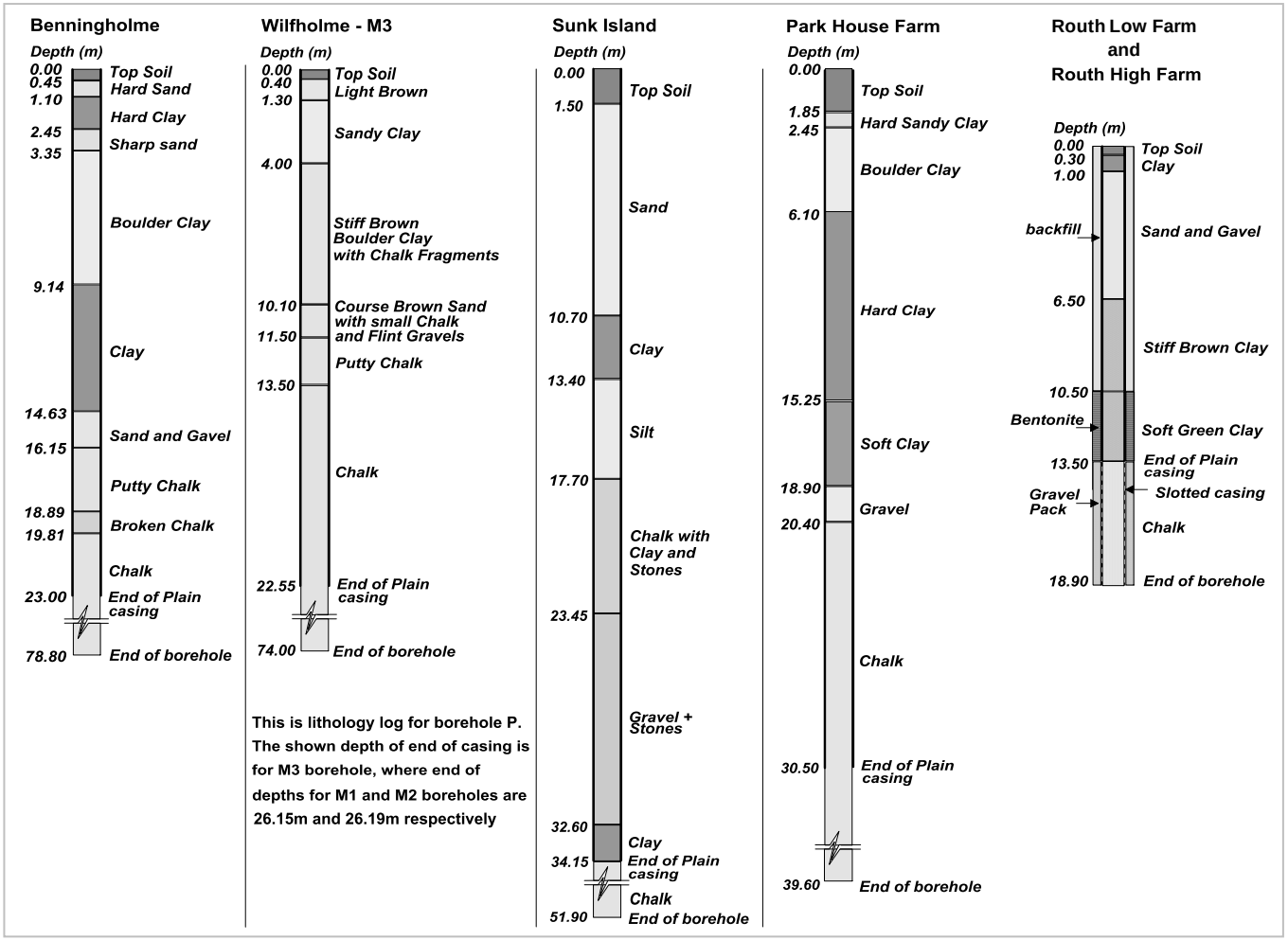

Figure 5.3. Lithology logs and completion details for Benningholme, Wilfholme Landing, Sunk Island, Park House Farm, Routh Low Farm and Routh High Farm boreholes.

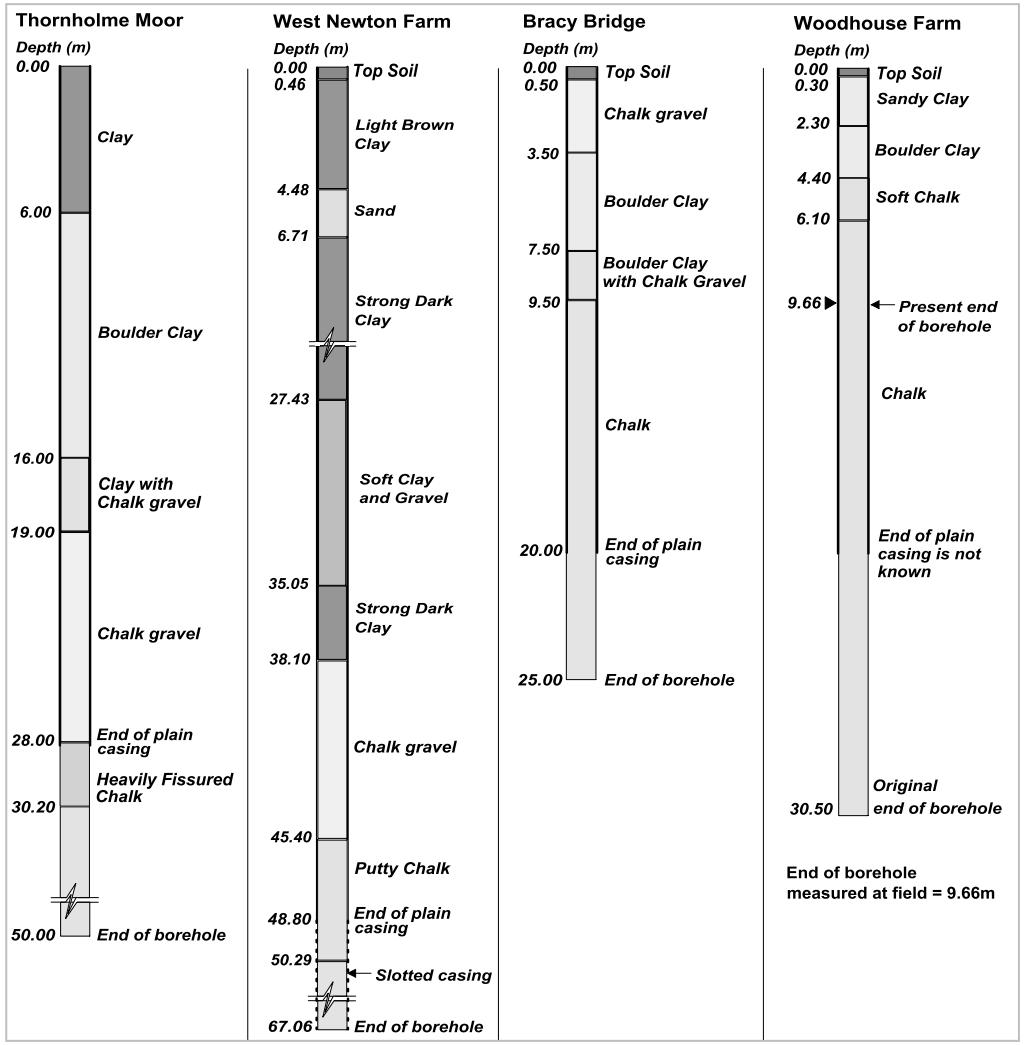

Figure 5.4. Lithology logs and completion details for Thornholme Moor, West Newton Farm, Bracy Bridge and Woodhouse Farm boreholes.

5.1.4. Instrumentation and recording

Absolute, non-vented, pressure transducers are used in this study to record time series data at 15 minutes intervals. A submerged pressure transducer is installed at each borehole to record the total head (water pressure plus barometric pressure) at a level below the minimum borehole water level obtained from EA monthly records (Figure 5.5a). A pressure transducer is also installed above the maximum borehole water level to record barometric pressure at four boreholes across the region (Benningholme, Wilfholme, Sunk Island and Park House Farm), see Figure 5.1. Barometric pressure data from Wilfholme site was used for data analysis at Routh Low Farm, Routh High Farm and Woodhouse Farm, located at ~ 7.5 km, 5.5 km and 6.0 km distant respectively. Barometric pressure data from Benningholme was used for data analysis at West Newton Farm borehole located at ~ 8.5 km distant. Barometric pressure data from Park House Farm was used for Thornholme Moor and Bracy Bridge boreholes located at ~ 2.0 km and 5.5 km respectively, Figure 5.1.

Data were collected over the period from September 2008 to October 2011, with record lengths in the range of 290-800 days. Illustrative records for water levels (m ASL) recorded during monitoring period at four boreholes are shown in Figure 5.6. As shown in Figure 5.5b and Table 5.2, two types of pressure transducers were used with resolutions ranged from 0.09 cmH_2O to 0.25 cmH_2O and accuracy ranged from ± 0.9 cmH_2O to ± 2.5 cmH_2O, depending on the make of the transducer (‘Diver’ by *www.swstechnology.com* or ‘Troll’ by *www.in-situ.com*). To maximize resolution pressure transducers with a maximum head range of 9-10.9 mH_2O were used.

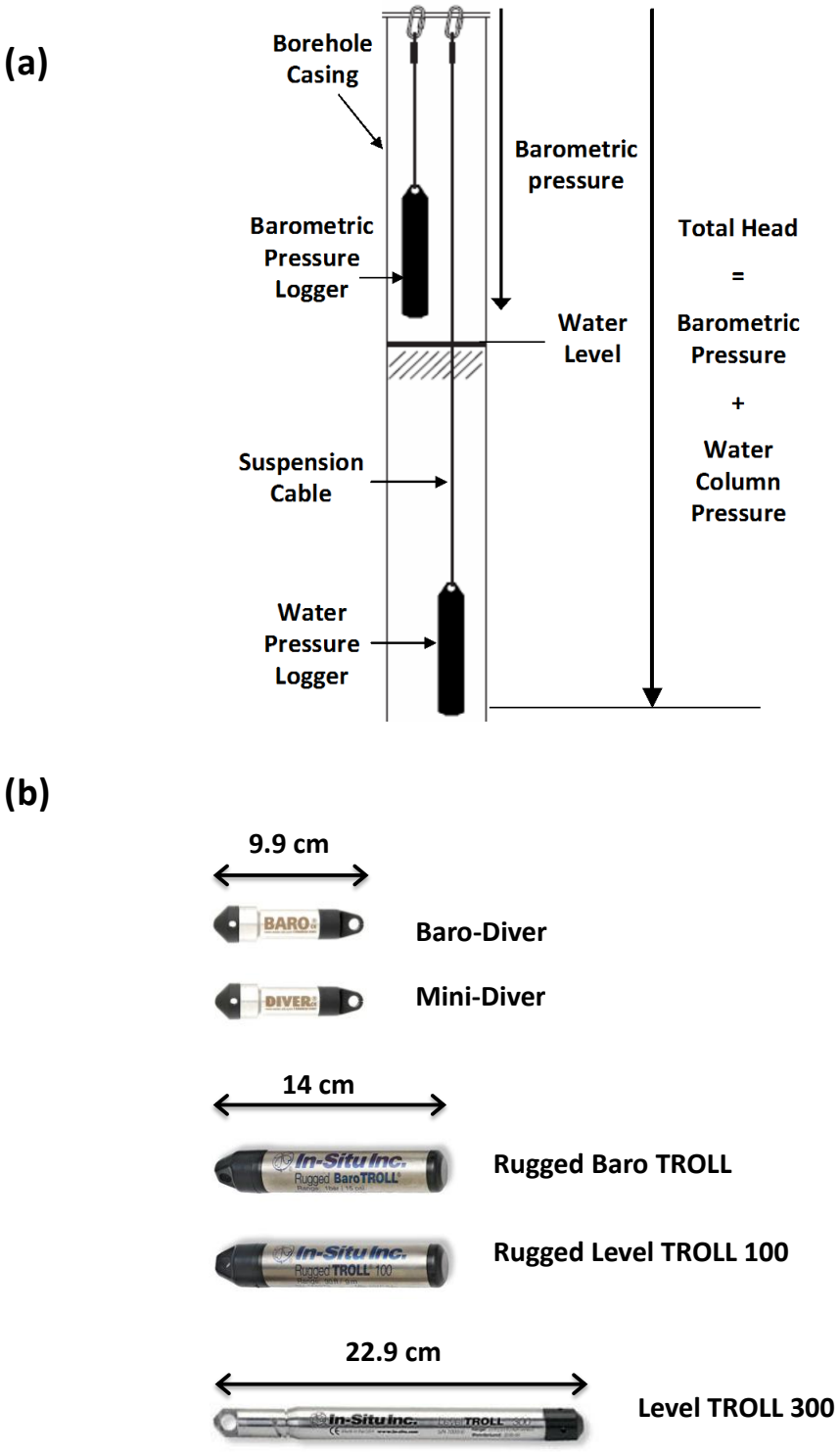

Figure 5.5. (a) Transducers installation. A pressure transducer is hung above the water surface to record barometric pressure and another submerged transducer records total head. (b) Different types of pressure transducers used in this study (after *Schlumberger Water Services* [2009] and *In-Situ Inc.* [2010]).

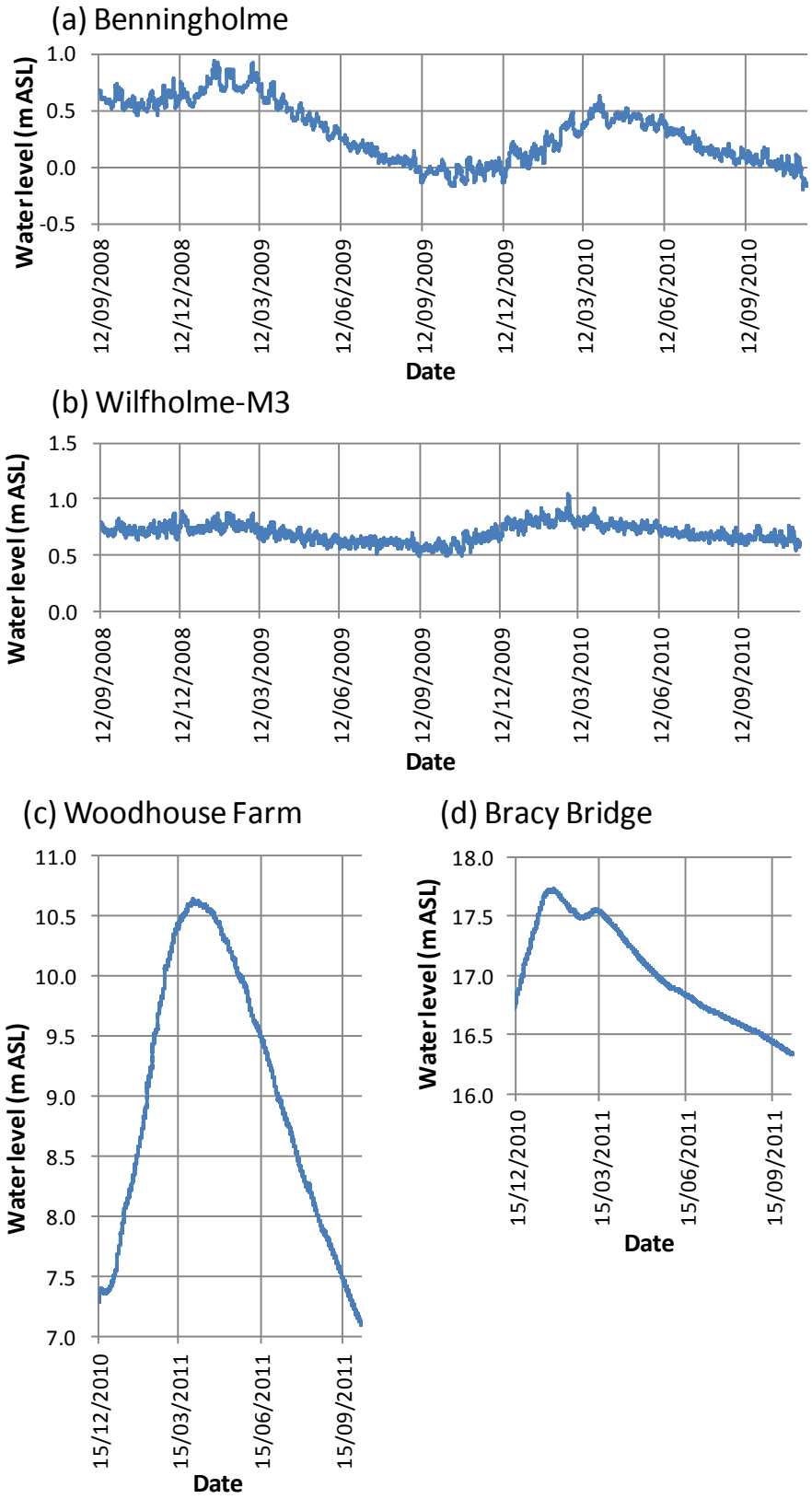

Figure 5.6. Illustrative records for water levels (m ASL) recorded during monitoring period at four boreholes; (a) Benningholme, (b) Wilfholme-M3, (c) Woodhouse Farm and (d) Bracy Bridge.

Table 5.2 . Details on instrumentation and data record length at each borehole

Borehole			Record start	Record end	Record length (days)	Transducer type	Transducer accuracy (cmH_2O)	Transducer resolution (cmH_2O)
1	Benningholme		12/9/2008	20/11/2010	799.1	Level Diver	± 2.5 cmH_2O	0.25 cmH_2O (or better)
						Baro Diver	± 0.5 cmH_2O	0.25 cmH_2O (or better)
2	Wilfholme	M1	23/6/2010	25/3/2011	275.5	Level Troll 300	± 1.03 cmH_2O	0.10 cmH_2O (or better)
		M2	23/6/2010	25/3/2011	275.5	Level Troll 300	± 1.03 cmH_2O	0.10 cmH_2O (or better)
		M3	12/9/2008	21/11/2010	800.0	Level Diver	± 2.5 cmH_2O	0.25 cmH_2O (or better)
						Baro Diver	± 0.5 cmH_2O	0.25 cmH_2O (or better)
3	Sunk Island		12/11/2008	20/11/2010	737.9	Level Diver	± 2.5 cmH_2O	0.25 cmH_2O (or better)
						Baro Diver	± 0.5 cmH_2O	0.25 cmH_2O (or better)
4	Park House Farm		26/5/2010	15/4/2011	324.2	Level Troll 100	± 0.9 cmH_2O	0.09 cmH_2O (or better)
						BaroTroll	± 1.0 cmH_2O	0.1 cmH_2O (or better)
5	Routh Low Farm		20/11/2010	7/10/2011	317.9	Level Troll 100	± 0.9 cmH_2O	0.09 cmH_2O (or better)
6	Routh High Farm		28/11/2010	6/10/2011	312.7	Level Troll 100	± 0.9 cmH_2O	0.09 cmH_2O (or better)
7	Thornholme Moor		28/11/2010	7/10/2011	312.0	Level Troll 100	± 0.9 cmH_2O	0.09 cmH_2O (or better)
8	West Newton Farm		29/10/2009	6/9/2011	677.1	Level Troll 100	± 0.9 cmH_2O	0.09 cmH_2O (or better)
9	Woodhouse Farm		15/12/2010	6/10/2011	293.6	Level Troll 100	± 0.9 cmH_2O	0.09 cmH_2O (or better)
10	Bracy Bridge		29/11/2010	6/10/2011	309.6	Level Troll 100	± 0.9 cmH_2O	0.09 cmH_2O (or better)

5.2. Identification of components in the water level signal

The main contributing components in borehole water level signal are barometric pressure, Earth tides and rainfall recharge. In addition, for boreholes located close to the coast effects from ocean tides are also present. Pumping effects from major abstractions and local farm boreholes are also detected in some locations. These components are explored in more details below.

Time series of barometric pressure and water level data recorded at Benningholme borehole (Figure 5.7) shows the characteristic mirror image between both signals which suggests that the aquifer is confined/semi-confined in the vicinity of this borehole. As shown in Figure 5.7, it is easy to observe from the mirror image, that barometric pressure is a major component in the borehole water level signal but other components are not so easily identified. The different components cannot be readily identified in the time domain because these components are superimposed at all times. However the Fast Fourier Transform (FFT) analysis can be used to show all harmonic components in the water level signal and to investigate the characteristics and frequency ranges of each component's contribution to the water level signal. In order to estimate the barometric response function, all components other than those generated by barometric pressure should be removed from the borehole water level signal.

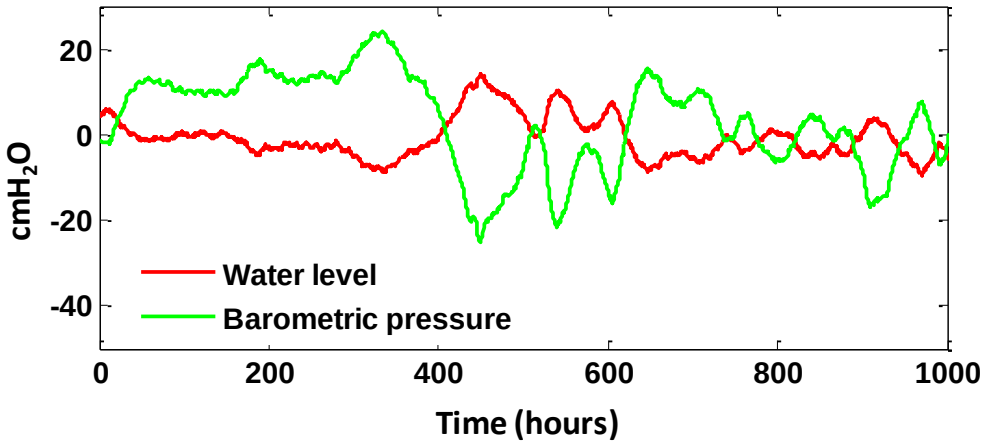

Figure 5.7. Example of water level and barometric pressure time series recorded at Benningholme borehole showing the characteristic mirror image pattern.

In this study, a Matlab code *SC* (Separate Components) has been developed to characterize and separate different components in the borehole water level signal using time series analysis. This code is then used to remove all components in the water level signal other than barometric pressure as a pre-processing step to estimate the barometric response function (see Chapter 6). The *SC* code and instructions for its use can be found in Appendix B. In this Matlab code, the Fast Fourier Transform (FFT) analysis is applied to recorded signals in order to show their harmonic components. Prior to Fast Fourier Transform analysis, each signal is pre-processed as follows according to steps recommended by *Gubbins* [2004].

1) Each signal is detrended (linear trend is removed and the mean subtracted). This is to remove any significant energy that is contained in slow varying trends across the time sequence as otherwise this energy, through leakage, can mask higher frequencies of interest.

2) The FFT is based on the Fourier integral transform which considers the recorded time series to be a continuous function of time. However in practice we have a discretised time series of a finite length. The FFT treats this finite time series as if it were periodically continuous. This requires the start and the end of the time series to have the same value otherwise the resulting discontinuity will introduce additional frequencies. The process by which the end points of both sides of a recorded time series are set to zero, is called 'tapering'. Tapering is the multiplication of a time series by a window function of the same length. Three window functions which are widely used are the Boxcar, Hanning and Tukey windows, see Figure 5.8. The Boxcar window has the advantage that no data downgrading occurs near the record ends (i.e. no data is thrown away) and that it gives a sharper definition of peaks in the harmonic content, but it has greater spectral leakage than other window shapes. The Hanning window minimizes spectral leakage but it involves loss of data away from the center of the record and gives broader peaks. A Tukey window with a tapering ratio (r) equal to zero is equivalent to a Boxcar window while a Tukey window with r equal to 50% of the record length, is equivalent to a Hanning window [*Bloomfield*, 2000]. Here, a Tukey window is applied as a compromise between the Boxcar and Hanning windows, with r of 20% of the record length as recommended in [*Bloomfield*, 2000]. This

suppresses spectral leakage and minimizes loss of data far from the center of the record while showing peaks that are sharp enough for visualization of the harmonics.

3) In some cases the time series is padded by zeros, i.e. the length of the series is extended by adding zeros to the end as if the signal was recorded over a longer time period. This smoothes the spectrum by interpolation and increases the spectral resolution of estimated frequencies.

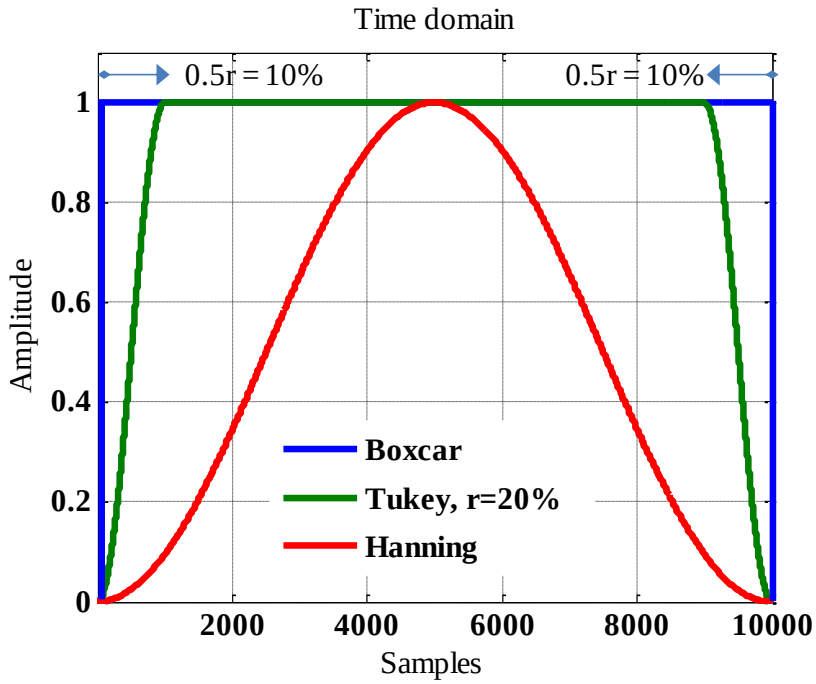

Figure 5.8. Shows the Boxcar, Hanning and Tukey (with r=20%) window functions.

In the *SC* Matlab code, the coherence, $C_{WB}(f)$ (Equation 5.1), is used as a useful measure of the linear correlation between the water level and barometric pressure time series at each frequency and is calculated using a Matlab function called '*mscohere*' [*MathWorks Inc.*, 2011]. If fluctuations in water level (output signal) are solely due to fluctuations in barometric pressure (input signal) coherence would be unity (perfectly correlated data). If fluctuations in the water level signal are not due to barometric pressure coherence would be zero. Coherence levels between zero and unity can be caused by (a) high levels of noise present in the measurements, and (b) additional influences other than barometric pressure [*Bendat and Piersol*, 2010].

$$C_{WB}(f) = \frac{|P_{WB}(f)|^2}{P_{WW}(f)\ P_{BB}(f)}, \quad (5.1)$$

where: $P_{WB}(f)$ is the cross-spectrum between water level and barometric pressure and $P_{WW}(f)$ and $P_{BB}(f)$ are the auto-spectra for water level and barometric pressure signals respectively. More details on auto-spectral and cross-spectral density functions can be found in Chapter 6 (section 6.3.3).

The time series recording interval of 15 minutes theoretically allows exploration of the harmonic components in the signal up to a frequency of around 35 cycles/day (estimated at 75% of the Nyquist or maximum frequency of 48 cycles/day). The lowest frequency that can be detected is a function of the recorded time series length where the minimum frequency or the fundamental frequency = 1/ record time length. The range of recorded time series lengths is from 275.5 to 800.0 days (Table 5.2) which correspond to minimum frequency range from 0.0036 to 0.0013 cycles/day respectively. The Benningholme borehole record (800 days) is used in the following to illustrate the separation and identification of components in the water level signal. Figures 5.9 and 5.10 show the main components contributing to borehole water level signal at Benningholme and these components are discussed below in detail.

5.2.1. Barometric pressure component

Fluctuations in barometric pressure are; (a) aperiodic fluctuations due to movement of higher and lower pressure air masses (frequency band below 1 cycle/day) which include most of the power in the barometric pressure signal, and (b) periodic fluctuations caused by atmospheric tides driven mainly by thermal solar forces [*Maréchal et. al.*, 2002], see Figures 5.9a, 5.10a and c. The remaining frequencies in the barometric pressure spectrum have amplitudes that are below the resolution of barometric pressure transducer (0.09-0.25 cmH_2O). The atmospheric tides are primarily excited by the periodic daily heating of the atmosphere by the Sun. Atmospheric tides are thus generated at periods related to the solar day, comprising diurnal tides at 24 hour periods (S_1) and semi-diurnal tides at 12 hour periods (S_2) [*Chapman and Lindzen*, 1970], see section 2.5 in Chapter 2.

In this case study, the S_1 and S_2 components of atmospheric tides are observed at 1.00 and 2.00 cycles/day respectively, see Figures 5.9a, 5.10a, c and 5.11. As shown in Figure 5.11 the observed S_1 component varies in magnitude between locations. Significant amplitudes for S_1 are observed at Wilfholme and Park House Farm (located in the north of the study area) while no significant amplitude is observed at either Benningholme or Sunk Island (located in the south of the study area). It is also observed that at Wilfhome the S_1 component is the most significant compared with other locations. These variations can be attributed to the diurnal variations of air temperature and wind at ground level causing different magnitude oscillation in the barometric pressure signal at different locations [*Chapman and Lindzen*, 1970; *Dia and Wang*, 1999], see section 2.5 in Chapter 2.

Coherence is used to investigate barometric pressure variations across the study area and the required spacing of pressure transducers. Figure 5.12 shows the coherence between pairs of recorded barometric pressure signals at four boreholes Benningholme, Wilfholme, Sunk Island and Park House Farm. High smooth coherence is observed below ~ 0.9 cycles/day and increasingly noisy coherence is observed above this frequency, which in general can be attributed to lower energy in the barometric pressure signal at these higher frequencies. Variable coherence is observed at 1.0 cycle/day (S_1 component) which can be linked to variations in S_1 amplitude (Figure 5.11). The highest overall coherence (largely above 0.8) is observed between the closest pair of barometric pressure records from Benningholme and Wilfholme which are located 11.1 km apart. This suggests that pressure transducers spaced at around 12 km will provide an adequate coverage for barometric pressure. This is in good agreement with the recommendation by *Schlumberger Water Services* [2006] that a barometric pressure transducer is representative for an area within a radius of 15 km.

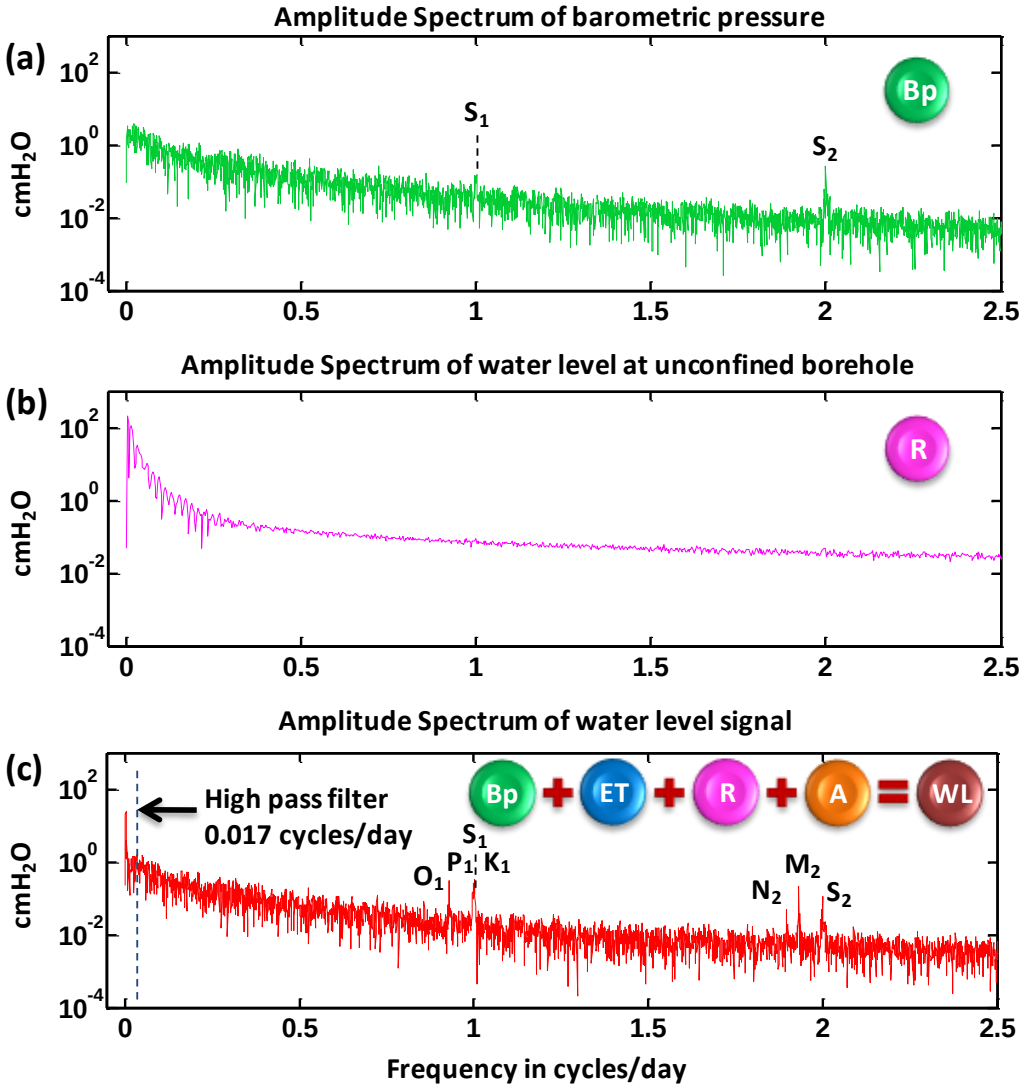

Figure 5.9. Example of water level signal frequency components (Benningholme borehole). a) Barometric pressure (B_p, green), b) recharge signal (R, magenta) from an unconfined borehole, c) resulting water level signal (WL, red), showing the frequency cut-off of high pass filter to remove recharge at below 0.017 cycles/day. At low frequencies the water level signal amplitude is about 3.5 times the barometric pressure signal amplitude due to recharge signal contributions. O_1, P_1, S_1 and K_1 are the diurnal and N_2, M_2 and S_2 are the semi-diurnal Earth tide components. A denotes anthropogenic effects.

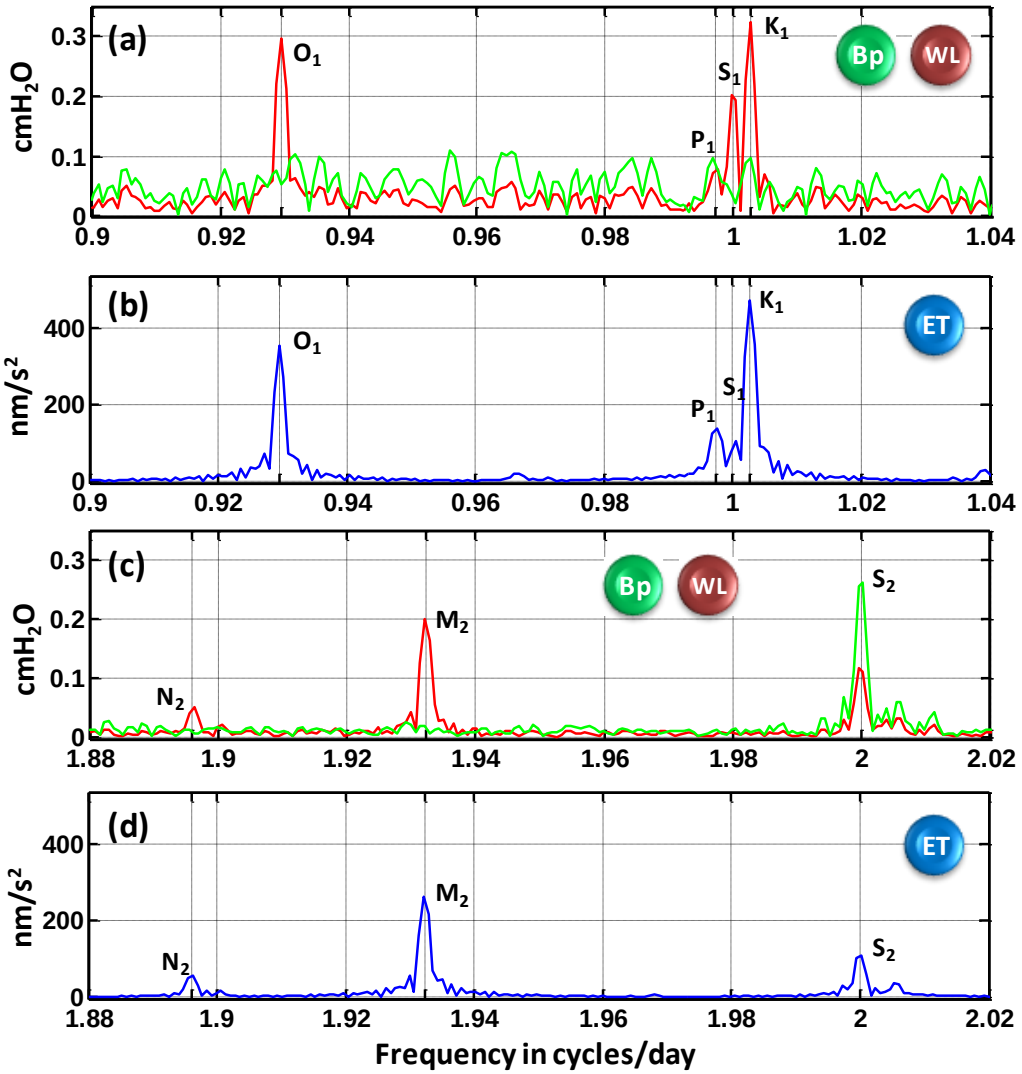

Figure 5.10. Details showing water level signal components at tidal frequencies (Benningholme borehole). a) and c) Barometric pressure (B_p, green) and water level (WL, red) at diurnal and semi-diurnal frequencies respectively. b) and d) show the theoretical Earth tides (ET, blue) calculated using *TSoft* at diurnal and semi-diurnal frequencies.

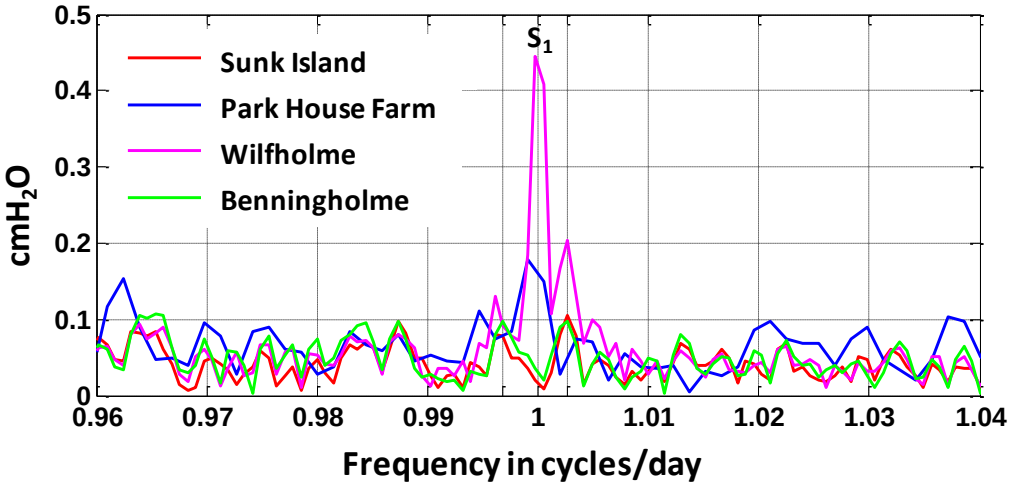

Figure 5.6. Comparison between amplitude spectra of barometric pressure at four boreholes locations (Benningholme, Wilfholme, Park House Farm and Sunk Island) at diurnal atmospheric tide (S_1). It is shown that a significant S_1 component is observed at only Wilfholme and Park House Farm locations.

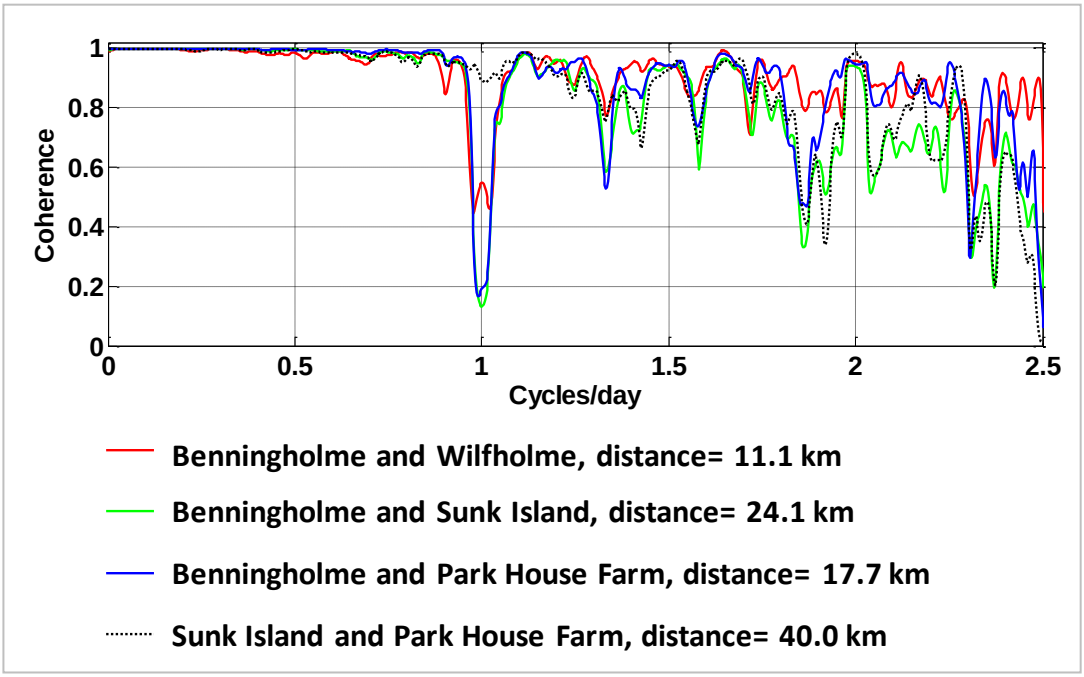

Figure 5.12. Coherence estimates between recorded barometric pressure signals recorded at four boreholes Benningholme, Wilfholme, Sunk Island and Park House Farm. It is shown that high coherence is observed between different barometric pressure records at all significant amplitudes except at frequency of 1.00 cycle/day (S1 component).

The coherence between the barometric pressure and water levels signals at the Benningholme borehole (Figure 5.13) is large and smooth over a wide frequency band (from ~0.03 to ~0.85 cycles/day). Due to the lack of energy above 0.85 cycles/day in both the water level and barometric pressure signals, noise becomes dominant and highly variable coherence is observed above 1 cycle/day.

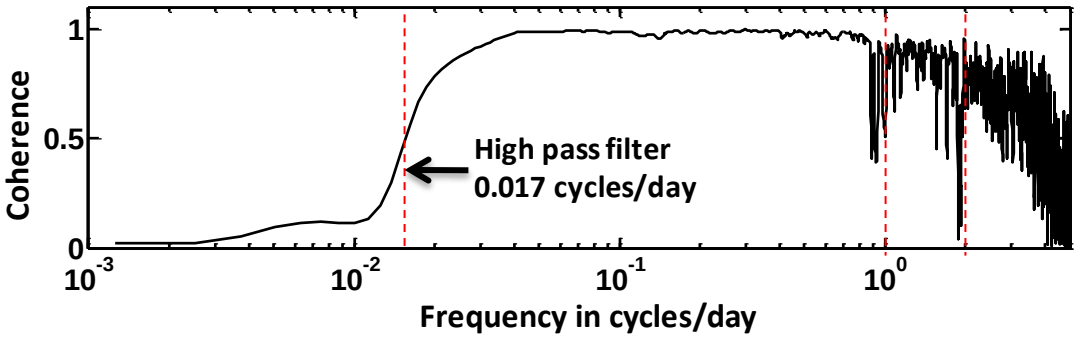

Figure 5.7. Example coherence between water level and barometric pressure raw signals at Benningholme borehole. The frequency cut-off of high pass filter to remove recharge at 0.017 cycles/day.

Comparing the amplitude spectra for barometric pressure and water levels signals (Figure 5.9a and 5.9c and Figure 5.10a and 5.10c), two main differences can be seen. The first difference is at low frequencies where the water level signal amplitude (maximum ~28.0 cmH_2O) is significantly higher than the barometric pressure signal amplitude (maximum ~3.3 cmH_2O). This is due to the contribution of the rainfall recharge which causes low coherence between water level and barometric pressure below 0.017 cycles/day. The second difference is at diurnal and semi-diurnal tidal frequencies O_1, P_1, S_1, N_2 and M_2 which is due to the Earth tide contribution, reflected by sudden drops in coherence at these frequencies (Figure 5.13).

5.2.2. Recharge component

The regional groundwater flow direction is towards the east to south-east as shown in Figure 5.1. The water level signals in unconfined boreholes located near the edge of the confining deposits are not significantly affected by either barometric pressure or Earth tides as would be anticipated for fully unconfined aquifers. Therefore, these signals can be assumed to represent the maximum recharge signal which contributes to

water level signals of boreholes in the confined aquifer. Time series data from seven unconfined boreholes (provided by EA, numbered from 11 to 17 in Figure 5.1), are used to characterize the recharge signal. Figure 5.14 shows water level data over one year for these seven boreholes and an example of the amplitude spectrum for the water level signal at the Gameslack borehole (number 15 in Figure 5.1) is shown in Figure 5.9b. The length of record used for FFT analysis at this borehole is 353 days with data at 15 minutes intervals. Figure 5.14 shows that recharge occurs dominantly in the winter months (November-March). Figure 5.15 shows that the recharge signal has high amplitude compared with water level and barometric pressure signals, up to about 0.1 cycles/day and Figure 5.9b shows that there is no significant response to either barometric pressure (at higher frequencies) or Earth tides at diurnal and semi-diurnal frequencies.

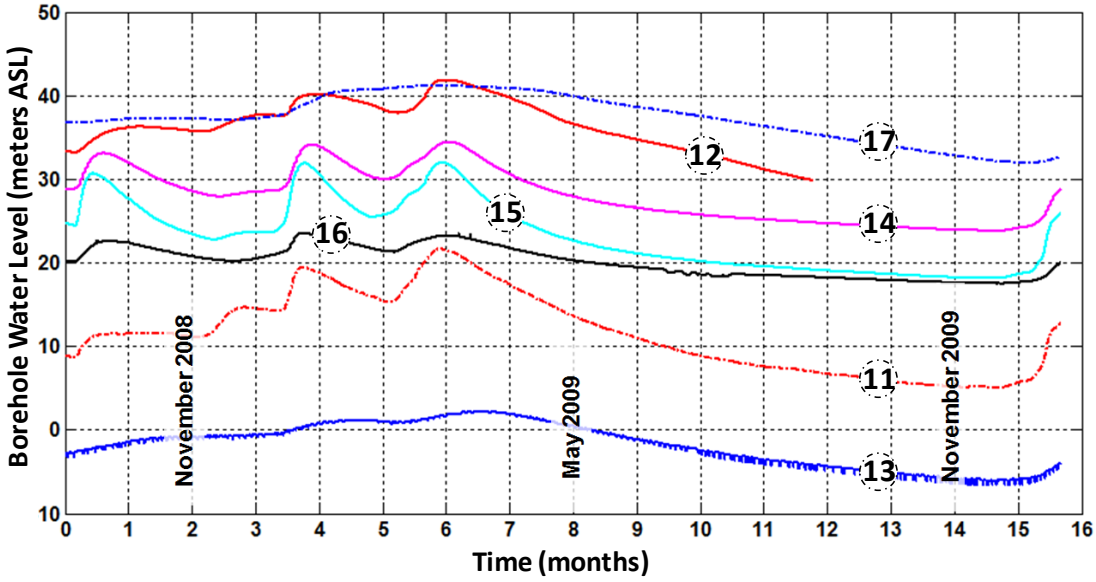

Figure 5.8. Water level data (provided by the EA) from seven unconfined boreholes representing the recharge signal. Circled numbers from 11 to 17 refers to locations shown in Figure 5.1. The recharge signals show similar trends with higher water levels during winter season.

Comparing the amplitude spectra for the recharge at Gameslack and the water levels signal at Benningholme at low frequencies (Figure 5.15) shows that the recharge signal amplitude is reduced by more than an order of magnitude at Benningholme, some 13 km from the edge of the confined aquifer. This indicates that the recharge signal

gradually looses energy as it migrates through the confined aquifer. In addition, Figure 5.15 shows that dissimilarity between water level and barometric pressure amplitude due to recharge contribution is observed up to the cut-off frequency of 0.017 cycles/day. It also shows that the earliest recharge signal peak which can be observed due to the limited record length (353 days) occurs at frequency of 0.0028 cycles/day, however it is observed at 0.0022 cycles/day in the water level signal at Benningholme (see Figure 5.17b).

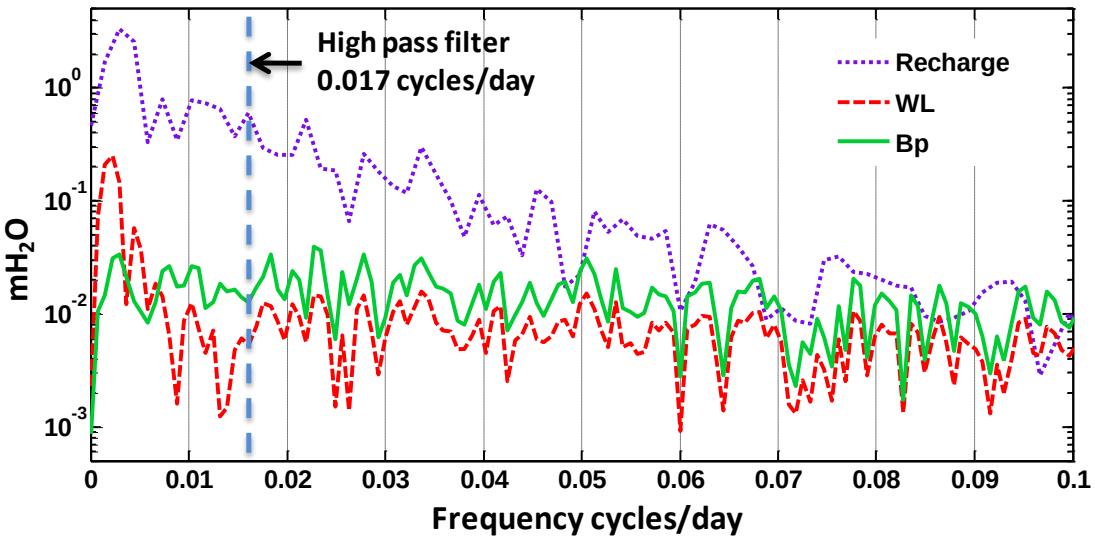

Figure 5.9. Comparison between amplitude spectra of water level (WL) and barometric pressure (B_p) signals recorded at Benningholme (confined aquifer) borehole and amplitude spectrum of the recharge signal recorded at Gameslack borehole (unconfined aquifer). The dissimilarity between water level and barometric pressure amplitude is observed up to the cut-off frequency of 0.017 cycles/day. It also shows that the recharge signal peak at a frequency of 0.0028 cycles/day.

5.2.3. Anthropogenic effects

The most significant anthropogenic effect on borehole water level signals is due to abstraction of groundwater for public and private water supplies. Only Wilfholme and Park House Farm boreholes were significantly impacted by pumping. For the three boreholes located at Wilfholme (M1, M2 and M3), water level time series show sharp

drawdown spikes in the range of 1-3 cm, and the water level spectral plot shows clear pumping effects in the frequency range 3.8 to 6 cycles/day (Figure 5.16). The pumped borehole is located some 100 m south east the site.

At the Park House Farm borehole, the local farmer is pumping from a borehole located some 100 m south. The time series of water level at this borehole shows clear pumping effects over wide range of frequencies with a drawdown range of 4-30 cm. A spectral plot of water level at this borehole shows no distinct pumping signal as at the Wilfholme borehole and pumping affects a wide range of frequencies causing the amplitude spectrum at this borehole to be noisy comparing with other boreholes (Figure 5.16).

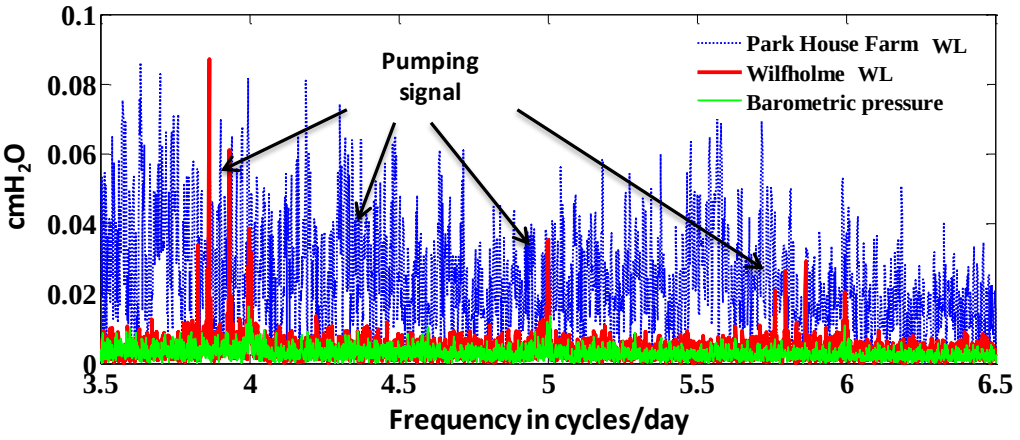

Figure 5.16. Amplitude spectra of water level (WL) and barometric pressure signals recorded at Wilfholme-M3 and at Park House Farm boreholes. Pumping effects at Wilfholme are in the frequency range 3.8 to 6 cycles/day, whereas, at Park House Farm pumping affects a wide range of frequencies.

5.2.4. Earth tide component

Earth tides are caused by the gravitational effects of the Moon and Sun on the Earth. Borehole water levels respond to Earth tides due to deformation of the aquifer matrix, see section 2.5 in Chapter 2. The more elastic the aquifer, the greater the deformation due to Earth tides and the greater the borehole water level response [*Inkenbrandt et al.*,

2005]. In addition the more confined the aquifer, the greater the response to Earth tides. However this response can be limited by the flow rate between the aquifer and the borehole where the aquifer is of low transmissivity and/or significant borehole storage/skin effects are present. The main Earth tide harmonic components are the five semi-diurnal/ diurnal periodic tidal frequencies O_1, K_1, N_2, M_2 and S_2 (Figure 5.10b and d), Table 5.3 after *Merritt* [2004] and *Roeloffs* [1996]. These five components represent 95% of the tidal potential [*Bredehoeft*, 1967] and can cause significant sinusoidal fluctuations in groundwater levels in confined/semi-confined aquifers [*Batu*, 1998]. In this study, two additional components P_1 and S_1 are seen to be significant in theoretical Earth tides (Figure 5.10b) and are observed in the water level signal (Figure 5.10a). Therefore these two components are included, giving a total of seven Earth tides components (see Table 5.3) considered for further analysis in section 5.3.3.

Table 5.3. Frequency and origin of observed Earth tides after *Merritt* [2004] and *Roeloffs* [1996].

Component	Frequency (cycles/day)	Origin
O_1	0.9295	Lunar diurnal
P_1	0.9973	Solar diurnal
S_1	1.0000	Solar diurnal
K_1	1.0027	Lunar-Solar diurnal
N_2	1.8959	Lunar semi-diurnal
M_2	1.9323	Lunar semi-diurnal
S_2	2.0000	Solar semi-diurnal

Figure 5.10b and d shows the spectra of the theoretical Earth tides in gravity units (nm/s^2) at the location of the Benningholme borehole, calculated using *TSoft* freeware [*Van Camp and Vauterin*, 2005]. To calculate these theoretical Earth tides, the tidal potential was first determined at each borehole location using *WPARICET* free software [*International Center for Earth Tides*, 2009] assuming a rigid Earth model [*Dehant et al.*, 1999]. This software uses latitude, longitude and ground elevation at the borehole location to determine the tidal potential which is then used as input to *TSoft* freeware to produce a theoretical time series of Earth tides in gravity units (nm/s^2). In this study, these theoretical Earth tides are compared with harmonic

components in the observed water level signals and with reconstructed Earth tide signals (see section 5.3.3).

Figure 5.10b and d shows that the theoretical Earth tides components at the Benningholme borehole location are O_1, P_1, S_1, K_1, N_2, M_2 and S_2, see Table 5.3. These tidal components are observed in the water level signal at Benningholme and do not correspond to barometric pressure except for the S_2 component, Figure 5.10. Therefore, at Benningholme both barometric pressure and Earth tides contribute to the water level signal at S_2.

5.3. Pre-processing the water level signal

In order to obtain the best possible estimation of the barometric response function, the effects of recharge, Earth tides, ocean tides and pumping are removed using the procedures described below. Before analysis, any gaps in the recorded time series of water levels are filled by linear interpolation. Corresponding periods in the barometric pressure time series are also similarly treated to minimize spectral damage as noted by *Beavan et al.* [1991]. Records gaps occurred only at Park House Farm and Routh Low Farm boreholes with gaps of 0.83 and 7.11 days respectively and are due to interference from slug tests (Chapter 9). Due to the lack of energy in the barometric pressure signal above the semi-diurnal S_2 component at 2 cycles/day, noise becomes dominant and highly variable coherence is observed between the water level and barometric pressure signals as shown in Figure 5.13. Therefore, a low pass Butterworth zero-phase filter with a cut-off frequency at 3 cycles/day is applied to both the water level and barometric pressure signals to remove high frequency noise.

5.3.1. Removal of recharge

Coherence (Equation 5.1) between water level and barometric pressure signals is used to determine a high pass filter cut-off to remove recharge. This cut-off is the frequency up to which the recharge signal contributes significantly to the water level signal. The cut-off is selected where coherence levels fall below 0.5, see Figure 5.13. These cut-offs ranges from 0.014 to 0.050 cycles/day, see Table 5.4.

Table 5.4. Approximate distance from the confined edge and cut-off frequency for recharge removal at each borehole.

Borehole		Distance from confined edge (Km)	Recharge high pass filter (cycles/day)
1	Benningholme	13.0	0.017
2	Wilfholme-M1	9.5	0.025
	Wilfholme-M2		
	Wilfholme-M3		
3	Sunk Island	30.0	0.014
4	Park House Farm	6.5	0.035
5	Routh Low Farm	15.2	0.035
6	Routh High Farm	13.0	0.035
7	Thornholme Moor	4.5	0.045
8	West Newton Farm	22.5	0.020
9	Woodhouse Farm	3.3	0.050
10	Bracy Bridge	0.9	0.050

In the *SC* code, high pass and low pass filters are applied using a combination of two Matlab functions '*butter*' and '*filtfilt*' [*MathWorks Inc.*, 2011]. The function '*butter*' is used to design a Butterworth filter by assigning a filter order and a cut-off frequency. Increasing the filter order increases the steepness and decreases the transition bandwidth of the applied filter. However, the larger the filter order, the more distortion it causes in the phase of the signal. The function '*filtfilt*' is used to apply this designed filter to the signal in forward and reverse directions (two pass filter) to correct for phase distortion introduced by a one pass filter. Figure 5.17a shows high pass Butterworth filters with filter order 4, 6 and 8 together with amplitude spectrum of water level at Benningholme borehole after applying these filters. As shown in Figure 5.17, increasing filter order above 6 does not substantially improve the steepness of the filter and the resultant water level spectra using filters with orders 6 and 8 is almost the same. For this reason, a filter order of 6 was chosen as a compromise between the steepness of the filter and phase distortion. Figure 5.17b compares raw water level signal at Benningholme with water level signal after the application of the high pass

filter with a cut-off frequency at 0.017 cycles/day, showing effective removal of the recharge signal.

In general, the cut-off frequency required to remove recharge decreases with the increasing distance between the borehole and the edge of the confined aquifer as shown in Figure 5.18 and Table 5.4. This decrease in cut-off frequency indicates that the higher frequencies of the recharge signal become progressively damped with distance. Thus the greater the distance from the edge of the confined aquifer, the lower the required cut-off to remove the recharge signal. Time series of the reconstructed recharge signals for all boreholes are shown in Figure 5.19 for the period September 2008 to September 2011. The seasonal recharge signal trend is observed with recharge occurring mainly during winter (November to March). The recharge signal amplitudes range from about 15 cm at Routh High Farm borehole to about 365 cm at Woodhouse Farm borehole. The largest amplitudes of reconstructed recharge signals are observed at Woodhouse Farm, Park House Farm, Thornholme Moor and Bracy Bridge boreholes (Figure 5.19) located the nearest to the confined edge and to zone of artesian flow, see Figure 5.1. The average amplitude for recharge signals at unconfined boreholes recorded near the confined edge (Figure 5.14) is about 5 m, while the average time series amplitude for reconstructed recharge signals at boreholes in the confined aquifer (Figure 5.19) is about 0.35 m. This confirms the earlier observation that a dampening occurs of an order of magnitude or more as the recharge signal migrates through the confined aquifer.

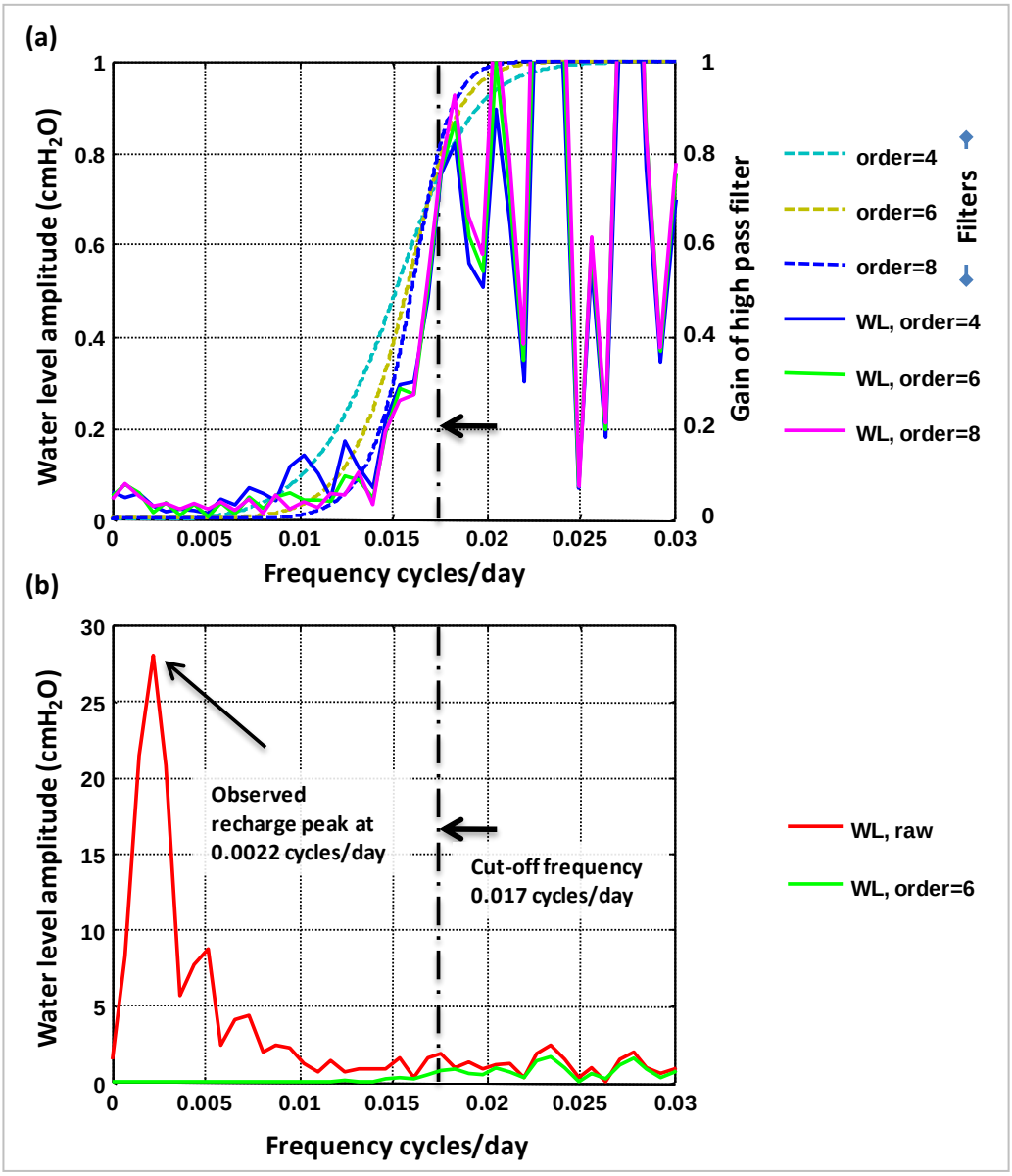

Figure 5.10. (a) Shows frequency response gain for a range of high pass Butterworth filters at the cut-off to remove recharge (0.017 cycles/day) with filter order 4, 6 and 8 with amplitude spectrum of water level (WL) at Benningholme borehole after applying these filters. (b) Comparison between water level signal before and after application of the high pass filter.

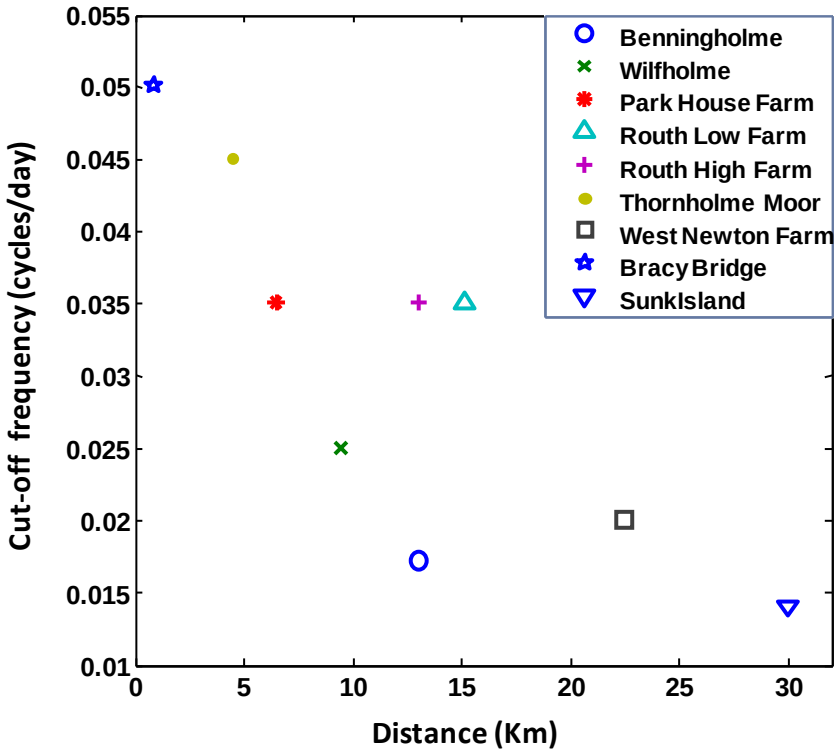

Figure 5.11. Cut-off frequency required to remove recharge decreases with the increasing distance between borehole and the confined edge of the aquifer.

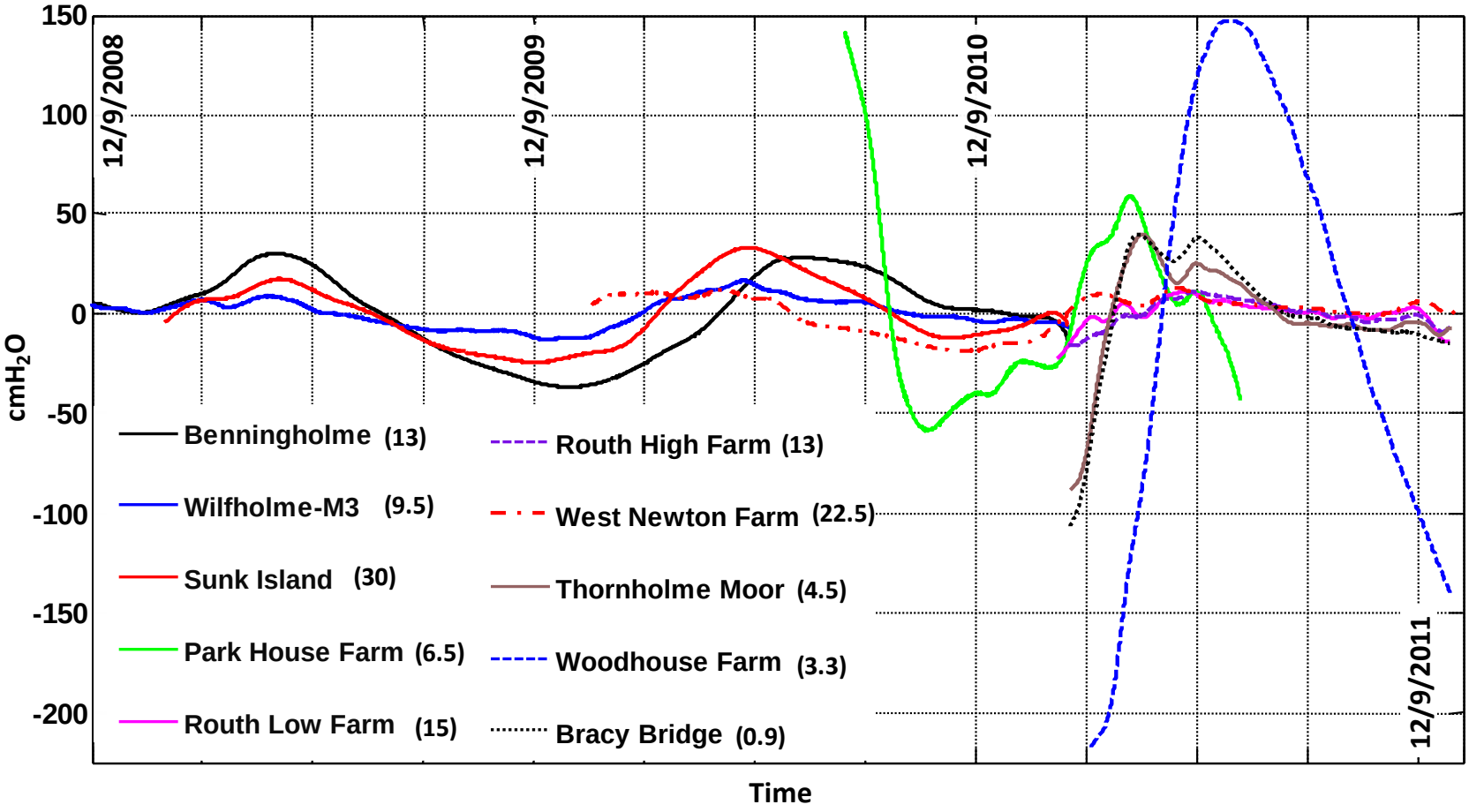

Figure 5.12. Time series of reconstructed recharge signals at all boreholes from September 2008 to September 2011. The seasonal recharge occurs during winter (November to March). Distance from each borehole to the confined edge is shown in km. The Recharge signals range from about 15 cm at Routh High Farm borehole to about 365 cm at Woodhouse Farm borehole.

5.3.2. Removal of anthropogenic effects

Effects of pumping are particularly clear at Wilfholme (M1, M2 and M3) and Park House Farm boreholes, Figure 5.16. The low pass Butterworth filter with a cut-off frequency at 3 cycles/day applied for removal of high frequency noise; also removes all pumping effects (which occur at a frequency range of 3.8-6.0 cycles/day) at Wilfholme boreholes. At Park House Farm borehole, the same filter only removes high frequencies of the pumping signal.

5.3.3. Removal of Earth and ocean tides

Earth and ocean tide components in the borehole water level signal are reconstructed and removed by applying a periodic time domain filter using the method of *Rasmussen and Mote* [2007], implemented in the *SC* code and explained below. The sum ($\xi(t)$) of the seven observed tidal frequencies (O_1, P_1, S_1, K_1, N_2, M_2, and S_2) in the water level signal (Table 5.3) is first calculated and then subtracted in the time domain from the water level signal. The summation formula shown in Equation 5.2 [*Rasmussen and Mote*, 2007, Equation 13] includes the Fourier trigonometric representation of a periodic sinusoidal wave $\left(a_j\, cos\, \omega_j t + b_j\, sin\, \omega_j t\right)$. Inputs are time, t, of each time step and the angular frequency, ω, of each tidal component from j=1 to 7. Equation 5.2 is solved for a_j and b_j unknown coefficients for each tidal component.

$$\xi(t) = \sum_{j=1}^{7} \left(a_j \cos \omega_j t + b_j\ \sin \omega_j t\right). \tag{5.2}$$

The change in borehole water level, ΔWL_{B_p}, due to change in barometric pressure is given by the convolution of the corresponding change in the barometric pressure, ΔB_p, with the impulse barometric response function, $\mu(\tau)$ [*Rasmussen and Mote*, 2007, Equation 11]:

$$\Delta WL_{B_p}(t) = \sum_{\tau=0}^{m} \mu(\tau)\ \Delta B_p(t-\tau)\,, \tag{5.3}$$

where: τ is the number of lags from 0 to *m*.

Therefore Equation 5.4 represents the change in borehole water level, ΔWL, due to both Earth tides and barometric pressure (Equations 5.2 and 5.3 respectively):

$$\Delta WL(t) = \sum_{\tau=0}^{m} \mu(\tau)\ \Delta B_p(t-\tau) + \sum_{j=1}^{7} \left(a_j \cos \omega_j t + b_j \sin \omega_j t\right). \qquad (5.4)$$

To calculate the sum, $\xi(t)$, Equations 5.4 is solved using the least squares regression approach shown in Equation 5.5a, where inputs for both Equations (5.2 and 5.3) are combined to form the coefficient matrix, $[\Delta B_p \vdots ET]$. The right hand side in Equation 5.5a is the solution vector which is composed of two concatenated vectors; the impulse barometric response function, $\mu(\tau)$, and coefficients for all tidal components, a_j and b_j. This separates the Earth tide contribution from the barometric pressure contribution in the borehole water level signal at diurnal and semi-diurnal frequencies.

$$[\Delta WL] = [\Delta B_p \vdots ET] \times \begin{bmatrix} \mu_0 \\ \vdots \\ \mu_m \\ a_1 \\ b_1 \\ \vdots \\ a_7 \\ b_7 \end{bmatrix}. \qquad (5.5a)$$

Equation 5.5b is simply Equation 5.5a written out in full matrix notation (after *Rasmussen and Mote,* 2007 and *Toll and Rasmussen*, 2007, Equation 4). In the *SC* code, Equation 5.5b is solved using the '*lscov*' Matlab function [*MathWorks Inc.*, 2011], from which standard errors (a_{j_err} and b_{j_err}) for calculated tidal coefficients are obtained. In addition, mean squared error (average sum of squares) value for solving Equation 5.5b, M_{SE}, is obtained. M_{SE} represents a single quantitative criterion of the error to achieve the best solution for Equation 5.5b.

$$\begin{bmatrix} \Delta WL_m \\ \Delta WL_{m+1} \\ \Delta WL_{m+2} \\ \vdots \\ \Delta WL_n \end{bmatrix} = \begin{bmatrix} \Delta Bp_m & \Delta Bp_{m-1} & \Delta Bp_{m-2} & \dots & \Delta Bp_1 & \vdots \\ \Delta Bp_{m+1} & \Delta Bp_m & \Delta Bp_{m-1} & \dots & \Delta Bp_2 & \vdots \\ \Delta Bp_{m+2} & \Delta Bp_{m+1} & \Delta Bp_m & \dots & \Delta Bp_3 & \vdots \\ \vdots & \vdots & \vdots & \vdots & \vdots & \vdots \\ \Delta Bp_n & \Delta Bp_{n-1} & \Delta Bp_{n-2} & \dots & \Delta Bp_{n-m+1} & \vdots \end{bmatrix}$$

$$\begin{bmatrix} \vdots & \cos\omega_1 t_m & \sin\omega_1 t_m & \dots & \cos\omega_7 t_m & \sin\omega_7 t_m \\ \vdots & \cos\omega_1 t_{m+1} & \sin\omega_1 t_{m+1} & \dots & \cos\omega_7 t_{m+1} & \sin\omega_7 t_{m+1} \\ \vdots & \cos\omega_1 t_{m+2} & \sin\omega_1 t_{m+2} & \dots & \cos\omega_7 t_{m+2} & \sin\omega_7 t_{m+2} \\ \vdots & \vdots & \vdots & & \vdots & \vdots \\ \vdots & \cos\omega_1 t_n & \sin\omega_1 t_n & \dots & \cos\omega_7 t_n & \sin\omega_7 t_n \end{bmatrix} \times \begin{bmatrix} \mu_0 \\ \mu_1 \\ \mu_2 \\ \vdots \\ \mu_m \\ \\ a_1 \\ b_1 \\ \vdots \\ a_7 \\ b_7 \end{bmatrix}, \quad (5.5b)$$

where: n is the total number of samples in the time series record.

The cumulative sum of the impulse barometric response function, $\mu(\tau)$, gives the step barometric response function ($R(\tau)$, Equation 5.6) which represents the time-domain barometric response function [after *Rasmussen and Mote*, 2007, Equation 12 and *Toll and Rasmussen*, 2007, Equation 3].

$$R(\tau) = \sum_{\tau=0}^{m} \mu(\tau)\,, \quad (5.6)$$

where: τ is the number of lags from 0 to *m*.

The number of lags, *m*, used in the analysis (Equation 5.5b) is 100, which with a data interval of 15 minutes is 25 hours. However, as shown in Figure 5.20, 50 lags (=12.5 hours) should be enough as the local maximum of the step barometric response function, $R(\tau)$, for all boreholes occurs in the range of 10-15 lags and that the step response more or less stabilizes above 50 lags, except at Park House Farm, which can be attributed to pumping effects. Thus above ~ 50 lags the impulse barometric response function ($\mu(\tau)$) is essentially zero and gives no contribution to the response.

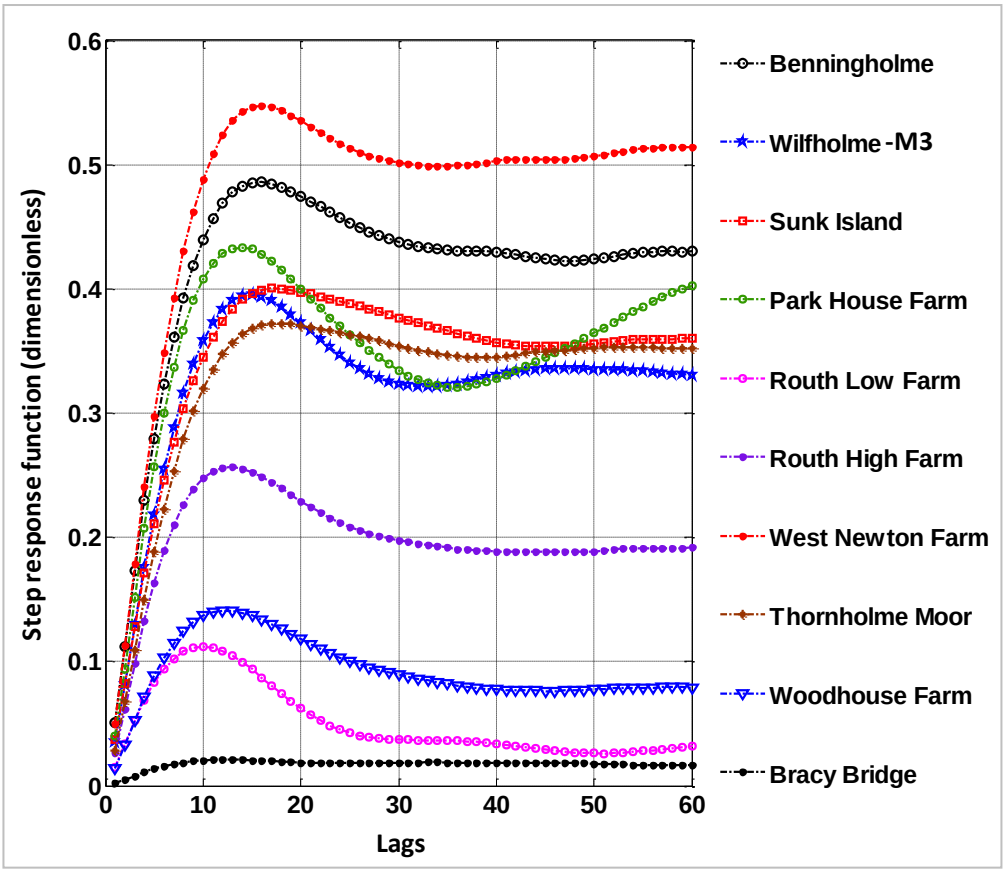

Figure 5.20. Shows the step barometric response function at all boreholes, 1 lag unit is 15 minutes. The local maximum for all boreholes occurs in the range of 10-15 lags and the step barometric response more or less stabilizes above 50 lags, except at Park House Farm.

Removing recharge before solving Equation 5.5b improves the solution accuracy, where the least squares mean squared error (M_{SE}) is reduced by about an order of magnitude. Further increase in accuracy is obtained if pumping effects are also removed, as explained in section (5.3.2), before removing Earth tides, if possible.

The Earth tide sum, $\xi(t)$, is then calculated using Equations 5.7 and 5.8. Inputs are the calculated tidal coefficients from Equation 5.5b and the right hand side (ET) of the combined matrix, $[\Delta B_p \vdots ET]$.

$$\begin{bmatrix} \Delta W_{ET}(m) \\ \Delta W_{ET}(m+1) \\ \Delta W_{ET}(m+2) \\ \vdots \\ \Delta W_{ET}(n) \end{bmatrix} = \begin{bmatrix} \cos\omega_1 t_m & \sin\omega_1 t_m & \dots & \cos\omega_7 t_m & \sin\omega_7 t_m \\ \cos\omega_1 t_{m+1} & \sin\omega_1 t_{m+1} & \dots & \cos\omega_7 t_{m+1} & \sin\omega_7 t_{m+1} \\ \cos\omega_1 t_{m+2} & \sin\omega_1 t_{m+2} & \dots & \cos\omega_7 t_{m+2} & \sin\omega_7 t_{m+2} \\ \vdots & \vdots & & \vdots & \vdots \\ \cos\omega_1 t_n & \sin\omega_1 t_n & \dots & \cos\omega_7 t_n & \sin\omega_7 t_n \end{bmatrix} \times \begin{bmatrix} a_1 \\ b_1 \\ \vdots \\ a_7 \\ b_7 \end{bmatrix}, \quad (5.7)$$

where: $\Delta W_{ET}(t)$ are the reconstructed unit Earth tide signals, and

$$\xi(t) = \sum_{t=m}^{n} \Delta W_{ET}(t) \ . \quad (5.8)$$

The reconstructed sum, $\xi(t)$, is then subtracted from the water level time series to remove the Earth and ocean tide contributions. The amplitude and phase of each tidal component can be calculated using Equations 5.9 and 5.10, where a_j and b_j are magnitude coefficients of each tidal component obtained from Equation 5.5b.

$$A\omega_j = \sqrt{(a_j)^2 + (b_j)^2} \ . \quad (5.9)$$

$$\theta\omega_j = \arctan\ (b_j/a_j) \ . \quad (5.10)$$

The standard error of amplitude for each tidal frequency, $A\omega_{i\_\mathrm{err}}$, is calculated using Equation 5.11.

$$A\omega_{j\_\mathrm{err}} = \sqrt{(a_{j\_\mathrm{err}})^2 + (b_{j\_\mathrm{err}})^2} \ , \quad (5.11)$$

where: a_{j_err} and b_{j_err} are the standard errors obtained from the '*lscov*' Matlab function [*MathWorks Inc.*, 2011] that is used to solve Equation 5.5b.

Figure 5.21 shows amplitude spectrum for water level signal before and after removing Earth tides and barometric pressure signal for the Benningholme borehole using the method described above. This shows that the O_1, P_1, S_1, K_1, N_2 and M_2 Earth tides components have been removed while the contribution of barometric pressure at S_2 component remains in the water level signal. Figure 5.22 shows the improvement in coherence at diurnal and semi-diurnal frequencies for the Benningholme borehole after Earth tides removal. Figure 5.23a and b shows an example of time series of the

calculated theoretical and reconstructed Earth tides for the Benningholme borehole. The similarity in the timing of spring and neap tides in both signals is clear.

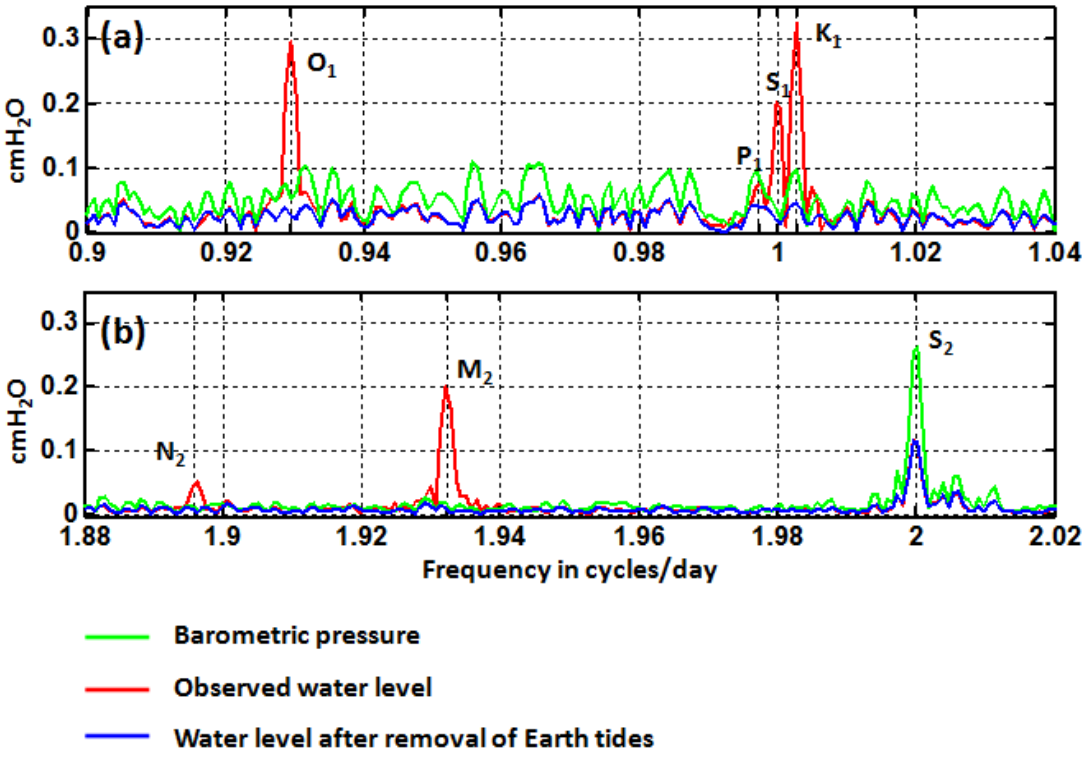

Figure 5.13. Comparison of amplitude spectra for barometric pressure, observed water level and water level before and after removal of Earth tides at the Benningholme borehole. O_1, P_1, S_1, K_1, N_2 and M_2 Earth tides components have been fully removed while S_2 atmospheric tides present in the barometric pressure signal remain in the water level signal.

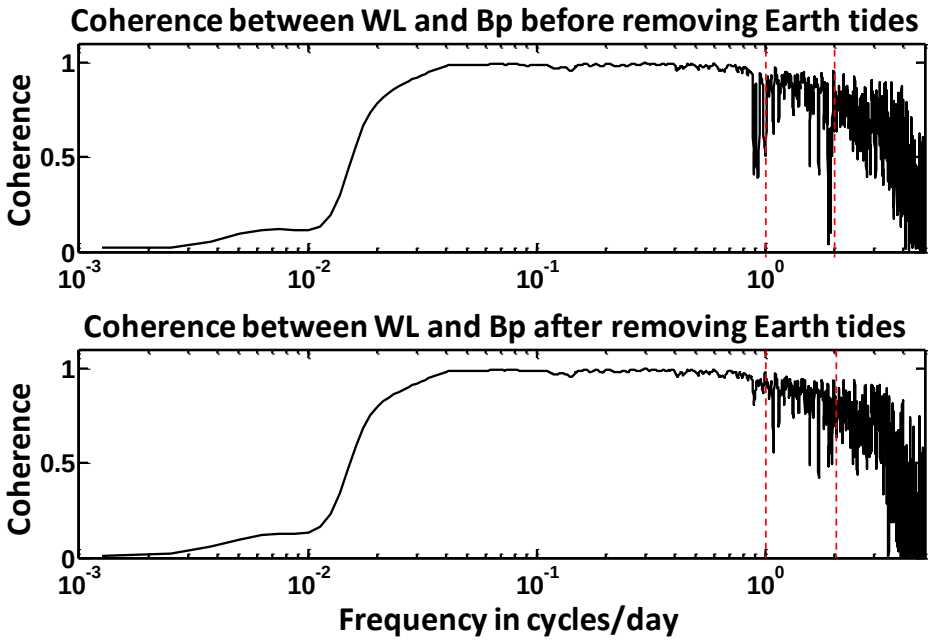

Figure 5.14. Coherence between water level and barometric pressure signals for the Benningholme borehole, showing a slight improvement in coherence after removal of Earth tides at 1 and 2 cycles/day.

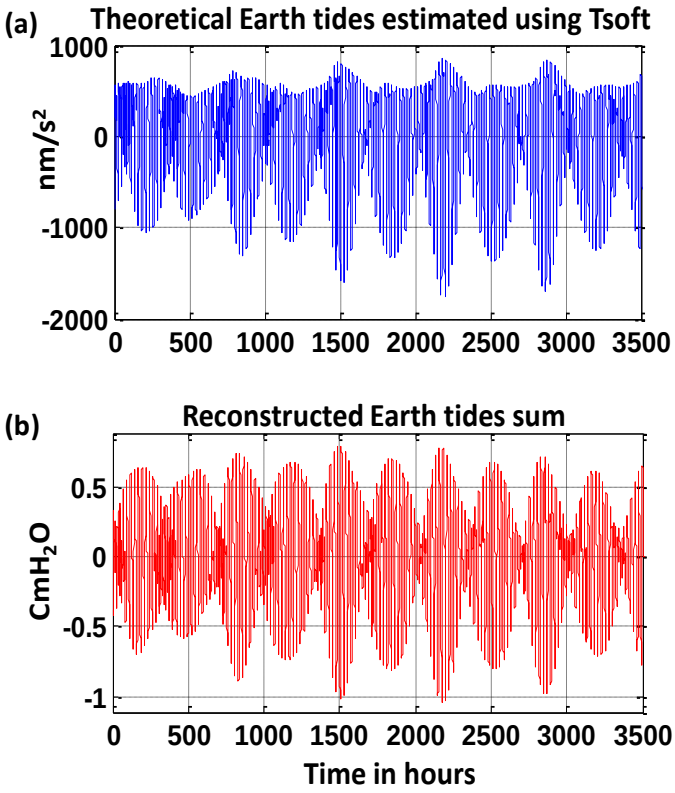

Figure 5.15. Earth tide analysis at the Benningholme borehole for an illustrative time series of 146 days length. a) Theoretical Earth tides time series calculated using *TSoft* [*Van Camp and Vauterin*, 2005]. b) Earth tides reconstructed from water level data.

Reconstructed amplitudes, $A\omega_j$, of the observed seven tidal components, calculated using Equation 5.9, are shown in Table 5.5 along with estimated standard error (expressed as a percentage) of amplitude for each tidal frequency, $A\omega_{j\_\mathrm{err}}$, calculated using Equation 5.11. Ranges of water level variations due to the sum of all Earth tides for all boreholes are shown in Table 5.6. These variations are calculated from the reconstructed time series of Earth tides, $\xi(t)$ (Equation 5.8), as averages of amplitudes of spring and neap tides. Table 5.6 shows that Earth tides induce water level variations ranging from 0.01 to 3.48 cm. Boreholes close to the sea may also show changes in water level due to ocean tides. The largest constituent of sea tides is the principal lunar semi-diurnal component, M_2, with a frequency of 1.9323 cycles/day, which coincides with the Earth tide component M_2 at the same frequency. For boreholes located close to the sea the reconstructed Earth tide sum ($\xi(t)$) also contains the ocean tide signal. This explains the large M_2 amplitude of 1.17 cm (Table 5.5) and the large water level variations between spring and neap tides (1.28 to 4.10 cm respectively, Table 5.6) at Sunk Island borehole, which is located at about 2 km from the sea. By contrast no significant trace of ocean tides is observed either at West Newton Farm (4.8 km from the sea) or Thornholme Moor (6 km from the sea).

A significant borehole water level response to Earth tides, specifically the O_1 and M_2 components, is a good indicator that the aquifer is confined [*Kümple*, 1997]. Low values for O_1 and M_2 components at Routh Low Farm, Routh High Farm, Woodhouse Farm and Bracy Bridge therefore suggest that these boreholes are less well confined than the other boreholes. However, borehole water level response to Earth tides can be damped due to the limited rate of flow between the borehole and the aquifer. The largest mean squared error, M_{SE}, (value of 0.02 cm^2) is seen at Park House Farm borehole. This is likely due to pumping effects which cannot be removed and cause noise in the water level signal.

Table 5.5. Results of Earth and ocean tides analysis for all boreholes. O_1, P_1, S_1, K_1, N_2, M_2, and S_2 are reconstructed amplitudes ± $A\omega_{j\_\mathrm{err}}$ %, which is the standard error (Equation 5.11) percentage of each reconstructed tidal component. M_{SE} is the least squares mean-squared-error. M_2 component includes the ocean tide signal.

Borehole		O_1 amplitude cmH_2O (0.9295 cycles/day)	P_1 amplitude cmH_2O (0.9973 cycles/day)	S_1 amplitude cmH_2O (1.0000 cycles/day)	K_1 amplitude cmH_2O (1.0027 cycles/day)	N_2 amplitude cmH_2O (1.8959 cycles/day)	M_2 amplitude cmH_2O (1.9323 cycles/day)	S_2 amplitude cmH_2O (2.0000 cycles/day)	M_{SE} cm^2
1	Benningholme	0.29 ± 1.1	0.14 ± 1.8	0.16 ± 1.9	0.32 ± 0.7	0.06 ± 2.8	0.21 ± 0.6	0.03 ± 3.0	0.0005
2	Wilfholme-M1	0.23 ± 3.6	0.17 ± 5.0	0.62 ± 1.6	0.11 ± 7.8	0.10 ± 4.5	0.40 ± 1.0	0.14 ± 4.5	0.002
	Wilfholme-M2	0.22 ± 4.0	0.19 ± 5.0	0.61 ± 1.7	0.10 ± 9.5	0.08 ± 5.1	0.36 ± 1.2	0.14 ± 4.9	0.002
	Wilfholme-M3	0.26 ± 1.9	0.06 ± 9.1	0.87 ± 0.6	0.28 ± 1.7	0.10 ± 2.5	0.40 ± 0.6	0.10 ± 4.0	0.002
3	Sunk Island	0.20 ± 1.5	0.09 ± 3.4	0.01 ± 20.6	0.23 ± 1.3	0.21 ± 0.7	1.17 ± 0.1	0.46 ± 0.5	0.0005
4	Park House Farm	0.21 ± 12.2	0.12 ± 20.8	0.49 ± 50.0	0.09 ± 28.6	0.06 ± 20.3	0.10 ± 12.4	0.24 ± 8.7	0.02
5	Routh Low Farm	0.01 ± 50.3	0.18 ± 5.1	0.62 ± 1.9	0.26 ± 3.6	0.01 ± 24.5	0.03 ± 10.1	0.12 ± 4.2	0.0005
6	Routh High Farm	0.06 ± 9.3	0.04 ± 13.3	0.16 ± 3.2	0.06 ± 8.2	0.002 ± 30.0	0.02 ± 12.8	0.11 ± 3.7	0.0007
7	Thornholme Moor	0.22 ± 1.5	0.09 ± 3.8	0.03 ± 11.9	0.25 ± 1.3	0.05 ± 3.5	0.20 ± 0.8	0.06 ± 4.4	0.0003
8	West Newton Farm	0.20 ± 4.1	0.14 ± 5.5	0.07 ± 11.4	0.19 ± 4.0	0.05 ± 8.9	0.12 + 3.6	0.14 ± 4.1	0.004
9	Woodhouse Farm	0.04 ± 22.2	0.1 ± 7.7	0.19 ± 4.3	0.06 ± 13.0	0.01 ± 44.7	0.01 ± 26.9	0.08 ± 7.1	0.0008
10	Bracy Bridge	0.01 ± 23.3	0.03 ± 7.4	0.06 ± 3.1	0.02 ± 8.5	0.01 ± 9.0	0.01 ± 16.3	0.01 ± 11.6	0.0002

Table 5.6. Observed ranges of water level variations due to Earth and ocean tides at all boreholes.

Borehole		Spring tides amplitude range (cm)	Neap tides amplitude range (cm)
1	Benningholme	1.00 – 2.08	0.15 – 0.56
2	Wilfholme-M1	1.73 – 2.48	1.20 -1.30
	Wilfholme-M2	1.65 – 2.30	1.17 – 1.68
	Wilfholme-M3	2.04 – 3.48	1.05 – 2.30
3	Sunk Island	3.10 – 4.10	1.28 – 2.11
4	Park House Farm	1.00 – 1.63	0.20 – 0.59
5	Routh Low Farm	0.50 – 0.60	0.35 – 0.40
6	Routh High Farm	0.27 – 0.66	0.19 – 0.21
7	Thornholme Moor	0.84 – 1.46	0.33 – 0.57
8	West Newton Farm	0.50 – 1.50	0.06 – 0.67
9	Woodhouse Farm	0.30 – 0.70	0.20 – 0.60
10	Bracy Bridge	0.11 – 0.13	0.01 – 0.07

Figure 5.24 shows illustrative water level signals at the Benningholme, Sunk Island, Wilfholme-M3 and Park House Farm boreholes before and after recharge, high frequency noise and Earth and ocean tide removal. This shows that removing recharge and high frequency noise smoothes the signal and that Earth tides removal has a significant effect. The final corrected signal shows the characteristic inverse relationship between barometric pressure and water level signals. Figure 5.24b shows the removal of ocean tides at Sunk Island borehole.

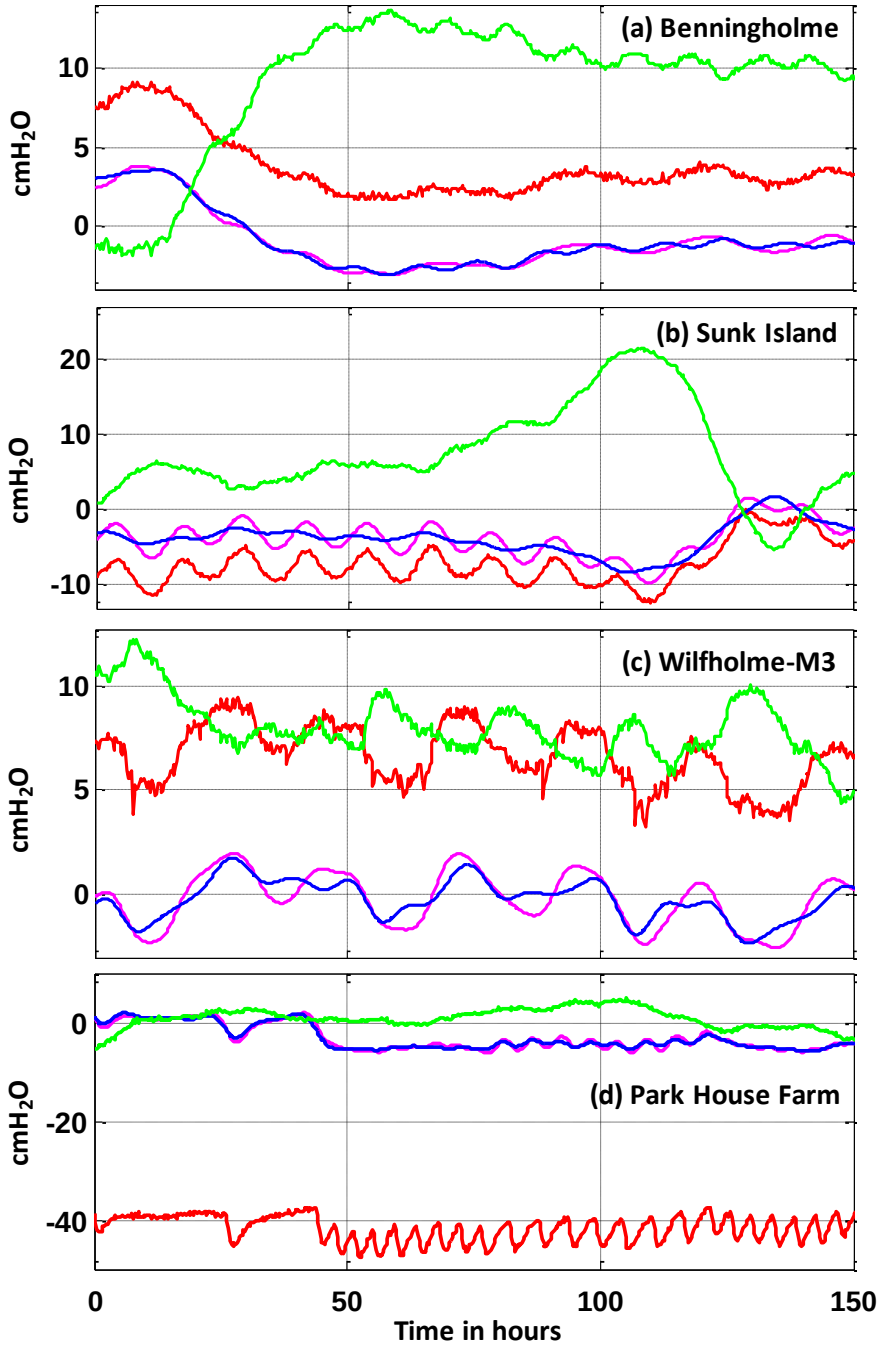

Figure 5.16. Illustrative segments of the time series for barometric pressure (green) and water level at different pre-processing stages for four boreholes; a) Benningholme, b) Sunk Island, c) Wilfholme-M3 and d) Park House Farm. Original water level input signal (red), after removing recharge, pumping and high frequency noise (magenta) and after removing Earth tides and ocean tides (blue). Figure 5.24c also illustrates removal of the pumping signal at Wilfholme-M3 and Figure 5.24d shows the removal of high frequency pumping signal at Park House Farm. The final corrected signals (blue) are smooth and show the characteristic inverse relationship with barometric pressure indicating confined to semi-confined behaviour.

5.4. Summary:

Time series data for borehole water levels and barometric pressure were collected using automatic pressure transducers from 12 boreholes located in the East Yorkshire Chalk Aquifer, UK. The main contributions to the borehole water level signals are barometric pressure, Earth and ocean tides, recharge and anthropogenic effects (pumping). Using the *SC* code developed in this work, the different influences on the water level time series were analyzed. The *SC* code was then used to remove the influences of recharge, Earth and ocean tides and pumping to isolate the influence of barometric pressure. This is a pre-processing step that is necessary prior to estimating barometric response functions. Barometric pressure is a major source of borehole water level fluctuations and contributes to the water level signal over most of the observed frequency band. The recharge signal contributes to the water level signal at low frequency up to ~0.05 cycles/day. Time series data of water levels from seven unconfined boreholes located along the edge of the confining unit were used to characterize the recharge signal. Coherence between water level and barometric pressure was used to determine a high pass filter cut-off frequency to remove the influence of recharge. A low pass filter is applied to remove low energy noise at high frequency and some pumping effects. Both atmospheric tides, present in the barometric pressure signal, and Earth tides contribute to the water level signals at S_1 and S_2 frequencies where the energy of barometric pressure signal is significant. This highlights the importance of separating the atmospheric tides and Earth tide effects at these frequencies in order to extend the frequency range of barometric response function. A periodic time domain filter [*Rasmussen and Mote,* 2007] has been used to reconstruct Earth and ocean tide contributions to the borehole water level signal. The reconstructed signal is then subtracted from the water level signal to remove tidal effects. The final filtered water level signals show the characteristic inverse relationship with barometric pressure. These filtered signals are used in Chapter 6 for determination of barometric response functions.

CHAPTER 6: ESTIMATION OF THE BAROMETRIC EFFICIENCY AND THE BAROMETRIC RESPONSE FUNCTION

6.1. Introduction

This chapter describes methods used in this study to estimate the static barometric efficiency and barometric response function. The least-squares regression method described by *Rasmussen and Crawford* [1997] was implemented using the *BE* Matlab code (see Appendix C) to compute the long and short-term barometric efficiencies. These were used in this study to diagnose the aquifer degree of confinement and the presence of borehole storage/skin effects in the vicinity of each borehole. The long and short-term barometric efficiencies are simple to compute and represent the borehole water level response to slow and rapid variations in barometric pressure respectively. However, the barometric response function represents the borehole water level response to the full range of frequencies in the barometric pressure signal but requires the use of the deconvolution technique to be computed. Filtered water levels and barometric pressure signals (see Chapter 5 for pre-processing steps) were used to estimate the barometric response functions using the "cross-spectral deconvolution by ensemble averaging" technique after *Welch* [1967] and *Beavans et al.* [1991]. In this study, the *RF* Matlab code (see Appendix D) was developed to combine and implement these techniques.

6.2. Estimation of static barometric efficiency

Static barometric efficiency is defined as the ratio of water level change to corresponding barometric pressure change, in boreholes tapping purely confined aquifers [*Jacob*, 1940]. *Rasmussen and Crawford* [1997] describes how to use barometric efficiency to diagnose the degree of confinement of the aquifer and borehole storage/skin effects. Their approach is based on a comparison between the long-term ($\propto_L$) and short-term ($\propto_S$) barometric efficiencies, given by Equations 6.1 and 6.2:

$$\Delta WL = -\propto_L \ \Delta B_p \ , \tag{6.1}$$

$$\Delta WL = -\propto_S \ \Delta B_p \ , \tag{6.2}$$

where: ΔWL and ΔB_p are the changes in water level and barometric pressure respectively, for a given time interval Δt.

The long-term barometric efficiency ($\propto_L$) is dominated by borehole water level fluctuations in response to low frequency changes in barometric pressure, and the short term barometric efficiency ($\propto_S$) is dominated by the borehole water level response to the rapid high frequency barometric pressure fluctuations. However estimates for short and long-term efficiencies from Equations 6.1 and 6.2 can be significantly in error if borehole water levels are also fluctuating in response to stresses other than barometric pressure, such as pumping, recharge and Earth tides.

Rasmussen and Crawford [1997] describe the relationship between $\propto_L$ and $\propto_S$:

- Where there are negligible borehole storage or skin effects, $\propto_L$ should equal $\propto_S$ in purely confined aquifers, i.e. barometric efficiency is constant and is independent of barometric pressure frequency.
- Where there are negligible borehole storage or skin effects in semi-confined aquifers, $\propto_L$ should be smaller than $\propto_S$. This is because long-term pressure changes have time to dissipate through the borehole-aquifer system, compared to short-term changes.
- Where there are significant borehole storage or skin effects, $\propto_L$ should be larger than $\propto_S$. This occurs when flow exchange between the aquifer and the borehole is restricted, and does not allow water level to respond to high frequency (rapid) changes in barometric pressure.

Here both unfiltered (raw) and filtered water level signals (i.e. with recharge, pumping effects, Earth and ocean tides and high frequency noise removed, see Chapter 5) were used to estimate $\propto_L$ and $\propto_S$. The *BE* Matlab code (Appendix C) was developed to do this and the *SC* Matlab code (Appendix B) was developed to filter water level records

as detailed in Chapter 5. In the *BE* code, $\propto_L$ and $\propto_S$ (Equations 6.1 and 6.2) were determined using the '*robustfit*' Matlab function, which uses an iteratively reweighted linear least squares approach to obtain a regression coefficient that is less influenced by outliers than an ordinary linear-least-squares fit [*MathWorks Inc.*, 2011].

Figure 6.1 shows an illustrative example from the Benningholme borehole where long-term and short-term barometric efficiencies are calculated for both unfiltered and filtered water level and barometric pressure signals (at 15 minutes interval) using the *BE* Matlab code. This shows that the correlation between water level and barometric pressure and thus the estimate of barometric efficiency is greatly improved after removal of recharge, Earth tides and high frequency noise. The filtered signals show a trend that can be seen in the unfiltered signals but which regression does not identify, see Figure 6.1. At Benningholme borehole the estimated long term barometric efficiencies, $\propto_L$, for unfiltered and filtered signals are 22.2% ± 3.4% and 47.4% ± 0.1% respectively, and the estimated short term barometric efficiencies, $\propto_S$, for unfiltered and filtered signals are 71.8% ± 0.5% and 47.9% ± 0.1% respectively. Thus the presence of influences other than barometric pressure in the unfiltered signals causes $\propto_L$ to be lower and $\propto_S$ to be higher in this case.

Table 6.1 lists calculated $\propto_L$ and $\propto_S$ for all boreholes. Estimates of $\propto_L$ and $\propto_S$ for filtered signals ranges from 1.8% to 47.4% and from 2.2% to 47.9% respectively (see Table 6.1). Results show that not filtering the signals leads to significant underestimation of $\propto_L$ (up to a maximum of 25% at Benningholme) and significant overestimation of $\propto_S$ (up to a maximum of 66% at Woodhouse Farm). Thus, estimating barometric efficiency using the unfiltered signals can lead to significant error. It is also shown that $\propto_S$ is larger than $\propto_L$ for most boreholes, implying that they show a semi-confined response to barometric pressure changes. At Routh Low Farm and Routh High Farm, $\propto_S$ is less than $\propto_L$ indicating significant borehole storage or skin effects. At Park House Farm $\propto_S$ and $\propto_L$ are statistically identical inferring that this borehole shows more or less purely confined behaviour. However, the water level signal at this borehole shows interference from nearby pumping which cannot be removed by simple filtering (see Chapter 5). This is likely to introduce significant bias in $\propto_S$ and $\propto_L$, as reflected in the high standard error (0.5% for $\propto_L$ and 0.8% for $\propto_S$)

and low R^2 values (0.57 for $\propto_L$ and 0.17 for $\propto_S$) compared to other boreholes. Benningholme and Sunk Island boreholes show the least difference between $\propto_S$ and $\propto_L$ implying that these boreholes show high degrees of confinement. The glacial sediments cover at the Benningholme borehole is 16.2 m thick and is composed of clay-rich materials, whereas at the Sunk Island borehole the glacial sediments cover is composed of sand, gravel and clay with a thickness (34.2 m) twice that at Benningholme consistent with a high degree of confinement. Low values for both $\propto_S$ and $\propto_L$ at Woodhouse Farm and Bracy Bridge boreholes infer that the aquifer at these boreholes is the least confined. These two boreholes are nearest to the confined edge, 3.3 km and 0.9 km respectively, with a thin cover of glacial sediments, 4.4 m and 9.5 m respectively, which include sand and chalk gravel (Figure 5.4), consistent with a low degree of confinement.

6.3. Estimation of the barometric response function

6.3.1. Introduction

In purely confined aquifers, a constant barometric efficiency adequately characterizes the borehole water level response to barometric pressure fluctuations. However, in the semi-confined cases, where the confining layer has non-zero hydraulic conductivity, a change in the aquifer pore pressure in response to changing barometric pressure will slowly depressurize by groundwater flow to or from the water table. In this case, the response, and thus barometric efficiency, depends on the frequency of the barometric pressure signal. Under these conditions, a barometric response function is required to represent the borehole-aquifer system response to the full range of frequencies in the barometric pressure signal.

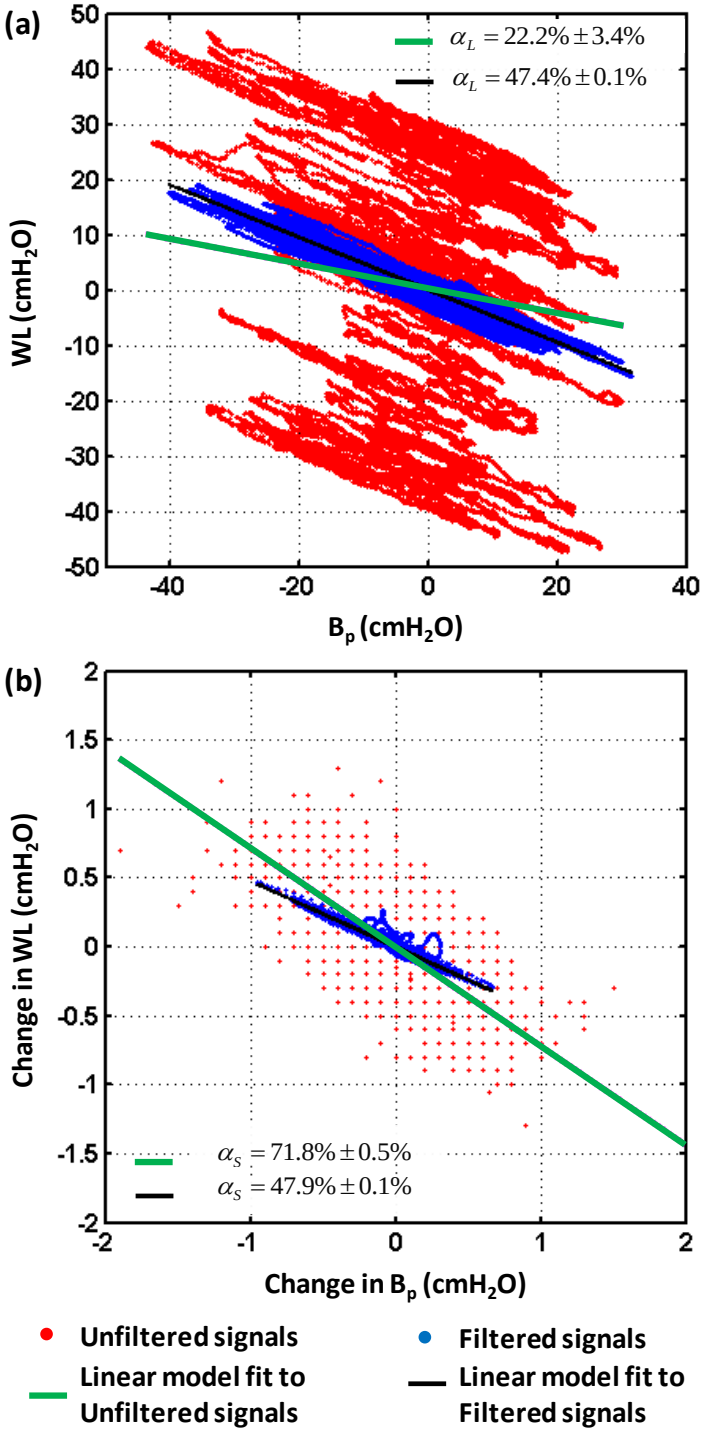

Figure 6.1. Estimation of $\propto_L$ and $\propto_S$ from water level (WL) and barometric pressure (B_p) signals at the Benningholme borehole using 15 minute intervals, for a) long-term barometric efficiency and b) short-term barometric efficiency. Points in (b) lie on a discrete grid due to the precision of data recorded by pressure transducer. The barometric efficiency is given by the slopes of the plots in a) and b). It is evident that the correlation between water level and barometric pressure, and therefore accuracy of the estimated barometric efficiency, is greatly improved after removing recharge, Earth tides and high frequency noise.

Table 6.1. Long-term ($\propto_L$) and short-term ($\propto_S$) barometric efficiencies for all boreholes. SE is the standard error. ---- indicates negative values of barometric efficiency due to influences in the water level signal other than barometric pressure, such as recharge and Earth tides.

Borehole			Barometric efficiency for unfiltered water level and barometric signals				Barometric efficiency for filtered water level and barometric signals			
			$\propto_L$ % ± SE %	R^2	$\propto_S$ % ± SE %	R^2	$\propto_L$ % ± SE %	R^2	$\propto_S$ % ± SE %	R^2
1	Benningholme		22.2 ± 3.4	0.02	71.8 ± 0.5	0.43	47.4 ± 0.1	0.95	47.9 ± 0.1	0.95
2	Wilfholme	M1	17.9 ± 1.4	0.18	77.1 ± 0.7	0.23	33.2 ± 0.6	0.64	38.9 ± 0.4	0.62
		M2	17.5 ± 1.4	0.17	80.7 ± 0.6	0.25	32.6 ± 0.4	0.60	38.4 ± 0.5	0.56
		M3	20.8 ± 1.1	0.11	76.5 ± 0.5	0.26	28.9 ± 0.2	0.71	37.7 ± 0.3	0.62
3	Sunk Island		30.5 ± 1.8	0.05	68.2 ± 0.6	0.30	37.9 ± 0.1	0.88	39.1 ± 0.1	0.89
4	Park House Farm		----	----	74.5 ± 1.1	0.12	41.9 ± 0.5	0.57	41.8 ± 0.8	0.17
5	Routh Low Farm		11.5 ± 3.6	0.04	68.7 ± 2.1	0.29	17.4 ± 1.0	0.28	7.6 ± 1.9	0.52
6	Routh High Farm		11.7 ± 3.5	0.03	77.2 ± 0.8	0.35	32.2 ± 0.2	0.88	27.6 ± 0.4	0.57
7	Thornholme Moor		----	----	77.0 ± 1.0	0.27	29.7 ± 0.3	0.81	37.2 ± 0.2	0.90
8	West Newton Farm		42.8 ± 0.8	0.20	85.8 ± 0.5	0.34	38.3 ± 0.1	0.59	45.4 ± 0.1	0.56
9	Woodhouse Farm		----	----	79.5 ± 0.8	0.38	9.7 ± 0.9	0.16	13.5 ± 0.9	0.18
10	Bracy Bridge		----	----	65.8 ± 1.3	0.16	1.8 ± 1.3	0.12	2.2 ± 2.3	0.06

The general approach for estimating the barometric response function of a borehole-aquifer system is to deconvolve the barometric pressure signal from the water level signal. As shown in Figure 6.2a, multiple inputs including barometric pressure, Earth tides, recharge and anthropogenic effects are convolved with the response of borehole-aquifer system to give the single output water level signal. In other words, the inputs are merged together in the combined response provided by the borehole-aquifer system to give the output signal [*Press et al.,* 2007]. In this study and as described in Chapter 5, the observed water level signal is first filtered to achieve a single-input/single-output system so that as far as possible, barometric pressure is the only influence on the water level signal, see Figure 6.2b. In this case the response function is assumed to represent the borehole-aquifer system response only to the input barometric pressure signal, and is named as the barometric response function (BRF).

Deconvolution can be applied in either the time domain [*Rasmussen and Crawford,* 1997; *Butler et al.,* 2011] or in the frequency domain [*Rojstaczer,* 1988a; *Galloway and Rojstaczer,* 1988; *Rojstaczer and Riley,* 1990; *Ritizi et al.,* 1991; *Quilty and Roeloffs,* 1991; *Beavans et al.,* 1991]. However, the time domain calculations are not straightforward analytically [*Furbish,* 1991]. In addition, the time domain deconvolution is computationally expensive compared to frequency domain deconvolution. In the time domain, the actual response to barometric pressure and other influences occur at each time step, while in the frequency domain influences can occur at frequencies far from the frequencies of interest and can be easily removed.

In this study, to estimate the barometric response function the *RF* Matlab code (see Appendix D) has been developed to implement the cross-spectral deconvolution by ensemble averaging method [*Welch,* 1967], see section 6.3.3. In this code Welch's method was combined with an overlapping frequency band technique described by *Beavan et al.* [1991], see section 6.3.4. These techniques were applied incorporating recommendations on overlap and filtering given by *Bendat and Piersol* [2010] and *Press et al.* [2007]. A similar procedure to that used by *Rojstaczer and Riley* [1990] was implemented to select the viable frequency range of estimated barometric response functions.

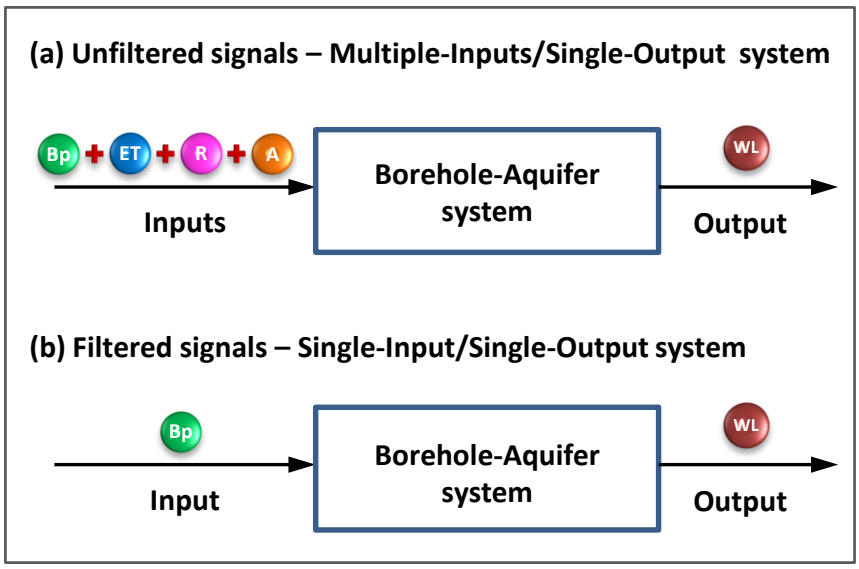

Figure 6.2. Schematic diagram for borehole-aquifer system response. (a) Multiple-Inputs/Single-Output system. Inputs are barometric pressure (B_p), Earth tides (ET), recharge (R) and anthropogenic effects (A) and the output is the water level signal (WL). (b) Single-Input/Single-Output system, the single input is barometric pressure (B_p) and the output is the water level signal (WL).

6.3.2. Ordinary frequency deconvolution

The frequency domain deconvolution is equivalent to division of the Discrete Fourier Transforms, DFTs, of the time series data (Equation 6.3):

$$BRF(f) = WL(f)/B_p(f)\ , \tag{6.3}$$

where: $BRF(f)$ is the barometric response function, and $WL(f)$ and $B_p(f)$ are the DFTs of the water level and the barometric pressure time series.

The barometric response function ($BRF(f)$) estimated by Equation 6.3 is a complex number which can be expressed as a gain or admittance component, $A^{BRF}(f)$, and a phase component, $\theta^{BRF}(f)$, which are given by the modulus and the argument of $BRF(f)$ respectively (Equations 6.4 and 6.5):

$$A^{BRF}(f) = |BRF(f)|, \tag{6.4}$$

and,

$$\theta^{BRF}(f) = \arctan(\text{Im}\, BRF(f)/\text{Re}\, BRF(f)). \quad (6.5)$$

The drawback of Equation 6.3 is that it becomes unstable at frequencies where $B_p(f)$ is very small or zero, leading to artificial magnification of the $BRF(f)$ at these frequencies. Figure 6.3 shows an example for the $BRF(f)$ estimate at the Benningholme borehole using Equations 6.3, 6.4 and 6.5. Amplitude spectra for the barometric pressure and water level at Benningholme borehole are shown in Figures 5.9 and 5.10 and an illustrative example of time series is shown in Figure 5.24. Prior to deconvolution the mean and linear trend of both barometric pressure and water level filtered records are subtracted and a tapering Tukey window (r= 20%, see Figure 5.8 for explanation) is applied to minimize spectral leakage. Here Hanning and Hamming windows were also tested and the Tukey window found to give the smoothest BRF estimate. $WL(f)$ and $B_p(f)$ were calculated using the '*FFT*' Matlab function [*MathWorks Inc.*, 2011]. As seen in Figure 6.3, both gain and phase components are very noisy. The high level of noise, particularly at frequencies above 1 cycle/day, is due to the lack of energy in the barometric pressure and water level signals. This level of noise is unacceptable as it makes it unfeasible to constrain theoretical model fits to estimated barometric response functions, as investigated in section 7.2.5 where it is shown that the aquifer-confining layer parameters are sensitive to small variations in gain and phase curves.

6.3.3. The cross-spectral deconvolution by ensemble averaging method

In this study, a more robust approach than direct deconvolution is used. This is the method of cross-spectral deconvolution by ensemble averaging [*Welch*, 1967] which is also used by a number of previous investigators [*Rojstaczer*, 1988a; *Rojstaczer and Riley*, 1990; *Beavan et al.* 1991; *Quilty and Roeloffs*, 1991]. In this method, the barometric response function is obtained by dividing the cross-spectral density between the water level and barometric pressure signal, $P_{WB}(f)$, by the auto-spectral density of the barometric pressure signal, $P_{BB}(f)$, Equation 6.6.

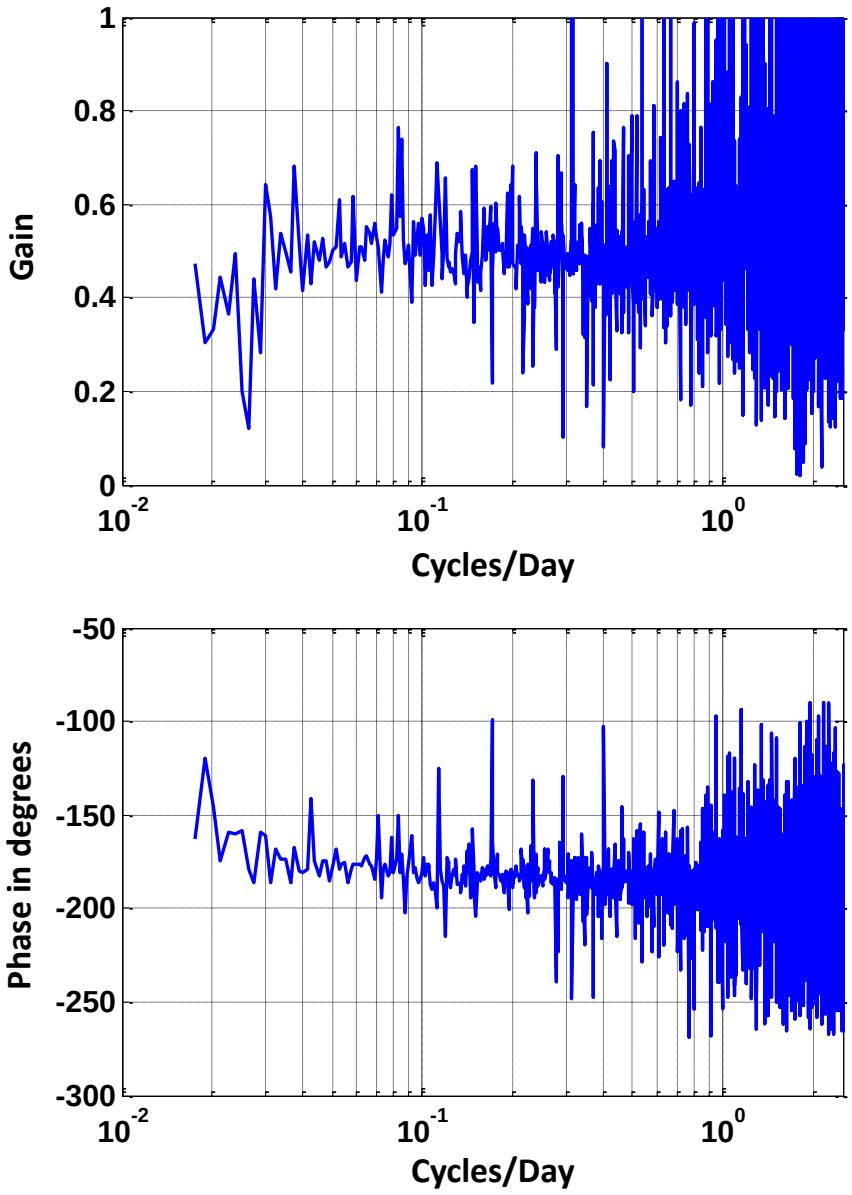

Figure 6.3. Example of a BRF estimated for the Benningholme borehole using ordinary DFT deconvolution. Both gain and phase show very noisy behaviour, particularly above 1 cycle/day, which makes it unfeasible to fit theoretical model to estimated barometric response function.

$$BRF(f) = \frac{P_{WB}(f)}{P_{BB}(f)} . \quad (6.6)$$

In this study, the *RF* Matlab code (see Appendix D) has been developed to apply the Welch method using the '*tfestimate*' Matlab function [*MathWorks Inc.*, 2011] to estimate the barometric response function. This function computes the cross-spectral density between the water level and barometric pressure signal, $P_{WB}(f)$, and the auto-spectral density of the barometric pressure signal, $P_{BB}(f)$, and then forms their quotient to obtain the barometric response function, $BRF(f)$. Steps for BRF estimation using *RF* Matlab code are as follows:

1) Filtered time series of the water level and barometric pressure signals are created using methods described in Chapter 5. Zero-phase, high and low pass filters are applied to water level signal to remove the recharge signal and high frequency noise, respectively. These filters are also applied to the barometric pressure signal to treat both signals equally to ensure compatibility between them. Finally both signals are detrended (mean and linear trend are removed).

2) Records of both signals are divided into a specified number of segments, N, with an overlap, δ, of 50% between segments. An overlap of 50% doubles the number of calculations to perform in Equation 6.6. However by using this percentage about 90% of the stability lost due to tapering operations can be recovered [*Bendat and Piersol*, 2010]. Figure 6.4 illustrates the segmentation of the ensemble averaging method after [*Welch*, 1967].

In the *RF* Matlab code, the maximum number of segments (N) that can be used is calculated, using Equations 6.7 and 6.8, as a function of both the lowest frequency of interest (F_{min}) and the number of samples in the full record (C). F_{min} controls the length of each segment (L), see Figure 6.4 and Equation 6.7; the longer the segment, the lower the frequency that can be resolved. C controls how many segments (N) can be generated for a given segment length (L) and percentage of overlap of δ=50%, Equation 6.8.

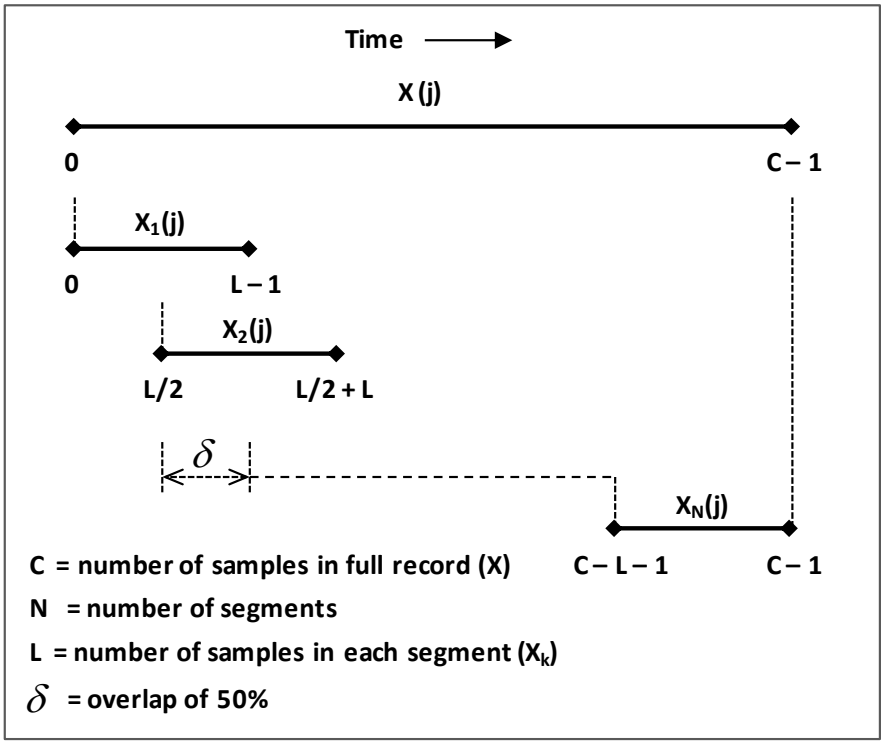

Figure 6.4. Illustration of record segmentation in the ensemble averaging method, after [Welch, 1967]. The filtered time series for water level and the barometric pressure are divided into a number of segments, N, with overlap, δ, between segments.

$$\lceil \mathrm{L} \rceil = \frac{(1/\mathrm{F_{min}})}{\Delta \mathrm{t}}, \tag{6.7}$$

where: L is the number of samples in each segment rounded to the nearest integer and Δt is the sampling interval. The number of segments, N, is given by:

$$\lfloor \mathrm{N} \rfloor = \left(\frac{\mathrm{C}}{\mathrm{L}/2}\right) - 1, \tag{6.8}$$

where: C is the number of samples in the full record.

3) For each segment a tapering periodic Hanning window is applied to minimize spectral leakage, as recommended by *Welch* [1967] and *Bendat and Piersol* [2010]. Here both a periodic Hamming window and a Tukey window (r= 20%) were tested. The periodic Hamming window gave the same result as the applied periodic Hanning window, while the Tukey window give similar results but less smooth. To avoid

artifacts of undesired periodicity each segment is padded with zeros at its end, as recommended by *Press et al.* [2007], to make up the number of points in the Fast Fourier Transform, FFT, to the next power of two. This also results in increasing resolution of the barometric response function estimate, as it increases the number of data points.

4) Each pair of corresponding segments is then used to compute a single cross-spectral density function between the water level and barometric pressure signals as the product of the Fast Fourier Transform of the water level segment, FFT_{WL}, and the conjugate of the Fast Fourier Transform of the barometric pressure segment, FFT^*_{Bp}. The final cross-spectral density, $P_{WB}(f)$, is then averaged over the number of segments (N) using Equation 6.9 [*Bendat and Piersol* 2010].

$$P_{WB}(f) = \frac{2}{NL\Delta_t}\sum_{k=1}^{N}\left[FFT^*_{Bp}(k)\, FFT_{WL}(k)\right], \tag{6.9}$$

where: k =1, 2, 3,……, N and Δ_t is the recording time interval.

5) Each segment of the filtered record of barometric pressure is used to compute a single auto-spectral density function as the squared magnitude of the Fast Fourier Transform. The final auto-spectral, $P_{BB}(f)$, is then averaged over the number of segments (N) using Equation 6.10 after *Bendat and Piersol* [2010].

$$P_{BB}(f) = \frac{2}{NL\Delta_t}\sum_{k=1}^{N}\left|FFT_{Bp}(k)\right|^2. \tag{6.10}$$

6) Finally, Equation 6.6 is used to estimate the barometric response function, $BRF(f)$, using $P_{WB}(f)$ and $P_{BB}(f)$ obtained from Equations 6.9 and 6.10 respectively. An implicit assumption when using this 'averaging' approach is that the estimated $BRF(f)$ is stationary in time, i.e. time series of the same length but different time periods give the same barometric response function. This assumption is tested in section 6.3.5.

Figure 6.5 shows an example of a barometric response function estimate at the Benningholme borehole using number of segments (N) of 5, 10, 15, 20 and 26. This shows that increasing number of segments reduces noise in the BRF estimate. It is also shown that 20 segments are sufficient to give a reliable BRF estimate and little difference can be observed between BRF estimates using 20 and 26 segments (see Figure 6.5). In this example shown in Figure 6.5, the full record length is 76565 samples with a 15 minute interval. The lowest frequency of interest is 0.017 cycles/day (the cut-off imposed by the high-pass filter applied to remove recharge) which requires a minimum segment length (L) of 5647 samples. This means that the maximum number of segments (N), based on overlap of δ=50%, is 26.

6.3.4. The cross-spectral deconvolution by ensemble averaging with overlapping frequency bands

Using Welch's averaging technique has the advantage of smoothing the estimated barometric response function but has the disadvantage of limiting it at lower frequencies, because dividing the time series into a number of segments means shortening individual segment record length. To minimize the impact of this effect, an overlapping frequency band technique as described by *Beavan et al.* [1991] is used where up to five overlapping frequency bands are used to estimate the barometric response function. A small number of segments is used to extend the barometric response function frequency band to low frequencies accepting the resulting lower accuracy. The number of segments is then incrementally increased to give more accurate estimation of the BRF for higher frequency bands. The cut-off frequency of the first frequency band is given by the cut-off frequency identified to remove recharge at each borehole; see Table 5.4. The cut-off frequency for each of the higher overlapping frequency bands is decided according to each borehole case. For each frequency band, a high-pass zero-phase Butterworth filter is applied, for both water level and barometric pressure signals, to prevent leakage from lower frequencies as described by *Beavan et al.* [1991] and the barometric response function is estimated according to the Welch's averaging technique as described above in section 6.3.3. Table 6.2 gives details of record lengths, segmentation and high-pass filters used in estimating the barometric response function at each borehole. The number of segments range from 20 to 1109 and segments lengths range from 1.06 to 58.83 days.

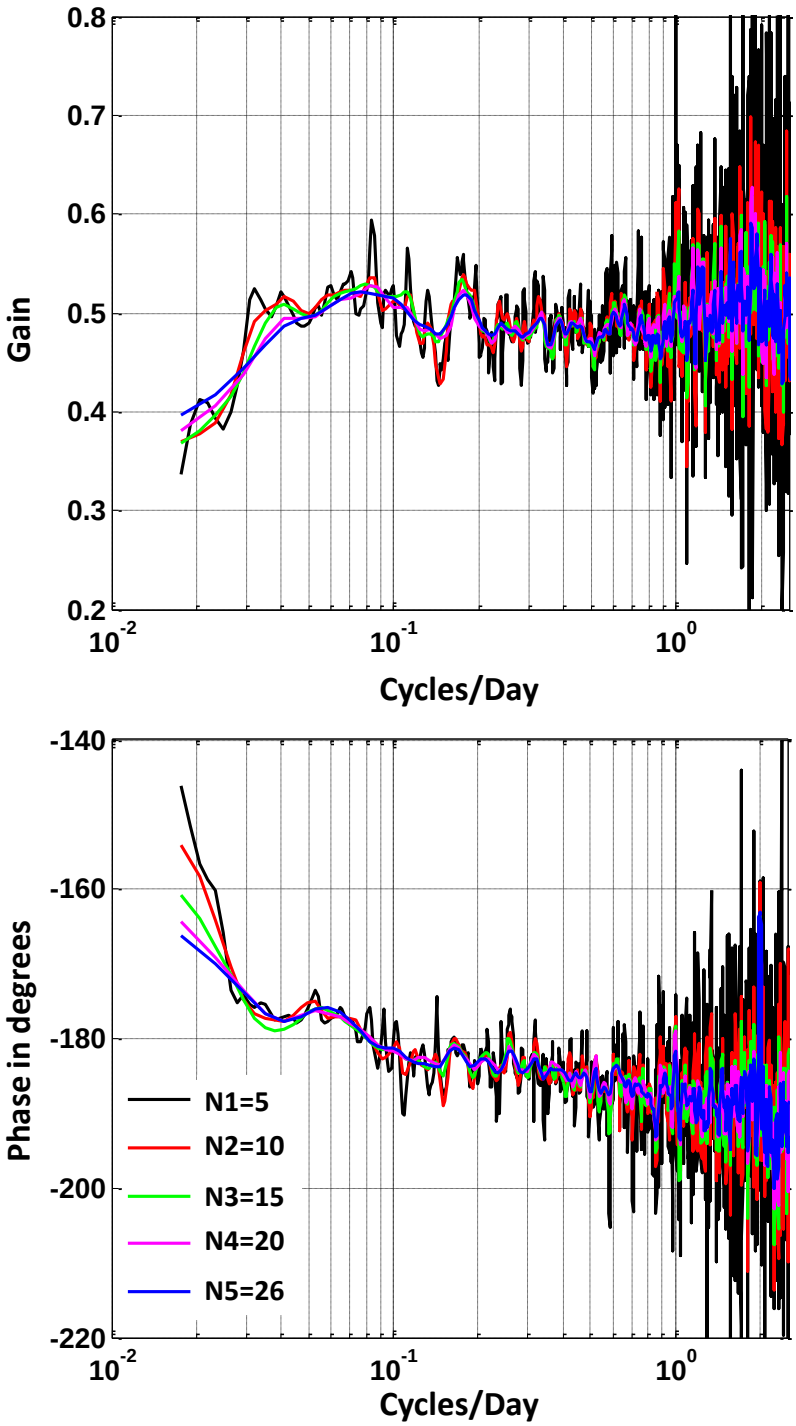

Figure 6.5. Example of BRF estimation at the Benningholme borehole using a range of number of segments (N) from 5 to 26. It is shown that increasing the number of segments reduces noise in the BRF estimate in both gain and phase components. Note that the minimum frequency in both gain and phase components is 0.017 cycles/day, the cut-off applied for recharge removal.

Table 6.2. Details on segmentation, overlapping frequency bands and high-pass filters used to estimate barometric response functions.

		Record length (days)	No. of segments (N)	Segment lengths (days)	Gaps (days)	No. of freq. bands	High-pass-filter cut-off frequencies (cycles/day)
1	Benningholme	799.1	26, 46, 158	58.83, 33.34, 10	-----	3	0.017, 0.03, 0.1
2	Wilfholme- M1 and M2	275.5	26, 42, 53, 163, 514	20, 12.5, 10, 3.33, 1.06	-----	5	0.05, 0.08, 0.1, 0.3, 0.95
	Wilfholme- M3	800.0	78, 126, 158, 478, 1109	20, 12.5, 10.0, 3.33, 1.44	-----	5	0.05, 0.08, 0.1, 0.3, 0.7
3	Sunk Island	737.9	28, 43, 72, 219, 512	58.83, 33.34, 20, 6.66, 2.86	-----	5	0.017, 0.03, 0.05, 0.15, 0.35
4	Park House Farm	324.2	60, 66, 95, 160, 223	10.53, 9.53, 6.67, 4, 2.86	0.83	5	0.095, 0.105, 0.15, 0.25, 0.35
5	Routh Low Farm	317.9	21, 49, 94, 189	28.57, 12.5, 6.67, 3.33	7.11	4	0.035, 0.08, 0.15, 0.3
6	Routh High Farm	312.7	20, 48, 92, 185, 526	28.57, 12.5, 6.67, 3.33, 1.18	-----	5	0.035, 0.08, 0.15, 0.35, 0.85
7	Thornholme Moor	312.0	26, 36, 60, 184, 494	22.23, 16.67, 10.0, 3.33, 1.25	-----	5	0.045, 0.06, 0.1, 0.3, 0.8
8	West Newton Farm	677.1	32, 59, 86, 134, 336	40.0, 22.23, 15.38, 10.0, 4.0	-----	5	0.025, 0.045, 0.065,0.1, 0.25
9	Woodhouse Farm	293.6	57, 87, 116, 145, 203	10.0, 6.67, 5.0, 4.0, 2.86	-----	5	0.1, 0.15, 0.2, 0.25, 0.35
10	Bracy Bridge	309.6	29, 110, 153, 215, 554	20.0, 5.56, 4.0, 2.86, 1.11	-----	5	0.05, 0.18, 0.25, 0.35, 0.9

The thresholds for coherence and signal amplitude were determined by trial and error for each borehole. In most cases, any frequencies where amplitude of the water level signal gain is lower than about 0.03 cmH_2O, or where the coherence between barometric pressure and water level signals is lower than around 0.5 were excluded from the final barometric response function. These thresholds are specific to this case study and boreholes described here. In general, it was found that the estimated BRF at which the water level signal amplitude and/or coherence are lower than these thresholds show implausible response function shapes, see Figures 6.6 and 6.7 for examples of application of these thresholds. A similar procedure is described by *Rojstaczer and Riley* [1990] where they excluded frequencies at which coherence is less than 0.7 and the power spectrum of the water level signal is less than 0.1 cm^2 day/cycle. Below these thresholds, they observed responses that had no theoretical basis. This limited their analysis to barometric response function with a frequency band of 0.09-0.4 cycles/day plus two data points at 1 and 2 cycles/day. This is a narrower frequency band compared with the barometric response function frequency range in this study which ranges from 0.017-0.095 to 0.56-1.0 cycles/day plus two data points at 1 and 2 cycles/day.

Sources of error in frequency response function estimation are described in *Bendat and Piersol* [2010]. For each individual frequency band, an averaged coherence estimate, $C_{WB}(f)$, over the number of segments N is calculated using Equation 6.11, using the same ensemble averaging technique described in section 6.2.3. In the *RF* Matlab code the coherence is computed for each frequency band using the '*mscohere*' Matlab function [*MathWorks Inc.*, 2011].

$$C_{WB}(f) = \frac{|P_{WB}(f)|^2}{P_{WW}(f)\ P_{BB}(f)}, \tag{6.11}$$

where: $C_{WB}(f)$ is coherence between water level and barometric pressure signals, $P_{WB}(f)$ and $P_{BB}(f)$ are estimated using Equations 6.9 and 6.10, and $P_{WW}(f)$ is the auto-spectral density function of the water level signal, Equation 6.12:

$$P_{WW}(f) = \frac{2}{NL\Delta_t}\sum_{k=1}^{N} |FFT_{WL}(k)|^2, \tag{6.12}$$

where: FFT_{WL} is the Fast Fourier Transform of the water level signal.

The normalized standard error, $\sigma(f)$, of the barometric response function is then estimated using Equations 6.13 and 6.14 as a function of coherence between barometric pressure and water level signals, $C_{WB}(f)$ (Equation 6.11), and the degrees of freedom, p,which is a function of the number of segments, N, and the percentage of overlap, δ, [*Beavan et al.*, 1991; *Bendat and Piersol*, 2010]. Equation 6.14 shows that for $C_{WB}(f)$ close to unity and/or for large p, the error $\sigma(f)$ approaches zero. Therefore, using a large number of segments reduces the error and smooths the barometric response function.

$$p = \mathrm{N} - (\mathrm{N} - 1)\,\delta \ , \tag{6.13}$$

$$\sigma(f) = \left\{\frac{1}{2p}\left(\frac{1}{C_{WB}(f)^2} - 1\right)\right\}^{1/2}. \tag{6.14}$$

For each frequency band, gain and phase components, $A^{BRF}(f)$ and $\theta^{BRF}(f)$, are calculated using Equations 6.4 and 6.5 respectively. The standard errors for both components, $\sigma A(f)$ and $\sigma\theta(f)$, are then calculated using Equations 6.15 and 6.16 respectively, after *Beavan et al.* [1991] and *Bendat and Piersol* [2010, P 310].

$$\sigma A(f) = \sigma(f)\, A^{BRF}(f), \tag{6.15}$$

$$\sigma\theta(f) = \sigma(f)\, \frac{180}{\pi}. \tag{6.16}$$

Figure 6.6 illustrates various stages of barometric response function estimation for the Benningholme borehole. The barometric response function is estimated using three overlapping frequency bands of 26, 46, 158 segments (Table 6.2). Figure 6.6a shows that as the number of segments becomes higher, the barometric response function becomes smoother but more restricted at low frequencies. In addition, as number of segments increases, coherence becomes smoother particularly at high frequencies (Figure 6.6b). The barometric response function constructed from these three overlapping frequency bands is shown in Figure 6.6d. The acceptable range of frequencies is determined using the coherence and signal energy, as described above,

from which the final frequency range of the barometric response function is determined. Figure 6.6b shows that coherence is higher than 0.8 over the entire frequency band from 0.017 to 2 cycles/day. However, Figure 6.6c shows that the water level signal amplitude at frequencies above 0.8 cycles/day is lower than the limit of 0.03 cmH_2O. Thus the final barometric response function ranges from 0.017 to 0.8 cycles/day with and additional point at 1 cycle/day. The point at 2 cycles/day was excluded as it shows an implausible phase value. The Benningholme borehole lies within zone 3 (total catchment) of the groundwater source protection zones of several abstraction stations lying between Beverley and Hull (see Figure 5.1). It is therefore possible that the water level signal at Benningholme shows some influence from these abstractions. These abstractions commonly have a 12 hour pumping cycle which may explain the implausible phase value at 2 cycles/day. The final selected barometric response function is shown in Figure 6.7 together with one standard error bars (Equations 6.15 and 6.16). It is shown that due to the lower number of segments error bars at low frequencies are larger compared with higher frequencies.

Figure 6.8 illustrates various stages of barometric response function estimation for the Routh Low Farm borehole, as an example of analysis of boreholes with a short time series record. The full record length at this borehole (317.9 days) is about 40% of that at the Benningholme borehole (799.1 days). Figure 6.8b shows that frequencies above 0.7 cycles/day have coherence largely below the chosen threshold of 0.5. In addition, water level signal amplitudes at frequencies above 0.6 cycles/day are below the threshold of 0.03 cmH_2O except at 1 and 2 cycles/day (Figure 6.8c). Therefore, frequencies above 0.6 cycles/day were excluded from the final determined barometric response function. Low values for coherence and water level amplitude at high frequencies suggest a low level of connectivity between the aquifer and the borehole, i.e. that the flow rate between aquifer and borehole is not sufficient for borehole water levels to respond to high frequency barometric pressure changes. This is later confirmed using slug tests, explained in detail in Chapter 9. The final selected barometric response function is shown in Figure 6.9 together with one standard error bars. The estimated barometric response functions for all boreholes with one standard error bars are presented in Chapter 8.

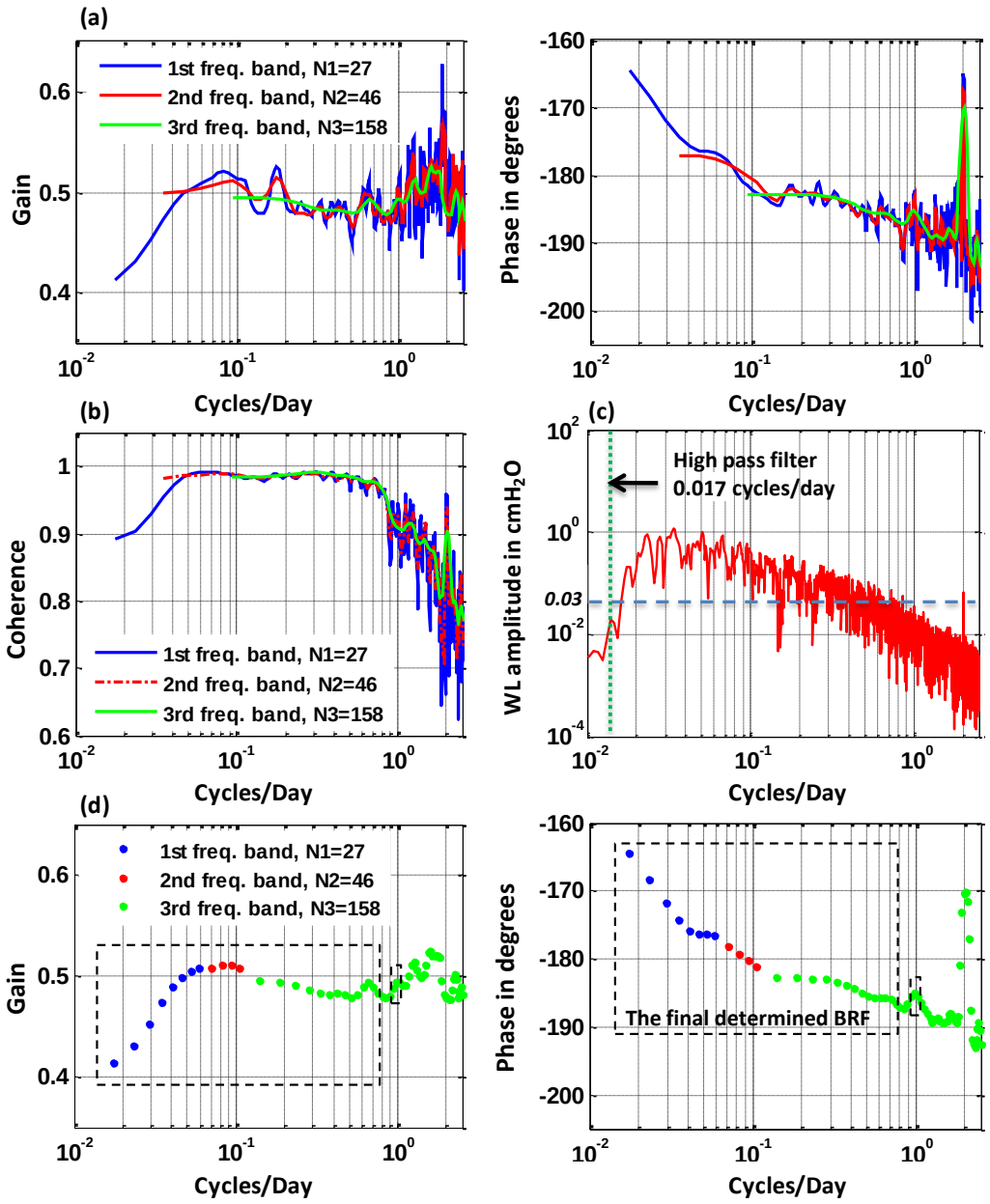

Figure 6.6. Steps in estimating the barometric response function (Benningholme borehole). a) Gain and phase plots showing estimated barometric response functions for three overlapping frequency bands. b) Coherence for the three overlapping frequency bands in (a). c) Water level signal with amplitude threshold of 0.03 cmH_2O. d) The final selected barometric response function (dashed box) determined from three overlapping frequency bands in (a). This illustrates that using the deconvolution-averaging method integrated with three overlapping frequency bands results in a smooth barometric response function.

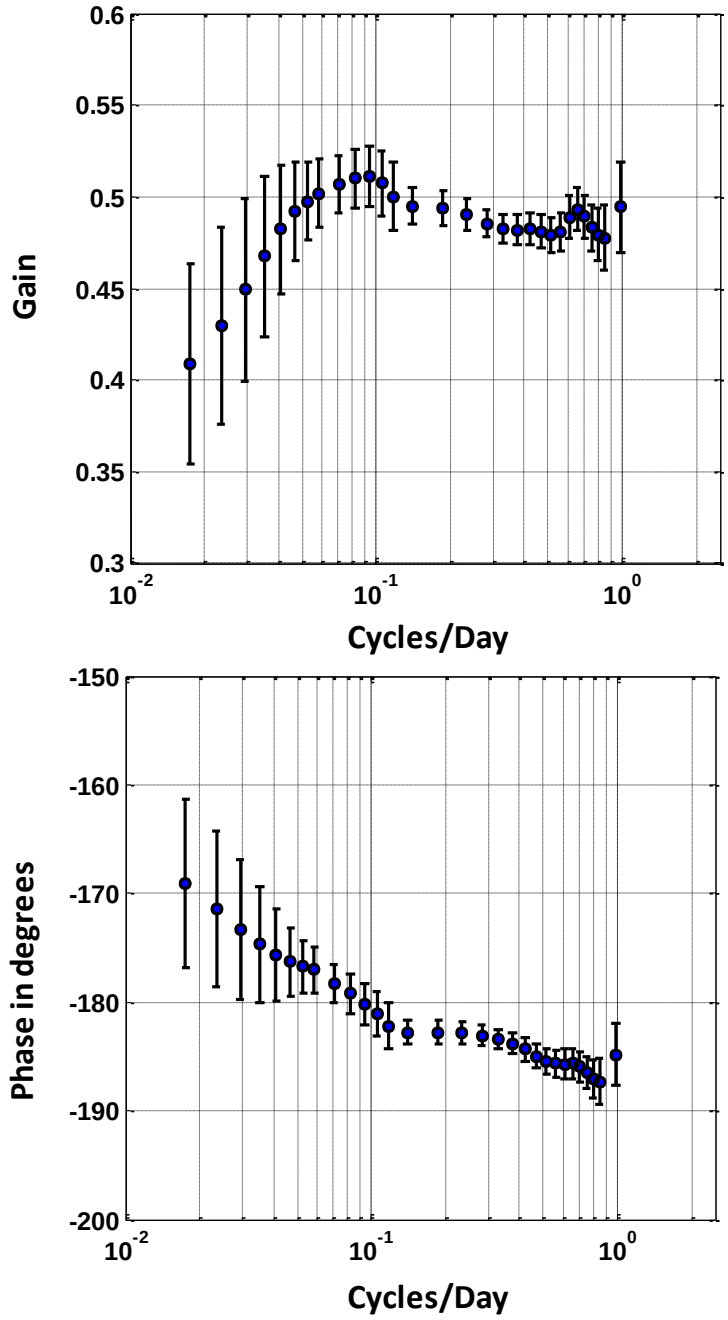

Figure 6.7. The final selected barometric response function at the Benningholme borehole together with one standard error bars. Error bars are larger at lower frequencies due to lower number of segments used in estimation of the barometric response function.

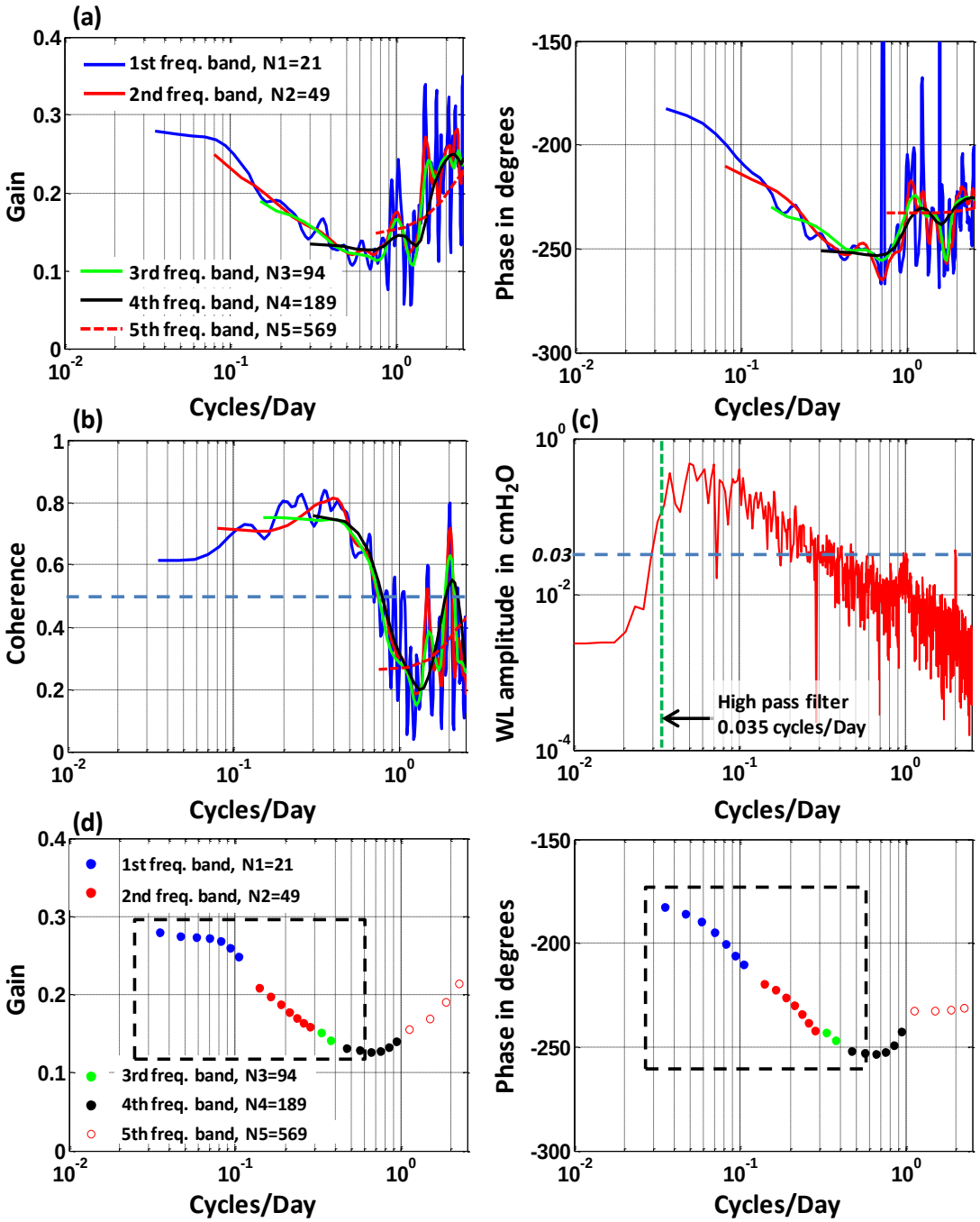

Figure 6.8. Steps in estimating the barometric response function (Routh Low Farm borehole). a) Gain and phase plots showing estimated barometric response functions over five overlapping frequency bands. b) Coherence for the five overlapping frequency bands, frequencies above 0.7 cycles/day have coherence below threshold of 0.5. c) Water level signal amplitude where frequencies above 0.6 cycles/day have amplitudes below threshold of 0.03 cmH_2O except at 1 and 2 cycles/day. d) The final selected barometric response function (dashed box).

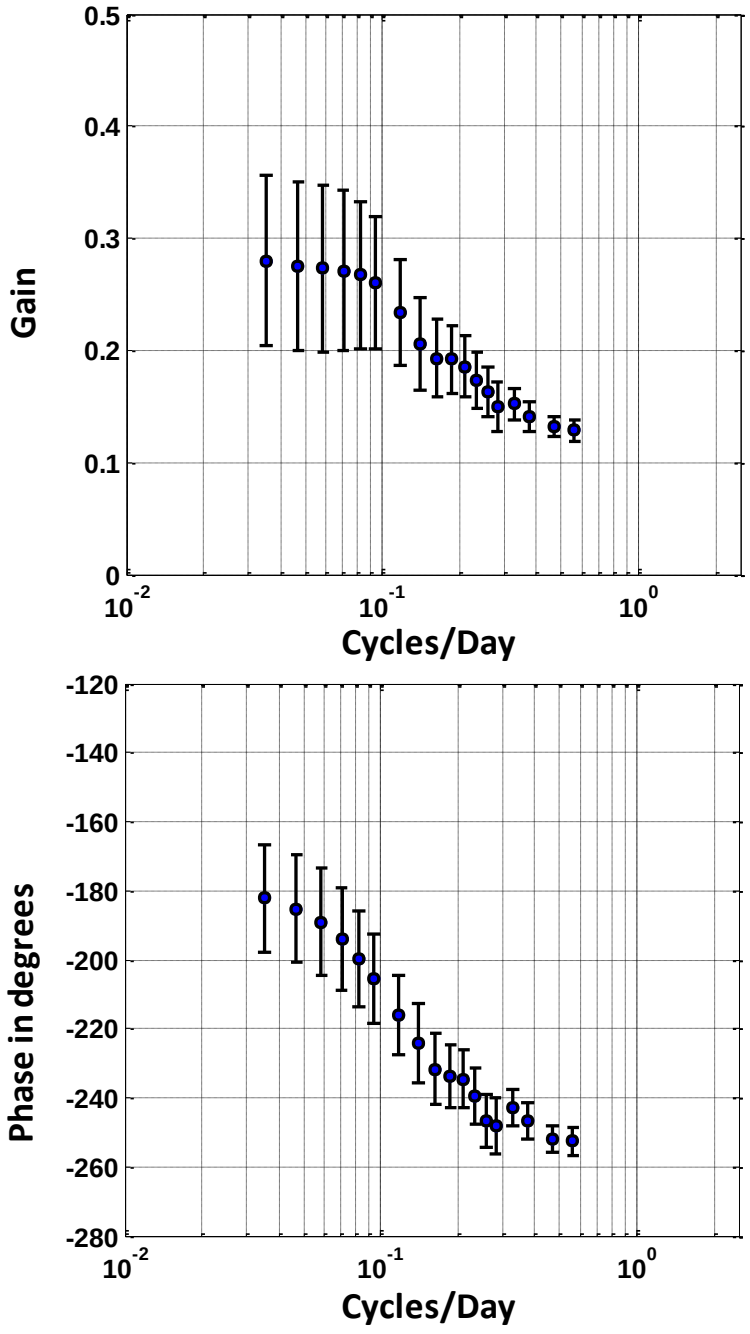

Figure 6.9. The final selected barometric response function at the Routh Low Farm borehole together with one standard error bars. Error bars are larger at lower frequencies due to lower number of segments used in the estimation of the barometric response function.

6.3.5. Testing the assumption of stationarity

The technique of "cross-spectral deconvolution by ensemble averaging" [*Welch,* 1967] described in sections 6.3.3 and 6.3.4 implicitly assume that the estimated $BRF(f)$ is stationary in time (time-invariant), i.e. time series of the same length but from different time periods give the same barometric response functions. This assumption of stationarity is tested using the Benningholme record (796 days) divided into four sub-records each of 199 days. Each of these sub-records was used to estimate the barometric response function using the "averaging" technique and three overlapping frequency bands (with 5, 8, 38 segments and cut-off frequencies of 0.017, 0.025 and 0.1 respectively), see Figure 6.10. The estimated barometric response functions are generally in good agreement with each other within the one standard error bars. Better agreement is shown at the second and third frequency bands (high frequencies) due to the larger number of segments (8 and 38). For the first frequency bands (low frequencies), the agreement between barometric response functions is less due to the small number of segments (N=5), which is reflected by the large error bars compared with higher frequencies. Previous test (Figure 6.5) showed that a minimum number of 20 segments is needed to give a reliable estimate of barometric response function. Data collected in this study have longer records, than 199 days used in this test, giving larger number of segments even at low frequencies, see Table 6.2. However, in general this test here, Figure 6.10, indicates that the stationarity assumption for the barometric response function with relative to time is valid if a suitable number of segments can be achieved.

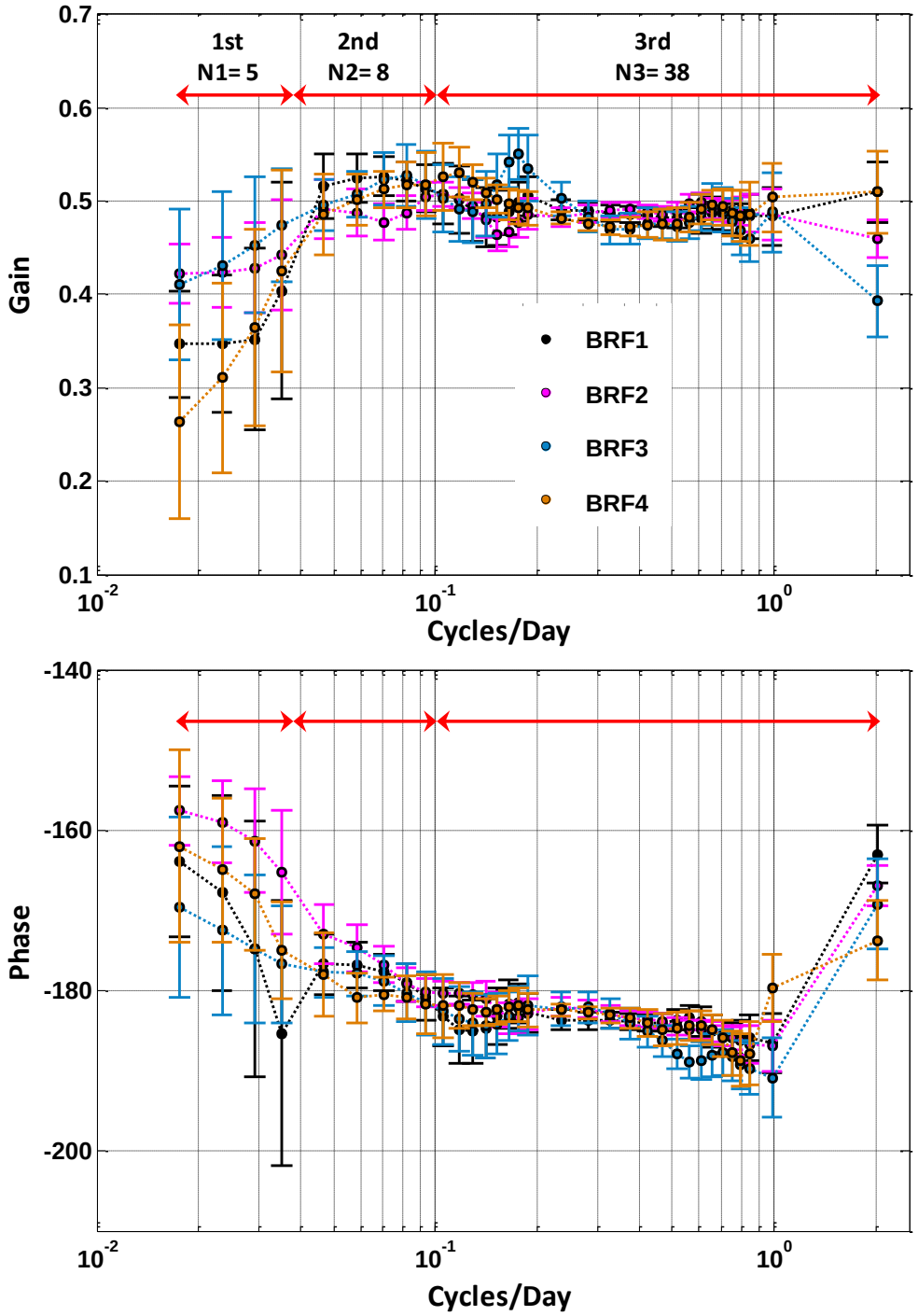

Figure 6.10. Stationarity test for the barometric response function using four equal length sub-records at the Benningholme borehole. Estimated barometric response functions show good agreement with each other within one standard error bars particularly for frequency bands 2 and 3. Frequency band 1 shows less good agreement due to the small number of segments that were used.

6.3.6. Importance of removing recharge and Earth tides

To illustrate the importance of removing recharge and Earth tides, Figure 6.11 shows a comparison between estimated barometric response functions using filtered (continuous lines) and unfiltered (dotted lines) water level and barometric pressure signals at the Benningholme borehole. This shows that removing Earth tides increases the accuracy of the barometric response function estimate at diurnal and semi-diurnal frequencies and that removing recharge has a significant effect on the barometric response function at low frequencies. The recharge signal contribution to the borehole water level signal introduces high energy at low frequencies, (see section 5.2.2). This energy can leak to higher frequencies and cause distortion of the spectra at higher frequencies [*Beavan et al.*, 1991 and *Hwang et al.*, 2003]. To avoid this high-pass zero-phase Butterworth filters are applied to each frequency band to remove frequencies lower than the fundamental frequency for the segment as described by *Beavan et al.* [1991]. Figure 6.12 shows the coherence between water level and barometric pressure signals for the three overlapping frequency bands using unfiltered signals at the Benningholme borehole. Low coherence is observed, compared to filtered signals (Figure 6.6b), at diurnal and semi-diurnal frequencies due to contamination from Earth tides. In addition, energy leakage from frequencies lower than the fundamental frequency of each band (0.017, 0.03 and 0.1 cycles/day respectively) causes very low coherence at low frequencies. Thus, the pre-processing of the water level and barometric pressure signals to remove recharge and Earth tides has a significant impact on the accuracy of the barometric response function particularly at low frequencies and diurnal and semi-diurnal frequencies of Earth tides.

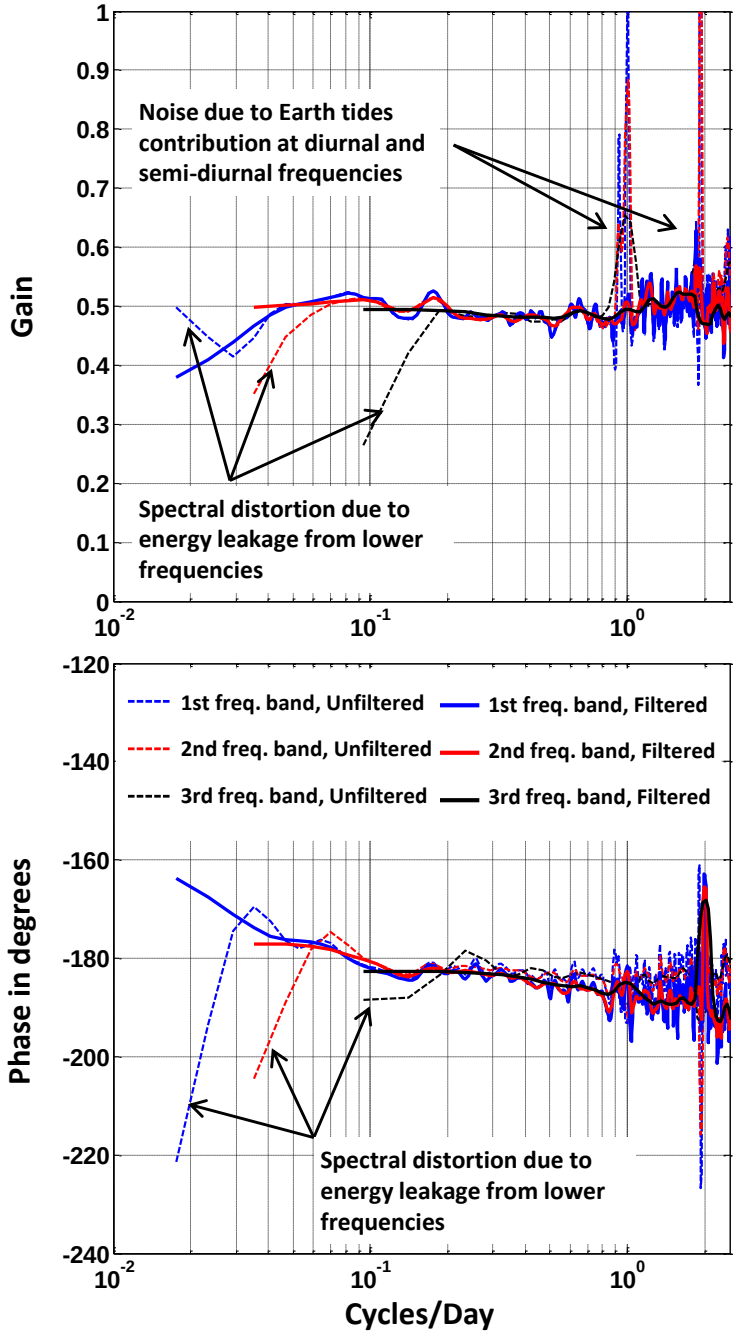

Figure 6.11. A comparison between estimated barometric response function using filtered (continuous lines) and unfiltered (dotted lines) signals at the Benningholme borehole. It shows the significant effect for removing recharge and Earth tides on estimating the barometric response function.

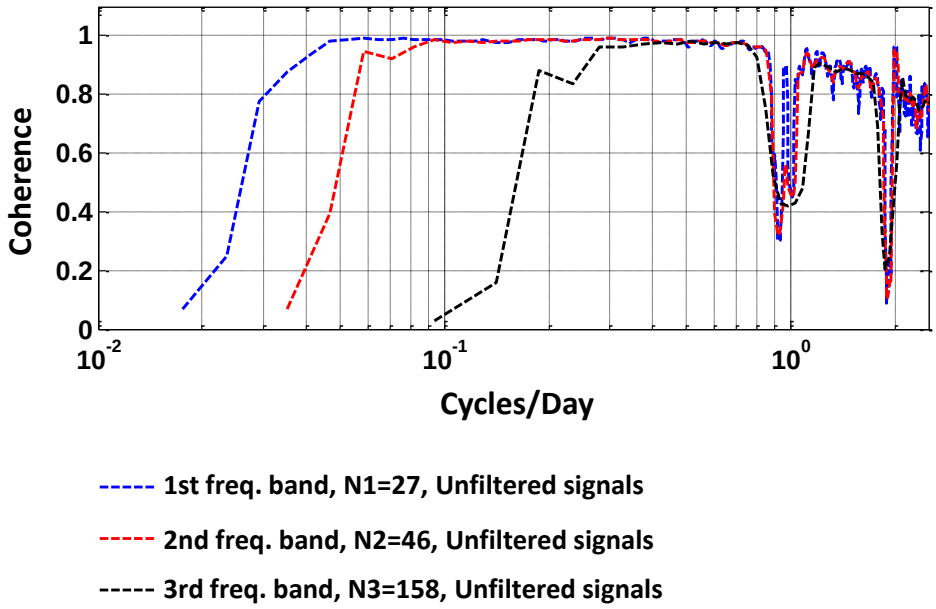

Figure 6.12. Coherence estimate between water level and barometric pressure unfiltered signals for the three overlapping frequency bands at the Benningholme borehole. Sudden drops are observed at diurnal and semi-diurnal frequencies due to contamination from Earth tides. For the three overlapping frequency bands low coherence is observed at low frequency due to energy leakage from lower frequencies.

6.4. Summary

The *BE* Matlab code (Appendix C) was developed to implement the least-squares regression methods detailed by *Rasmussen and Crawford* [1997] to compute short-term and long-term barometric efficiencies. Results were used as a diagnostic measure for the degree of aquifer confinement. Results predict that the aquifer at all boreholes is semi-confined except for Routh Low Farm and Routh High Farm boreholes where significant borehole storage/skin effects dominate the short-term barometric efficiency. The *RF* Matlab code (Appendix D) was developed to implement the cross-spectral deconvolution-averaging method [*Welch*, 1967] integrated with the technique of overlapping frequency bands described by *Beavan et al.* [1991] to estimate barometric response functions with uncertainty bounds. Estimates of barometric response function using these techniques showed significant improvement in smoothness and accuracy compared with the ordinary frequency deconvolution method. Testing the stationarity assumption of the barometric response function with respect to time showed that this assumption is valid if a suitable number of segments can be achieved. Comparing the barometric response function using filtered and unfiltered signals shows the benefits of removing the contributions of recharge and Earth tides to the water level signal. These techniques have been used to estimate barometric response functions for all boreholes and results are described in Chapter 8.

CHAPTER 7: THEORETICAL RESPONSE MODEL AND ESTIMATION OF SYSTEM PARAMETERS

7.1. Introduction:

For a purely confined aquifer where the confining layer is thick and/or has zero permeability, the barometric response function is independent of frequency (see Chapter 2, section 2.2.2). Thus, the gain component is constant at all frequencies with a value equal to the static barometric efficiency. The phase component is -180º at all frequencies, i.e. the water level signal is out of phase with the barometric pressure signal. In this case the low permeability of the confining layer does not allow a change in aquifer pore pressure to dissipate through vertical flow to/from the water table and is called the undrained response condition. However, the purely confined aquifer case is rarely found in nature and most aquifers are in fact semi-confined. Even aquifers with low permeability confining layers usually show a semi-confined response to sufficiently long periods (low frequencies) of barometric pressure change because these changes occur at a slow rate allowing time for the aquifer pore pressure to dissipate (termed drained response conditions). Under semi-confined conditions, close to undrained response to barometric pressure change can be observed over short periods, although this response may be attenuated at high frequencies if the aquifer has low lateral transmissivity and/or borehole storage or skin effects are significant [*Rojstaczer*, 1988a; *Roeloffs*, 1996]. Therefore, in most real cases, the barometric response function is frequency dependent and can be used to estimate aquifer and confining layer properties by fitting to theoretical response models. In this chapter, the governing equations for a theoretical model of borehole water level response to barometric pressure and the fitting technique used for estimating system parameters are described.

7.2. Theoretical response model for semi-confined aquifers

Rojstaczer [1988a] developed an analytical model for the borehole water level response to barometric pressure under semi-confined conditions. Conceptually his model is composed of two layers, a confining layer (which is divided into unsaturated and saturated zones) overlying an aquifer layer, see Figure 7.1. He assumes that these

two layers have similar loading efficiencies under undrained conditions, essentially assuming that the elastic properties for both layers are the same and vertically and laterally uniform. His model considers three flow processes driven by three pressure imbalances that are generated instantaneously by a step change in barometric pressure, see Figure 7.1:

1. vertical air flow driven by pressure imbalance between the Earth's surface and the water table through the unsaturated zone,
2. vertical groundwater flow driven by pressure imbalance between the water table and the aquifer through the saturated confining layer, and
3. horizontal groundwater flow driven by pressure imbalance between the aquifer and the borehole.

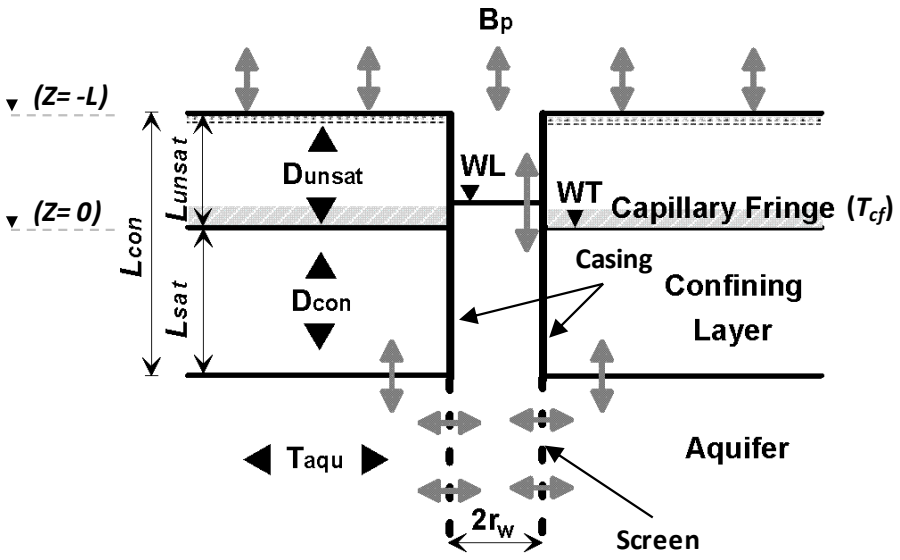

Figure 7.1. Diagram showing a cross section of aquifer and confining layer with key parameters controlling the borehole water level (WL) response to barometric pressure (B_p) changes after [*Rojstaczer*, 1988a and *Evans et al.*, 1991]. D_{unsat} is the vertical pneumatic diffusivity of the unsaturated zone, D_{con} is the vertical hydraulic diffusivity of the saturated zone, T_{aqu} is the aquifer transmissivity, T_{cf} is the capillary fringe attenuation factor and WT is the water table.

Evans et al. [1991] also developed an analytical model similar to that of *Rojstaczer* [1988a] but with three differences. Firstly, his model is composed of one layer divided into unsaturated and saturated zones; here he implicitly assumes that the aquifer and the confining layer have similar flow and elastic properties. Secondly, the model allows for attenuating effects of a capillary fringe on the air pressure pulse caused by compression of isolated air pockets within capillary fringe which are not connected with the atmosphere. This is a phenomenon also observed by *Peck* [1960] and *Turk* [1975]. Thirdly, *Evans et al.* [1991] includes the presence of a low permeability skin at the interface between the borehole screen and the aquifer formation.

In this study, the *Rojstaczer* [1988a] model is used as this model is better suited to an aquifer that is partially confined by a layer with a different hydraulic conductivity. However, the capillary fringe attenuation factor (T_{cf}) is added from the *Evans et al.* [1991] model, see section 7.2.4. The governing equations of *Rojstaczer* [1988a] model with the modification from *Evans et al.* [1991] are explained in the following subsections according to the three flow processes described above.

7.2.1. Vertical air flow between the Earth's surface and the water table

In *Rojstaczer* [1988a] model, the air flow between the Earth's surface and the water table is assumed to be strictly vertical. This implicitly assumes that barometric pressure is uniform over a large area [*Roeloffs*, 1996]. Vertical air flow through the unsaturated zone is represented by a simple homogenous diffusion equation [*Weeks*, 1979; *Rojstaczer*, 1988a, Equation 1]:

$$D_{unsat}\ \frac{\partial^2 P_a}{\partial z^2} = \frac{\partial P_a}{\partial t}\,, \tag{7.1}$$

where: D_{unsat} is the vertical pneumatic diffusivity of the unsaturated zone, the ratio of pneumatic conductivity to specific storage for isothermal air flow. P_a is the air pressure pulse, z is the vertical distance from the water table to the ground surface and t is time.

As shown in Equation 7.1, the rate of diffusion of the air pressure is directly proportional to D_{unsat}, i.e. the diffusion rate ($\partial P_a/\partial t$) increases with large values of D_{unsat}. Equation 7.1 is solved subject to the following boundary conditions [*Rojstaczer*, 1988a: Equations 2a and 2b]:

$$P_a(-L,t) = A\cos(\omega t), \text{ and} \tag{7.2a}$$

$$P_a(L,t) = A\cos(\omega t), \tag{7.2b}$$

where: $z = -L$ is the Earth's surface and the water table is at $z = 0$ (see Figure 7.1), A and ω are amplitude and angular frequency of the periodic barometric pressure pulse. Equation 7.2a states that the air pressure at ground surface is equal to barometric pressure represented by a periodic wave ($A\cos(\omega t)$). The boundary condition in Equation 7.2b is imposed to ensure that the vertical air flow at the water table ($z = 0$) is zero [*Rojstaczer*, 1988a].

The solution of 7.1, subject to 7.2 at the water table ($z = 0$) given by *Rojstaczer* [1988a, Equation 3] is:

$$P_a = (M - iN)\,A\,\exp(i\omega t), \tag{7.3}$$

where: i is the imaginary unit ($\sqrt{-1}$), and M and N are [*Rojstaczer*, 1988a, Equations 4a and 4b]:

$$M = \frac{2\cosh(R^{0.5})\cos(R^{0.5})}{\cosh(2R^{0.5}) + \cos(2R^{0.5})}, \text{ and} \tag{7.4a}$$

$$N = \frac{2\sinh(R^{0.5})\sin(R^{0.5})}{\cosh(2R^{0.5}) + \cos(2R^{0.5})}, \tag{7.4b}$$

where: R is the dimensionless frequency of the unsaturated zone given by [*Rojstaczer*, 1988a, Equation 5]:

$$R = \frac{{L_{unsat}}^2\omega}{2D_{unsat}}, \tag{7.5}$$

where: L_{unsat} is the unsaturated zone thickness.

Evans et al. [1991] introduced Equation 7.6 (his Equation A3) similar to Equation 7.3 for barometric pressure diffusion at the water table but with the addition of capillary fringe attenuation represented by an attenuation factor, T_{cf}:

$$P_a = T_{cf}\ A\ \exp\ i(\omega t + \theta), \tag{7.6}$$

where: θ is the phase of the pressure pulse.

As shown in Equation 7.6, the attenuation factor (T_{cf}) accounts for the fraction of the air pressure wave transmitted through the capillary fringe [*Evans et al.*, 1991]. Thus, a value of T_{cf} of unity means zero attenuation and allows 100% of the pressure wave to pass through the capillary fringe, while a value of T_{cf} of zero allows none of the pressure wave to be transmitted.

7.2.2. Vertical groundwater flow between the water table and the aquifer

Rojstaczer [1988a] assumes in his model that groundwater flow in the confining layer between the water table and the aquifer is strictly vertical. He also assumes that the loading efficiencies (ε) for the aquifer and the confining layer are the same. Loading efficiency is the ratio of the pore pressure change to the barometric pressure change under undrained conditions ($\varepsilon = 1 - BE$), where BE is the static barometric efficiency of the aquifer. This assumption ensures that the instantaneous transfer of the barometric pressure to the subsurface (confining layer and the aquifer) is vertically and horizontally uniform. The governing equation for pore pressure response due to periodic loading [*Rojstaczer*, 1988a, Equation 6] is:

$$\frac{\partial P}{\partial t} = D_{con}\ \frac{\partial^2 P}{\partial z^2} - \left(\varepsilon\ \frac{\partial P_a}{\partial t}\right), \tag{7.7}$$

where: P is the pore pressure change in excess of hydrostatic pressure. D_{con} is the vertical hydraulic diffusivity of the confining layer, the ratio of hydraulic conductivity to hydraulic specific storage of confining layer.

Equation 7.7 shows that the vertical hydraulic diffusivity of the saturated zone (D_{con}) governs the rate of diffusion of pore pressure change through confining layer. In other words, the hydraulic diffusivity controls the timescale of fluid flow from the water table to/from the aquifer [*Roeloffs*, 1996]. The right hand term (between brackets) in Equation 7.7 represents the instantaneous transmission of the surface load of the air pressure wave (P_a) via grain-to-grain contact (elastic deformation) to the underlying layers which is governed by the loading efficiency (ε).

Equation 7.7 is solved subject to the following boundary conditions [*Rojstaczer*, 1988a, Equations 7a and 7b]:

$$P(0,t) = M\,A\,\cos\,(\omega t) + N\,A\,\sin\,(\omega t), \text{ and} \tag{7.8a}$$

$$P(\infty,t) = A\,\varepsilon\,\cos\,(\omega t), \tag{7.8b}$$

where: $P(0,t)$ is the change in pore water pressure at the water table and $P(\infty,t)$ is the change in pore water pressure at a depth far from the water table.

The pore water pressure (P) at the water table, $z = 0$, (given by Equation 7.8a) must equal the air pressure (P_a) at the water table (given by Equation 7.3). The dimensionless frequency that characterizes flow in the saturated confining layer (Q) is [*Rojstaczer*, 1988a, Equation 10]:

$$Q = \frac{{L_{sat}}^2 \omega}{2D_{con}}, \tag{7.9}$$

where: L_{sat} is the thickness of the saturated zone.

7.2.3. Horizontal flow between the borehole and the aquifer

In the model of *Rojstaczer* [1988a], groundwater flow between the borehole and the aquifer is assumed to be strictly horizontal and is described in Equation 7.10 for non steady radial flow in a homogeneous isotropic aquifer. This is derived from the

solution after *Jacob* [1946] which includes a leakage term to incorporate the influence of the confining layer [*Rojstaczer*, 1988a, Equation 11]:

$$\frac{\partial^2 s}{\partial {r_r}^2} + \frac{1}{r_r}\,\frac{\partial s}{\partial r_r} - \frac{K_{con}\, s}{T_{aqu}\; L_{sat}} = \frac{S_{sa}}{K_{aqu}}\,\frac{\partial s}{\partial t}\,, \tag{7.10}$$

where: s is drawdown within the aquifer caused by periodic volumetric discharge in the borehole, r_r is radial distance from the borehole, T_{aqu} and K_{aqu} are the horizontal transmissivity and hydraulic conductivity of the aquifer respectively, S_{sa} is the specific storage of the aquifer under conditions of no horizontal deformation, and K_{con} is the vertical hydraulic conductivity of saturated confining layer [*Rojstaczer*, 1988a].

Equation 7.10 is solved subject to the following boundary conditions [*Cooper at al.*, 1965; *Rojstaczer*, 1988a, Equations 12a and 12b]:

$$s(\infty, t) = 0, \quad \text{and} \tag{7.11a}$$

$$\lim_{r_r \to 0} \frac{r_r \partial s}{\partial r_r} = \frac{\omega\, r_w^2\, x_0}{2\, T_{aqu}} \sin \omega t\,, \tag{7.11b}$$

where: r_w is the borehole radius and x_0 is the amplitude of fluctuations in borehole water level (measured positive upwards).

The boundary condition of Equation 7.11a states that the drawdown in the aquifer far from the borehole due to periodic discharge in the borehole is zero. The boundary condition in Equation 7.11b states that near the borehole screen radial flow is equal to the discharge from the borehole [*Reed*, 1980]. The dimensionless frequency that characterizes the flow between the borehole and the aquifer is [*Rojstaczer*, 1988a, Equation 14]:

$$W = \frac{r_w^2 \omega}{T_{aqu}}\,. \tag{7.12}$$

Rojstaczer [1988a] gives a solution for Equation 7.10 subject to boundary Equations 7.11a and 7.11b subject to four assumptions:

(1) the level of the water table does not change in response to periodic discharge from the borehole,
(2) the confining layer has negligible specific storage.
(3) changes in pore pressure due to fluctuations of borehole water level induce only vertical deformation (a standard assumption in groundwater hydraulics), and
(4) the borehole can be treated as a line source.

As reported by *Rojstaczer* [1988a], the errors involved in assumptions 1 and 2 have been examined by *Neuman and Witherspoon* [1969]. They found that these errors are negligible when the dimensionless parameters β_m and $(W/q)^{1/2}$ are less than 0.01, where: β_m and q are defined as [*Rojstaczer*, 1988a, Equations 15 and 9]:

$$\beta_m = \frac{r_w}{4L_{sat}(K_{con}\, S_{sc}/K_{aqu}\, S_{sa})^{1/2}} \quad , \tag{7.13}$$

where: S_{sc} is the specific storage of the confining layer, and

$$q = \frac{L_{sat}\,\omega}{K_{con}} \, . \tag{7.14}$$

Since in most cases the hydraulic conductivity of the aquifer will be larger than that of the confining layer, and the saturated thicknesses of the confining layer and the aquifer will be much larger than the borehole radius, then the dimensionless frequencies β_m and $(W/q)^{1/2}$ will normally be less than 0.01 [*Rojstaczer*, 1988a]. To check this for the Chalk Aquifer, typical average values given in Table 7.1 are substituted into Equations 7.12, 7.13 and 7.14, giving values of β_m of 0.007 and $(W/q)^{1/2}$ of 0.006. Thus errors caused by assumptions 1 and 2 can be ignored in our case study.

Table 7.1. Typical average values of the East Yorkshire Chalk Aquifer and monitoring boreholes [*Parker*, 2009; *Batu*, 1998].

Parameter	Value
Borehole radius, r_w	0.1 m
Thickness of unsaturated zone, L_{unsat}	1.5 m
Thickness of saturated zone, L_{sat}	15 m
Aquifer thickness	10 m
Hydraulic conductivity of confining layer, K_{con}	0.01 m/day
Aquifer transmissivity, T_{aqu}	20 m^2/day
Specific storage of confining layer, S_{sc}	10^{-3} m^{-1}
Specific storage of the aquifer, S_{sa}	10^{-5} m^{-1}
Static barometric efficiency of the Aquifer, *BE*	0.6

In the following section, the steps for determining the theoretical barometric response function from Rojstaczer's model are briefly described. Full details of his model derivation and assumptions can be found in *Rojstaczer* [1988a].

7.2.4. Determination of theoretical barometric response function

The model barometric response function of *Rojstaczer* [1988a] can be expressed as:

$$BRF_m = (U - 1)/(1 + (0.5\, i\, W\, V)\,) \quad , \tag{7.15}$$

where: i is the imaginary unit ($\sqrt{-1}$), and U and V are given by Equations 7.16 and 7.17:

$$U = \left(\left(M\, T_{cf} + iN\, T_{cf}\right) - \varepsilon\right) \exp\,(-(i + 1)\, Q^{0.5}) + \varepsilon \, , \tag{7.16}$$

where: M and N are given by Equations 7.4a and 7.4b, and ε is the loading efficiency of the aquifer. Here, the capillary fringe attenuation factor (T_{cf}) from the model of *Evans et al.* [1991] is added to *Rojstaczer* [1988a] model in Equations 7.16.

$$V = K_0\{\,[W^2(S_{aqu}^2 + \left(\tfrac{S_{con}}{2Q}\right)^2)]^{0.25} \exp\,[0.5\, i\, \tan^{-1}(2Q)]\,\} \, , \tag{7.17}$$

where: K_0 is the modified Bessel function of the second kind of order zero, S_{aqu} is the storage coefficient of the aquifer, S_{con} is the storage coefficient of the confining layer, and W and Q are given in Equations 7.12 and 7.9 respectively. The gain and phase are then given by the modulus and the argument of BRF_m respectively using Equations 6.4 and 6.5, section 6.3.2.

A typical barometric response function shape is shown in Figure 7.2 using parameters typical of the boreholes analyzed here (see Table 7.1). The response can be divided into three stages comprising low (A), intermediate (B) and high frequency (C) responses [*Rojstaczer,* 1988a].

Low frequency response (drained response)

At low frequencies in stage A, the gain increases and phase decreases with increasing frequency, see Figure 7.2. The response is principally governed by the ratio of the dimensionless frequencies of unsaturated and saturated zones, R/Q (Equation 7.18). At very low frequencies, equilibrium is maintained and the system behaves as if nearly unconfined where the gain component of barometric response function approaches zero. The ratio R/Q is a measure of the time needed for air pressure to pressurize the water table versus the time needed for water to flow to water table to depressurize pore pressure in the aquifer [*Roeloffs,* 1996]. Therefore, small values of the ratio R/Q infer negligible unsaturated zone effects, where the unsaturated zone thickness (L_{unsat}) is thin and/or the vertical pneumatic diffusivity (D_{unsat}) is large.

$$\frac{R}{Q} = \frac{{L_{unsat}}^2}{{L_{sat}}^2} \frac{D_{con}}{D_{unsat}} . \qquad (7.18)$$

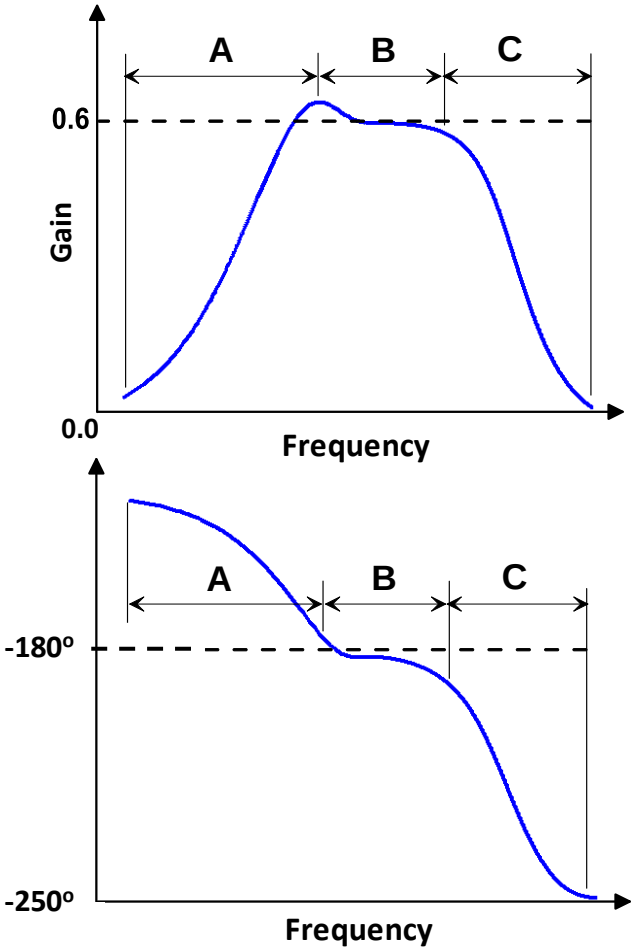

Figure 7.2. Example theoretical barometric response function gain and phase curves derived from the model of *Rojstaczer* [1988a] using parameters typical of the confined Chalk Aquifer (Table 7.1). Showing low (A), intermediate (B) and high (C) frequency response stages.

Intermediate frequency response (undrained response)

At intermediate frequencies in stage B, a plateau exists in both gain and phase (Figure 7.2) representing near confined conditions. The gain at this intermediate response plateau is the static barometric efficiency and phase is -180˚ using the convection used by *Rojstaczer* [1988a]. Changes in barometric pressure are too fast to allow exchange between the semi-confining layer and the aquifer, and the aquifer transmissivity is sufficient to allow unattenuated flow between the aquifer and the borehole. The response is governed by the loading efficiency of the aquifer ($\varepsilon = 1 - BE$) and is similar to that of a fully confined aquifer.

High frequency response (attenuated undrained response)

At high frequencies in stage C, gain decrease and phase increase with increasing frequency (Figure 7.2) due to the limited rate at which water can flow between the aquifer and the borehole. The response is governed principally by borehole design, horizontal aquifer transmissivity and aquifer storativity. If borehole storage/skin effects are negligible and/or the aquifer transmissivity is high, neither gain attenuation nor phase lag will be observed and the intermediate response plateau (stage B) will extend to higher frequencies.

7.2.5. Sensitivity of model parameters

Figures 7.3 and 7.4 illustrate the sensitivity of the model, where each parameter is changed within a range of values while fixing all other parameters. Initial parameters are based on typical values for the East Yorkshire Chalk Aquifer and given in Table 7.1. Figure 7.3a shows that the barometric efficiency, BE, controls only the magnitude of the gain. Figure 7.3b shows that changes in aquifer transmissivity, T_{aqu}, affect only the intermediate to high frequency response in both gain and phase. In addition, increasing T_{aqu} increases the width of the confined plateau in both gain and phase. Reducing the T_{aqu} value below a certain limit (here 10 m^2/day, Figure 7.3b) causes the confined plateau to vanish. Figure 7.3c shows that the model is relatively insensitive to aquifer storage coefficient S_{aqu} and only high frequencies are affected where reducing

S_{aqu} decreases both gain and phase with increasing frequency. Note that no sensitivity curves for storage coefficient of confining layer S_{con} are shown here because it has no significant effect on the response shapes, within a range of 10^{-2} - 10^{-4}, typical of the expected range for glacial sediments [*Batu,* 1998].

Figure 7.4 shows that the confining layer properties (hydraulic diffusivity of the saturated zone D_{con}, pneumatic diffusivity of the unsaturated zone D_{unsat}, the thickness of the unsaturated zone L_{unsat}, and the capillary fringe attenuation factor T_{cf}) affect the response at principally low to intermediate frequencies. Figure 7.4a shows that increasing D_{con} shrinks the width of the confined plateau, (i.e. reduces the degree of aquifer confinement) and the response becomes more semi-confined with a bell shaped gain and monotonic phase lag. It is also shown that using a very small value for D_{con} (0.01 m^2/day) gives a purely confined response where the gain equals the static barometric efficiency (BE=0.6) and the phase is -180˚. Figures 7.4b and 7.4d show that decreasing D_{unsat} and T_{cf} (i.e. increasing the attenuation of air wave through the unsaturated zone) can cause gain values larger than the static barometric efficiency (BE=0.6) at low frequencies. The attenuation of the air pressure wave delays transmission to the water table which in turn delays pressurization of the aquifer pore water. This can then cause the difference in pressure between the borehole and the aquifer to be larger than the static *BE* value.

7.3. Fitting model curves to estimated barometric response functions

Aquifer and confining layer parameters are estimated by fitting the above theoretical model curves to the estimated barometric response functions for both gain and phase components simultaneously. The objective function to be minimized is the sum of square differences in the complex plane between complex forms for estimated (BRF, Equation 6.3) and model (BRF_m, Equation 7.15) response functions. The real and imaginary parts of the response function in the complex plane are used to calculate the objective function rather than gain and phase values. This is because gain ranges from 0 to 1 and phase ranges from -120 to -260 which will emphasize or give more weight to phase over gain, but if the complex plane is used this imbalance is avoided.

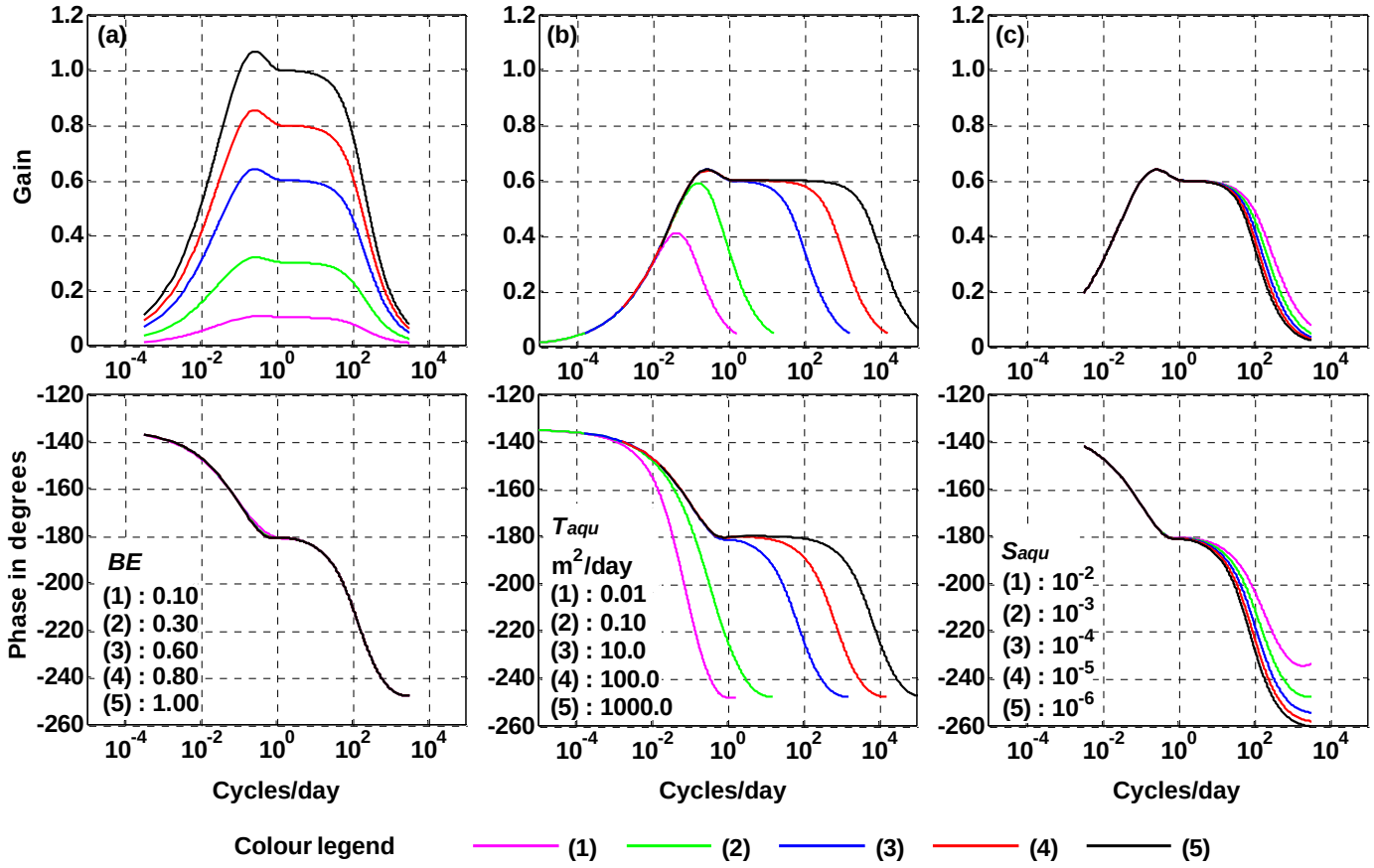

Figure 7.3. Sensitivity analysis for a) barometric efficiency, *BE*, b) aquifer transmissivity, T_{aqu}, and c) aquifer storage coefficient, S_{aqu}, based on the model of *Rojstaczer* [1988a]. Assumed parameters are as for Table 7.1. In each figure all parameters are fixed and one parameter changed to values shown in the phase plot of each figure. It is shown that *BE* controls only the gain magnitude, T_{aqu} affects only the intermediate to high frequency response in both gain and phase, and changes in S_{aqu} affects only the high frequency response.

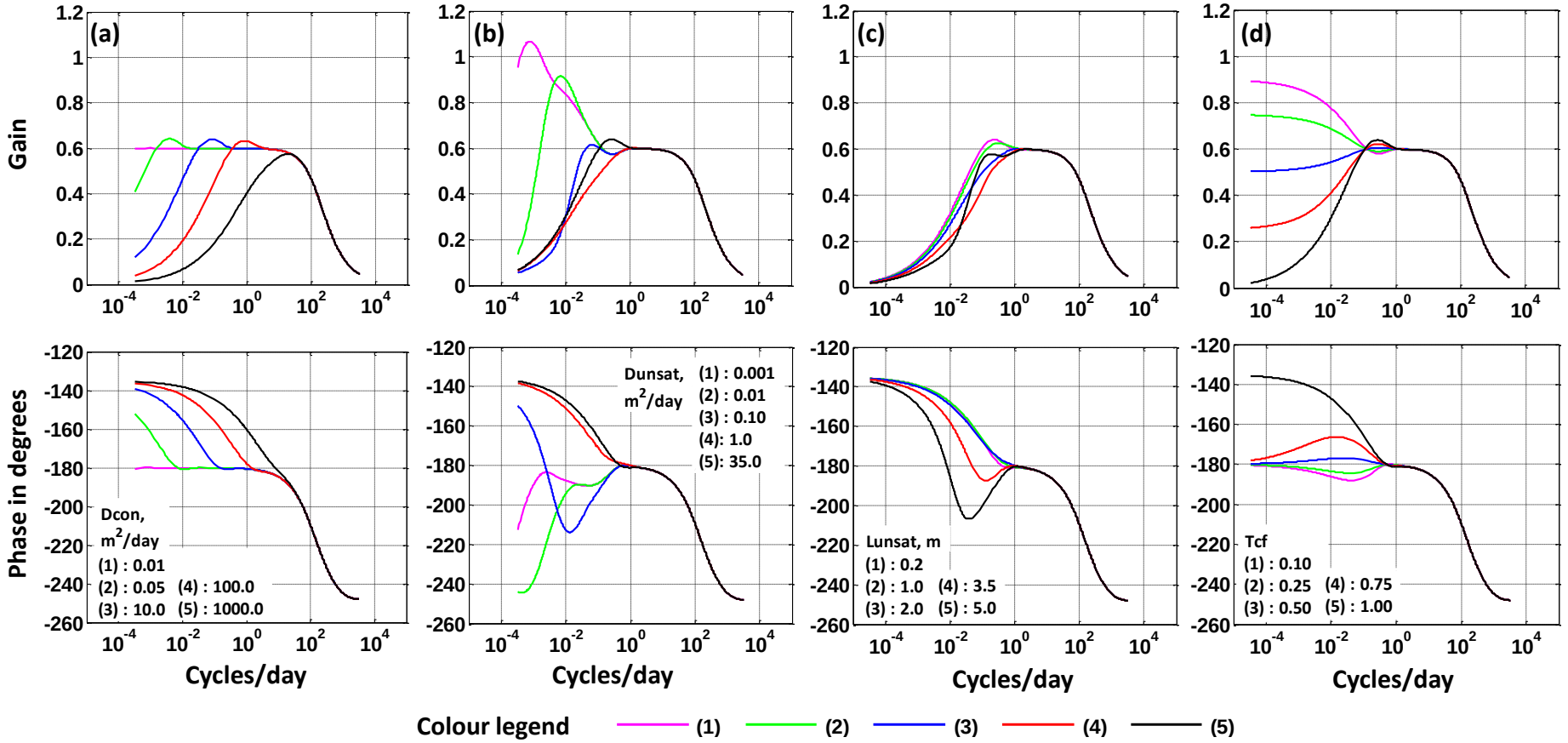

Figure 7.4. Sensitivity analysis for a) vertical hydraulic diffusivity of confining layer, D_{con}, b) vertical pneumatic diffusivity of unsaturated zone D_{unsat}, c) thickness of unsaturated zone, L_{unsat} and d) capillary fringe attenuation factor, T_{cf}, based on the model of *Rojstaczer* [1988a]. Assumed parameters are as for Table 7.1 and one parameter changed to values shown in phase plots. It is shown that confining layer properties D_{con}, D_{unsat}, L_{unsat} and T_{cf}, affect principally low to intermediate frequencies.

The best fit solution is obtained using the Matlab code developed here (*Automatic_Fitting.m*, see Appendix E) which is based on hybrid genetic (GA) and pattern search (PS) algorithms described by *Alsumait et al.* [2009] and *Liuni et al.* [2010]. In this code, the Matlab function '*HybridFcn*' is used to integrate the two Matlab functions '*ga*' (genetic search tool) and '*patternsearch*' (pattern search tool) [*MathWorks Inc.*, 2011] to construct the hybrid algorithm. Combining these two algorithms helps to overcome the drawbacks of using each one individually. The pattern search, PS, is a computationally efficient searching technique but is dependent on the initial guess point. If the initial chosen point does not lie on the same basin of attraction as the global minimum point (global solution) the PS searching algorithm will converge to a local minimum solution. The genetic algorithm, GA, is a random searching technique which is independent of the initial start point but is computationally intensive. The idea behind using the combined hybrid genetic algorithm (GA) and pattern search algorithm (PS) is to use GA to find a reasonable initial guess point and after that refine the solution using the PS technique [*Alsumait et al.,* 2009 and *Liuni et al.,* 2010]. Thus, the computational time is critically reduced and the best initial guess point is found by randomly searching the solution space. For more details about this hybrid technique the reader is referred to [e.g. *Payne and Eppstein,* 2005; *Alsumait et al.,* 2009; *Liuni at al.,* 2010; *Costa et al.*, 2012].

In GA a chosen number of possible solutions, the population, is randomly produced by sampling the solution space within specified lower and upper bounds for each fitting parameter. Each solution is a set of values of six fitting parameters. These six parameters are; barometric efficiency (BE), pneumatic diffusivity of the unsaturated zone (D_{unsat}), hydraulic diffusivity of the saturated zone (D_{con}), aquifer transmissivity (T_{aqu}), capillary fringe attenuation factor (T_{cf}), and the thickness of the unsaturated zone (L_{unsat}). Each solution is treated as an evolving individual who seeks to reach the optimum global solution through a specified number of generations. At each generation the GA evaluates all the possible solutions to detect the best one which gives the minimum value for the objective function [*Liuni et al.,* 2010]. The hybrid algorithm (GA-PS) switches from the genetic algorithm, GA, to the pattern search algorithm, PS, when the specified termination tolerance (10^{-6}) on the objective function is achieved or when the specified number of generations is reached or if it is asked manually to do so, through an option designed in the *Automatic_Fitting.m*

Matlab code. The pattern search algorithm then uses the best solution of the GA as an initial point to be refined, by first constructing a mesh of surrounding points. If one of the new points has a better value for the objective function the PS will use it as the new initial point through a new iteration, etc… [*Alsumait et al.,* 2009] until it reaches the point at which the difference in objective function value (F-value) between two consecutive solutions is less than the specified threshold of 10^{-6}. This threshold is the default value in Matlab and it has been found to be sufficiently small to achieve a global minimum solution for optimization problems in this study.

The Matlab code '*Automatic_Fitting.m' (see Appendix E*) is designed to apply lower and upper bounds for each fitting parameter during optimization to reduce the computational time and to optimize for feasible solutions. The lower and upper bounds for both the barometric efficiency (BE) and the capillary fringe attenuation factor (T_{cf}) are constrained to be from 0 to 1 respectively. For Benningholme and Sunk Island boreholes, the unsaturated zone thickness (L_{unsat}) is constrained using water level records collected during monitoring period from adjacent boreholes that are screened in the confining layer. For other boreholes, the applied lower and upper bounds for this parameter are 0.5m and 3.5m respectively based on prevailing hydrological knowledge and records from other boreholes in the confining layer (provided by EA). In most cases, lower and upper bounds for the aquifer transmissivity, T_{aqu}, the hydraulic diffusivity, D_{con}, and pneumatic diffusivity, D_{unsat}, are set to a wide range from 0 to 1000 m^2/day; however, this upper bound is increased as needed. Four parameters are held constant; confining layer total thickness ($L_{con} = L_{sat} + L_{unsat}$), storage coefficient of confining layer (S_{con}), aquifer storage coefficient (S_{aqu}), and borehole radius (r_w). Sensitivity to S_{con} and S_{aqu} are discussed in section 7.2.5 and values for these parameters are listed in section 8.1.

For the genetic algorithm (GA), the number of solutions (population size) used is 10000 and the number of generations is set to infinity. The final generation before switching to the PS is then chosen manually while the code is running, when the F-value stabilizes for 10 generations or so. It has been found that 25 generations is usually enough to reach this stabilization point. An illustrative example for the Benningholme borehole, Figure 7.5a and b, shows the optimum (best fit) solution for

the objective function, where real and imaginary components for both model and estimated barometric response function are fitted simultaneously.

The Matlab code '*Manual_Fitting.m' (see Appendix F*) plots the estimated barometric response function with one standard deviation error bars and the best fit model curve together with two additional model curves. This is used to check the sensitivity of each fitting parameter in the solution set, particularly when the best fit solution gives a value equal to specified upper or lower bounds. In addition, acceptable ranges of each parameter (upper and lower bounds) were determined from the range indicated by model curves that lie within one standard deviation error ($\pm \sigma$) of the estimated barometric response function. This is done by fixing all parameters except one, and changing only the parameter of interest. The example of the Benningholme borehole is listed in Table 7.2. All best fit estimates for parameters lie between assigned upper and lower bounds (explained above), except pneumatic diffusivity (D_{unsat}). The automatic best fit value for the pneumatic diffusivity (D_{unsat}) here is 1000.0 m^2/day, which is essentially the upper bound assigned to this parameter during optimization. Trials were done to re-run the automatic fit (GA-PS) using an upper boundary of infinity for this parameter. However the best fit solution was then different in each run and varied over several orders of magnitudes. During these trials all parameters other than D_{unsat} converged to similar values (Table 7.2) which is a good indication that no trade-off occurred. Hence, D_{unsat} cannot be inverted for this borehole case.

Table 7.2. Fitting parameters for the Benningholme borehole from the automatic (GA-PS) algorithm, the best fit and refined solution using the manual fitting code.

Fitting technique	*BE* (-)	$D_{con,}$ (m^2/day)	$D_{unsat,}$ (m^2/day)	$T_{aqu,}$ (m^2/day)	T_{cf} (-)	L_{unsat} (m)
Automatic fit GA-PS	0.49	10.0	1000.0	1.5	0.82	1.20
Lower bound using manual fitting	0.49	8.0	≥ 2.0	1.2	0.70	0.50
Upper bound using manual fitting	0.49	13.0	----	1.9	0.90	2.00
Final best fit solution	0.49	10.0	10.0	1.5	0.82	1.20

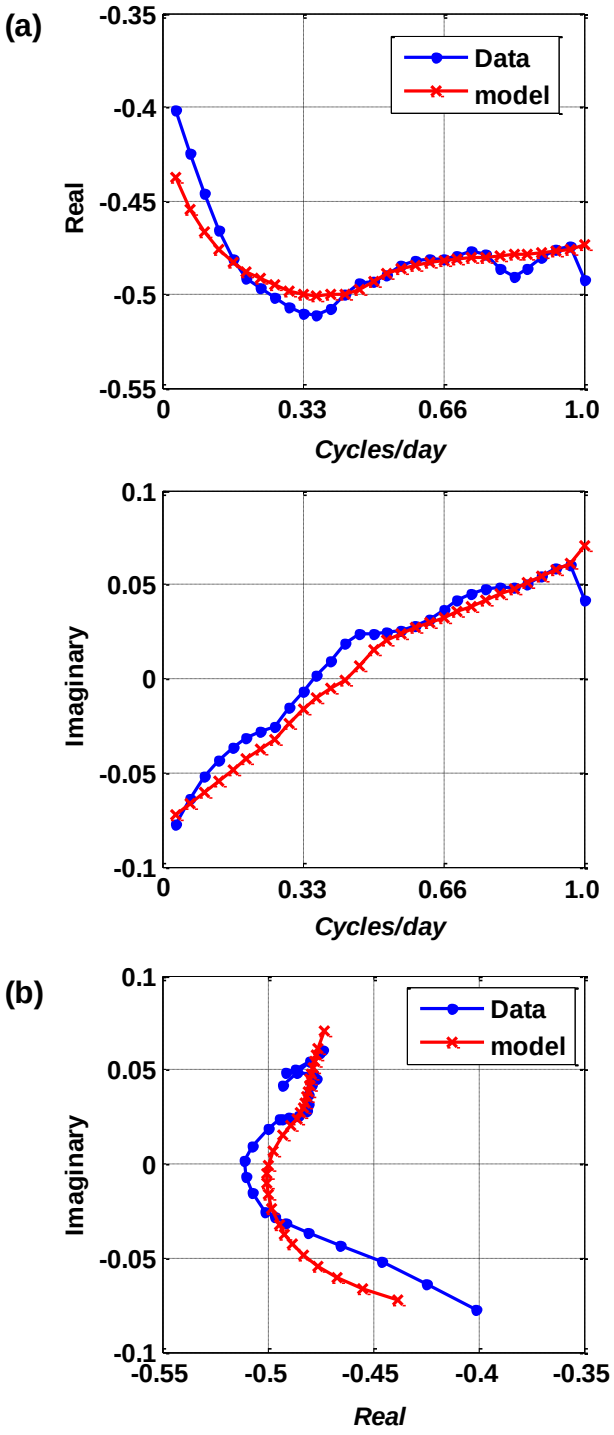

Figure 7.5. Illustrative example for best fit solution of the objective function at Benningholme borehole. (a) Best fit of theoretical model to the BRF for both real and imaginary parts (solved simultaneously) and (b) best fit in the complex plane.

The manual fitting code (*Manual_Fitting.m*) was used to check the sensitivity of the model curve to this parameter and it was found that the model is not sensitive to D_{unsat} values larger than 10.0 m^2/day with a lower bound of 2.0 m^2/day. Thus an estimate of the upper pound to this parameter was not determined and the manually refined best fit value is 10.0 m^2/day (Table 7.2).

7.4. Summary

Under pure confined conditions, the barometric response function (BRF) is independent of frequency, however under semi-confined conditions the barometric response function is a strong function of frequency. The confining layer properties affect low to intermediate frequencies. The intermediate frequency response is governed by the loading efficiency of the aquifer. Limited aquifer transmissivity and storativity and/or significant borehole skin effects cause the barometric response function to be a strong function of frequency at intermediate and high frequencies. The *Rojstaczer* [1988a] model was used to model observed barometric response functions with the capillary fringe attenuation factor added from the model of *Evans et al.* [1991]. The sensitivity to model parameters was implemented using initial values which are typical for the East Yorkshire Chalk Aquifer. Sensitivity (Figures 7.3 and 7.4) shows that each parameter changes the response shapes in a specific way. This, with the technique of fitting both gain and phase simultaneously, provides a powerful way to obtain a unique solution. In this study, the best fit solution is obtained using the Matlab code developed here (Automatic_Fitting.m, see Appendix E) which is based on hybrid genetic (GA) and pattern search (PS) algorithms. In some cases it was not possible to invert some parameters due to insensitivity of the model curve. However, by re-running additional optimization trials, in which upper or lower bounds for these parameters were varied, no indication of trade-off was observed. The best fit solution is then refined manually using the '*Manual_Fitting.m'* Matlab code (see Appendix F). These techniques have been used to fit *Rojstaczer* [1988a] model to estimated barometric response functions in order to derive properties of aquifer and confining layer, results for all boreholes are described in Chapter 8.

CHAPTER 8: BAROMETRIC RESPONSE FUNCTION AND HYDRAULIC AND PNEUMATIC PARAMETER ESTIMATION

8.1. Introduction

Methods described in previous chapters (5, 6 and 7), illustrated by the Benningholme borehole, were applied to the eleven other boreholes across the confined Chalk Aquifer. In Chapter 5, boreholes water level signals with records ranging from 275 to 800 days (recorded at 15 minutes interval) were pre-processed to remove contributions of recharge, pumping and Earth and ocean tides. The recharge signal contributes to the water level signal at low frequencies and is removed by applying a high pass filter with cut-off frequency range of 0.014-0.05 cycles/day for all boreholes. This cut-off is the frequency up to which the recharge signal contributes significantly to the water level signal and is selected using a cut-off coherence level of 0.5. Pumping influences were observed at Wilfholme in the frequency range of 3.8-6.0 cycles/day, and found to affect a wide frequency range at Park House Farm. The low pass filter, with a cut-off frequency at 3 cycles/day which is applied for removal of high frequency noise, removed all pumping effects at Wilfholme boreholes but only part of it at Park House Farm borehole. Contributions of Earth and ocean tide components in the borehole water level signal, with range of 0.01-4.1 cm, were removed by applying a periodic time domain filter using the method of *Rasmussen and Mote* [2007]. Ocean tides were only observed at the Sunk Island borehole, located at about 2 km from the sea. In Chapter 6, barometric response functions were estimated for each borehole, from pre-processed signals, using the cross-spectral deconvolution-averaging method [*Welch*, 1967] integrated with the technique of overlapping frequency bands described by *Beavan et al.* [1991]. All barometric response functions were estimated with one standard error bars which were determined as a function of coherence and number of segments, as described by *Beavan et al.* [1991] and *Bendat and Piersol* [2010]. Then acceptable ranges for the final barometric response functions were selected using amplitude and coherence thresholds of ~ 0.03 cmH_2O and 0.5 respectively. In Chapter 7, the model of *Rojstaczer* [1988a] was used to model observed barometric response functions with the capillary fringe attenuation factor added from the model of *Evans et al.* [1991]. The best fit of this model to observed barometric response functions, is obtained using a hybrid (GA-PS) automatic search algorithm. The best fit solution is a

set of values of six fitting parameters (Table 8.1), while four other parameters are held constant (confining layer total thickness (L_{con}), storage coefficient of confining layer (S_{con}), aquifer storage coefficient (S_{aqu}), and borehole radius (r_w)). In *Rojstaczer's* [1988a] model, the response can be divided into three stages comprising low (A), intermediate (B) and high frequency (C) responses. The low frequency stage A is governed by the properties and thickness of the confining layer, the intermediate frequency stage B is governed by the loading efficiency of the aquifer and the high frequency stage C is governed by the transmissivity of the aquifer, see Figures 7.3 and 7.4. In this chapter, observed barometric response functions are interpreted in the light of these stages.

In this chapter, barometric response functions are presented for twelve boreholes from the confined Chalk Aquifer in East Yorkshire. These boreholes penetrate a wide range of glacial sediments types overlying the aquifer, Figure 8.1. For each borehole, the best fit model curve to the estimated barometric response function is shown and acceptable ranges of each parameter (upper and lower bounds) were determined from model curves that lie within one standard error ($\pm \sigma$) of the estimated barometric response function. These ranges are obtained using the *Manual_Fitting* Matlab code, see Appendix F, by changing the parameter of interest while holding other parameters constant. A summary of the six estimated parameters at each borehole is shown in Table 8.1 together with their ranges. For each borehole the best fit model curve is plotted together with two curves representing upper and lower pounds for one or two parameters of interest. Phase is plotted according of the sign convection of *Rojstaczer* [1988a], see section 7.2.4. For all boreholes, a value of 10^{-3} is used for storage coefficient of the confining layer as an average representative value for glacial sediments cover with average thickness of 10 m [*Batu*, 1998] and an aquifer storage coefficient of 10^{-4} (for chalk) is used for all boreholes, as the model is not sensitive to these parameters within the frequency band of estimated barometric response functions of 0.017-2 cycles/day as shown in Figure 7.3c.

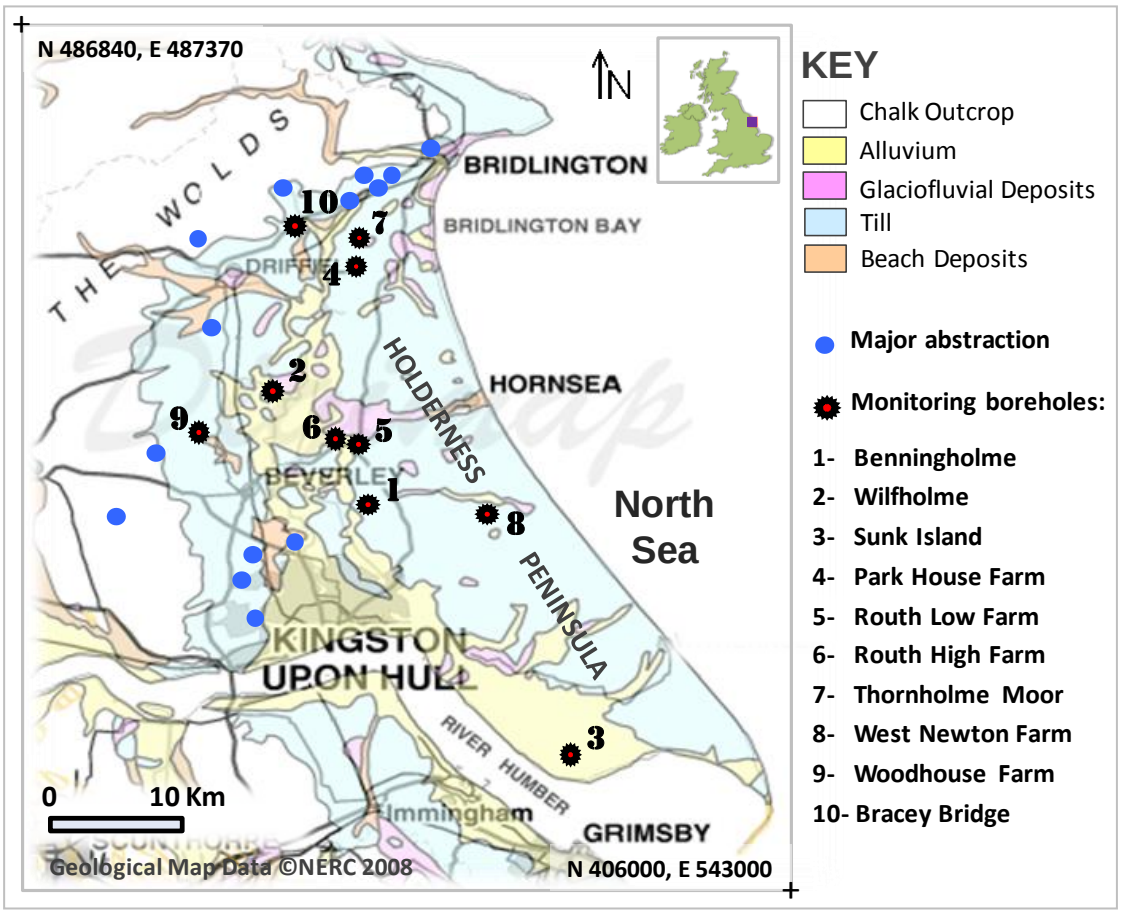

Figure 8.1. Locations of monitoring boreholes and major abstractions together with superficial deposits [*Edina-Digimap "Geological Map Data © NERC 2008"*; *Smedley et al.*, 2004; *Gale and Rutter*, 2006].

Table 8.1. Best fit parameter values and ranges for each borehole: *BE* barometric efficiency, D_{con} vertical hydraulic diffusivity of confining layer, D_{unsat} vertical pneumatic diffusivity of confining layer, T_{aqu} aquifer transmissivity, T_{cf} capillary fringe coefficient and L_{unsat} thickness of unsaturated zone.

Borehole		*BE* (-)		D_{con} (m^2/day)		D_{unsat} (m^2/day)		T_{aqu} (m^2/day)		T_{cf} (-)		L_{unsat} (m)	
		Best	Range	Best	Range	Best	Range	Best	Range	Best	Range	Best	Range
1	Benningholme	0.49	0.49	10.0	8.0–13.0	10.0	≥ 2.0	1.5	1.2-1.9	0.82	0.7-0.9	1.20	0.50–2.00
2	Wilfholme-M1	0.47	0.45-0.49	25.0	23.0–30.0	6.0	5.5–7.0	2.5	2.5–5.0	1.0	0.98–1.0	2.15	2.00 –2.30
	Wilfholme-M2	0.47	0.45-0.49	25.0	23.0–30.0	6.0	5.5–7.0	2.5	2.5–5.0	1.0	0.98–1.0	2.15	2.00 –2.30
	Wilfholme-M3	0.47	0.47	25.0	24.0 – 25.0	6.0	6.0 – 7.0	3.0	≥ 3.0	0.94	0.93 – 0.98	2.30	2.20 - 2.30
3	Sunk Island	0.39	0.37-0.39	15.0	≤ 25.0	0.9	≥ 0.15	1.8	≥ 1.8	0.40	0.25–0.81	1.70	≤ 3.50
4	Park House Farm	0.56	0.52-0.58	224.0	190.0-325.0	10.8	9.0–15.0	0.7	0.4-2.5	0.95	0.85–1.0	2.33	2.00-2.60
5	Routh Low Farm	0.42	0.38-0.45	34.6	25.0-45.0	8.9	6.0-15.0	0.001	0.001-0.002	0.87	0.65-1.0	3.15	2.70-2.30
6	Routh High Farm	0.51	0.5-0.53	133.2	120.0-160.0	12.3	10.0-15.0	0.008	0.007-0.008	0.79	0.78-0.82	2.29	2.10-2.50
7	Thornholme Moor	0.39	0.38-0.40	310.0	250.0-370.0	50.0	≥ 20.0	10.5	5.0-90.0	0.95	0.93-0.97	0.70	≤ 1.50
8	West Newton Farm	0.55	0.53-0.58	121.1	80.0-180.0	50.0	≥ 15.0	5.0	≥ 1.5	1.0	0.9-1.0	2.40	≤ 5.0
9	Woodhouse Farm	0.15	0.0-1.00	5.0×10^4	$\geq 3.0\times10^3$	12.0	10.0-15.0	10.0	≥ 0.1	0.89	0.85-0.92	0.72	0.65-0.75
10	Bracy Bridge	0.0	0.0-0.05	2.0×10^4	$\geq 7.0\times10^3$	128.0	110.0-140.0	3.0	≥ 3.0	0.98	0.98	1.56	1.10-2.00

8.2. Benningholme borehole

This borehole is situated 13 km from the edge of the confined aquifer, see Figure 8.1. The log of the Benningholme borehole (Figure 8.2b) shows that the confined layer is dominated by 16 m of clay-rich sediments. The estimated barometric response function gain and phase with one standard deviation errors are plotted in Figure 8.2a together with the best fit model curve. The barometric response function is determined over a relatively wide frequency band from 0.017 to 1.0 cycles/day. Gain ranges from 0.4 to 0.51 and phase from -187º to -169º. Two stages of response can be observed. At low frequencies up to ~0.09 cycles/day, the response shows gain attenuation and phase advance with decreasing frequency and above ~0.09 cycles/day gradual gain decrease and phase lag is observed with increasing frequency. There is some indication of a static confined plateau at intermediate frequencies, (stage B in Figure 7.2). The overall shape of the estimated barometric response function is in agreement with the theoretical best fit curve where gain is bell shaped and phase is monotonic. The phase fit is better than the gain fit, as the gain at low frequencies tends to show lower values than the model.

To obtain the best fit model curve, the unsaturated zone thickness, L_{unsat}, was constrained with upper and lower bounds of 2.5 m and 1.0 m based on data collected during field visits (2008-2010) from an adjacent shallow borehole (3.8 m deep) which taps the glacial sediments cover. Figure 8.2a also shows two model curves; one of them indicates upper bound for D_{con} (13 m^2/day) and lower bound for T_{aqu} (1.2 m^2/day), while the other curve indicates lower bound for D_{con} (8 m^2/day) and upper bound for T_{aqu} (1.9 m^2/day). Changing D_{con} affects the low frequency response (< 0.2 cycles/day) while changing T_{aqu} affects only the high frequency response (> 0.2 cycles/day). Only a lower bound to vertical pneumatic diffusivity is determined due to model insensitivity. Estimated model value for the static barometric efficiency (BE = 49.0%) is in good agreement with short-term barometric efficiency ($\propto_s$= 47.9%±3.37%) estimated using linear regression (see Chapter 6, section 6.2). The estimated value of horizontal aquifer transmissivity of 1.5 (1.2-1.9) m^2/day, is significantly lower than the value of 52.0 m^2/day from a 5 hour pumping test [*Parker*, 2009].

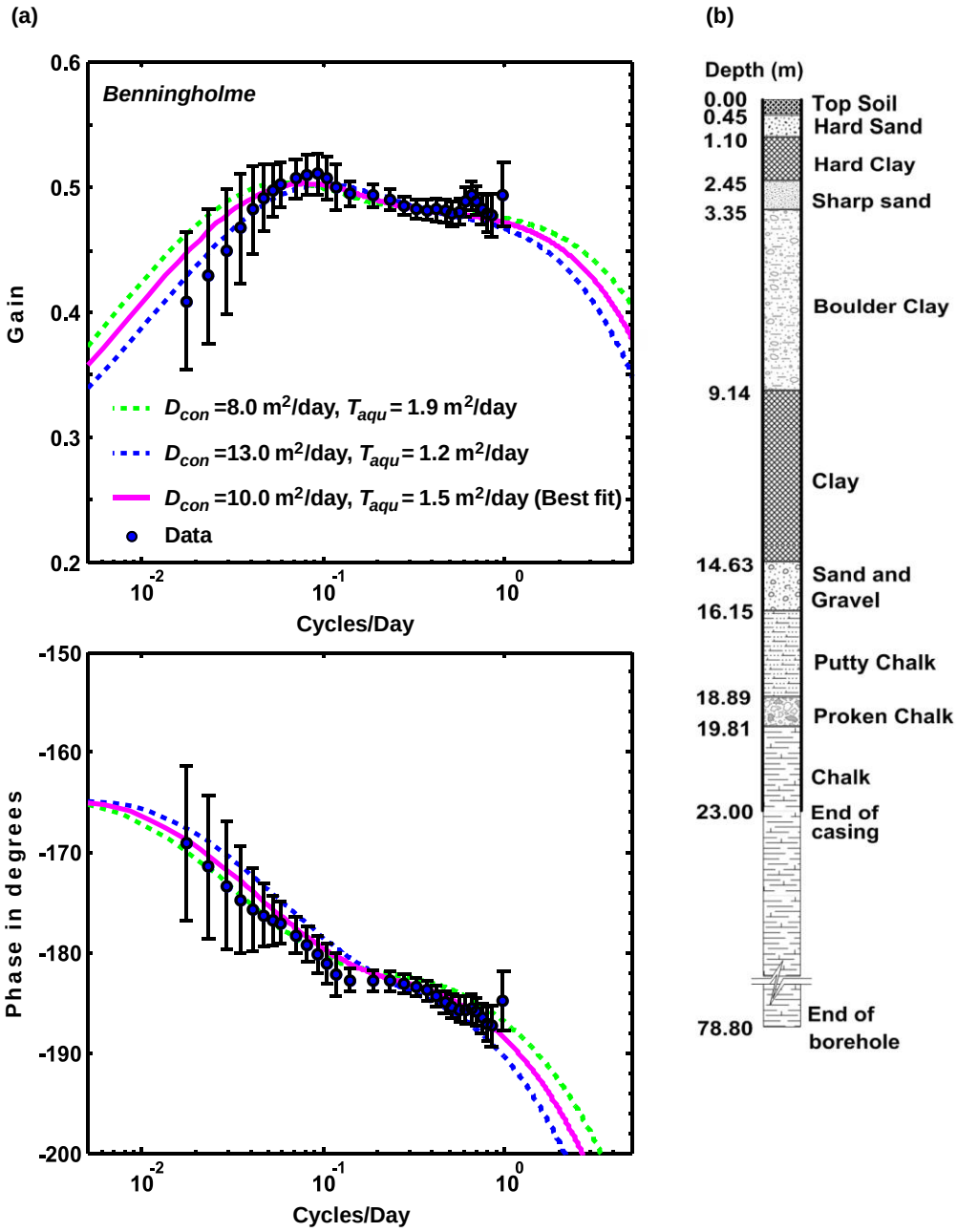

Figure 8.2. Results for the Benningholme borehole, record length 799 days; a) barometric response function with best fit theoretical models. The best fit curve (solid magenta) is shown together with two model curves (dashed) giving upper (blue) and lower (green) bounds for vertical hydraulic diffusivity of confining layer, D_{con}, (8-13 m^2/day), and aquifer transmissivity, T_{aqu}, (1.2-1.9 m^2/day). (b) Lithology log for Benningholme borehole (data provided by EA).

8.3. Wilfholme boreholes (M1, M2 and M3): A huddle test

The boreholes at Wilfholme are situated 9.5 km from the edge of the confined aquifer, see Figure 8.1. The main aim of analyzing these three boreholes (M1, M2 and M3) which are arranged in a triangle 43 m apart from each other (see Figure 8.3a) is to compare the results of closely spaced boreholes. This provides a "huddle test" in which the barometric response functions from these three closely spaced boreholes can be compared. The lithology penetrated by these boreholes, shown in Figure 8.3b, is for the central borehole P (Figure 8.3a) and shows a confining layer of 11.5 m dominated by boulder clay. Electromagnetic surveys and resistivity profiling show little variation in composition of confining layer over the three boreholes with thicknesses ranging from 10 m to 13 m [*Hartmann,* 2004]. Therefore relatively constant properties of confining layer would be anticipated. This is in good agreement with results where derived parameters for these three boreholes are very similar, especially M1 and M2, see Figure 8.4a. It is important to note that the recorded time series for M3 (2.2 years) is about three times longer than for M1 and M2 (0.76 years). The examined frequency band for these three boreholes is 0.025 to 2 cycles/day as shown in Figure 8.4. The estimated barometric response functions for the three boreholes show strong dependence on frequency, with gain ranging from 0.31 to 0.5 and phase ranging from -189º to -157º, Figure 8.4. A single stage of increasing gain and decreasing phase with increasing frequency is observed. For all three boreholes, the estimated barometric response function shape is in overall agreement with the theoretical best fit curve which shows a bell shaped gain when extended beyond the frequency range of estimated barometric response function. Data points in the frequency band 0.025-0.05 cycles/day were excluded from the fitting process as they show values that are not consistent with any possible model curve at low frequency.

The best fit model value for the static barometric efficiency (*BE*) for M1, M2 and M3 is 47.0% and larger by about 10% than the short-term barometric efficiency, $\propto_s$, (38-39%, see Table 6.1), estimated using linear regression. Figure 8.4b shows a *BE* range of 0.45-0.49. As shown in Table 8.1, for the three boreholes the best fit and range for vertical hydraulic diffusivity, D_{con}, of the saturated confining layer is 25 (23-30) m^2/day and the sensitivity to this parameter for M2 borehole is shown in figures 8.4c. It is estimated that the capillary fringe effect (T_{cf}) attenuates up to 7.5% of the air

pressure wave (Figure 8.4d). At M3 borehole the estimated horizontal aquifer transmissivity, T_{aqu}, is 3 m^2/day which is a lower bound only as the fit is not sensitive to larger values of this parameter. This is shown in Figure 8.4d, where curve achieved using T_{aqu} value of 3000 m^2/day still fits the observed barometric response function within one standard deviation error bars. The estimated range for aquifer transmissivity, T_{aqu}, at M1 and M2 is similar at 2.5 m^2/day constrained with upper and lower bounds of 2.5 to 5.0 m^2/day. These values for aquifer transmissivity are much lower than pumping test results of ~500 m^2/day [*Hartman*, 2004].

8.4. Sunk Island borehole

This borehole is located in the eastern part of the aquifer 30 km far from the edge of the confined aquifer. The log shows 34 m of glacial deposits (Figure 8.5b) with a wide range of sediment type (gravel, sand, silt and clay). The estimated barometric response function together with the best fit model curve are shown in Figure 8.5a. The frequency band of barometric response function is 0.017 to 0.65 cycles/day as above 0.65 cycles/day, the signal amplitude is below the threshold of 0.03 cmH_2O. The gain ranges from 0.36 to 0.4 and phase from -183º to -179º degrees. In general, the estimated barometric response function is somewhat noisy and shows close to confined behavior with little frequency dependence, although at low frequencies (< 0.07 cycles/day) a small gain attenuation and phase lag is observed.

Only a lower bound to vertical pneumatic diffusivity, D_{unsat}, and an upper bound to thickness of unsaturated zone, L_{unsat}, are determined due to the model insensitivity at low frequencies. Estimated best fit value for horizontal aquifer transmissivity, T_{aqu}, (1.8 m^2/day) is an order of magnitude less than pumping test result of 10.70 m^2/day [*Straughton*, 2008]. The best fit model is not sensitive to this parameter due to the lack of data points at higher frequencies and therefore an upper bound is not determined.

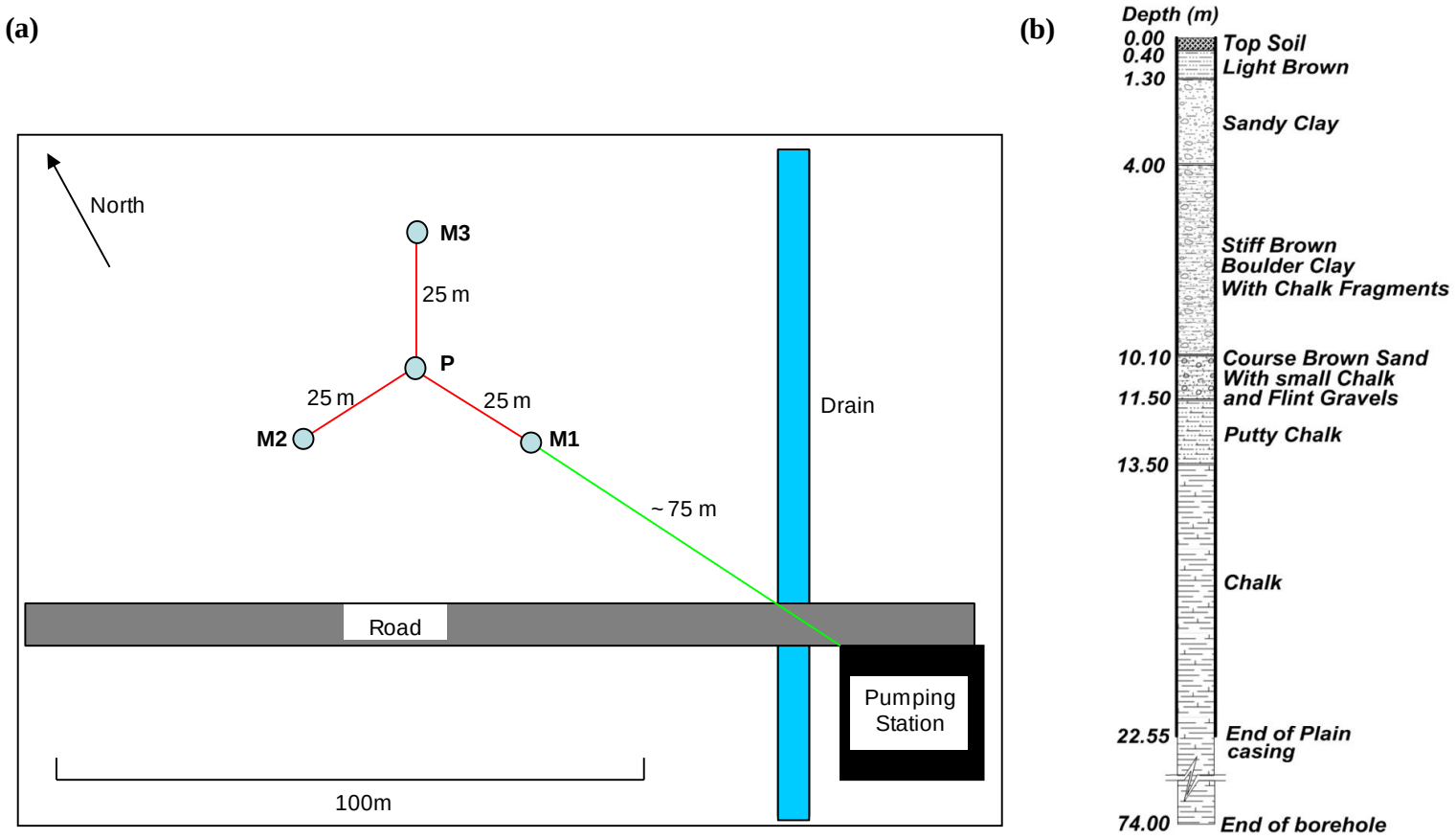

Figure 8.3. (a) Wilfholme site showing locations of M1, M2, M3 (43 m apart) and P borehole, adapted from *Hartmann* [2004]. (b) Lithology log for borehole P after [*Hartmann*, 2004]. Depths of base casing for M1, M2 and M3 are 26.15, 26.20 and 22.55m respectively.

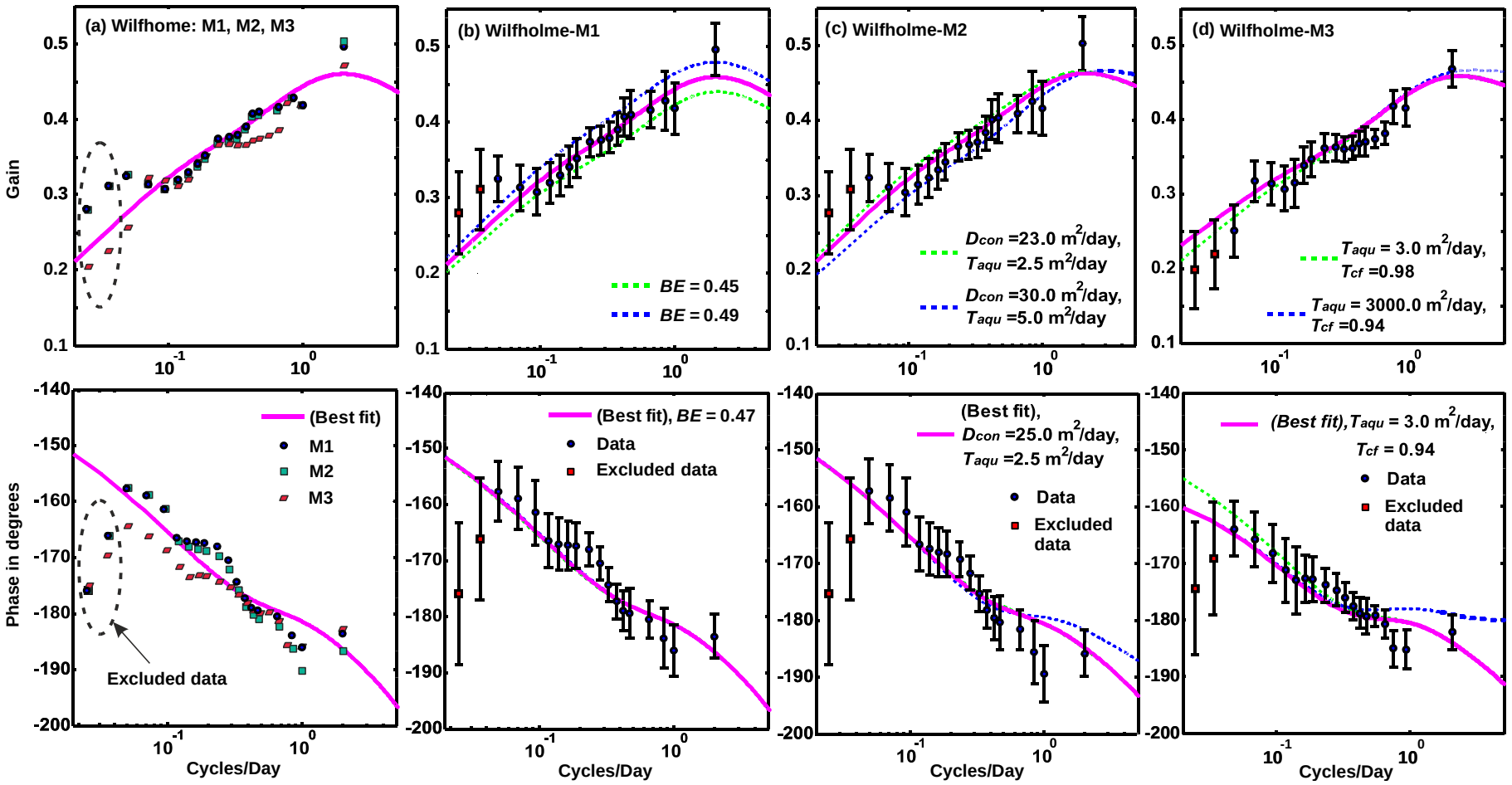

Figure 8.4. Wilfholme boreholes results; magenta curves are best model fits, and blue and green curves represent upper and lower bounds. (a) M1, M2 and M3 with best fit curves. (b) M1, best fit and two model curves for range of *BE* (0.45-0.49). (b) M2, best fit and two model curves for range of D_{con} (23-30) and T_{aqu} (2.5-5) in m^2/day. (c) M3, best fit and two model curves for range of T_{cf} (0.94-0.98) and T_{aqu} (3-3000) m^2/day.

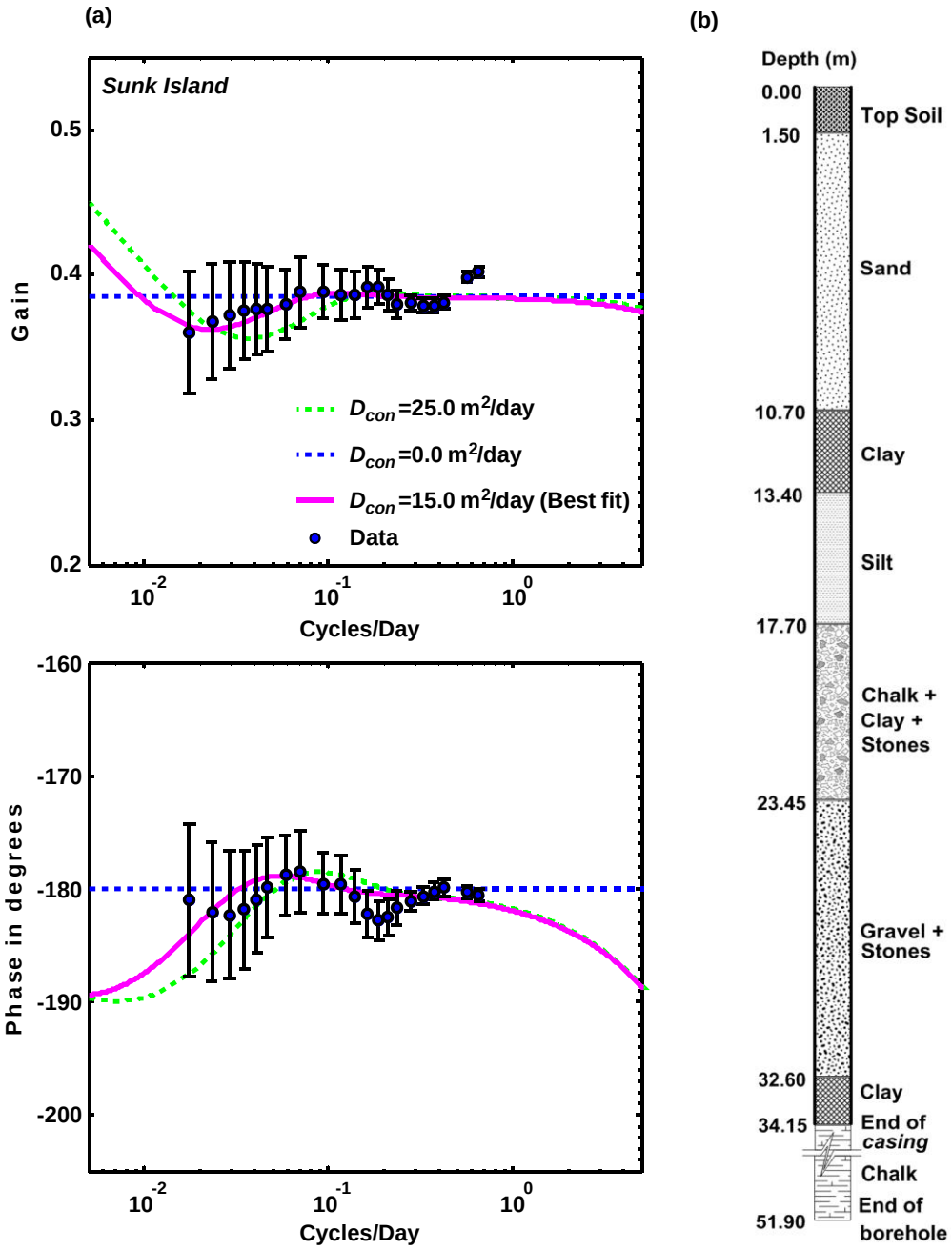

Figure 8.5. Results for Sunk Island borehole, record length 734 days; a) barometric response function with best fit theoretical models. The best fit curve (solid magenta) is shown together with two model curves (dashed) giving upper boundary (green) for vertical hydraulic diffusivity, D_{con}, (25 m^2/day) and a fully confined model (blue) using D_{con}= 0.0 m^2/day and T_{aqu} = 500.0 m^2/day. (b) Lithology log for Sunk Island borehole (data provided by BGS).

Only an upper bound to vertical hydraulic diffusivity, D_{con}, is determined (25.0 m^2/day), as shown in Figure 8.5a. This is because it is possible to fit a fully confined model (with gain of 0.39 and phase of -180°) lying within the error bars of the barometric response function, using a vertical hydraulic diffusivity of zero. Note that in order to do this, a high value for aquifer transmissivity (500 m^2/day) is required to flatten both gain and phase curves at the high frequency stage (C), i.e. to extend the intermediate frequency stage (B) to higher frequencies, see Figures 7.2 and 7.3. The estimated model value for the static barometric efficiency (*BE*=39.0%) is in good agreement with the short-term barometric efficiency ($\propto_s$=39.08±0.13%) estimated using linear regression, Chapter 6. The best fit capillary fringe attenuation (T_{cf}) is 60% of the air pressure wave, but due to the large error bars on the barometric response function at low frequencies this parameter is not well constrained (range of 19%-75%).

8.5. Park House Farm borehole

This borehole is situated 6.5 km from the edge of the confined aquifer, see Figure 8.1. The borehole log shows that the majority of the overlying glacial sediments (20.4 m thick) are composed of clay-rich sediments, as shown in Figure 8.6b. The best fit model curve to the estimated barometric response function is shown in Figure 8.6a. The observed gain and phase ranges from 0.37 to 0.46 and -192º to -164º respectively over a frequency range of 0.095 to 0.85 cycles/day. Data points in the frequency band 0.035-0.095 cycles/day where excluded in the fitting process as gain values are not consistent with any possible model curves at low frequency. Apart from these excluded points, the barometric response function shows a monotonic gain increase and phase decrease with increasing frequency. The water level signal at this borehole is significantly affected by local pumping activities, which were not possible to correct, occurring over a wide frequency band. This explains the large error bars which are due to reduced coherence between the water level and barometric pressure signals especially at high frequencies.

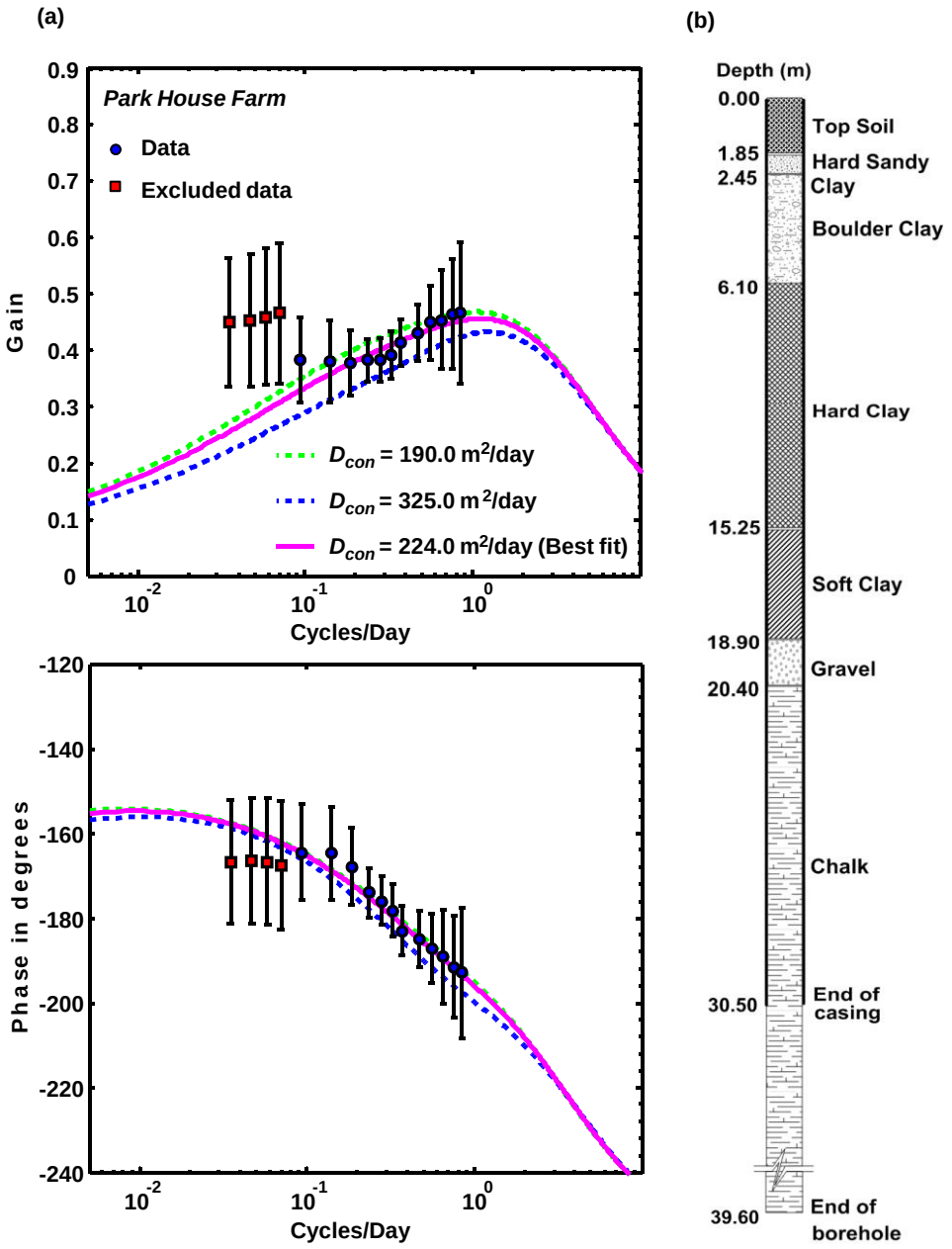

Figure 8.6. Results for Park House Farm borehole, record length 324 days. a) Barometric response function with best fit theoretical models. The best fit model curve (magenta) is shown together with two model curves (dashed) giving upper (blue) and lower (green) bounds for vertical hydraulic diffusivity, D_{con}, (190-325 m^2/day). (b) Lithology log for Park House Farm borehole (data provided by EA).

The estimated best fit model value for the static barometric efficiency (*BE*=56.0%) is larger than the short-term barometric efficiency ($\propto_s$=41.82±0.82%) estimated using linear regression (see Chapter 6). The estimated vertical hydraulic diffusivity, D_{con}, of the saturated confining layer is 224 (190 – 325) m^2/day and curves for upper and lower bounds for this parameter are shown in Figure 8.6a. These high values of diffusivity are not consistent with the confining layer lithology from the borehole log which includes 16.5 m of clay, suggesting low hydraulic diffusivity. Estimated horizontal aquifer transmissivity, T_{aqu}, is 0.7 (0.4-2.5) m^2/day which is similar to other boreholes, but no pumping test data is available here.

8.6. Thornholme Moor borehole

This borehole is situated 4.5 km from the edge of the confined aquifer, about 2.5 km south of the Park House Farm borehole, see Figure 8.1. The majority of the overlying glacial sediments (19.0 m thick) at this borehole are composed of clay-rich sediments as shown in Figure 8.7b. The best fit model curve to the estimated barometric response function is shown in Figure 8.7a. The observed gain and phase ranges from 0.27 to 0.42 and -159º to -182º respectively over a frequency range of 0.045 to 2.0 cycles/day. The overall shape of barometric response function is in good agreement with the theoretical best fit curve and shows gain increase and phase decrease with increasing frequency.

The estimated static barometric efficiency (*BE* = 39.0%) is in good agreement with the short-term barometric efficiency ($\propto_s$=37.2%±0.20%) estimated using linear regression (see Chapter 6). Only a lower bound to vertical pneumatic diffusivity and an upper bound to thickness of the unsaturated zone are determined due to the model insensitivity to constrain these parameters. The estimated vertical hydraulic diffusivity of the saturated confining layer, D_{con}, is 310.0 (250-370) m^2/day and not consistent with lithology log which contains 19 m of clay-rich sediments, suggesting a low hydraulic diffusivity. Model curves for this range of D_{con} are shown in Figure 8.7a. The estimated best fit value for horizontal aquifer transmissivity, T_{aqu}, is 10.5 m^2/day. No pumping test data is available at this borehole.

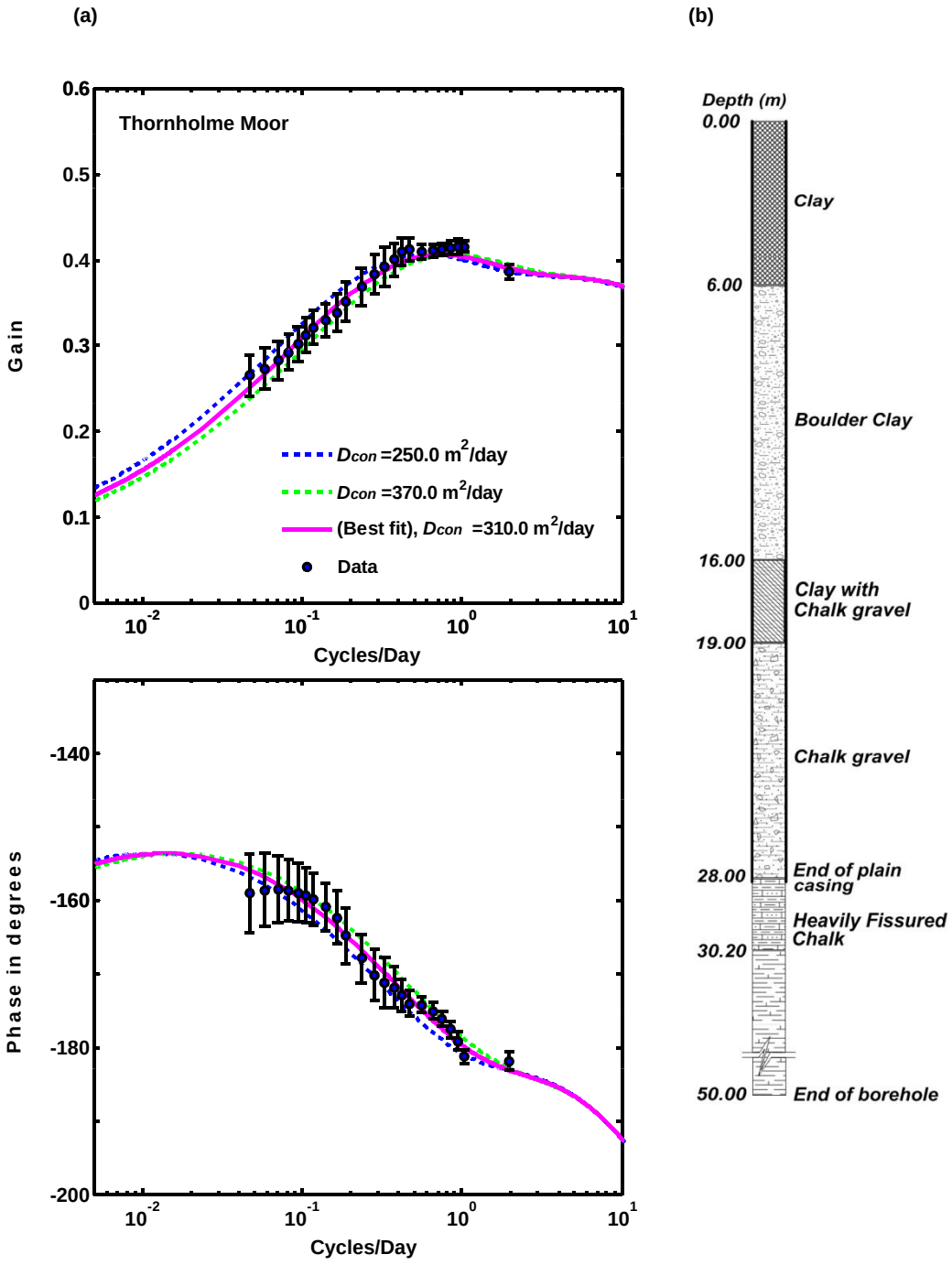

Figure 8.7. Results for Thornholme Moor borehole, record length 312 days. a) Barometric response function with best fit theoretical models. The best fit curve (solid magenta) is shown together with two model curves (dashed) giving upper (blue) and lower (green) bounds for vertical hydraulic diffusivity, D_{con}, (250-370 m^2/day). (b) Lithology log for Thornholme Moor borehole (data provided by EA).

8.7. Routh Low Farm borehole

This borehole is located in the center of the confined part of the aquifer, 2.2 km east of the Routh High Farm borehole (section 8.8), and 15.2 km from the confined edge as shown in Figure 8.1. The borehole log (provided by EA), shown in Figure 8.8b, shows 8 m of clay and 5.5 m of sand and gravel. The estimated barometric response function together with the best fit model curve are shown in Figure 8.8a. The barometric response function frequency band is 0.035 to 0.56 cycles/day. Frequencies above 0.56 cycles/day were excluded due to limitations of signals amplitude and coherence as explained in section 6.3.4. The gain ranges from 0.13 to 0.28 and phase from -182º to -253º degrees. The barometric response function shows strong dependence on frequency with monotonic gain and phase decrease with increasing frequency. The estimated barometric response function overall shape is in agreement with the theoretical best fit curve which shows a bell shaped gain when extended below the frequency range of estimated barometric response function.

The barometric response function shows low and high frequency responses, stages A and C in Figure 7.2, while the intermediate frequency response (stage B) is not present. This is due to the rather low transmissivity of the aquifer which dominates response stages at intermediate (B) and high (C) frequency stages. Figure 7.3b shows how very low aquifer transmissivity values, T_{aqu}, can cause the intermediate response stage (B) to disappear. This is reflected by the low and well constrained range of aquifer transmisivity, T_{aqu} = 0.001 (0.001-0.002) m^2/day. This is also supported by estimates of short-term (7.6%) and long-term (17.4%) barometric efficiencies, see section 6.2 and Table 6.1, which suggest limited flow between borehole and aquifer due to significant borehole storage or skin effects, or significantly low aquifer transmissivity. The estimated vertical hydraulic diffusivity, D_{con}, of the saturated confining layer is 34.6 (25.0–45.0) m^2/day, and model curves for this parameter range are shown in Figure 8.8a.

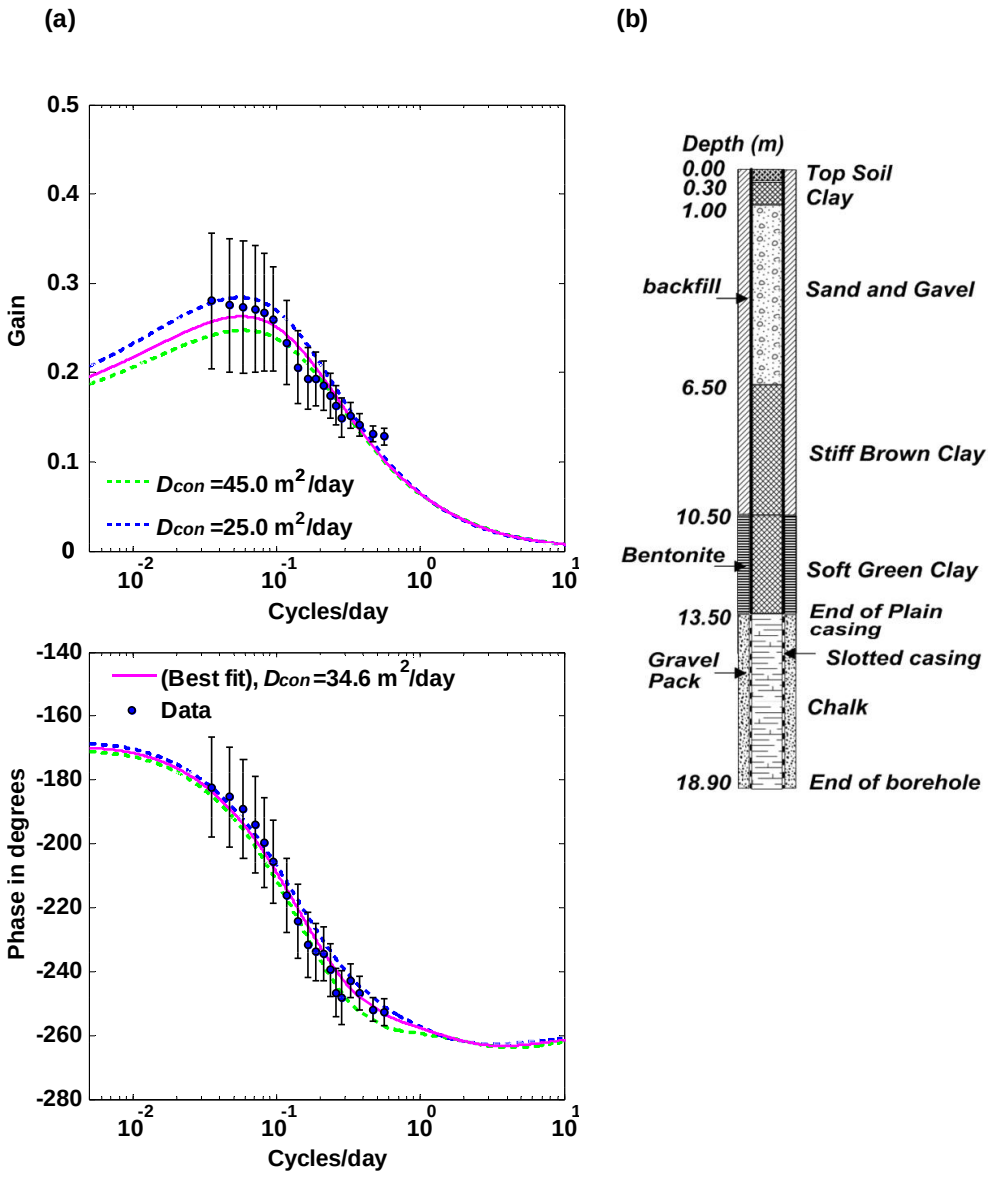

Figure 8.8. Results for Routh Low Farm borehole, record length 318 days. a) Barometric response function with best fit theoretical models. The best fit curve (solid magenta) is shown together with two model curves (dashed) giving upper (green) and lower (blue) bounds for vertical hydraulic diffusivity, D_{con}, (25-45 m^2/day). (b) Lithology log for Routh Low Farm borehole (data provided by EA). The end of borehole measured at field is 16.90 m.

8.8. Routh High Farm borehole

This borehole is situated 13 km from the edge of the confined aquifer, see Figure 8.1. According to data provided by the EA the lithology log at this borehole is the same as that for Routh Low Farm borehole, Figure 8.9b. The observed gain and phase ranges from 0.29 to 0.36 and from -169º to -227º respectively over a frequency range of 0.035 to 1.0 cycles/day. The estimated barometric response function shows strong dependence on frequency in agreement with the theoretical best fit curve and shows a bell shaped gain and monotonic phase lag with increasing frequency.

Similar to the Routh Low Farm borehole, the barometric response function at Routh High Farm borehole shows low and high frequency responses, stages A and C (Figure 7.2), while the intermediate frequency response (stage B) is not present due to the rather low transmissivity of the aquifer which dominates the response at intermediate and high frequency stages (B and C respectively). Estimated aquifer transmisivity, T_{aqu}= 0.008 (0.007-0.008) m^2/day, is low as at Routh Low Farm borehole. This is also supported by estimates of short-term (27.6%) and long-term (32.2%) barometric efficiencies see section 6.2 and Table 6.1, which suggest significant borehole storage or skin effects, or significantly low aquifer transmissivity. The estimated vertical hydraulic diffusivity of the saturated confining layer, D_{con}, is 133.2 (120-160) m^2/day, see Figure 8.9a. It is important to note that, although Routh High Farm and Routh Low Farm boreholes have similar lithology logs (according to EA records) and they are located only 2.2 km from each other, the barometric response functions are significantly different and the D_{con} estimate at Routh High Farm borehole is about four times larger than that of Routh Low Farm borehole.

8.9. West Newton Farm borehole

This borehole is located 22.5 km from the confined edge, see Figure 8.1, and penetrates the thickest (38 m) layer of clay-rich glacial sediments of all analyzed boreholes, Figure 8.10b. The observed gain and phase ranges from 0.45 to 0.68 and from -155º to -182º respectively over a frequency range of 0.023 to 2.0 cycles/day. The best fit model curve to the estimated barometric response function is shown in Figure 8.10a. The estimated barometric response function is rather noisy, particularly the gain, and the phase shows a better fit than the gain.

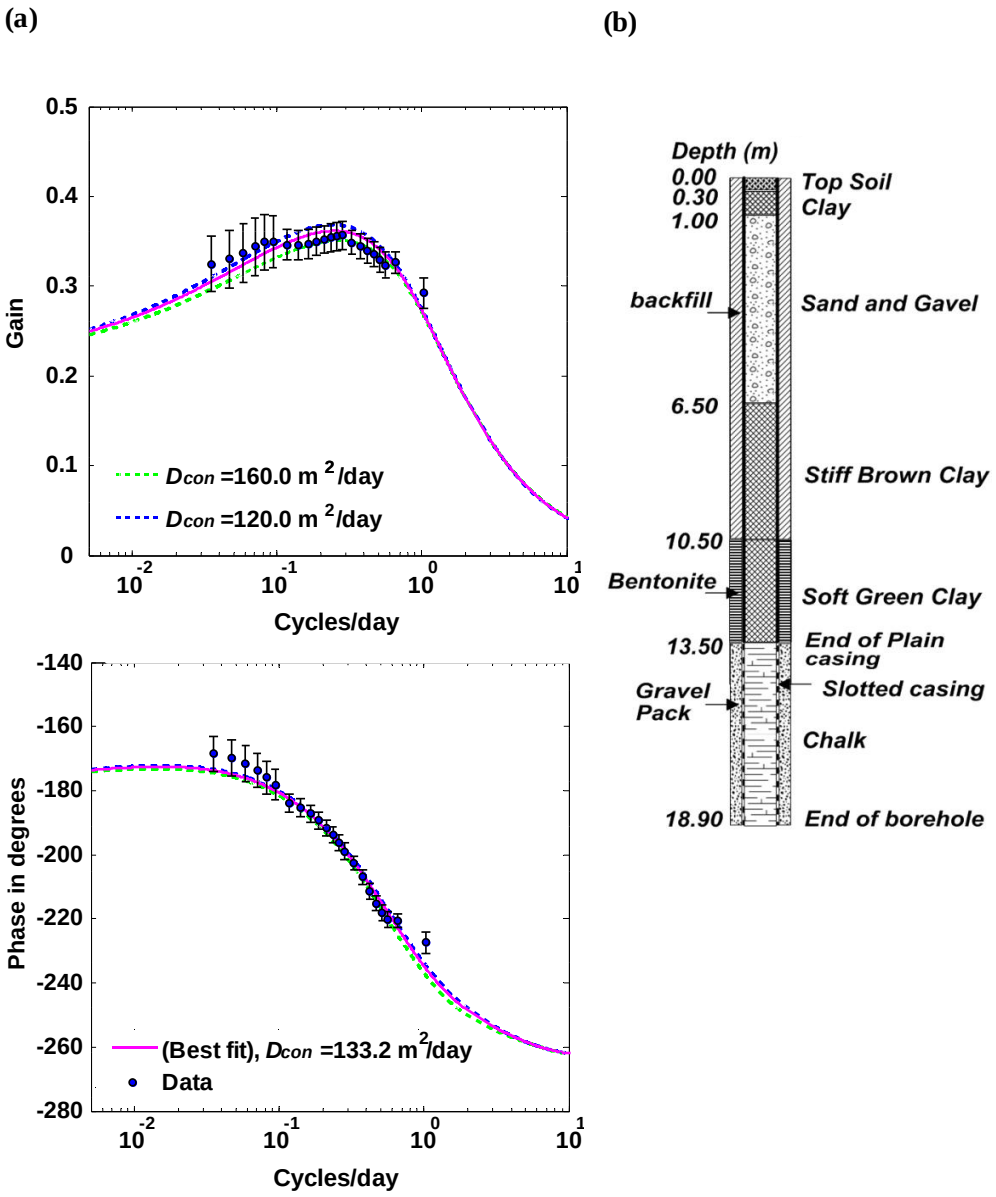

Figure 8.9. Results for Routh High Farm borehole, record length 313 days. a) Barometric response function with best fit theoretical models. The best fit curve (solid magenta) is shown together with two model curves (dashed) giving upper (green) and lower (blue) bounds for vertical hydraulic diffusivity, D_{con}, (120-160 m^2/day). (b) Lithology log for Routh High Farm borehole (data provided by EA).

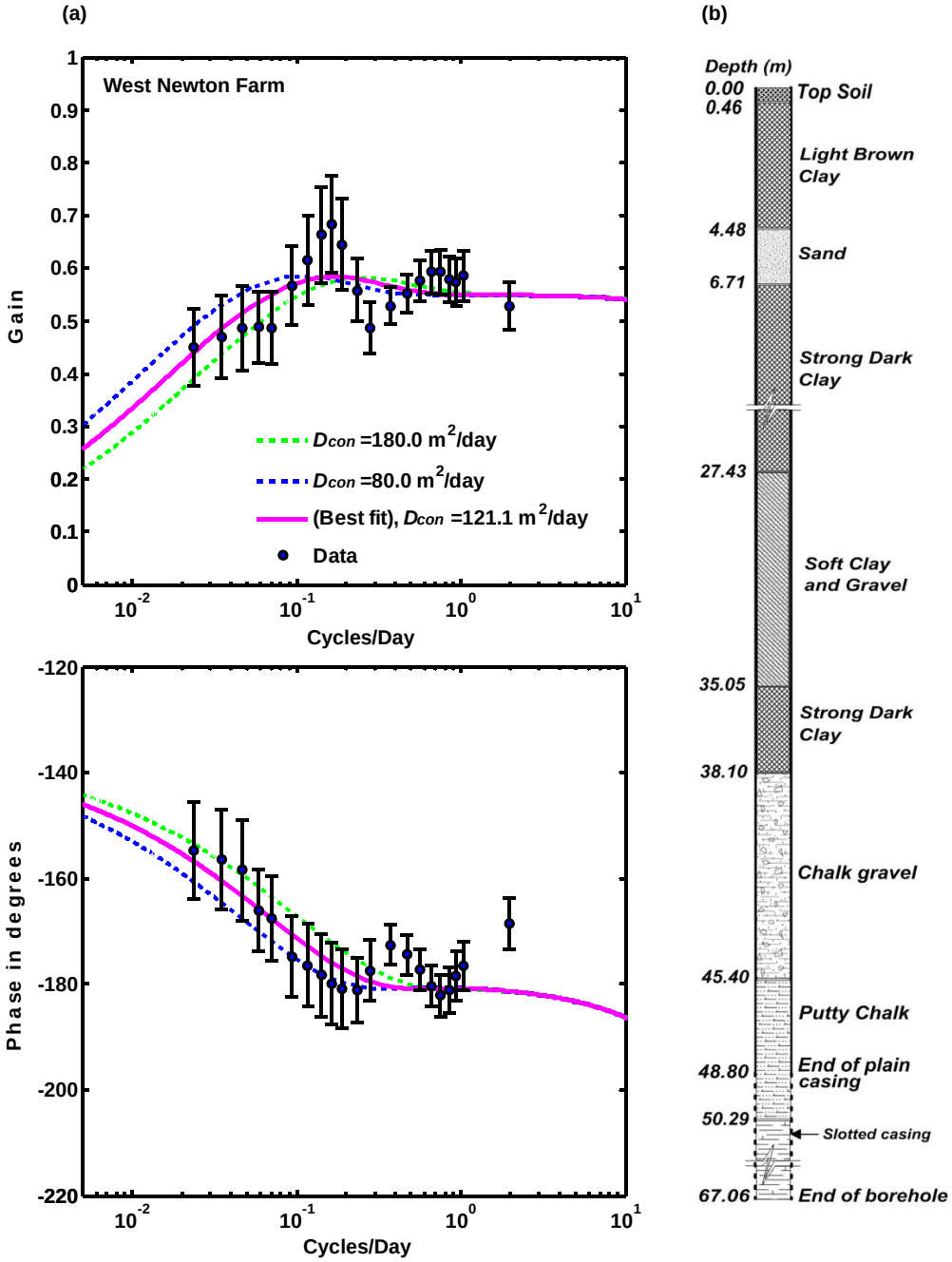

Figure 8.10. Results for West Newton Farm borehole, record length 677 days. a) Barometric response function with best fit theoretical models. The best fit curve (solid magenta) is shown together with two model curves (dashed) giving upper (blue) and lower (green) bounds for vertical hydraulic diffusivity, D_{con}, (80-180 m^2/day). (b) Lithology log for West Newton Farm borehole (data provided by EA).

The estimated static barometric efficiency (*BE* = 55.0%) is larger than short-term barometric efficiency ($\propto_s$=45.4%±0.14%) from linear regression (see Chapter 6, section 6.2). Only the lower bound to vertical pneumatic diffusivity, D_{unsat}, and upper bounds to thickness of unsaturated zone, L_{unsat}, and aquifer transmissivity, T_{aqu}, are determined due to the model insensitivity to constrain these parameters. The estimated vertical hydraulic diffusivity of the saturated confining layer, D_{con}, is 121.1 (80–180) m^2/day and model curves for this parameter range are shown in Figure 8.10a. This value is not consistent with the lithology log at this borehole, which is dominated by clay-rich sediments (Figure 8.10b), suggesting low diffusivity values and a high degree of confinement.

8.10. Woodhouse Farm borehole

This borehole is situated 3.3 km from the edge of the confined aquifer, see Figure 8.1. The glacial sediment cover at this borehole is the thinnest (4.4 m) of all analyzed boreholes, and is comprised of sandy clay and boulder clay (Figure 8.11b). At this borehole, coherence between water level and barometric pressure is in the range of 0.1-0.3, the lowest coherence of all boreholes analyzed. Therefore, no coherence threshold was applied in selecting the final barometric response function and this is reflected in the large size of the error bars. The best fit model curve to the estimated barometric response function is shown in Figure 8.11a. The observed gain and phase ranges from 0.09 to 0.27 and from -204º to -220º respectively over a frequency range of 0.05 to 2.0 cycles/day.

The best fit model curve shows that the barometric response function represents the low frequency end (stage A, Figure 7.2). Estimated static barometric efficiency (*BE*) is 15% but poorly constrained (0%-100%) due to the weak sensitivity of the model to this parameter. However this value for barometric efficiency is in good agreement with the short-term barometric efficiency ($\propto_s$=13.62%±1.40%) estimated using linear regression (see Chapter 6, section 6.2).

The estimated vertical hydraulic diffusivity of the saturated confining layer, D_{con}, 5.0×10^4 ($\geq 3.0\times10^3$) m^2/day, is the largest of all analyzed boreholes by two to three orders of magnitude with a lower bound only due to model insensitivity to larger values of this parameter. Model curves for this parameter range are shown in Figure 8.11a and the model insensitivity to large values is shown by using a rather high value of 5×10^7 m^2/day, which gave a model curve that still lie between the one standard error bars. The high value of hydraulic diffusivity is consistent with the thin cover of glacial sediments at this borehole although this cover is composed of clay-rich sediments that would suggest a relatively low value for diffusivity. Aquifer transmissivity is estimated at 10 m^2/day with only a lower bound to the aquifer transmissivity (0.1 m^2/day) is determined due to the model insensitivity to large values of this parameter. No pumping test data is available at this borehole.

8.11. Bracy Bridge borehole

This borehole is the nearest of all boreholes analyzed to the confined edge at 0.9 km, see Figure 8.1. The thickness of glacial sediment cover at this borehole is 9.6 m and is composed of chalk gravel and boulder clay as shown in Figure 8.12b. At this borehole, coherence between water levels and barometric pressure was low, in the range 0.1-0.45. The coherence threshold applied here to select the final barometric response function was 0.2, which excludes the frequency range of 0.07-0.18 cycles/day, Figure 8.13. The best fit model curve to the estimated barometric response function is shown in Figure 8.12a. The gain and phase ranges from 0.03 to 0.11 and -157º to -255º respectively over a frequency range of 0.05 to 2.0 cycles/day. The fit for both gain and phase is good above a frequency of 0.23 cycles/day.

Similar to Woodhouse Farm borehole, the best fit curve at Bracy Bridge shows that the barometric response function represents low frequencies (stage A, Figure 7.2). The estimated static barometric efficiency (*BE*) is 0.0 % (0.0-5.0) which is in reasonable agreement with low short-term barometric efficiency ($\propto_s$=2.2%±2.31%) estimated using linear regression (see Chapter 6, section 6.2).

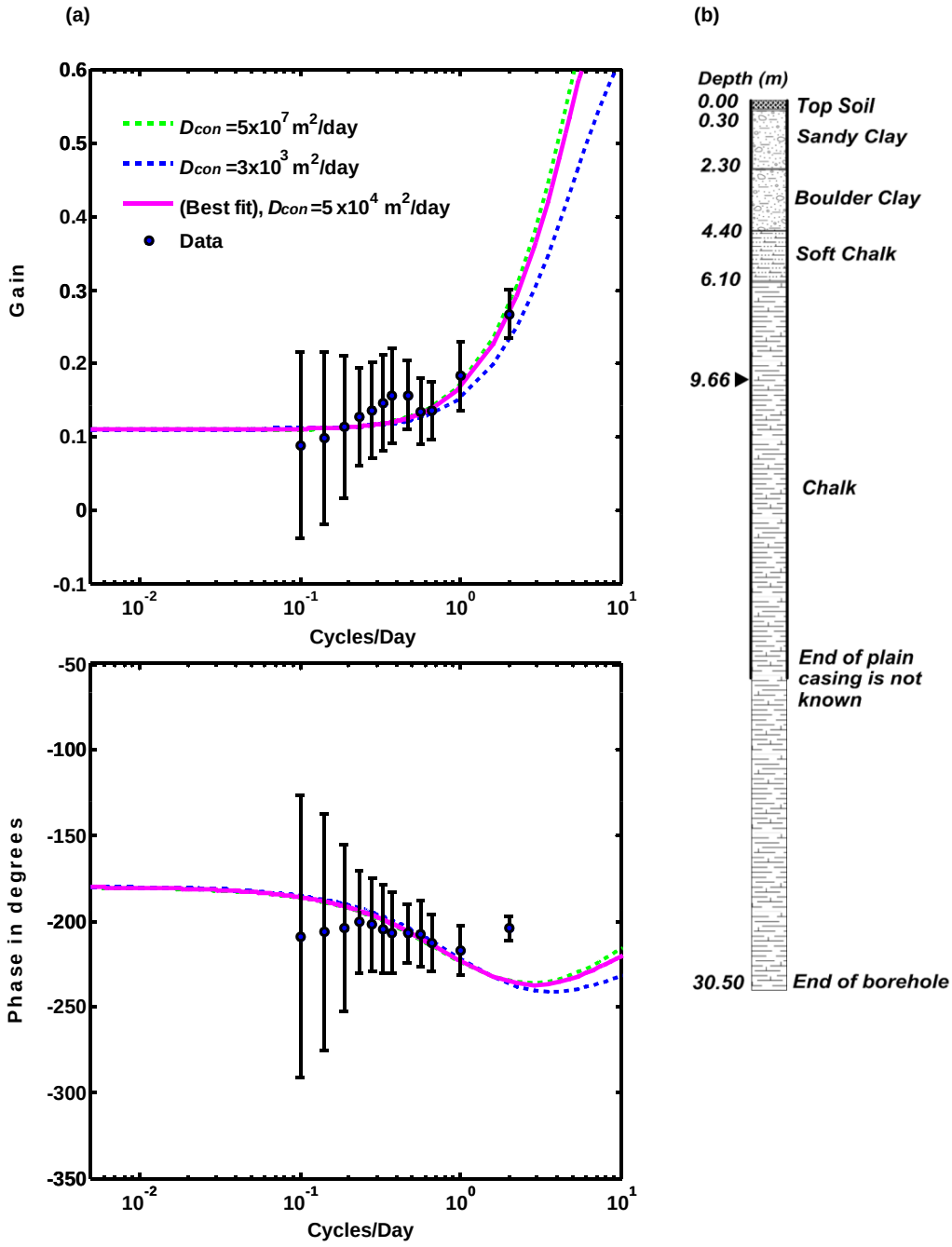

Figure 8.11. Results for Woodhouse Farm borehole, record length 294 days. a) Barometric response function with best fit theoretical models. The best fit curve (solid magenta) is shown together with two model curves (dashed) giving upper (blue) and lower (green) bounds for vertical hydraulic diffusivity, D_{con}, (3×10^3-5×10^7 m^2/day). (b) Lithology log for Woodhouse Farm borehole (data provided by EA).

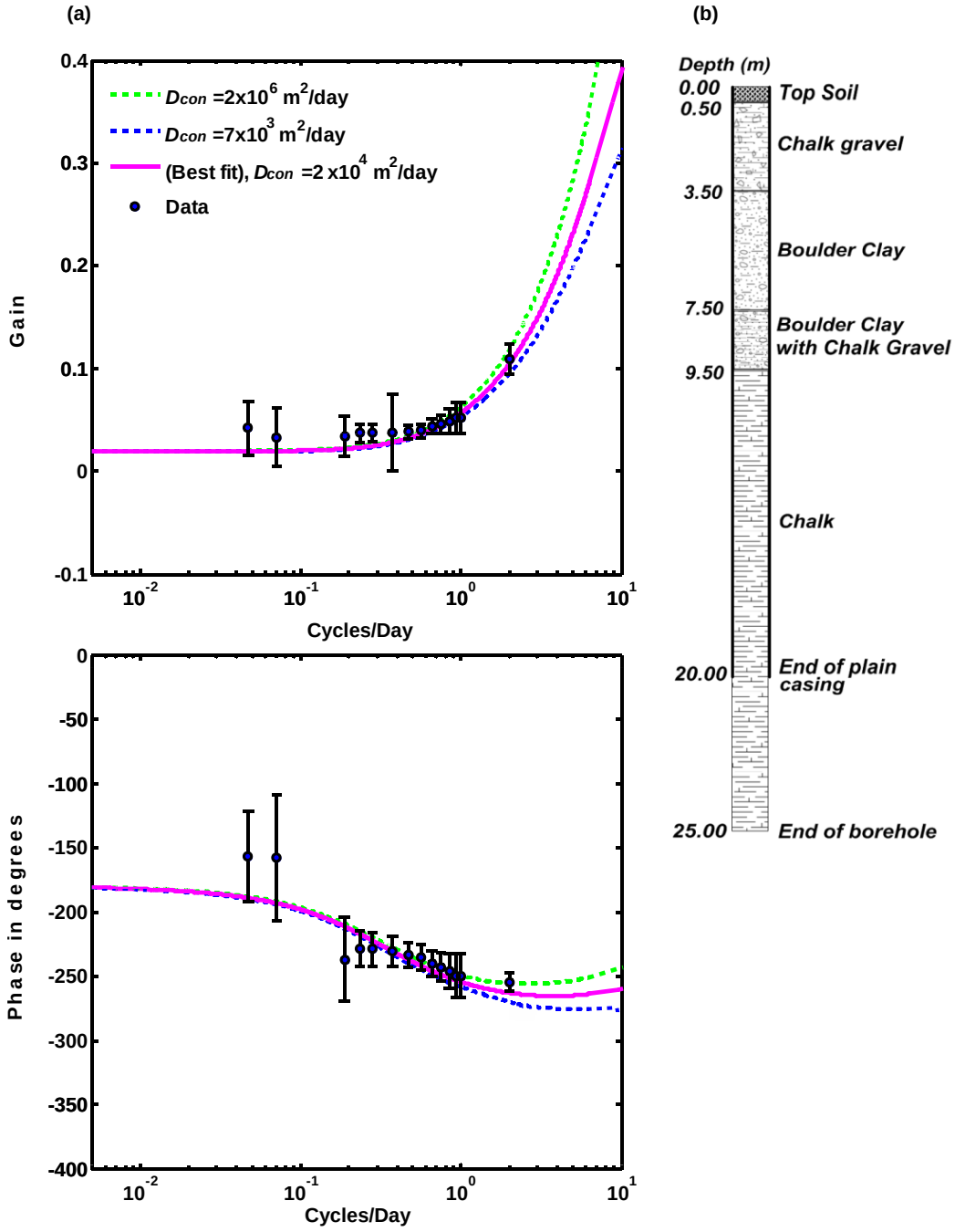

Figure 8.12. Results for Bracy Bridge borehole, record length 310 days. a) Barometric response function with best fit theoretical models. The best fit curve (solid magenta) is shown together with two model curves (dashed) giving upper (blue) and lower (green) bounds for vertical hydraulic diffusivity, D_{con}, (7×10^{3}-2×10^{6} m^2/day). (b) Lithology log for Bracy Bridge borehole (data provided by EA).

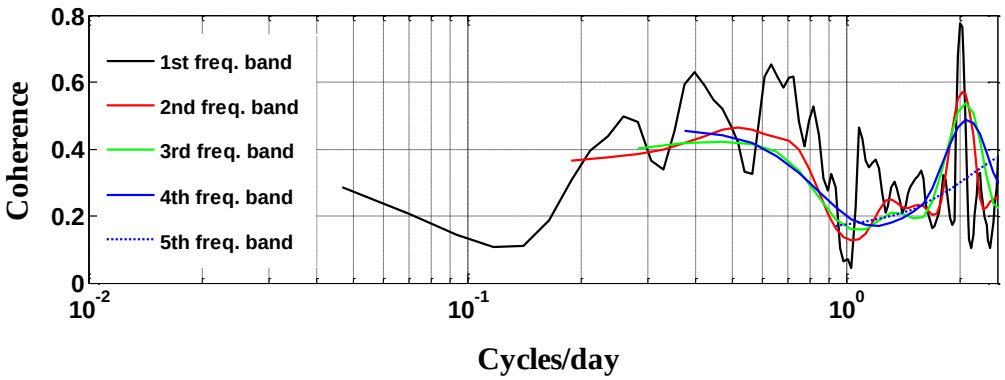

Figure 8.13. Coherence between water levels and barometric pressure at Bracy Bridge borehole for five overlapping frequency bands. Coherence range is 0.1-0.45 and a threshold at 0.2 excludes the frequency range of 0.07-0.18 cycles/day.

The estimated vertical hydraulic diffusivity of the saturated confining layer, D_{con}, of 2.0×10^4 ($\geq 7.0\times10^3$) m^2/day, is very high and of the same order of magnitude as that of Woodhouse Farm borehole (5.0×10^4 m^2/day). These are two to three orders of magnitude larger than that of the other boreholes. Only lower bound to hydraulic diffusivity, D_{con}, is determined due to model insensitivity to larger values. This illustrated by using a rather high value of 2×10^6 m^2/day, which gave a model curve that still lies within the one standard error bars, Figure 8.12a. To obtain the best fit, the unsaturated zone thickness was constrained to lie between 1 and 2 m based on EA records (for the year 2010) from a nearby borehole which taps the glacial sediments cover. The estimated pneumatic diffusivity at this borehole, 128 (110-140) m^2/day, is the highest of all analyzed boreholes which is consistent with lithology in the unsaturated zone of top soil and chalk gravel.

8.12. Summary

Results for twelve selected boreholes show a wide range of barometric response functions. At the Wilfhome (M1, M2 and M3) and Park House Farm boreholes, a few data points at the low frequency end of the barometric response function were excluded from the fitting as they lie far from any possible model curves. This can be due to heterogeneity of the confining layer which is not incorporated in the theoretical model by *Rojstaczer* [1988a] or due to other interferences like pumping which is observed at both locations. The role of confining layer heterogeneity is further explored in Chapter 9.

In some cases, it was possible to place only an upper or lower bound to parameters, see Table 8.1. In general, this is due to model insensitivity to larger or lower values of these parameters for model curves lying within the one standard error bars on the barometric response function. Only an upper bound was placed for hydraulic diffusivity, D_{con}, at Sunk Island (≤ 25 m^2/day), where the barometric response function is the flattest and where a fully confined model can be fitted using a D_{con} value of zero. At Woodhouse Farm and Bracy Bridge boreholes, located the nearest to the confined edge, it was only possible to estimate a lower bound for D_{con} ($\geq 3\times10^3$ m^2/day and $\geq 7\times10^3$ m^2/day), where model curves with very high values of this parameter can well fit the barometric response function within error bars. Only a lower bound for aquifer transmissivity, T_{aqu}, was obtained at five borehole, see Table 8.1. This is due to the lack of observed barometric response at high frequencies (stage C, Figure 7.2), which made it difficult to constrain this parameter. An exception to this is the Routh Low Farm and Routh High Farm boreholes where the high frequency stage C was observed due to the rather low transmissivity of the aquifer (0.001-0.008 m^2/day) which dominates the response.

The best fit range for the vertical hydraulic diffusivity, D_{con}, is from 10 m^2/day to 5.0×10^4 m^2/day. None of the boreholes show a purely confined behaviour at all frequencies, although nearly confined behaviour is observed at Sunk Island borehole and some sign of a confined plateau (Stage B, Figure 7.2) is observed at Benningholme borehole. Estimated values for this parameter are consistent with lithology logs at all boreholes except at Park House Farm, Thornholme Moor and West Newton Farm

boreholes. At these three boreholes, lithology logs are comprised of clay-rich sediments suggesting low diffusivity values whereas model values for hydraulic diffusivity are high. Estimated D_{con} value at Routh High Farm borehole is about four times larger than Routh Low Farm borehole although they have similar lithology logs. This conflict is likely to be due to the highly heterogeneous nature of the confining layer which is explored further in Chapters 9 and 10.

In general, estimated model values for aquifer transmissivity, T_{aqu}, (0.001-10.5 m^2/day) are up to six orders of magnitudes lower than results of pumping tests and prevailing hydrogeological knowledge of the East Yorkshire Chalk Aquifer. At Benningholme, Sunk Island and Wilfholme boreholes estimated values for this parameter (1.5, 1.8 and 2.5 m^2/day respectively) are one to two order of magnitude less than pumping tests results of 52, 10.7 and 500 m^2/day respectively [*Parker*, 2009; *Straughton*, 2008; *Hartman*, 2004]. The lowest estimates for aquifer transmissivity, T_{aqu}, of 0.001 m^2/day and 0.008 m^2/day were observed at Routh Low Farm and Routh High Farm boreholes respectively. This is further explored in Chapter 9.

Model estimates for static barometric efficiency, *BE*, are equal to or larger than both short-term ($\propto_S$) and long-term ($\propto_L$) barometric efficiencies estimated by linear regression analysis (see Chapter 6, section 6.2), but in better agreement with short-term barometric efficiency ($\propto_s$). The estimated model range for *BE* at Bracy Bridge and Woodhouse Farm boreholes, the nearest two boreholes to the confined edge, is 0.0%-0.15% which is much smaller compared to the range of 0.39%-0.56% at other boreholes. This is likely because these boreholes show nearly unconfined behaviour and consistent with the thin glacial sediments cover at these boreholes. A full comparison between model and linear regression barometric efficiencies is detailed in Chapter 10 (section 10.4).

Two main issues have emerged in this chapter and are explored in more detail in Chapter 9. The first is a discrepancy of up to six orders of magnitudes between model estimates for aquifer transmissivity, T_{aqu}, and results of pumping tests and prevailing hydrogeology knowledge of the East Yorkshire Chalk Aquifer. This is explored using

slug tests at five boreholes (section 9.2). The second conflict is the inconsistency between derived model values for confining layer diffusivity and boreholes lithology logs. This suggests that parameters derived from barometric response functions are likely to represent the confining layer properties not only in the immediate vicinity of the borehole but for an area surrounding the borehole. Therefore, the impact of confining layer heterogeneity on barometric response function is explored using a simple 2D flow modeling (section 9.3).

CHAPTER 9: IMPACT OF HETEROGNEITY AND BOREHOLE CONSTRUCTION ON BAROMETRIC RESPONSE FUNCTION

9.1. Introduction

This chapter presents further investigations of two issues which came to light within Chapter 8 where barometric response functions for twelve boreholes are presented and modelled to determine aquifer and confining layer properties. These are:-

i. Discrepancy in aquifer transmissivity determined from barometric response function and pumping tests. This is investigated using a series of slug tests at five boreholes; Benningholme, Wilfholme-M2, Sunk Island, Park House Farm and Routh Low Farm.
ii. Inconsistencies between estimated properties of confining layer and borehole lithology at some boreholes, e.g. at Park House Farm, Thornholme Moor and West Newton Farm. This is explored by employing a simple model to investigate the influence of confining layer heterogeneity on the barometric response function.

9.2. Model versus pumping test value of aquifer transmissivity

The estimated aquifer transmissivity, T_{aqu}, from the barometric response functions for all boreholes (0.001-10.5 m^2/day) are significantly lower than pumping tests values where available and the reported range of transmissivity (50 to 5000 m^2/day) from the Chalk Aquifer in East Yorkshire [*Smedley* et al., 2004; *Hartmann*, 2004; *Straughton*, 2008; *Parker*, 2009] by up to several orders of magnitude. Variations in borehole water levels due to barometric pressure changes is of the order of a centimetre whereas pumping tests induce drawdown of the order of a meter or more. To explore the discrepancies between the estimates of aquifer transmissivity from barometric response function analysis and pumping tests, a series of slug tests was performed at each borehole using slug volumes ranging from 0.37 to 20 liters to investigate aquifer response to variations in induced head change. Most slug tests were performed by adding volumes of water to the boreholes and a few by insertion/ removal of a metal bar to induce head change. Slug test data for borehole total head and barometric

pressure were collected using automatic pressure transducers at 1 second intervals. At Benningholme, Wilfholme-M2 and Sunk Island boreholes, barometric pressure changes over tests periods were very small due to the short duration of the performed slug tests (1-8 minutes). At Park House Farm and Routh Low Farm boreholes, test durations are larger, 1.5 and 8 hours respectively. Due to the short duration of the slug tests, only small changes in barometric pressure occurred. Therefore, barometric pressure was simply subtracted from the total head to obtain the water level signals which were used for further analysis.

Slug tests analyses were performed (with AquiferWin32 software) using three methods *Hvorslev* [1951] for full and partial penetration, *Cooper at al.,* [1967] for full penetration and KGS model *Hyder et al.,* [1994] for partial penetration. The Cooper at al. and KGS methods incorporates aquifer storage while the Hvorslev's method assumes negligible storage effects. Slug tests data at each borehole were analyzed by two methods, Hvorslev and another method according to borehole construction. A brief description of each method is explained below. For more details about these methods the reader is referred to [*Hyder et al.,* 1994; *Butler,* 1998; *Batu,* 1998; *Kruseman and Ridder,* 2000].

Cooper's method (full penetration)

The *Cooper et al.,* [1967] solution gives estimates for aquifer transmissivity and storativity and is based on the following main assumptions [*Batu,* 1998; *Kruseman and Ridder,* 2000]:

- The aquifer is confined and has an infinite areal extent.
- The aquifer is homogeneous and isotropic.
- The borehole fully penetrates the aquifer and has a finite diameter.
- The slug is introduced instantaneously to the borehole.

The analytical solution of the *Cooper et al.* [1967] method is shown in Equation 9.1 [*Butler,* 1998]:

$$H(t)/H_0 = f(\beta,\alpha) = \frac{8\alpha}{\pi^2}\int_0^\infty \exp\left(-\frac{\beta u^2}{\alpha}\right)\frac{1}{u\Delta(u)}\,du \ , \tag{9.1}$$

where: $H(t)$ is the head deviation from static at time *t*, H_0 is the initial head displacement at *t=0*, β is the dimensionless time parameter and α is the dimensionless storage parameter [*Butler*, 1998]:

$$\beta = K_r bt/r_c^2 \ , \tag{9.1a}$$

$$\alpha = r_w^2 S_s b/r_c^2 \ , \tag{9.1b}$$

where: K_r is the radial component of hydraulic conductivity, b is the aquifer thickness, r_c is the radius of borehole casing, r_w is the radius of borehole screen and S_s is the specific storage of the aquifer. As shown in Equation 9.1a, if r_w is almost equal to r_c, then $\alpha = S_s b$, thus α in this case is equal to the aquifer storage coefficient *S*. This is assumed to be the case for all boreholes analyzed here.

In Equation 9.1, u and $\Delta(u)$ are given by [*Butler*, 1998]:

$$u = {r_r}^2 S/4Tt \ , \text{ and} \tag{9.1c}$$

$$\Delta(u) = [uJ_0(u) - 2 \propto J_1(u)]^2 + [uY_0(u) - 2 \propto Y_1(u)]^2 \ , \tag{9.1d}$$

where: r_r is the radius of head change in the aquifer at time *t*, T is the transmissivity of the aquifer and J_0 and Y_0, J_1 and Y_1 are zero-order and first-order Bessel functions of the first and second kind, respectively.

KGS method (partial penetration)

Hyder et al. [1994] developed an extension of the method of *Cooper et al.* [1967] to the case of a partially penetrating borehole, known as the KGS model, which gives estimates for hydraulic conductivity and storativity of the aquifer. Other than allowing for the partial penetration case and a possible component of vertical flow, the assumptions of the KGS method are the same as those of the Cooper et al. method. The solution Equation 9.1 is modified to [*Butler*, 1998]:

$$H(t)/H_0 = f(\beta, \alpha, \psi, d/b_w, b_w/b), \tag{9.2}$$

where: β and α are defined in Equations 9.1a and 9.1b. b is the aquifer thickness, d is the depth of the screen of the borehole measured from the top of the aquifer, b_w is the screen length and ψ is the square root of the anisotropy ratio $(K_z/K_r)^{1/2}$, where K_z and K_r are the vertical and horizontal components of flow respectively.

In solutions of both Cooper et al. and KGS methods, the normalized heads $(H(t)/H_0)$ are plotted on the vertical axis versus the logarithm of the dimensionless time parameter (β) with a range of type curves each of which corresponds to a different value of the dimensionless storage parameter (α) [*Butler*, 1998]. Equations 9.1 and 9.2 incorporate aquifer storage. However, the estimation of aquifer storativity from these methods is highly uncertain due to a number of reasons. One of them is the uncertainty in the effective screen radius, r_w [*Butler*, 1998]; due to lack of information about borehole construction, or that the borehole is open to the aquifer with no screen which makes it difficult to decide an exact value for this parameter. Also, as seen from Equation 9.1b, the estimate of aquifer storativity depends on accurate estimation of α. At low values of α the shapes of the type curves become very similar making an exact estimate of α difficult to determine [*Butler*, 1998]. Fortunately, both methods are rather insensitive to α so that this does not introduce large errors in estimates of hydraulic conductivity. If α is less than 10^{-5}, which is the case at Benningholme (section 9.2.1) and Sunk Island (section 9.2.3), an error of two orders of magnitude in α will cause an error of less than 30% in hydraulic conductivity [*Papadopulos et al.*, 1973].

Hvorslev's method (full and partial penetration)

The Hvorslev model [1951], for both full and partial penetration borehole cases, differs from that of *Cooper et al.* [1967] in three main points. First, the effect of aquifer storage is assumed to be negligible, and thus an induced head change in the borehole is only affected by flow to/from the aquifer. Second, it is not necessary for the slug to be instantaneously introduced. Third, the lateral extent of the induced head change impacts up to a finite distance (R_e) from the borehole [*Butler*, 1998].

Hvorslev's solution for the full penetration case is:

$$K_r = \frac{r_c^2 \ln(R_e/r_w)}{2bT_0}, \tag{9.3}$$

where: T_0 is the time at which a normalized head ($H(t)/H_0$) of 0.368 is achieved and R_e is the effective radius of the slug test, an empirical parameter which is either equal to the borehole screen length or to 200 times the radius of the borehole screen [*Butler*, 1998].

Hvorslev solution for the partial penetration case is:

$$K_r = \frac{r_c^2 \ln\left[1/(2\psi)+\left(1+\left(1/(2\psi)\right)^2\right)^{1/2}\right]}{2bT_0}, \tag{9.4}$$

where: ψ is the square root of the anisotropy ratio $(K_z/K_r)^{1/2}$, where K_z and K_r are the vertical and horizontal components of flow respectively.

In both Hvorslev's solutions for full and partial penetration (Equations 9.3 and 9.4) a plot of the logarithm of normalized head on the vertical axis versus time on the horizontal axis is a straight line. The slope of this line is used to estimate the radial component of conductivity, K_r [*Butler*, 1998]. The straight line fit to normalized data should be done over the interval of 0.15-0.25 in normalized head as recommended by *Butler* [1998]. This recommendation is applied to the slug tests analysis in the following sections.

9.2.1. Benningholme borehole

A series of six slug tests (0.37 (added and removed), 2, 5, 8 and 15 liters) were performed at Benningholme borehole inducing head changes in the range 2 to 41 cm, see Table 9.1. The log of this borehole (Figure 8.2b) show that the casing penetrates 4.10 m into the Chalk Aquifer. *Parker et al.* [2010] showed from impeller flow logs that most transmissivity occurs over a 9 m section immediately below base of casing. Thus it is probable that the casing penetrates into the high transmissivity layer and that the borehole partially penetrates the aquifer. The slug tests were therefore analyzed using both *Hvorslev* [1951] and KGS [*Hyder et al.*, 1994] partial penetration methods, and results are shown in Table 9.1, where aquifer transmissivity values were obtained using the aquifer thickness open to the borehole of 62.65 m. The data shows good fits for both methods, (Figures 9.1 and 9.2), except for the smallest slug size (0.37 liters) where data is noisy due to the small size of the initial head displacement (0.02 m). The noise in the data means that it is difficult to use the KGS model as type curves are close together. In general, hydraulic conductivities (K_r) obtained using KGS method are 10-25% larger that those obtained using Hvorslev method. The dimensionless storage parameter (α, Equation 9.1b) represents the storage coefficient of the aquifer where the casing radius (r_c) is considered to be equal to the borehole screen radius (r_w). The estimated range for α of 10^{-6}-10^{-7} using the KGS model infers aquifer storativities two to three orders of magnitude less than the typical average value (10^{-4}) for the East Yorkshire Chalk Aquifer [*Parker,* 2009]. However, as explained in section 9.2, estimates of aquifer storage from KGS model are highly uncertain [*Butler,* 1998; *Papadopulos et al.,* 1973].

Results of all slug tests at Benningholme (Figure 9.3) show a power-law relationship between initial head displacement and estimated aquifer transmissivity with an exponent of 0.66-0.69 and R^2 value of 0.97. The barometric response function model value for aquifer transmissivity T_{aqu} of 1.5 m^2/day (where head displacement is around 0.25 cm) and the pumping test value of 52 m^2/day with a drawdown of 45 cm [*Parker,* 2009] also lie on this trend.

Table 9.1. Slug tests volumes, initial displacements and results at the Benningholme borehole. *T* values were obtained using the aquifer thickness open to the borehole of 62.65 m.

Slug volume (liter)	Initial displacement (m)	Hvorslev method			KGS method		
		T_0 (Seconds)	K_r (m/day)	T (m^2/day)	K_r (m/day)	T (m^2/day)	α (--)
0.37	0.02	550	0.09	5.4	----	----	----
0.37	0.02	782	0.06	3.8	----	----	----
2	0.07	273	0.17	10.9	0.20	12.5	10^{-6}
5	0.16	163	0.29	18.2	0.37	22.9	10^{-7}
8	0.25	115	0.41	25.8	0.46	28.7	10^{-7}
15	0.41	81	0.58	36.5	0.64	40.0	10^{-7}

9.2.2. Wilfholme-M2 borehole

A series of eleven slug tests were performed at Wilfholme-M2 borehole. Before analysis the data was corrected for other effects (Earth tides, pumping effects and background water level changes) using water level data from the nearby borehole P, see Figure 8.3a. As shown in Figure 8.3b, the borehole casing penetrates 14.70 m into the Chalk Aquifer. *Parker* [2009] concluded from impeller flow logs that the greatest conductivities are confined to a thin layer about 0.15 m thick just below the base of the casing. This suggests that the casing partially penetrates the aquifer. A series of eleven slug tests (0.37, 0.5, 1, 2, 3, 4, 6, 7, 8, 9 and 10 liters), Table 9.2, were performed inducing head changes of 2 to 52 cm. These are analyzed using the *Hvorslev* [1951] and KGS [*Hyder et al.*, 1994] methods for partial penetrating boreholes.

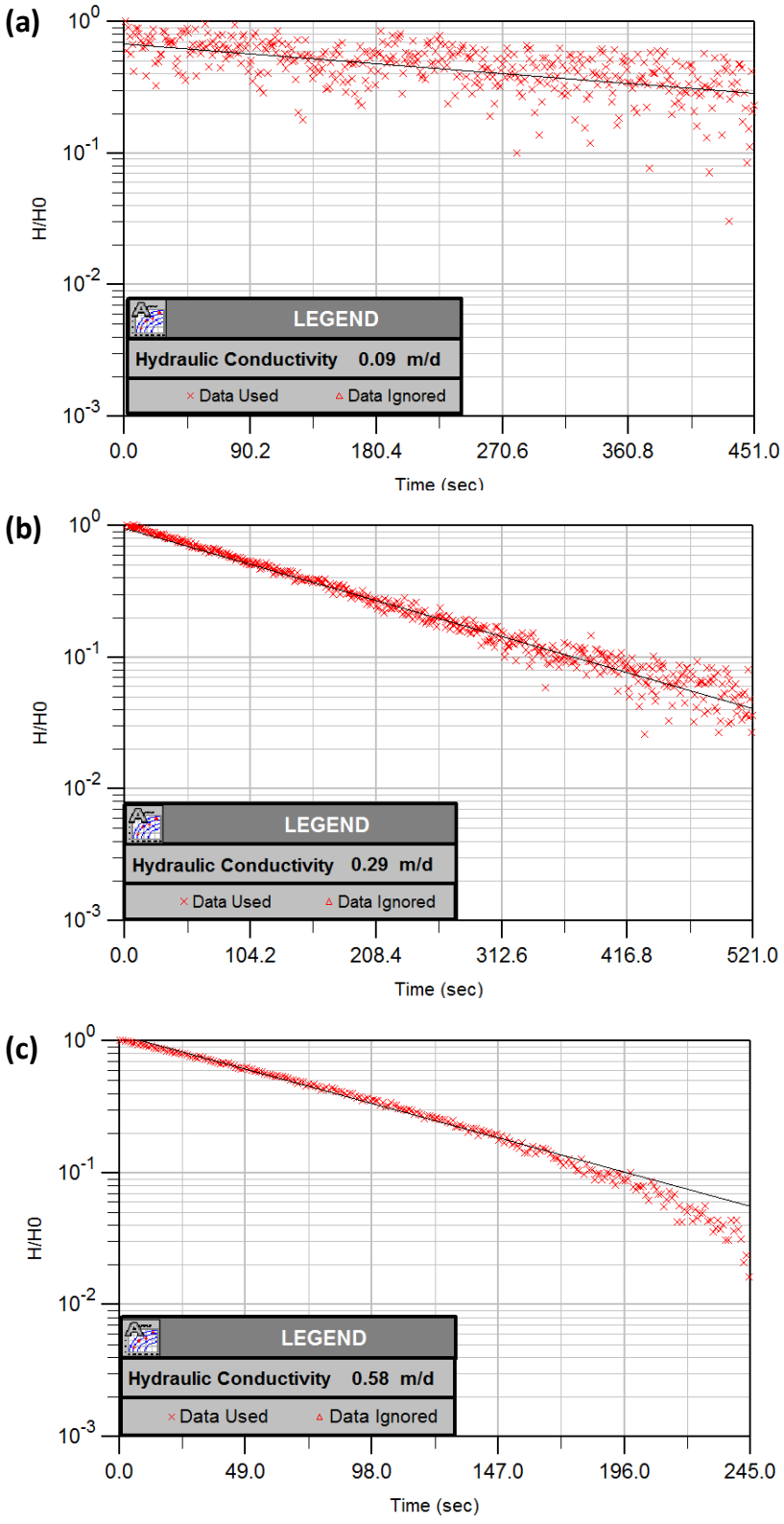

Figure 9.1. Illustrative fits for slug test analysis using Hvorslev method for partial penetration at the Benningholme borehole for a) 0.37 liter (added) slug - K_r=0.09 m/day, b) 5 liters slug - K_r=0.29 m/day and c) 15 liters slug- K_r=0.58 m/day, where (H/H_0) is the normalized head. Data shows good fits to Hvorslev model although data for the smallest slug (0.37 liters) is noisy due to the small size of slug.

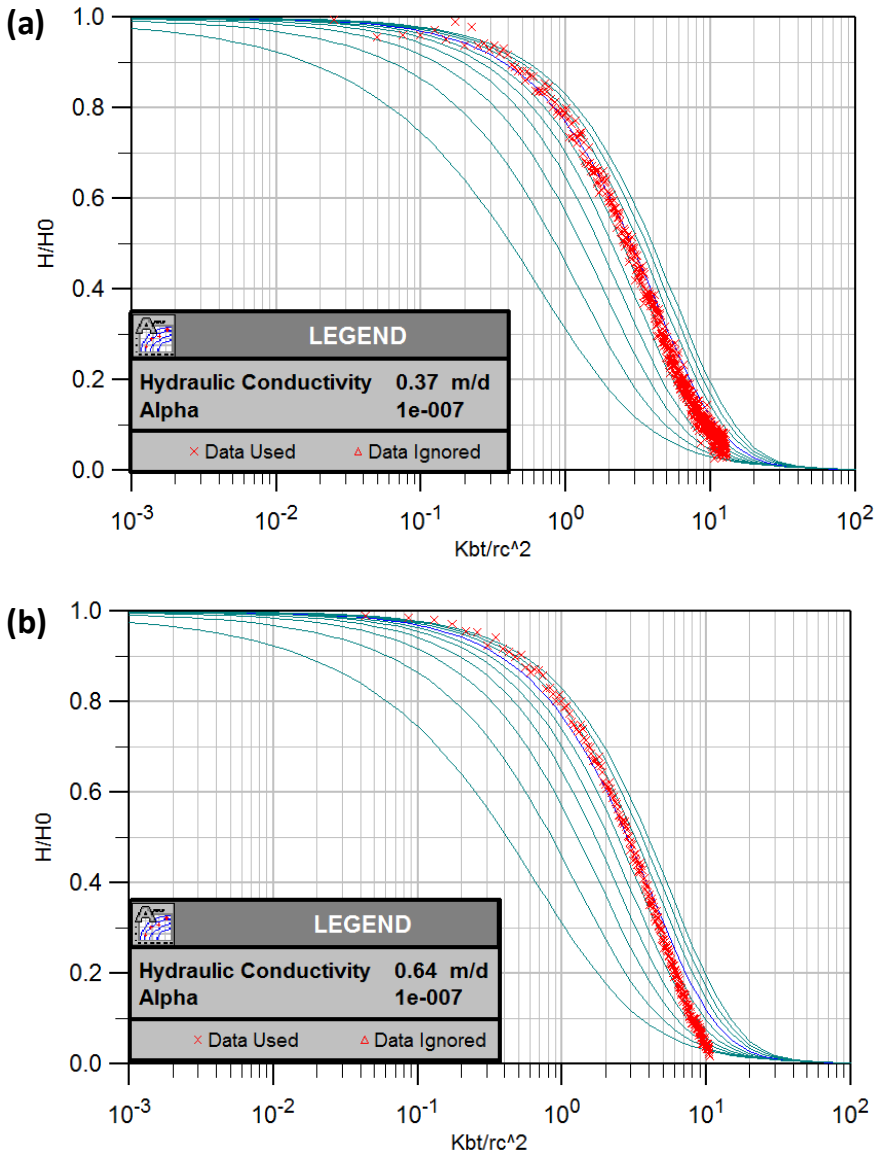

Figure 9.2. Illustrative fits for slug test analysis using KGS method for partial penetration at the Benningholme borehole for a) 5 liters slug - K_r=0.37 m/day, and b) 15 liters slug - K_r=0.64 m/day. The horizontal axis is the logarithm of the dimensionless time parameter, β, (Equation 9.1a). In general the data shows good agreement with the KGS model type curves and estimated K_r values are in good agreement with results from the Hvorslev method. However the estimated α (10^{-7}) implies S values ~ 3 orders of magnitude less than average typical values for the East Yorkshire Chalk Aquifer.

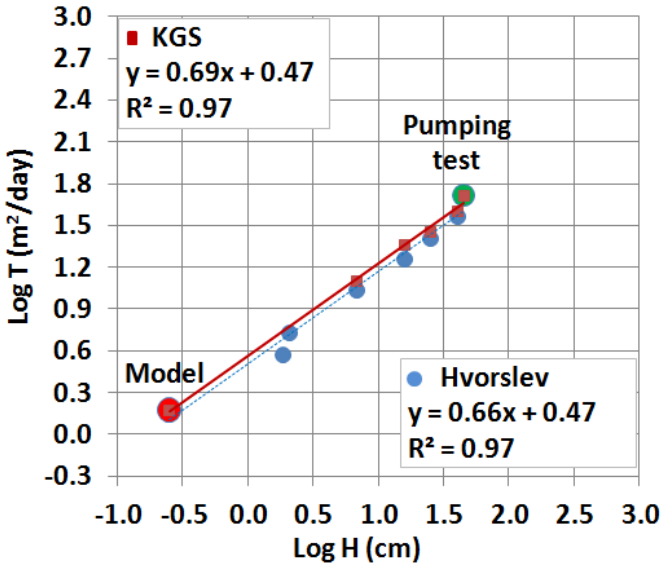

Figure 9.3. Slug test analysis results for Benningholme show a power-law relationship between initial head displacement, H (cm), and estimated aquifer transmissivity, T (m^2/day). The barometric response function model value for aquifer transmissivity T_{aqu} of 1.5 m^2/day and the pumping test value of 52 m^2/day [*Parker*, 2009] also lie close to this trend.

Table 9.2. Slug tests volumes, initial displacements and results at the Wilfholme-M2 borehole. *T* values were obtained using the aquifer thickness open to the borehole of 62.5 m.

Slug volume (liter)	Initial displacement (m)	Hvorslev method			KGS method		
		T_0 (Seconds)	K_r (m/day)	T (m^2/day)	K_r (m/day)	T (m^2/day)	α (--)
0.37	0.02	65	0.56	34.9	----	----	----
0.5	0.03	75	0.48	30.0	0.55	34.1	10^{-4}
1	0.06	44	0.81	50.7	0.67	41.9	10^{-4}
2	0.11	41	0.87	54.6	0.67	42.1	10^{-4}
3	0.17	41	0.87	54.6	0.70	43.9	10^{-4}
4	0.23	42	0.86	54.0	0.67	42.1	10^{-4}
6	0.34	42	0.87	54.7	0.70	43.9	10^{-4}
7	0.40	42	0.86	53.5	0.69	43.2	10^{-4}
8	0.45	42	0.87	54.2	0.65	40.9	10^{-4}
9	0.50	42	0.87	54.2	0.65	40.9	10^{-4}
10	0.52	43	0.85	52.9	0.63	39.8	10^{-4}

Slug tests results for aquifer transmissivity, shown in Figure 9.4a and Table 9.2, based on an aquifer thickness open to the borehole of 62.5 m, are in the range of 30-55 m^2/day which is one order of magnitude higher than the barometric response function model value of T_{aqu} of 2.5 m^2/day and one order of magnitude lower than pumping test results (drawdown of 65cm) of 485 m^2/day [*Hartmann et al.*, 2007]. Estimated range for α of 10^{-4} using the KGS model infers an aquifer storativity consistent with typical values for the East Yorkshire Chalk Aquifer [*Parker*, 2009]. Figure 9.4b shows drawdown data for Wilfholme-M2 borehole when borehole P (25 m distant), was pumped at a constant rate of 423 m^3/day for 0.725 days. The drawdown curve does not show a good fit to Theis model and only late time data was used to determine transmissivity [*Kilpatrick*, 2008]. However, by fitting different parts of the drawdown curve to the Theis curve, a range of aquifer transmissivity values can be obtained from 3.5 m^2/day (early data) to 430 m^2/day (late data). The early data gives a value of transmissivity close to the barometric response function model value of 2.5 m^2/day. Using intermediate time data gives 43 m^2/day close to the slug test value of 30-55 m^2/day. This suggests that there is a similar relationship between initial head displacement and estimated aquifer transmissivity at this borehole to that observed at Benningholme and Sunk Island boreholes.

9.2.3. Sunk Island borehole

A series of six slug tests (0.37 (added and removed), 2, 5, 8 and 10 liters) giving head changes in the range of 3 to 64 cm were performed at Sunk Island borehole, Table 9.3. This borehole is open over the whole chalk interval and is therefore fully penetrating (Figure 8.5b). A pumping test was performed at this borehole by *Straughton* [2008] using pumping rate of 64.3 m^3/day inducing 6.73 m of drawdown and interpreted using *Logan* [1964] approximation to give a transmissivity value of 10.70 m^2/day. Ambient dilution tests at Sunk Island borehole identified no specific inflows or outflows, suggesting that fractures are uniformly distributed over the open borehole interval [*Parker*, 2009]. The slug tests were analyzed using methods of both *Hvorslev* [1951] and *Cooper at al.* [1967] for fully penetrating boreholes, see Table 9.3 and Figures 9.5 and 9.6, and derived estimates for aquifer transmissivity are based on an aquifer thickness open to the borehole of 17.75 m.

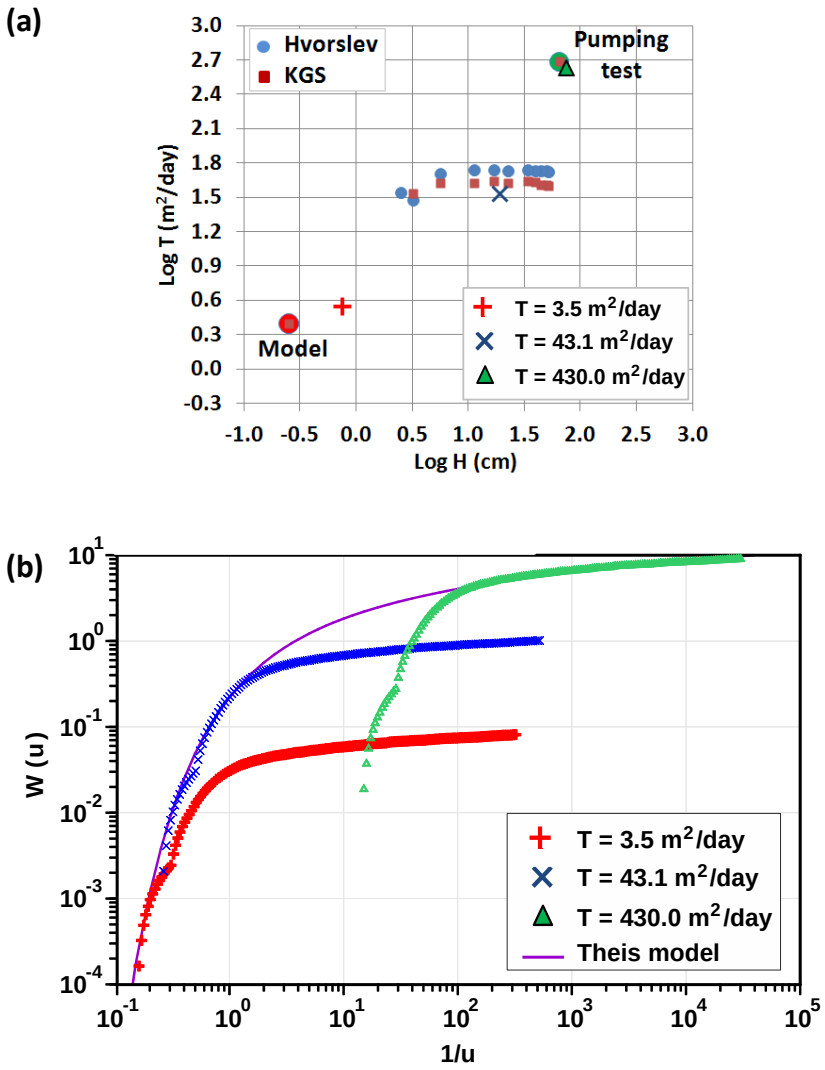

Figure 9.4. Slug test analysis results for Wilfholme-M2 borehole showing, a) log-log plots of initial displacement, H (cm), versus estimated aquifer transmissivity, *T* (m^2/day). Aquifer transmissivity estimates from the slug tests results (30-55 m^2/day) are one order of magnitude higher than the T_{aqu} value of 2.5 m^2/day from barometric response function and one order of magnitude lower than pumping test results of 485 m^2/day [*Hartmann et al.*, 2007]. b) Pumping test results from the Wilfholme-M2 and interpretation using the model of *Theis* [1935]. Early, intermediate and late stages of drawdown curve are fitted to the Theis curve giving estimated aquifer transmissivities of 3.5, 43.1, and 430.0 m^2/day.

Similar to the Benningholme borehole test results but with more scatter, the slug test results at Sunk Island borehole suggest a power-law relationship between initial head displacement and estimated aquifer transmissivity with an exponent in the range 0.32-0.4, somewhat lower than that of Benningholme (0.66-0.69), and an R^2 value range of 0.74-0.87. The best fit line to the slug test data is in good agreement with both the estimated barometric response function model value for T_{aqu} of 1.8 m^2/day and the pumping test result of 10.70 m^2/day. The estimated range of aquifer storativity (10^{-5}-10^{-7}) is one to three 3 orders of magnitude less than typical values for the East Yorkshire Chalk Aquifer.

Table 9.3. Slug tests volumes, initial displacements and results at the Sunk Island borehole. T values are based on aquifer thickness open to borehole of 17.75 m.

Slug volume (liter)	Initial displacement (m)	Hvorslev method			Cooper et al. method	
		T_0 (Seconds)	K_r (m/day)	T (m^2/day)	T (m^2/day)	α (--)
0.37	0.03	132	0.25	4.4	----	----
0.37	0.03	175	0.20	3.6	----	----
2	0.13	167	0.12	2.1	3.5	10^{-5}
5	0.25	121	0.30	5.3	7.3	10^{-7}
8	0.50	102	0.26	4.5	6.3	10^{-7}
10	0.64	64	0.53	9.4	14.5	10^{-7}

9.2.4. Park House Farm borehole

Four slug tests were performed (2.5, 6.5, 10, 20 liters) giving head changes in the range 8 to 66 cm at Park House Farm borehole. These were analyzed using methods of both *Hvorslev* [1951] and KGS, [*Hyder et al.*, 1994] for partial penetrating boreholes, Table 9.4, as the borehole casing penetrates 10.1 m into the aquifer. There is no information on the vertical distribution of hydraulic conductivity and no pumping test has been performed here. The slug tests give a range for aquifer transmissivity of 1.5-3.3 m^2/day, based on an aquifer thickness open to the borehole of 19.2 m, close to the barometric response function model value of 0.70 m^2/day, and show no clear trend, Figure 9.7. The scatter in the data may be due to interference from nearby pumping activities. Estimated aquifer storativity of 10^{-4} using the KGS model is consistent with the typical values for the East Yorkshire Chalk Aquifer [*Parker,* 2009].

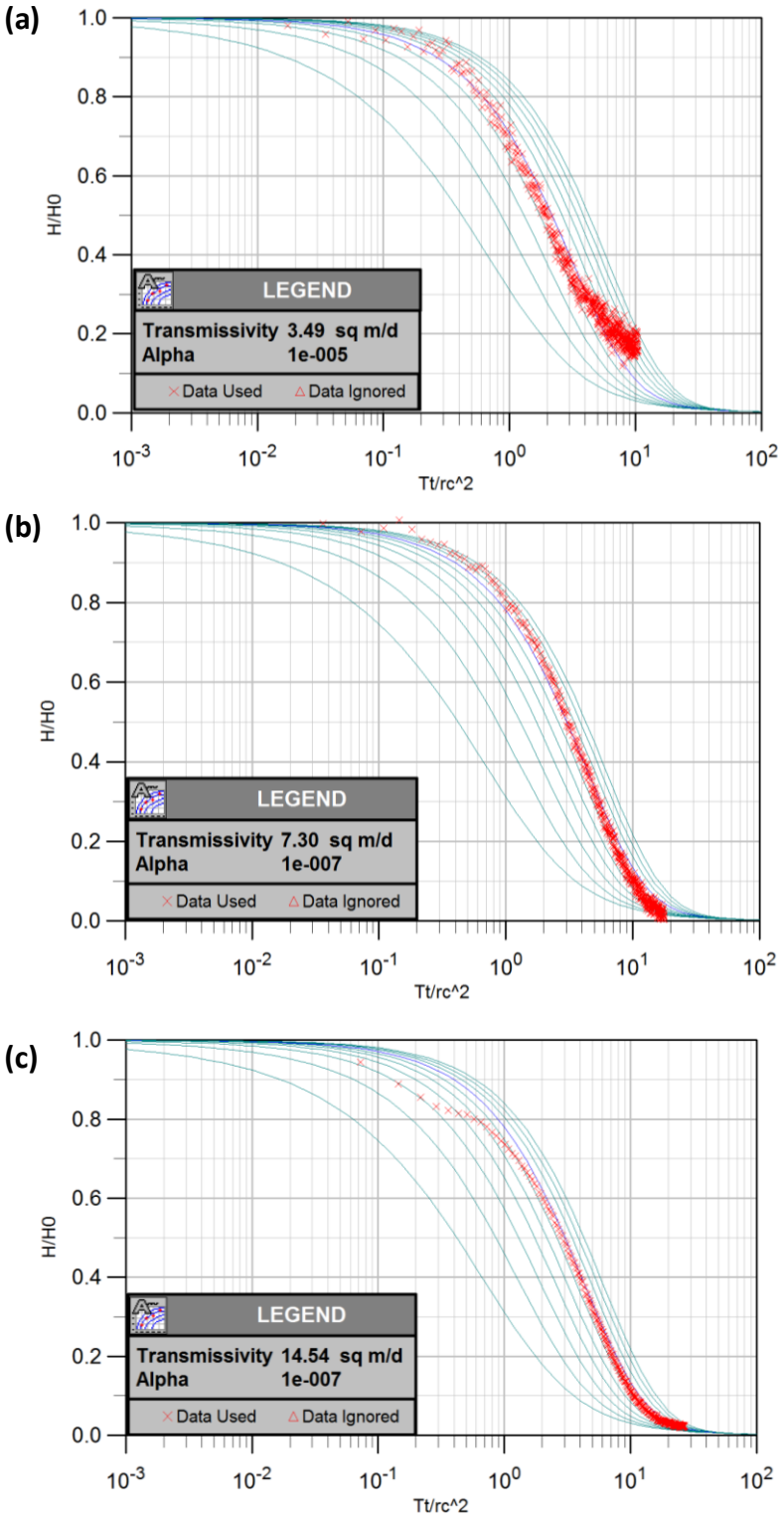

Figure 9.5. Illustrative fits for slug test analysis using Cooper et al. method for full penetration at the Sunk Island borehole for a) 2 liters slug - T=3.49 m/day, b) 5 liters slug - T=7.3 m/day, and c) 10 liters slug - T=14.54 m/day. The horizontal axis is the logarithm of the dimensionless time parameter, β, (Equation 9.1a). Estimated α (10^{-5}-10^{-7}) implies an aquifer storativity that is one to three 3 orders of magnitude less than typical values for the East Yorkshire Chalk Aquifer.

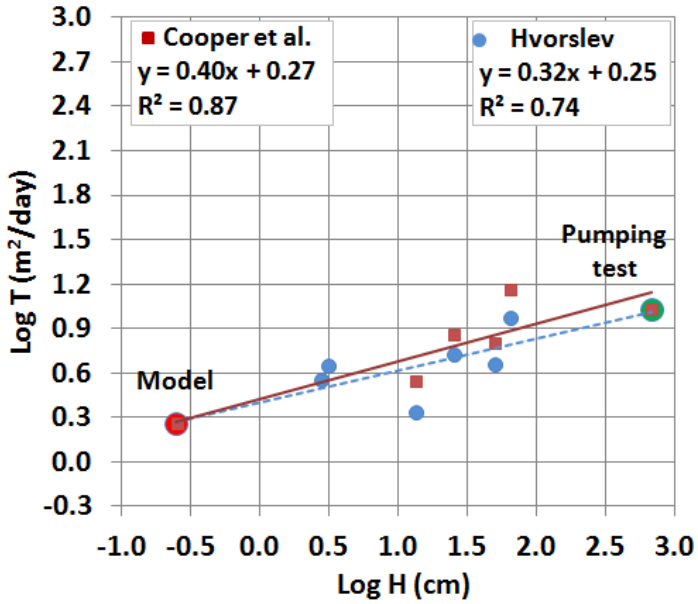

Figure 9.6. Slug test analysis results for the Sunk Island borehole show a power-law relationship between initial head displacement, H (cm), and estimated aquifer transmissivity, T (m^2/day). This trend is in good agreement with both the barometric response function model value for T_{aqu} of 1.8 m^2/day and the pumping test result of 10.70 m^2/day.

Table 9.4. Slug tests volumes, initial displacements and results at the Park House Farm borehole. T values are based on aquifer thickness open to the borehole of 19.2 m.

Slug volume (liter)	Initial displacement (m)	Hvorslev method			KGS method		
		T_0 (Seconds)	K_r (m/day)	T (m^2/day)	K_r (m/day)	T (m^2/day)	α (--)
2.5	0.08	2192	0.10	1.9	0.10	1.9	10^{-4}
6.5	0.20	1352	0.17	3.3	0.13	2.6	10^{-4}
10	0.33	2621	0.09	1.7	0.08	1.5	10^{-4}
20	0.66	1493	0.16	3.0	0.14	2.7	10^{-4}

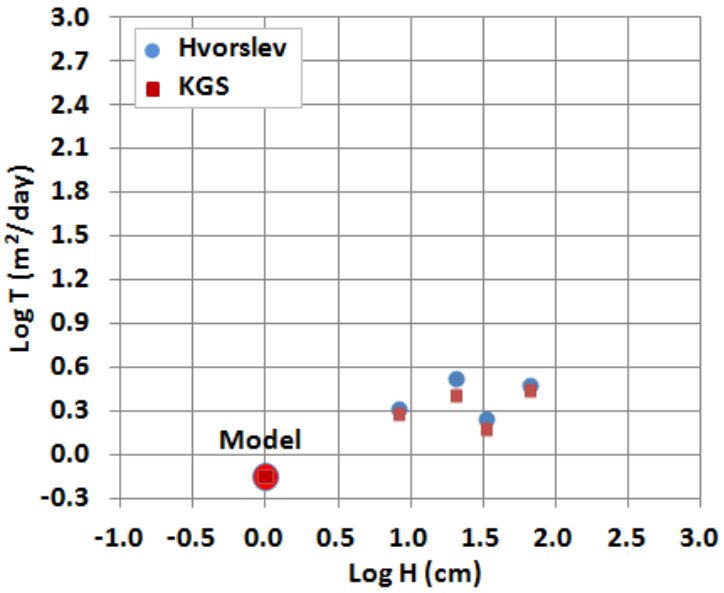

Figure 9.7. Slug test analysis results for the Park House Farm borehole shows a log-log plots of initial displacement, H (cm) versus estimated aquifer transmissivity, *T* (m^2/day). The range for aquifer transmissivity of 1.5-3.3 m^2/day is close to the barometric response function model value of 0.70 m^2/day, and result show no clear trend. No pumping test data is available at this borehole. The scatter in the data may be due to interference from nearby pumping activities.

9.2.5. Routh Low Farm borehole

One slug test (0.25 liters) was performed at Routh Low Farm borehole giving a head change of 0.12 cm. This borehole is screened over the whole chalk interval and is therefore fully penetrating (Figure 8.8b). Therefore, the slug test was analyzed using *Hvorslev* [1951] full penetration method and results are shown in Figure 9.8. Very slow recovery was observed during the test and only 40% of the initial displacement was recovered after 8 hours. Estimated aquifer conductivity is 0.001 m/day which gave aquifer transmissivity of 0.0034 m^2/day considering an aquifer thickness of 3.4 m (full penetrated length of chalk open to the borehole). This transmissivity value is significantly less than the reported range of transmissivity (50 to 5000 m^2/day) from the Chalk Aquifer [*Smedley* et al., 2004], however it is in good agreement with the estimated barometric response function model value for T_{aqu} of 0.001 m^2/day.

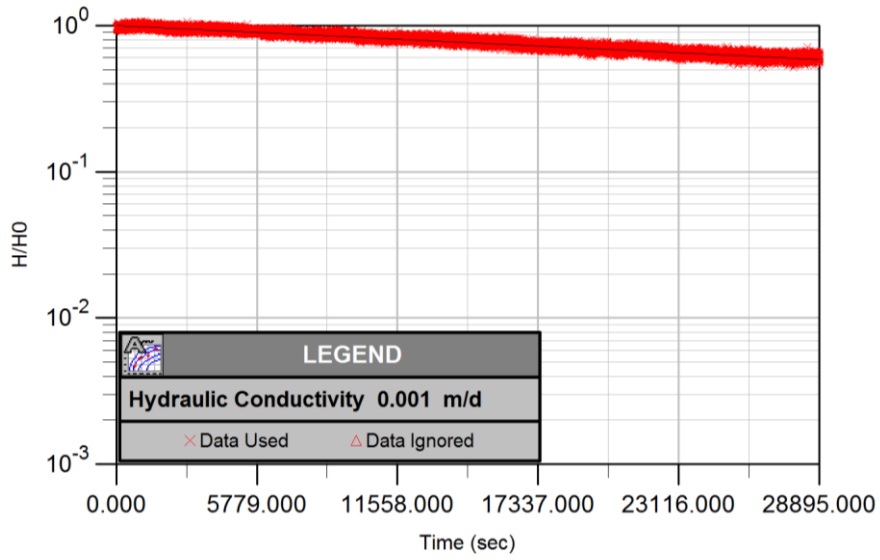

Figure 9.8. Slug test analysis using Hvorslev method for full penetration at the Routh Low Farm borehole, 0.25 liters slug giving K_r=0.001 m/day. Only 40% recovery of initial displacement was achieved after 8 hours due to the very low hydraulic conductivity.

9.3. Impact of confining layer heterogeneity

The discrepancies between estimated properties of confining layer (Hydraulic diffusivity, D_{con}) and borehole lithology at some boreholes, e.g. at Park House Farm, Thornholme Moor and West Newton Farm, raise an important question. How large an area around the borehole is reflected by the barometric response function and what is the impact of heterogeneity within the confining layer? This question is explored by modelling the impact of barometric pressure changes on aquifer response where the confining layer is heterogeneous.

9.3.1. Construction of 2D MODFLOW model

A 2D cross-sectional, saturated, transient flow model (10000 m by 20 m with 14800 cells) was built using Visual MODFLOW [*Waterloo Hydrogeologic, Inc.*] to explore barometric pressure signal propagation through a heterogeneous confining layer, Figure 9.9. Four scenarios are explored. In all scenarios the model consists of two layers, each 10 m thick, representing the confining layer and the aquifer. Hydraulic conductivities are 0.01 m/day for confining layer which is typical of glacial clay-rich

sediments and 10 m/day is chosen as a typical value for Chalk Aquifer, Table 9.5 [*Batu,* 1998; *Parker,* 2009]. Typical values of porosity (0.3 and 0.01) and specific storage (10^{-3} and 10^{-5} m^{-1}) were chosen for the confining layer and the aquifer, respectively [*Hartmann,* 2004; *Quinn,* 2009]. The first scenario (A) is a model in which the confining layer is homogeneous, Figure 9.10a. Conceptual models for the second (B) and third (C) 'heterogeneous' scenarios are shown in Figure 9.10b and c in which the confining layer heterogeneity is represented by a highly conductive block with a hydraulic conductivity of 10 m/day and width (W) of 500 m and 20 m respectively. In the fourth scenario (D), the high conductive block has a width of 500 m but penetrates only halfway through the confining layer, Figure 9.10d. All model hydraulic parameters are listed in Table 9.5.

MODFLOW does not model air flow in the unsaturated zone. For that reason, it is assumed that the unsaturated zone causes no significant attenuation of the barometric pressure signal and the upper model boundary is modelled as a constant head boundary (CHB) with a head that is variable with time and is represented by an actual barometric pressure time series recorded at Benningholme borehole of 100 days length (September 2008 to late December 2008). Heads at the eastern and western model boundaries are set to be the mean value of this barometric pressure signal (10.31 m) and are represented by constant head boundaries (CHB). The bottom model boundary is represented as no-flow, Figure 9.9. The initial head throughout the model is set to zero. The total simulation time is 100 days based on 4 hour time steps. The propagation of the barometric pressure signal in the model is monitored by a number of observation boreholes, screened in the aquifer at the level of -15 m, distributed horizontally at a range of distances D (100 m, 200 m, 300 m and 500 m) from the edge of the highly productive block, see Figure 9.9.

Table 9.5. Hydraulic parameters for MODFLOW model layers

Layer	Kx=Ky=Kz m/day	S_s m^{-1}	Effective porosity
Confining layer	K1= 0.01	10^{-3}	0.30
Aquifer layer	K2= 10.0	10^{-5}	0.01
Highly conductive block	K3= 10.0	10^{-4}	0.20

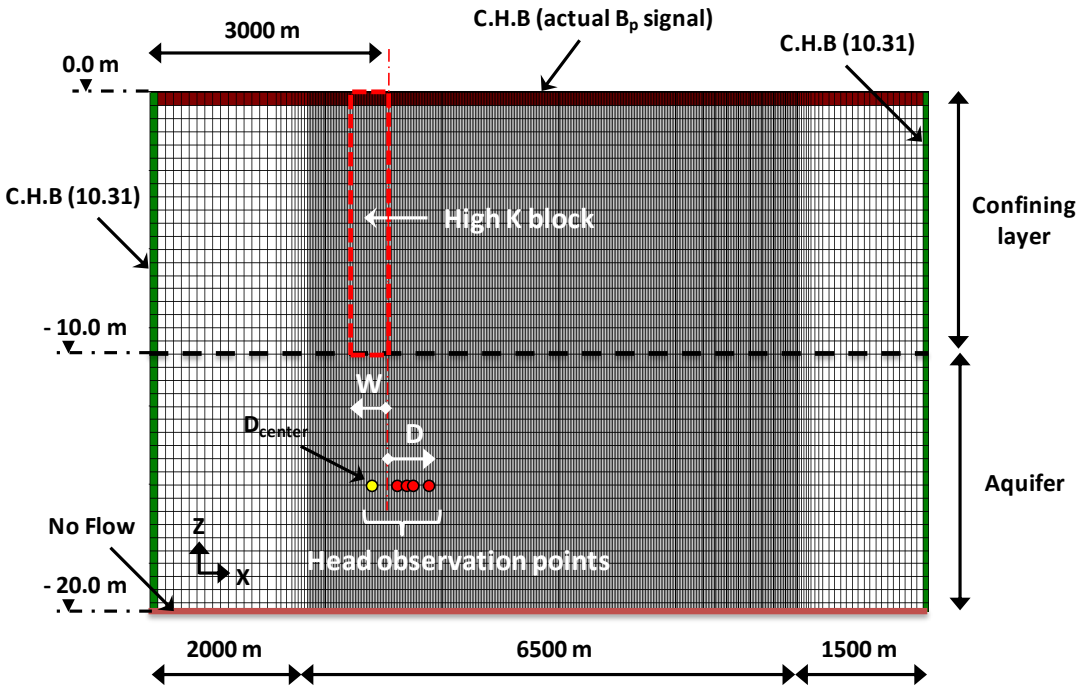

Figure 9.9. Layers, boundary conditions and grid construction of the 2D cross-sectional MODFLOW model. The model is constructed of two layers (10 m thick) with a total of 14800 cells ranging in size from 20×0.5 m to 100×0.5 m. The top boundary is a constant head boundary (CHB) represented by an actual barometric pressure signal (B_p). Eastern and western boundaries are constant head boundaries (CHB) at 10.31 m and the bottom boundary is no flow. W is the width of the high conductive block and D is the distance to the observation borehole, measured from the edge of the high conductive block.

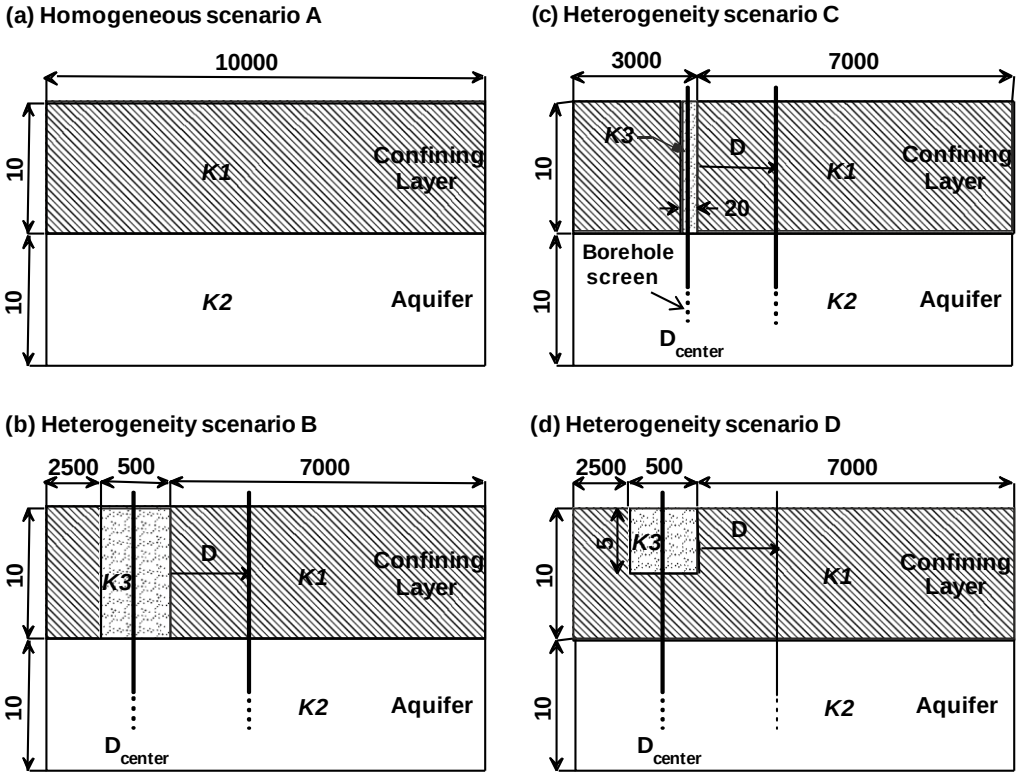

Figure 9.10. Four modelling scenarios (all dimensions in meters). a) Homogeneous scenario (A). b) In heterogeneous scenario (B), the high conductive block fully penetrates the confining layer and has a width of W=500 m. c) In heterogeneous scenario (C), the high conductive block fully penetrates the confining layer and has a width of W=20 m. d) In heterogeneous scenario (D), the high conductive block penetrates halfway through the confining layer and has a width of W=500 m.

9.3.2. Results of MODFLOW model

The effects of initial head conditions lasted for 20 days as shown in Figure 9.11. Therefore, results shown in Figures 9.12 and 9.13 are for a 10 day period of modelling results (day 50 to day 60), that avoid the influence of initial conditions. The impact of heterogeneity can be seen by comparing the experienced head in the aquifer in Figure 9.12 b, c and d (Heterogeneous scenarios B, C and D) with Figure 9.12a (homogeneous scenario A) at the same time of 53.5 days. Both full penetration scenarios B and C (Figure 9.12b and c) show similar head pattern, to the right of the high conductive block where observation boreholes are located, regardless the difference in width of the high conductive block. The pressure signal is instantaneously transmitted through the high conductive block in the confining layer, to the full thickness of the aquifer that lies immediately below the high conductivity block. The pressure signal then propagates horizontally through the aquifer. In heterogeneous scenario D, Figure 9.12d, only part of the atmospheric pressure signal is instantaneously transmitted to the aquifer due to the limited vertical extent of the high conductive block.

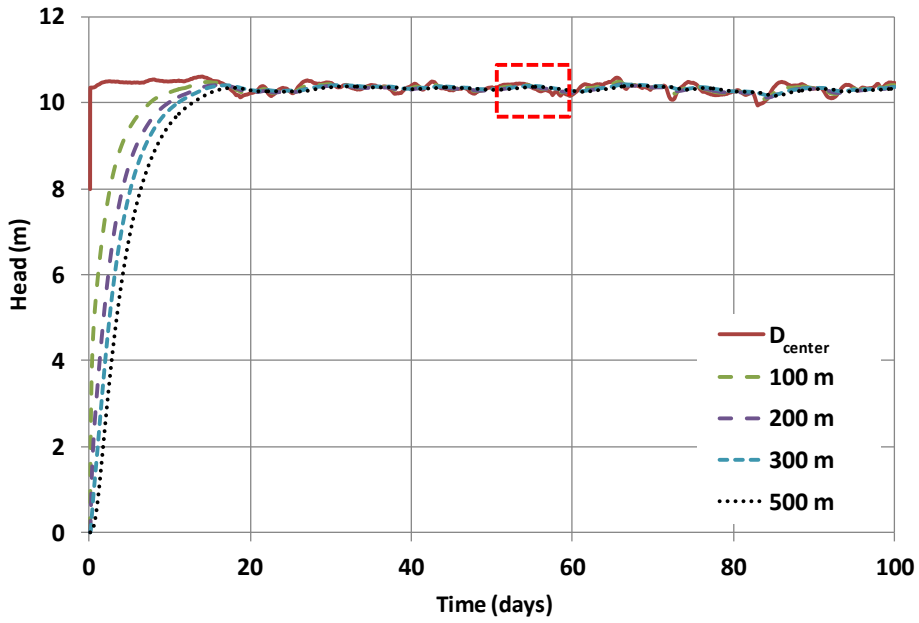

Figure 9.11. Results of heterogeneity scenario B showing that effects of the initial head conditions are up to about 20 days. The red box indicates the time period of results shown in Figure 9.13.

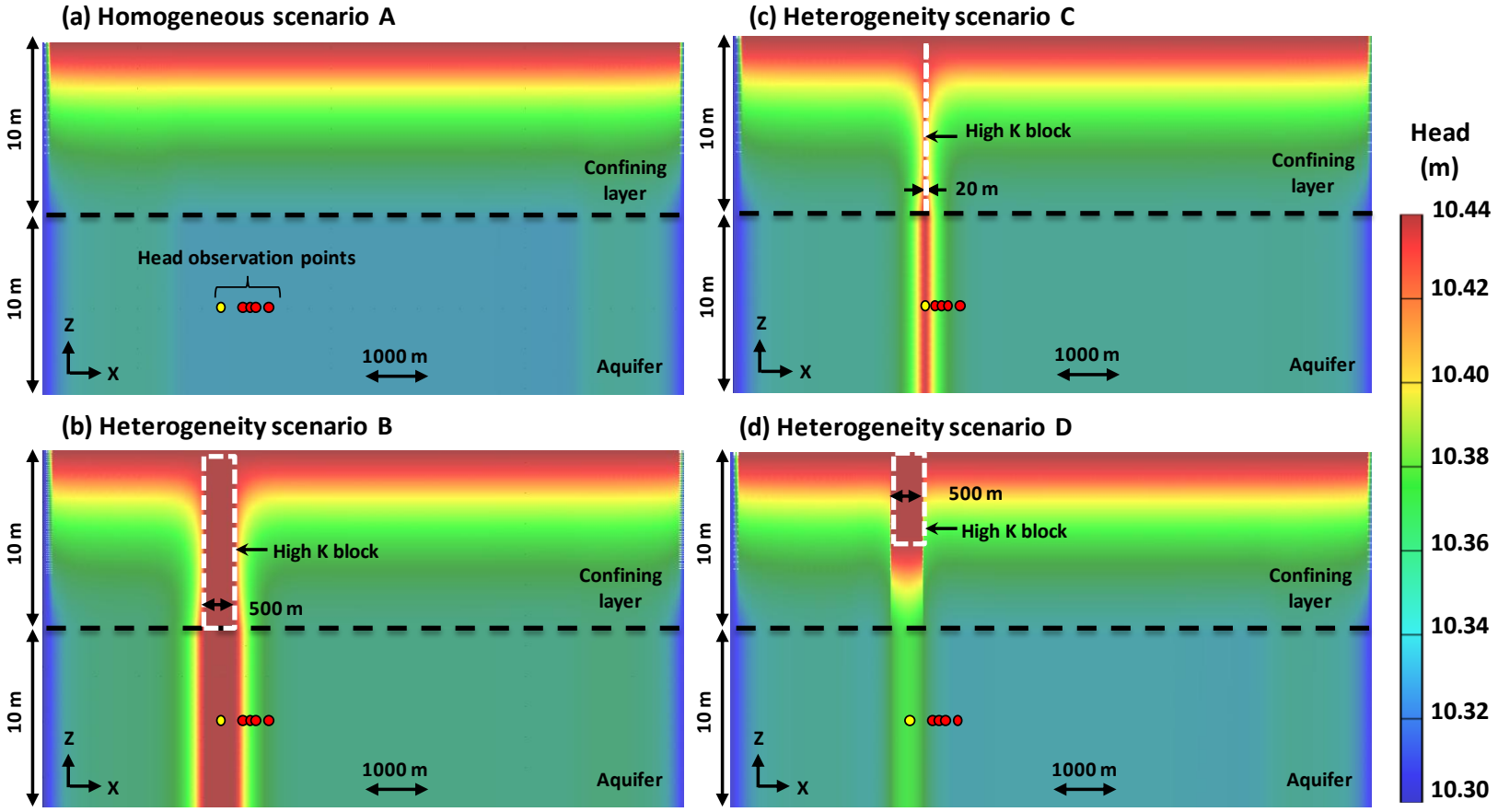

Figure 9.12. Head patterns for the four scenarios at the time of 53.5 days. a) Homogeneous scenario A, b) heterogeneous scenario B, c) heterogeneous scenario C and d) heterogeneous scenario D. B and C show similar patterns, the pressure signal is instantaneously transmitted, through the high conductive part of the confining layer, to the aquifer full thickness lying immediately below the high conductivity block.

The impact of the high conductive block at different distances from the edge of the high conductive block can be seen by comparing the observed head in the aquifer (for the heterogeneous scenarios B, C and D) with that of the 'homogenous model' scenario A, Figure 9.13. In the homogenous scenario A, the head in the aquifer induced by the barometric pressure signal is highly damped and lagged by the low conductivity confining layer, Figure 9.13a. Both scenarios B and C gave similar results with respect to distance from the edge of the high conductive block and thus Figure 9.13a represents results for both scenarios. These scenarios show that the barometric pressure signal is progressively damped and lagged with increasing distance D from the edge of the high conductivity block. High frequencies are more severely damped than low frequencies, while low frequencies are observed at larger distances. This indicates that the high frequency response in the aquifer is dominated by properties of the confining layer near by the borehole while the low frequency response reflects confining layer properties over greater distances. If a difference of 0.5 cm (i.e. twice the lowest transducer resolution of 0.25 cm) is considered to be the minimum that can distinguish between results of the homogeneous and heterogeneous scenarios, effect of the high conductive block can be distinguished up to a distance of some 500 m from the edge of the block, see Figure 9.13a.

In the fourth scenario D, shown in Figure 9.10d, the highly conductive block penetrates only halfway through the confining layer. The aim of this scenario is to examine the effect of vertical heterogeneity in the confining layer. Results show that the signal in the aquifer immediately below the high conductive block (D_{center}) is now significantly damped particularly with respect to high frequencies. In this scenario, the effect of the high conductive block can be detected to a distance up to around 200 m, Figure 9.13b. No difference from the homogeneous model was observed when this scenario is run using a high conductive block of 20 m width, i.e. results were identical to the homogeneous scenario A.

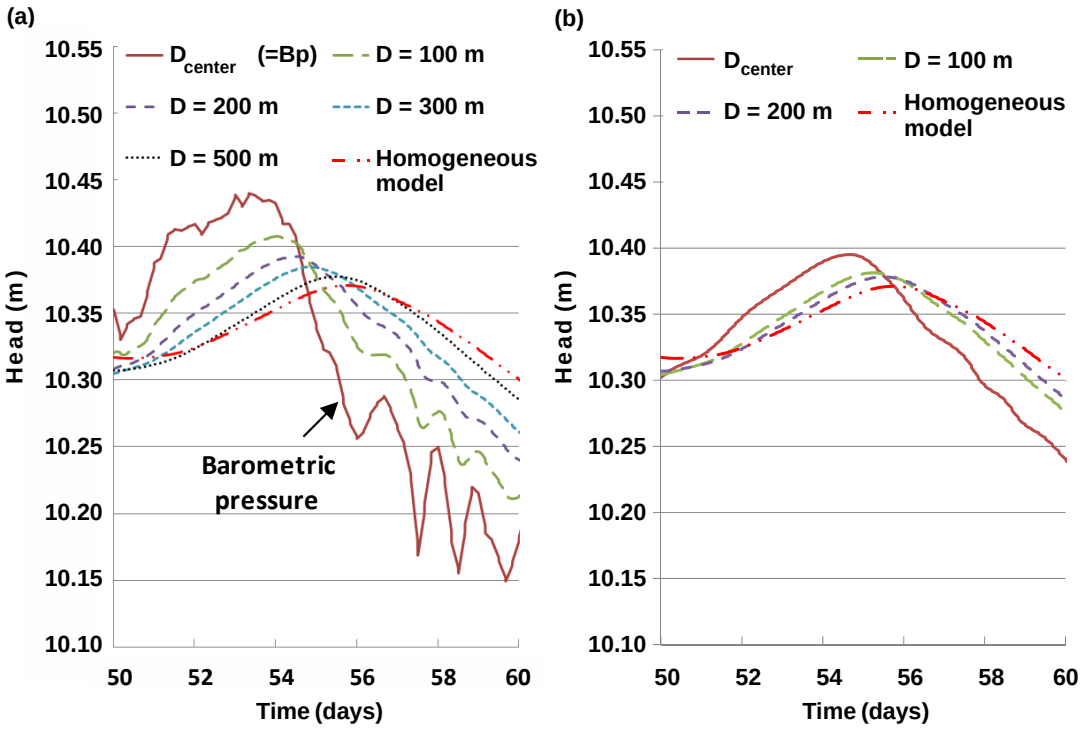

Figure 9.13. Results of flow modelling for a 10 day period (from day 50 to day 60), showing impact of heterogeneity with high hydraulic conductivity. a) Similar results are obtained for scenarios B and C where the high conductive block has a width of 500 m and 20 m respectively and fully penetrates the confining layer. b) Results for scenario D where the high conductive block penetrates halfway through the confining layer with a width of 500 m. The input barometric pressure signal, shown in brown is progressively dampened and lagged with increasing distance D from the edge of the heterogeneity.

9.4. Summary

9.4.1. Summary of slug tests

Series of slug tests were performed at five monitoring boreholes to explore the discrepancy in estimated aquifer transmissivity from the barometric response function and pumping tests. Slug tests results at both Benningholme and Sunk Island show a clear power-law relationship between the initial head change and aquifer transmissivity with exponents of 0.66-0.69 and 0.32-0.4 respectively. At Park House Farm and Routh Low Farm, no clear trend is observed and results show close agreement between the transmissivities estimated from the barometric response function and slug tests. At Wilfholme-M2, where the borehole casing is known to penetrate through a significant proportion of the highly conductive part of the aquifer, the estimate for aquifer transmissivity also strongly depends on the duration of the slug or pumping test. Overall the slug tests results suggest that the discrepancy between the barometric response function and pumping tests values for aquifer transmissivity is due to the differences in magnitude and duration of the head change applied. Induced head changes in response to barometric pressure are in the order of a centimetre while during pumping tests head changes are of the order of meters. This is supported by the observation that estimation of transmissivity from pumping test data at Wilfholme-M2 using Theis is highly dependent on the chosen time interval. The power-law relationship between initial head change and estimated transmissivity is thought to be caused by the partially penetrating nature of the borehole. Small head changes affect only the region very close to the borehole while large head change affects a larger region, and therefore a greater thickness, of the aquifer thus causing an increase in estimated aquifer transmissivity with increasing applied head change. It is likely that many boreholes in the Chalk Aquifer are partially penetrating since boreholes casings (which are always solid) often extend through the highly fractured and weak parts of the aquifer and will therefore be impacted by these effects.

9.4.2. Summary of heterogeneity modelling

Four modelling scenarios were explored using a transient 2D flow model. One of these scenarios represents the homogeneous confining layer case and the other three represent different scale heterogeneities in that layer. Modelling results suggest that a

heterogeneity consisting of a high conductive block with a width of 20-500 m, which fully penetrates the confining layer, will significantly affect the water level signal reaching a monitoring borehole situated at up to some 500 m distant from the conductive block. Thus, if the heterogeneity provides a pathway through whole thickness of the confining layer, a significant impact on head response, and thus the barometric response function, is likely to be observed regardless the width of this pathway, at least down to 20 m. Results from the fourth scenario show that the effect of high conductive block of 500 m width, which partially penetrates the confining layer is detected up to about 200 m distant from borehole, while no significant response change is observed when the block is only 20 m wide. It can be expected therefore that the barometric response function will be highly sensitive to presence of high conductive, connected pathways through the confining layer and will reflect confining layer properties of an area around the monitoring borehole of up to around one km across. Results show that the impact of low frequencies can be seen further from the heterogeneity and thus the low frequency band of estimated barometric response functions may reflect confining layer properties distant from the monitoring borehole, while the high frequencies reflects properties near to the borehole. This sensitivity to confining layer heterogeneity may explain misfits between estimated barometric response functions and model at low frequencies (e.g. Wilfholme and Park House Farm boreholes, Chapter 8). This can also explain the discrepancy between derived model values for diffusivity of confining layer and borehole logs (e.g. Park House Farm, Thornholme Moor and West Newton Farm boreholes), which is further explored in Chapter 10.

CHAPTER 10: SUMMARY AND DISCUSSION

10.1. Summary

Time series analysis is used to characterize the contributions to water level signals for twelve boreholes located in the East Yorkshire Chalk Aquifer. The different influences on the water level time series were analyzed using the *SC* Matlab code developed in this work (Appendix B). Influences other than barometric pressure were then removed using this code as a processing step that is necessary prior to estimating barometric response functions. Results show that these influences are Earth and ocean tides, recharge and pumping effects. Contributions of Earth and ocean tides to the borehole water level signal are significant, up to 4.0 cm. This highlights the importance of removing these contributions in order to extend the frequency range of estimated barometric response functions up to the diurnal and semi-diurnal tidal frequencies. The recharge contribution to borehole water level signals is significant, and the cut-off frequency to remove recharge is up to 0.05 cycles/days. Pumping interferences were observed at Wilfholme and Park House Farm boreholes. While it was possible to fully remove these influences at Wilfholme, pumping effects could only be partially removed at Park House Farm borehole.

Filtered borehole water level signals with all influences other than barometric pressure removed were used to compute short-term and long-term barometric efficiencies using the *BE* Matlab code developed in this study (Appendix C). Results indicate that the aquifer at all boreholes is semi-confined and that significant borehole storage/skin effects are present at Routh Low Farm and Routh High Farm boreholes. Filtered water level signals from twelve boreholes were used to estimate barometric response functions using cross-spectral deconvolution with up to five overlapping frequency bands, using the *RF* Matlab code developed in this study (Appendix D). The *Rojstaczer* [1988a] model was used to model barometric response functions with the capillary fringe attenuation factor added from the model of *Evans et al.* [1991]. The best fit solution is obtained using the hybrid genetic (GA) and pattern search (PS) technique, implemented in the *Automatic_Fitting* Matlab code developed in this study (Appendix E). The best fit solution is then refined manually for some cases using the

Manual_Fitting.m Matlab code developed in this study (Appendix F). The ranges of vertical hydraulic diffusivity (10.0 to 5.0×10^4 m^2/day) and pneumatic diffusivity (0.9 to 128.0 m^2/day) reflect the wide variation in composition of the glacial sediments confining the Chalk Aquifer. Estimated aquifer transmissivities using barometric response functions are up to several orders of magnitude less than pumping test values from the East Yorkshire Chalk Aquifer. This discrepancy was explored using slug tests. Results indicate a power-law relationship between slug test initial displacement and aquifer transmissivity. Overall the slug tests results suggest that this discrepancy is due to the differences in magnitude and duration of the head change applied. The discrepancy between estimated properties of confining layer and borehole lithology at some boreholes was explored by modeling the impact of barometric pressure changes on aquifer response where the confining layer is heterogeneous. Modeling results show that the response at high frequencies reflects the borehole log, while at lower frequencies it reflects confining layer properties further from the borehole. This modeling indicates the sensitivity of the barometric response functions to connected flow pathways provided by heterogeneities in the confining layer.

In the following sections the components contributing to borehole water level signals, the estimation of barometric response functions and derived parameters, and methods by which borehole water level responses to barometric pressure can be used as an indicator of intrinsic aquifer vulnerability are discussed.

10.2. Borehole water level signal components

Analysis of water level signals from twelve boreholes located on the confined/semi-confined part of the East Yorkshire Chalk Aquifer show that the main contributing components are barometric pressure, Earth and ocean tides, recharge and pumping. Although the barometric pressure is the main driving force for borehole water level fluctuations, contributing to the water level signal over most of the observed frequency band, the other contributions are also significant and further discussed below.

Influence of recharge

Analysis of water level signals from seven boreholes located in the unconfined aquifer show that they are influenced solely by recharge and do not respond to a significant degree to either barometric pressure or Earth tides. Water level signals from these unconfined boreholes were used to determine the frequency range of the recharge contribution to the water level signals in boreholes located in the confined/semi-confined aquifer. Coherence estimates were used to determine a frequency cut-off up to which the recharge signal affects the response relation between water level and barometric pressure signals at each borehole. The recharge signal contributes to water level signal from ~0.0022 cycles/day and up to ~ 0.05 cycles/day. The recharge contribution to water signal is clear and differs from one borehole to another. Recharge removal by applying a high pass filter at this cut-off helps to minimize spectral leakage from the lower high energy frequencies due to recharge. The upper limit for the recharge frequencies range from 0.014 cycles/day at Sunk Island borehole to 0.05 cycles/day at Woodhouse Farm and Bracy Bridge boreholes. The cut-off frequency of the high pass filter applied to remove recharge, decreases with the increasing distance between each borehole and the confined edge (Figure 5.18). However exceptions occur. The recharge contribution to the water level signal at the Routh Low Farm and Routh High Farm boreholes (located 13-15 km from the confined edge) is up to 0.035 cycles/day which is significantly larger than the contribution at the Benningholme borehole (up to 0.017 cycles/day) located at a similar distance from the confined edge (13 km), Figure 5.18. This suggests that there may be some local recharge near the Routh Low Farm and Routh High Farm boreholes. A group of flooded sand and gravel pits (the former Routh Quarry) exists a few hundred meters away from these boreholes. These flooded pits are thought to be hydraulically connected to the aquifer and hence could potentially represent a source of local recharge.

Influences of Earth tides and ocean tides

Earth tides contribute to the borehole water level signal at O_1, P_1, S_1, K_1, N_2, M_2 and S_2 tidal components (0.9295, 0.9973, 1.0, 1.0027, 1.8959, 1.9323 and 2.0 cycles/day respectively). Atmospheric tides contribute to the borehole water level signal at S_1 and S_2 (1.0 and 2.0 cycles/day respectively) and at these specific tidal frequencies the energy of barometric pressure signal is significant while it is almost zero above and

between them. This highlights the importance of separating atmospheric and Earth tide effects at these frequencies in order to extend the frequency range of estimated barometric response function.

The Earth tides and ocean tide contributions to the water level signals were determined and reconstructed using method detailed by *Rasmussen and Mote* [2007]. *Rasmussen and Mote* [2007] found a lack of similarity between theoretical and reconstructed Earth tides which they attributed to aquifer heterogeneity. Unlike their results, there is an obvious similarity between these signals at all boreholes in this study except at Park House Farm which could be due to pumping activities close to this borehole. In addition, the reconstructed amplitude range of the major Earth tidal components O_1 (0.01-0.29 cm) and M_2 (0.01-0.4 cm) are up to two orders of magnitudes larger compared with the results of *Rasmussen and Mote* [2007]. This is likely because in their case the aquifer is poorly confined showing a low barometric efficiency (~ 6%) compared to this study (~ 45%). A significant response of borehole water level to Earth tides, particularly O_1 and M_2 components, is an indicator of that the aquifer is confined [*Kümple*, 1997]. Thus, the small reconstructed ranges of tidal amplitudes for O_1 and M_2 at Woodhouse Farm and Bracy Bridge boreholes (0.01-0.04 cm and 0.01 cm respectively) suggest a relatively low degree of confinement (Table 5.5). This is in good agreement with derived hydraulic diffusivity of the confining layer at these two boreholes which are up to three orders of magnitude larger than the other boreholes (Table 8.1). Ocean tides are clearly observed ~ 2 km from the sea at Sunk Island borehole at which the largest M_2 amplitude is observed (1.17 cm), while no trace of ocean tides is observed at West Newton Farm (~ 4.8 km from the sea, M_2 amplitude of 0.12 cm) or Thornholme Moor (~ 6 km from the sea, M_2 amplitude of 0.2 cm). This shows that ocean tides affect the water level signals at boreholes located up to about 2-3 km from the coast.

10.3. Estimation of the barometric response function

To estimate the barometric response function, the cross-spectral deconvolution and averaging method [*Welch*, 1967] integrated with a technique of overlapping frequency bands described by *Beavan et al.* [1991] are implemented in the *RF* Matlab code (Appendix D) developed in this study.

Instrument accuracy and frequency range of the barometric response function

Due to limitations of signal energy and coherence, the frequency band width of the derived barometric response functions is 0.017-2 cycles/day. This range is similar to the frequency ranges reported by *Rojstaczer* [1988a], *Galloway and Rojstaczer* [1988], and *Rojstaczer and Riley* [1990]. *Evans et al.* [1991] reported barometric response functions over the greater frequency range of 0.02-50 cycles/day. This was possible due to their use of higher resolution pressure sensors (vented to the atmosphere) with an accuracy of ±0.14 cmH_2O which compares to the accuracy of pressure transducers used in this study of ±0.9-2.5 cmH_2O. This is reflected in the high coherence estimates between water level and barometric pressure signals of 0.9 to 1.0 over most of the observed frequency band in *Beavan et al.* [1991]. Vented pressure sensors are more expensive than non-vented and more complicated to install. However, the resolution of non-vented pressure sensors is steadily improving which will allow the estimation of more accurate barometric response functions over wider frequency bands in the future. The most restricted frequency band of the barometric response function (0.035-0.56 cycles/day) is observed at Routh Low Farm borehole and is due to limitations of signal energy and coherence at high frequencies. These limitations are thought to be due to the very low transmissivity of the aquifer at this borehole (0.0034 m^2/day) which damps the water level response to barometric pressure at high frequencies. This is confirmed by a low short-term barometric efficiency of 7.6% at this borehole which is smaller than the long-term barometric efficiency of 17.4%, implying significant borehole storage/skin effects [*Rasmussen and Crawford*, 1997].

Impact of data record length

In this study, the method of cross-spectral deconvolution by ensemble averaging [*Welch*, 1967] is used to obtain smooth estimates of barometric response functions with reduced error bars. In this method, records of both water level and barometric pressure signals are divided into a specified number of segments, N, of equal length with an overlap, δ, of 50% between segments. The final barometric response function is averaged over the number of segments (N), see section 6.3.3. In general, the longer the record length, the larger the number of segments used and the smoother and more accurate is the barometric response function estimate as shown in Figure 6.5. Also a larger number of segments results in smaller error bars (Equations 6.13 and 6.14). Data records lengths in this study range from 275 days at Wilfholme-M1 and Wilfholme-M2 to 800 days at Benningholme and Wifholme-M3 boreholes. Note that estimated barometric response functions for M1, M2 and M3 boreholes at the Wilfholme "huddle test" are very similar although the record length at M3 is about 3 times longer than the others. *Rojstaczer* [1988a] and *Rojstaczer and Riley* [1990] used data records of only 150 days from which they obtained plausible barometric response functions. The minimum record length needed in order to obtain a reliable estimate of the barometric response function depends on the required minimum number of segments and length of each segment. The minimum number of segments to give a reliable response was found to be about 20 (section 6.3.4). The minimum length of each segment is controlled by the lowest frequency required which is the cut-off frequency to remove recharge (0.014-0.05 cycles/day). Thus, if an average cut-off of 0.03 cycles/day is considered for this case study, the minimum segment length is 33.34 days (=1/0.03). This gives a minimum record length of about 334 days based on 20 segments and an overlap of 50% between segments (see Equations 6.7 and 6.8). In this study, the number of segments used to estimate barometric response functions ranges from 20 to 1109 segments, Table 6.2. The minimum number of segments used by *Beavan et al.* [1991] is 5; again this is possible because of the higher resolution of the pressure sensors they used. The technique of ensemble averaging [*Welch*, 1967] implicitly assume that the estimated barometric response function is stationary in time. The assumption of stationarity was tested using the longest record (Benningholme borehole) divided into four segments of 199 days, section 6.3.5. The test showed that the barometric response function is reproducible within the errors and thus that the stationarity assumption is valid.

10.4. Determining aquifer and confining layer properties

Range of barometric response functions

Aquifer and confining layer properties were estimated through fitting the model of *Rojstaczer* [1988a] to estimated barometric response functions. In general, results show good fits but in some cases, the fit is relatively poor for the gain at low frequencies. This may be due in part to the use of low number of segments which increases uncertainty and the size of error bars at these low frequencies but may be also attributed to heterogeneity in the confining layer as revealed by MODFLOW modeling (section 9.3).

According to *Rojstaczer* [1988a] model, the response can be divided into three stages comprising low (A), intermediate (B) and high frequency (C) responses, Figure 10.1. Stage A (low frequencies) is governed by the properties of both the unsaturated and saturated zones of the confining layer. Stage B (intermediate frequencies) is governed by the static barometric efficiency which is a function of the elastic properties of the aquifer. Stage C is governed principally by borehole design, horizontal aquifer transmissivity and aquifer storativity. The barometric response functions estimated here are compared in Figure 10.2 and show a wide range of curve shapes which are a strong function of frequency. Barometric response functions are determined over a frequency range of 0.017-2 cycles/day which is about one third of the total frequency band shown in Figures 7.3 and 7.4, which are based on the theoretical model of *Rojstaczer* [1988a]. Thus it is not possible to observe the entire low, intermediate and high frequency response stages (stages A, B and C, Figure 10.1) in estimated barometric response functions, and only the low and intermediate frequency response stages (A and B) are observed at most boreholes. Exceptions are seen at Routh Low Farm and Routh High Farm where low and high response stages (A and C) are observed due to low aquifer transmissivity which dominates over the intermediate stage B. Thus, the observed frequency range of 0.017-2 cycles/day favors estimation of confining layer properties, which are essentially sensitive to low and intermediate frequencies (A and B), Figure 7.4. Aquifer transmissivity mainly influences the high frequency band (C), Figure 7.3b and for this reason, it was only possible to estimate a lower bound for aquifer transmissivity at five of the boreholes, see Table 8.1.

A clear confined plateau (stage B) is observable for Benningholme and Sunk Island boreholes, Figure 10.2, where the relatively flat gain and phase curves indicate low hydraulic diffusivities (10 and 15 m^2/day, respectively). In contrast, the response curves at Woodhouse Farm and Bracy Bridge boreholes which show the lowest gain values and steepest phase curves indicating high hydraulic diffusivities (2×10^4-5×10^4 m^2/day). The estimated barometric response function at West Newton Farm is relatively noisy compared to those of other boreholes. Response curves of Wilfholme, Park House Farm and Thornholme Moor boreholes show monotonic gain increase and phase decrease with increasing frequency. The responses at these boreholes are a strong function of frequency corresponding to stage A (low frequencies) and are dominated by the confining layer properties.

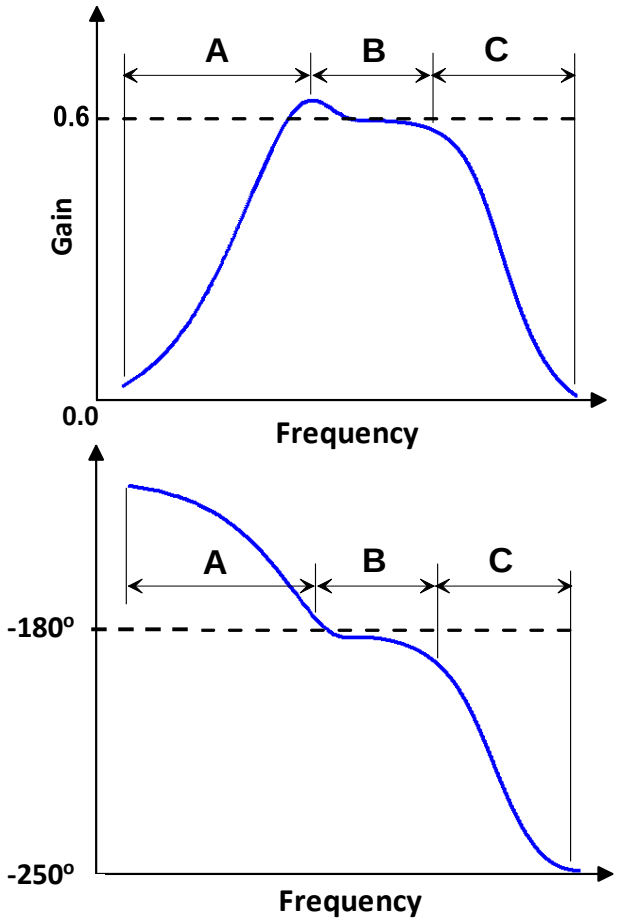

Figure 10.1. Example theoretical barometric response function gain and phase curves derived from the model of *Rojstaczer* [1988a] using parameters typical of the confined Chalk Aquifer (Table 7.1), showing low (A), intermediate (B) and high (C) frequency response stages.

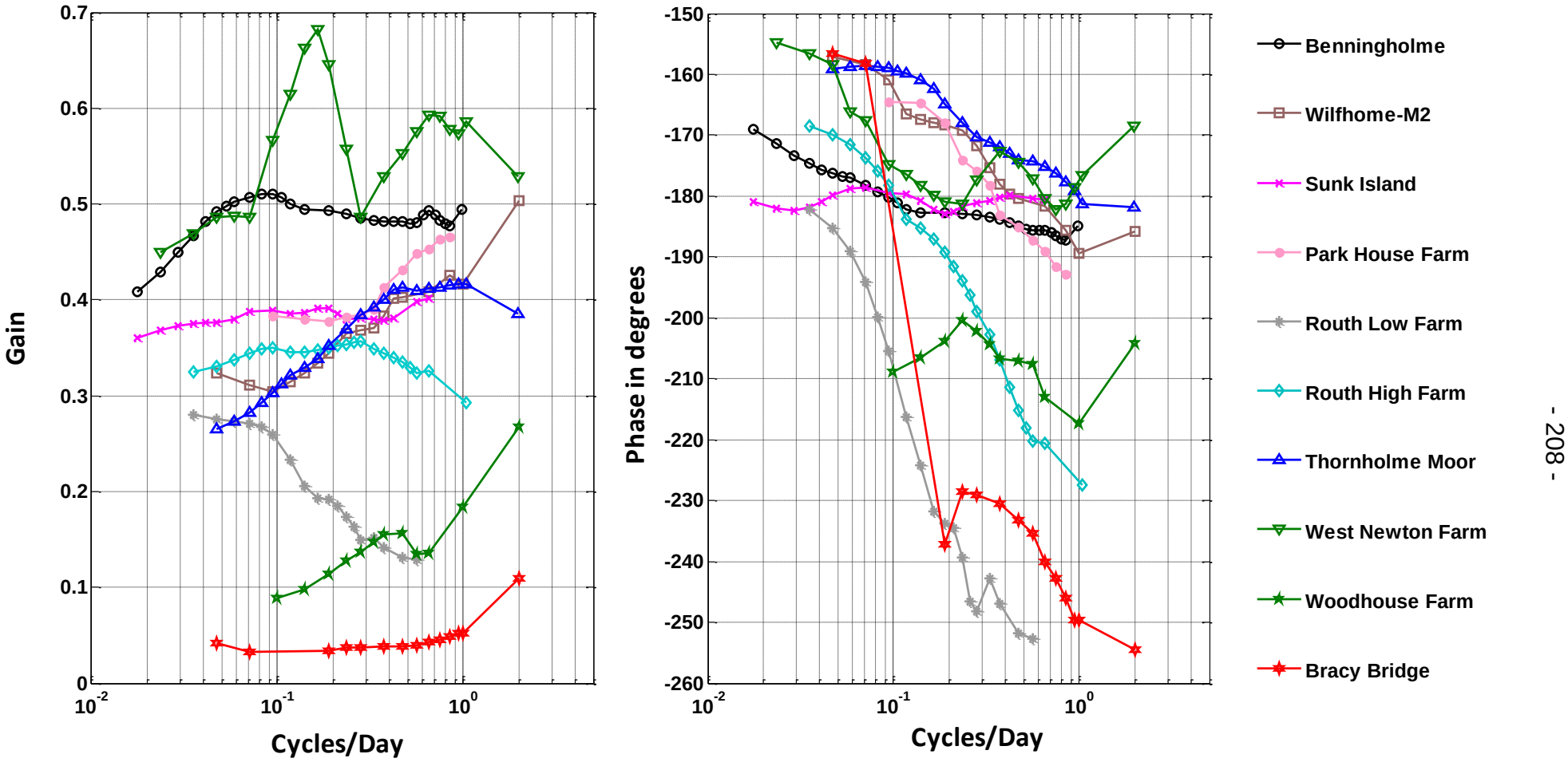

Figure 10.2. Comparison of gain and phase curves for estimated barometric response functions for all boreholes, showing a frequency range of 0.017-2.0 cycles/day. A wide range of response shapes is observed.

Influence of the capillary fringe

The addition of the capillary fringe attenuation factor, T_{cf}, introduced in *Evans et al.* [1991] to the model of *Rojstaczer* [1988a] improves the fit of theoretical response curves to observed data at low frequencies in some cases. The capillary fringe attenuation effect is due to the change in volume of encapsulated air bubbles within the capillary fringe or just below the water table with changing barometric pressure which results in a partial absorption of the air pressure pulse as it passes through the unsaturated zone [*Evans et al.*, 1991]. Varying T_{cf} influences the slope of both gain and phase curves at low frequencies (see Figure 7.4d). The unsaturated zone in the confined East Yorkshire Chalk Aquifer is thin (about 0.5-3.5 m) and the capillary fringe attenuation factor, T_{cf}, is therefore controlled by the nature of the glacial sediments at shallow depths. Capillary fringe attenuation effects are greatest at Sunk Island borehole (T_{cf} = 0.4), while they are small or negligible at all other boreholes (0.82-1.0). Encapsulation of air bubbles within the capillary fringe is most pronounced for coarse sediments and soils [*Honig and Murphy*, 2001] and *Evans et al.* [1991] estimated capillary fringe coefficients of 0.4-0.5 for an unsaturated zone in sandstones. This is consistent with a significant value for T_{cf} of 0.4 at the Sunk Island borehole where a 9 m thick layer of sand is found at shallow depth containing the water table at 1.7 m depth. The composition of the unsaturated zone at this borehole contrasts with other boreholes where more clay-rich sediments are found. *Peck* [1960] detected an attenuation of 5% (T_{cf} of 0.95) caused by encapsulated air in a column experiment with sandy soil and *Turk* [1975] observed an attenuation of 20% (T_{cf} of 0.8) in an experiment in silty loam soil. Both of these materials are expected to be finer grained and have lower hydraulic and pneumatic conductivity than sand. These values for T_{cf} are close to the estimated range for T_{cf} of 0.82-1.0 for the other boreholes in the present study.

Short and long-term barometric efficiencies versus static barometric efficiency

In this study, short-term ($\propto_S$) and long-term ($\propto_L$) barometric efficiencies were computed using simple methods described by *Rasmussen and Crawford* [1997], see section 6.2. In addition, static barometric efficiencies (*BE*), were derived by fitting the *Rojstaczer* [1988a] model to estimated barometric response functions. Here short-term

($\propto_S$) and long-term ($\propto_L$) barometric efficiencies are compared with the static barometric efficiency (*BE*) estimated at each borehole, see Table 10.1 and Figure 10.3. It is shown that model estimates for *BE* are equal to or larger than both short-term ($\propto_S$) and long-term ($\propto_L$) barometric efficiencies. Greater discrepancy between *BE* and $\propto_S$ and $\propto_L$ is seen at Routh Low Farm and Routh High Farm which show reversed relationship between $\propto_S$ and $\propto_L$. At Benningholme and Sunk Island boreholes, model estimates for *BE* are more or less equal to both short-term ($\propto_S$) and long-term ($\propto_L$) barometric efficiencies, and correspond to the more highly confined behavior at these boreholes. The same observation is made at Woodhouse Farm and Bracy Bridge boreholes. However this is due to conditions close to unconfined where the borehole water levels show a weak response to barometric pressure at all frequencies and therefore give low values of barometric efficiency.

The static barometric efficiency (*BE*) is principally governed by the elastic properties of the aquifer and represents borehole water level response to barometric pressure changes under undrained response conditions. Under such conditions negligible flow occurs between the aquifer and water table to dissipate the change in pore water pressure. The short-term ($\propto_S$) barometric efficiency represents the borehole water level response to fast (high frequency) changes in barometric pressure. These changes can be sufficiently fast to achieve undrained response conditions and it is therefore anticipated that the static barometric efficiency (*BE*) will be close to the short-term barometric efficiency ($\propto_S$). However, short-term barometric efficiency ($\propto_S$) can be limited to an upper bound due to limitations on barometric pressure signal energy at high frequencies or due to limited flow rate between the aquifer and borehole caused by low aquifer transmissivities. *BE* from model is determined from the response across all frequencies and thus has no such upper bound, Figure 7.3a. It is therefore expected that model *BE* will be either equal to or larger than short-term barometric efficiency ($\propto_S$) which is consistent with observations shown in Figure 10.3. In semi-confined aquifers $\propto_L$ should be smaller than $\propto_S$, because long-term pressure changes have time to dissipate through the borehole-aquifer system, compared to short-term changes, see section 6.2. This is consistent with observed relationship between $\propto_S$ and $\propto_L$ except at Routh Low Farm and Routh High Farm boreholes where low rate of flow between the borehole and the aquifer causes this relationship to be reversed, Figure 10.3.

Table 10.1. Comparison between model [*Rojstaczer*, 1988a] and linear regression estimates of barometric efficiency, Tables 6.1 and 8.1.

Borehole			Model Barometric efficiency, *BE* %		Barometric efficiency for filtered signals using linear regression	
			Best	Range	$\propto_L$ % ± SE %	$\propto_S$ % ± SE %
1	Benningholme		49	49	47.4 ± 0.1	47.9 ± 0.1
2	Wilfholme	M1	47	45-49	33.2 ± 0.6	38.9 ± 0.4
		M2	47	45-49	32.6 ± 0.4	38.4 ± 0.5
		M3	47	47	28.9 ± 0.2	37.7 ± 0.3
3	Sunk Island		39	37-39	37.9 ± 0.1	39.1 ± 0.1
4	Park House Farm		56	52-58	41.9 ± 0.5	41.8 ± 0.8
5	Routh Low Farm		42	38-45	17.4 ± 1.0	7.6 ± 1.9
6	Routh High Farm		51	50-53	32.2 ± 0.2	27.6 ± 0.4
7	Thornholme Moor		39	38-40	29.7 ± 0.3	37.2 ± 0.2
8	West Newton Farm		55	53-58	38.3 ± 0.1	45.4 ± 0.1
9	Woodhouse Farm		15	0-100	9.7 ± 0.9	13.5 ± 0.9
10	Bracy Bridge		0.0	0-5	1.8 ± 1.3	2.2 ± 2.3

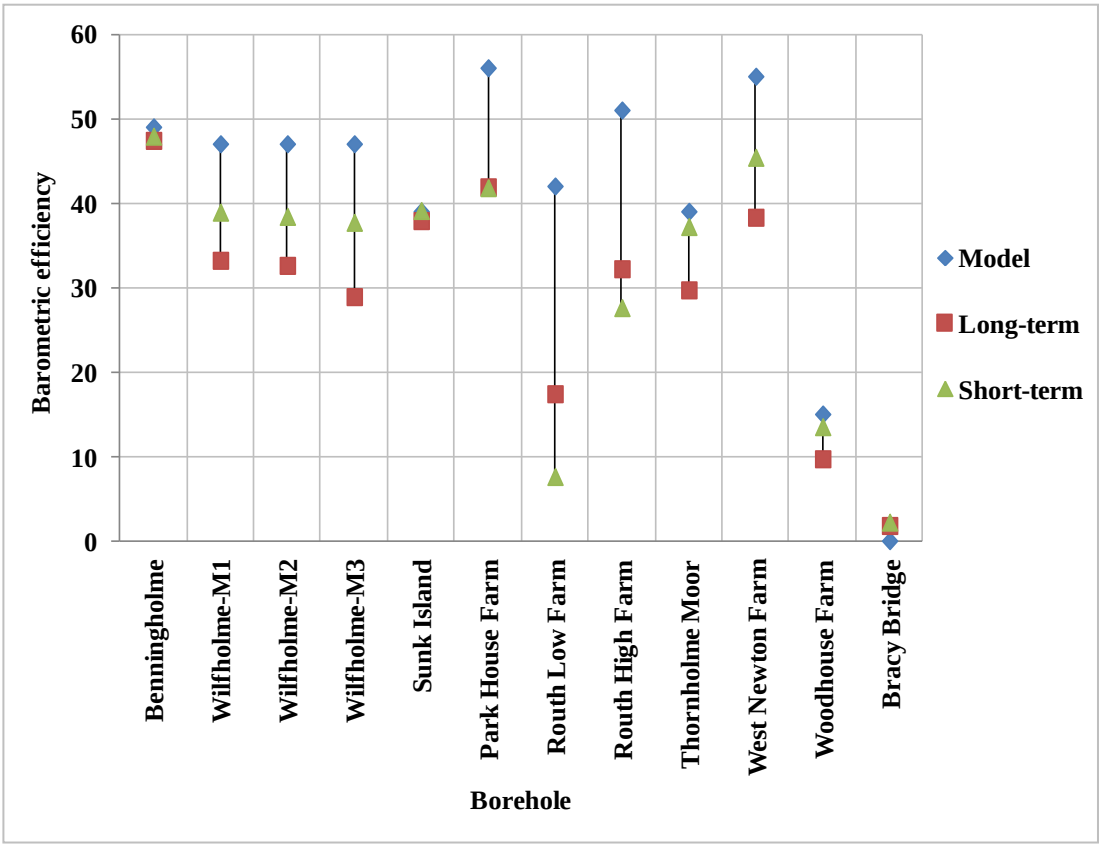

Figure 10.3. Barometric efficiencies obtained from model [*Rojstaczer*, 1988a] and linear regression (long-term, $\propto_L$, and short-term, $\propto_S$).

Aquifer transmissivity derived from the barometric response function

Discrepancies of up to two orders of magnitude between barometric response function and pumping tests values for aquifer transmissivity have been explored using slug tests. Induced changes in borehole water levels due to barometric pressure changes are of the order of a centimeter whereas pumping tests induce drawdown of the order of a meter or more. Theoretically slug tests results should give the same transmissivity value irrespective of the applied initial head displacement. However, results show a power-law relationship between the initial head change and aquifer transmissivity with varying exponents (0.32-0.66), similar to that observed by *Lee et al.* [1999] for slug tests in highly fractured gneiss with exponents range of 0.29-0.8. This relation can be attributed to partial penetration effects that are likely due to the design of monitoring boreholes with plain casings that penetrate 4-15 m through the top high conductivity layer of the Chalk Aquifer. It is thought that changing the slug volume changes the tested volume and effective thickness of the aquifer, and therefore changes the estimated aquifer transmissivity. This is also supported by pumping test data from Wilfholme-M2 borehole which shows that the estimated aquifer transmissivity (using Theis method) increases as increasingly larger time intervals are considered. The results of the slug test therefore suggest that estimated aquifer transmissivity, T_{aqu}, using barometric response function method is sensitive to borehole construction and should be considered as a lower bound only for actual aquifer transmissivity.

Pneumatic and hydraulic diffusivities derived from the barometric response function

Values for pneumatic and hydraulic diffusivities for different sediment types are not commonly discussed in literature. Therefore, estimated values for these parameters in this study are here compared with previous studies (Table 10.2). In this study, derived ranges for pneumatic (D_{unsat}) and hydraulic (D_{con}) diffusivities of glacial sediments are from 0.9 to 128 m^2/day and from 10 to 5×10^4 m^2/day respectively. These ranges are generally consistent with values derived by *Rojstaczer* [1988a] and *Evans et al.* [1991] for cases where the confining layer is composed of marine sediments, sandstone or mixture of sandstone and claystone, see Table 10.2. In contrast, values estimated by *Weeks* [1979] and *Galloway and Rojstaczer* [1988] for pneumatic diffusivity, D_{unsat}, for alluvium and highly fractured tuffs are one order of magnitude larger (Table 10.2)

inferring more diffusive unsaturated zones. In the literature, pneumatic diffusivity values are principally smaller than hydraulic diffusivity values with a ratio (D_{unsat}/D_{con}) that ranges from ~ 10^{-4} to 1, Table 10.2. This is generally consistent with ratios of 2.4×10^{-4} to 1 observed in this study. In reality conditions in the top soil layer such as water content, clay content and capillary fringe effects may significantly influence air diffusivity through the unsaturated zone. Therefore, a clear and consistent relationship between estimates of D_{unsat} and D_{con} particularly in cases where the confining layer is highly heterogeneous should not be expected.

Table 10.2. Estimated pneumatic and hydraulic diffusivities from previous studies.

	Composition of confining layer	Depth to water table (m)	D_{con} (m^2/day)	D_{unsat} (m^2/day)
Weeks [1979]	Alluvial aquifer	38	-----	5.1×10^3
Rojstaczer [1988a]	Marine sediments	18	4.3×10^3	77.5
	Fine to medium sandstone	14	1.7×10^3	0.15
Galloway and Rojstaczer [1988]	Highly fractured tuffs	400	3×10^3	2.3×10^3
Evans et al. [1991]	Sandstone	38-98	545	150
	Sandstone and claystone		1.1×10^3 - 1.6×10^5	86 - 130
	Sandstone and clay-rich beds		33.3 - 397.5	17.3 - 86

10.5. Impact of confining layer heterogeneity

The estimated hydraulic diffusivity (D_{con}) for all boreholes ranges from 10 to 5×10^4 m^2/day (Table 8.1) which varies over 4 orders of magnitude, reflects the wide range of glacial deposits overlying the East Yorkshire Chalk Aquifer. D_{con} estimates at Benningholme, Wilfholme, Sunk Island, Woodhouse Farm and Bracy Bridge boreholes are consistent with lithology logs at these boreholes. However, D_{con} estimates at other boreholes are not consistent with their lithology logs. Results of MODFLOW modeling suggests that a heterogeneity consisting of a high diffusivity

material, located up to 500 m from the observation borehole, in a confining layer of low diffusivity can significantly contribute to the estimated barometric response function. Low frequencies "see" further from the borehole while high frequencies mostly reflect the borehole log. Estimated barometric response functions are dominated by low frequencies due to limitations of signal energy and coherence between water level and barometric pressure. Thus barometric response functions are likely to be influenced by heterogeneities in the confining layer, creating inconsistencies between estimates of D_{con} and borehole lithology logs.

Selected boreholes cases are shown (Figures 10.4 and 10.5) to illustrate situations where estimates of D_{con} are consistent and inconsistent with borehole lithology logs, by comparing the lithology logs (EA and BGS) with superficial deposit maps [*Edina-Digimap "Geological Map Data © NERC,* 2011"] and 'Lithoframe' cross sections provided by the EA [*BGS © NERC*, 2008. *All Rights Reserved*]. A circle of 500 m radius around each borehole is used to represent the probable limit of expected influence of heterogeneity on the barometric response function.

Figure 10.4 shows two boreholes (Benningholme and Woodhouse Farm) where estimates of D_{con} are consistent with lithology logs. D_{con} at Benningholme is low (10 m^2/day) and the log at this borehole shows 16.2 m of clay-rich glacial deposits (Figure 8.2b). Two additional BGS lithology logs (B1 and B2), at 300-500 m distance, show that the confining layer is composed of boulder clay with a few thin layers of sand and gravel (0.5-1 m thick). This is consistent with both the map of superficial deposits and cross sections (Figure 10.4a and b) which show that the glacial sediments are largely composed of 10-20 m till, with some alluvium and river terrace deposits which do not penetrate the full thickness of the confining layer. Thus the confining layer sediments are dominated by clay-rich lithologies, reflected in low values of D_{con}.

At Woodhouse Farm borehole (Figure 10.4c and d), the estimated D_{con} is large (5.0×10^4 m^2/day) and the borehole lithology log (Figure 8.11b) shows a thin 4 m thick confining layer, composed of 2 m of boulder clay overlain by 2 m of sandy clay. The map and cross section of superficial deposits (Figure 10.4c and d) show a confining layer of 7 m thick thinning to almost zero 500 m east of the borehole where glaciofluvial (sands and gravels) deposits are dominant. This is consistent with the

high hydraulic diffusivity which reflects a thin confining layer and presence of glaciofluvial deposits. Similarly Wilfholme, Sunk Island and Bracy Bridge boreholes showed consistency between derived D_{con} and lithology logs, superficial deposits and geological cross sections. Similar barometric response functions and hence similar derived parameters are seen at M1, M2 and M3 boreholes at Wilfholme, forming a "huddle test", which suggests a relatively homogeneous confining layer at least on the scale of 45 m distant between these boreholes.

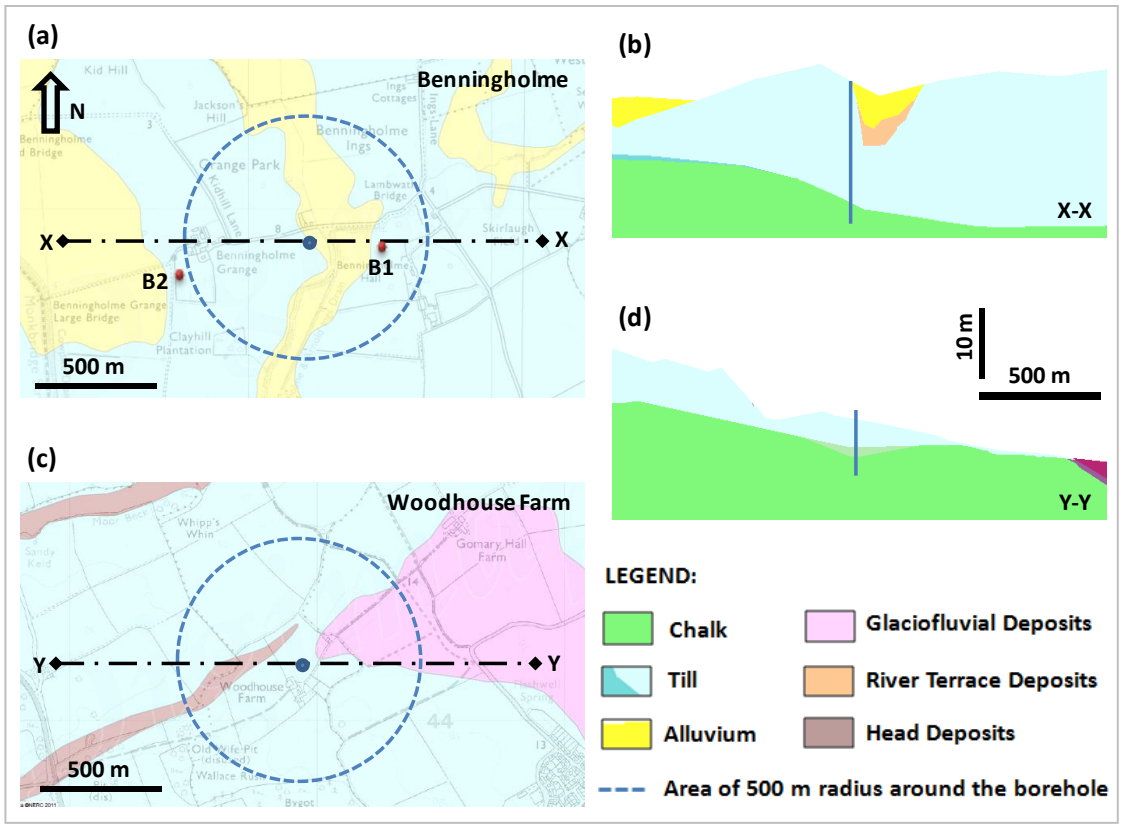

Figure 10.4. Superficial deposits maps; (a) Benningholme borehole and (c) Woodhouse Farm borehole, after [*Edina-Digimap "Geological Map Data © NERC 2011"*] and two cross sections through superficial deposits; (b) at Benningholme borehole and (d) at Woodhouse Farm borehole, provided by the EA after [*BGS © NERC, 2008. All Rights Reserved*]. Around the Benningholme borehole, superficial deposits are 10-20 m thick and are largely composed of glacial till with shallow alluvium deposits. Around the Woodhouse Farm borehole, superficial deposits are 0-7 m thick and are largely composed of glacial till and glaciofluvial deposits.

Figure 10.5 shows the location of Park House Farm borehole where the estimated D_{con} (224 m^2/day) is not consistent with the lithology log (Figure 8.6b) which shows 20 m of clay-rich deposits and therefore suggests a low D_{con} value. The map of superficial deposits (Figure 10.5a) shows a highly heterogeneous confining layer (till, river terrace deposits, alluvium, glaciofluvial and channel deposits) around this borehole. There are also sand and gravel pits located at ~ 500 m from this borehole (Figure 10.5a). Four additional BGS borehole logs (P1, P2, P3 and P4) close to Park House Farm (Figure 10.4a) indicate a sediment cover composed solely of sand and gravel. This infers that the large estimate of D_{con} at Park House Farm reflects high diffusivity heterogeneities (sands and gravels) in the confining layer within a radial distance of some hundreds of meters surrounding the Park House Farm borehole. In addition, the significant thinning of confining layer composed of channel deposits (largely sand and gravel), at the Gransmoor Quarry 1 km distant from the Park House Farm borehole (Figure 10.5b, section Y-Y) may have significant impact. The presence of high diffusivity deposits and thinning of the confining layer may explain the misfit of the model to the barometric response function at low frequencies at the Park House Farm borehole (Figure 8.6a).

The above shows that derived properties of confining layer using barometric response function technique, particularly D_{con}, are representative of the local geology in an area surrounding monitoring boreholes of about 500 m radius. However, information about the local geology derived from superficial deposits maps, geological cross sections and lithology logs is of limited resolution due to limitations of the density of data (e.g. borehole logs, exposures, geophysics ...etc) which were used to compile these geological maps and sections. Thus barometric response functions give information on D_{con} that may not be apparent in maps of confining layer lithology.

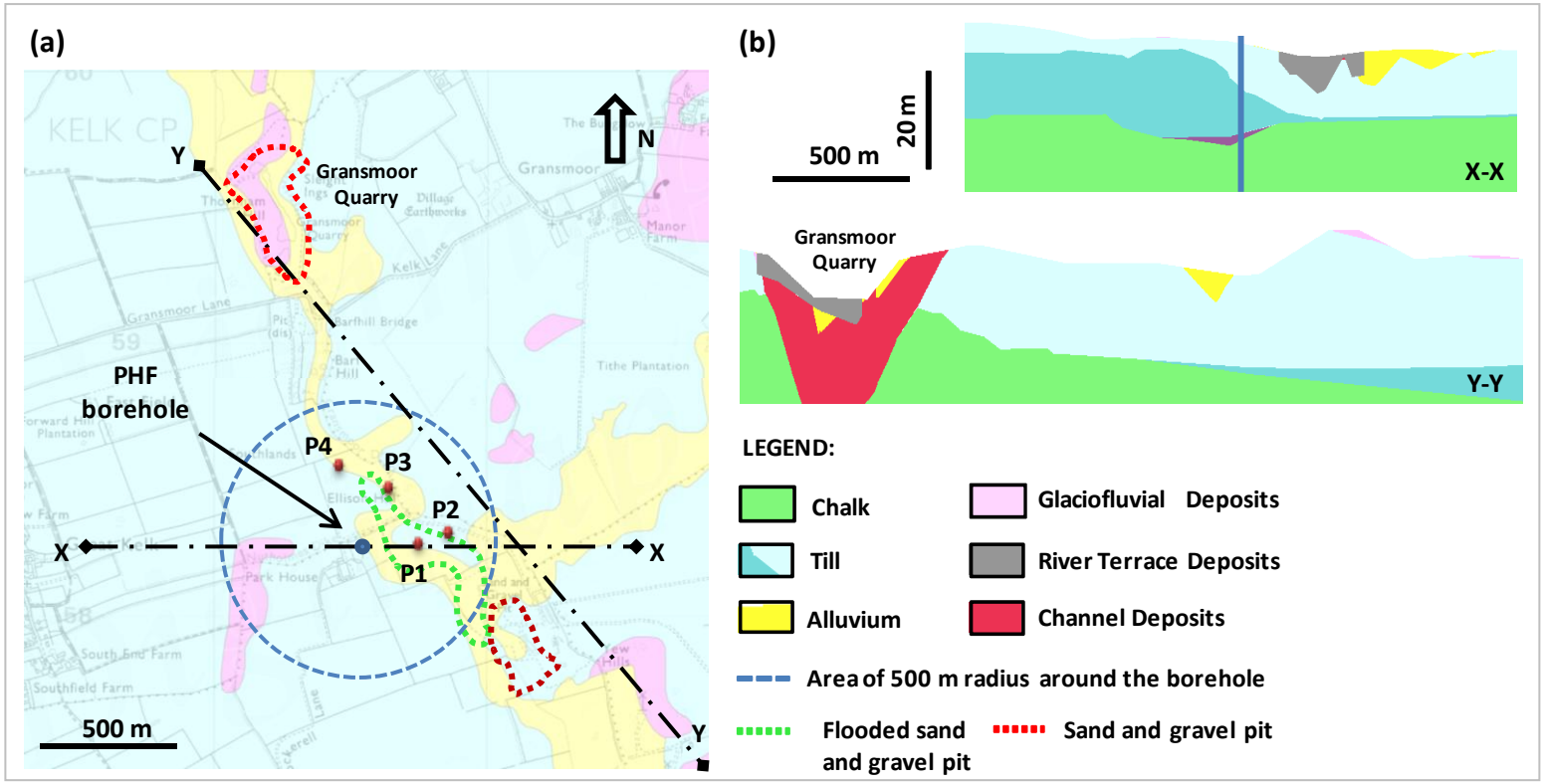

Figure 10.5. (a) Superficial deposit map at Park House Farm borehole after [*Edina-Digimap "Geological Map Data © NERC 2011"*]. (b) Two cross sections through superficial glacial deposits at Park House Farm, provided by the EA [*after BGS © NERC, 2008. All Rights Reserved*]. The superficial deposits around this borehole are 15-25 m thick and largely composed of glacial till with some shallow glaciofluvial and river terrace deposits. Sand and gravel pits are located 500-600 m away and the Gransmoor Quarry at a distance of 1000 m. Four BGS lithology logs (red dots), near Park House Farm borehole, show sediments composed solely of sand and gravel.

10.6. The link to aquifer vulnerability

According to *Boland et al.* [1999] 'Groundwater vulnerability is a measure of the significance of a pathway and receptor' reflecting the importance characterizing the vertical pathways from the ground surface to the aquifer. Intrinsic vulnerability is a function of the nature and thickness of the overlying confining layer, depth to water table and characteristics of the aquifer materials [*United States National Research Council*, 1993]. In general, the greater the clay content within the confining glacial sediments, the lower the hydraulic conductivity and the more protective it is to the aquifer. However high permeability materials within clay-rich glacial sediments (e.g. sands and gravels) may provide preferential pathways for contaminants to the aquifer. The land use in the Holderness Peninsula, East Yorkshire is dominated by arable farming and use of agricultural fertilizers since the 1950s have caused increasing nitrate levels in groundwater.

The local scale structure of the glacial deposits covering the Chalk Aquifer can vary over a few meters and is not well known everywhere. *Kilner et al.,* [2005] conducted a geophysical study to characterize the glacial sediments cover at two sites located in the confined aquifer. Borehole logs 20-30 m apart suggested the presence of small channels of sand and gravels within the confining layer which is otherwise composed of clay-rich materials. Significant high conductive pathways (composed of sand and gravel) through the confining layer were revealed by combining data from borehole logs with geophysical data (resistivity and electromagnetic induction). They also observed till which was weathered and fractured down to 5 m depth at coastal exposures, where fractures could provide significant pathways for contaminants. The existing maps of the glacial sediments are based largely on sparse borehole logs and thus cannot provide detailed local information on lithology and the continuity of permeable layers, which are key information for aquifer vulnerability assessment [*Kilner et al.,* 2005]. Available information on local geology can be misleading due to the highly heterogeneous nature of the glacial sediments, as shown in section 10.5.

Little information is available on the hydraulic conductivity (K_{con}) and specific storage (S_{sc}) of the glacial sediments of the area. Pumping and slug tests give estimates of the horizontal hydraulic conductivity, but vertical hydraulic conductivity is more

important for aquifer vulnerability. The flow rate of water carrying pollutants such as nitrate through a confining layer is controlled by vertical hydraulic conductivity and the head gradient where it is downwards. The barometric response function method gives vertical hydraulic diffusivity (K_{con}/S_{sc}) but it is not possible to separate the hydraulic conductivity unless the specific storage is known from other sources. However, diffusivity has been used in previous literature as an indicator of the existence of high flow pathways. *Knudby and Carrera* [2006] conducted a modeling study to simulate the impact of aquifer heterogeneity on diffusivity estimated from pumping tests. Their results suggested that hydraulic diffusivity is a reliable indicator of the degree of connectivity of high diffusivity pathways for both flow and/or solute transport. Data on hydraulic conductivity (K_{con}) and specific storage (S_{sc}) for a range of glacial sediments collected from literature [*Urish,* 1981; *Younger,* 1993; *Martin and Frind,* 1998; *Batu,* 1998; *Kilner,* 2004; *Quinn,* 2009] are plotted on a log-log plot in Figure 10.6. It shows that the hydraulic diffusivity (K_{con}/S_{sc}) for confining layer composed of a mix of glacial sediments is more sensitive to the hydraulic conductivity, which varies over 11 orders of magnitude, than to specific storage, which varies only over 2-3 orders of magnitude. This suggests that the hydraulic diffusivity may be used as a measure of aquifer vulnerability.

Results of modeling the impact of confining layer heterogeneity show that barometric response function represents the confining layer properties of an area surrounding, and not only the immediate vicinity, of the borehole. It shows that the barometric response function will reflect the presence of high diffusive pathways where present within an area surrounding the borehole with a radius of several hundred meters. It also shows that low frequencies can "see" further from the borehole than high frequencies, and thus low frequencies are more important for assessing the presence of high diffusive pathways and for indicating aquifer vulnerability. Hence, the barometric response function technique is a useful indicator for aquifer vulnerability as it can be easily estimated at these lower frequencies where the barometric pressure signal has greatest energy. In this study a high pass filter is used to remove recharge and the barometric response function is limited to frequencies above the cut-off of this filter. This suggests that a better filter to remove recharge which does not remove the response to barometric pressure at low frequencies, would be useful to extend the barometric response function to yet lower frequencies.

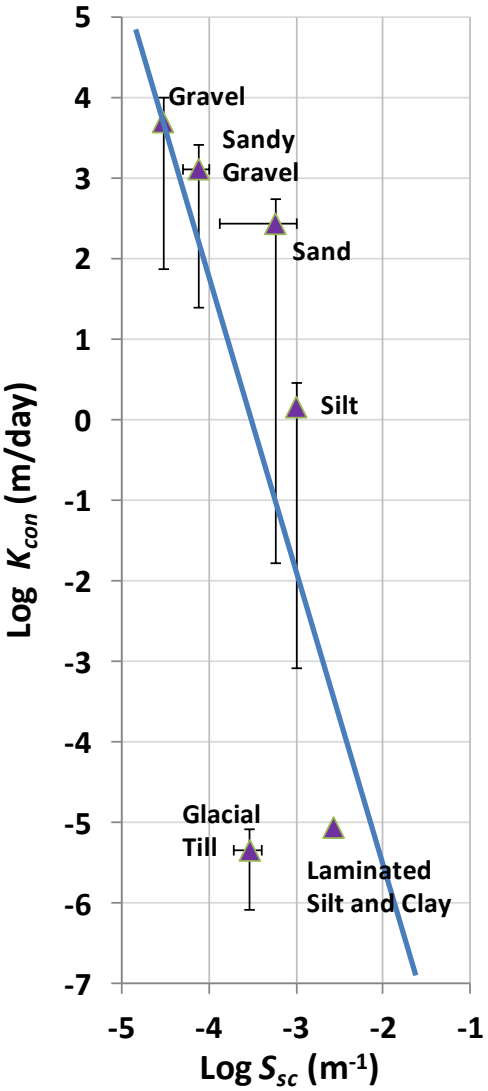

Figure 10.6. Log-log plot of specific storage (S_{sc}, m^{-1}) versus hydraulic conductivity (K_{con}, m/day) for glacial sediments [*Urish*, 1981; *Younger*, 1993; *Martin and Frind*, 1998; *Batu*, 1998; *Kilner*, 2004; *Quinn*, 2009] showing a strong variation of K_{con} over 11 orders of magnitude, while S_{sc} varies only over 2-3 orders of magnitude.

10.7. Towards a measure of aquifer confinement

The vertical pneumatic diffusivity governs the rate of air pressure diffusion through the unsaturated zone, while the vertical hydraulic diffusivity governs the rate of head diffusion through the saturated confining layer. In case of a homogeneous confining layer, estimated vertical diffusivities will be dominated by the clay content of materials along the diffusion pathway, i.e. high diffusivity values are likely to be found where the confining layer has less clay content and the vice versa [*Roeloffs*, 1996]. However in case of a heterogeneous confining layer, vertical diffusivities estimated from the barometric response function are likely to be dominated by high diffusivity pathways.

A measure of intrinsic vulnerability

Kruseman and Ridder [2000] suggested the use of hydraulic resistance (K_{con}/L_{sat}) as a measure of resistance to vertical flow, where K_{con} and L_{sat} are the hydraulic conductivity and saturated thickness of the confining layer respectively. This could be used as a measure of groundwater vulnerability, since it reflects the ease with which contaminants can travel through the confining layer. However, the barometric response function gives only diffusivities. The ratio of the square of layer thickness to the vertical diffusivity gives a characteristic time scale for the vertical diffusion of head and can be used as a useful measure of confinement [*Barker*, 1993; *Roeloffs*, 1996]. *Roeloffs* [1996] used this ratio to estimate the time scale for the dissipation of aquifer pore pressure through vertical diffusion to the water table as a function of the saturated zone thickness and hydraulic diffusivity. A related characteristic time scale parameter (C_{ts}, in time units, Equation 10.1) which is a function of the unsaturated and saturated confining layer diffusivities and thicknesses is introduced here as a measure of the degree of aquifer confinement:

$$C_{ts} = \frac{L_{unsat}^2}{D_{unsat}} + \frac{L_{sat}^2}{D_{con}} . \qquad (10.1)$$

Since C_{ts} depends on D_{con} and D_{unsat} it characterizes the presence of high conductive vertical pathways within some hundred meters of the borehole, which is a key advantage for the assessment of groundwater vulnerability where the confining layer is highly heterogeneous. In other vulnerability assessment methods the presence of such pathways can be easily missed due to limited resolution of information on local geology.

Application to the Chalk Aquifer in East Yorkshire

The characteristic time scale (C_{ts}) in Equation 10.1 is composed of an unsaturated zone term and a saturated zone term. Due to the nature of the Chalk Aquifer in East Yorkshire, C_{ts} estimates are dominated by the saturated zone term because the unsaturated zone thickness (L_{unsat}) is always small comparing with the thickness of saturated confining layer (L_{sat}). Low values of C_{ts} reflect low degrees of confinement, i.e. thin and/or highly diffusive confining layer, and the vice versa. Table 10.3 shows the estimated values of C_{ts} for all boreholes which varies over four orders of magnitude. Sunk Island borehole shows the greatest confined behavior (least vulnerable location) with a C_{ts} value of 73.4 days, while Bracy Bridge borehole shows the least confined behavior (most vulnerable location) with a C_{ts} value of only 0.01 days. Note that no consistent correlation is seen between C_{ts} and percentage of clay-rich sediments in the borehole log (Table 10.3). For instance at Bracy Bridge, Park House Farm and Thornholme Moor boreholes, the percentage of clay-rich sediments is large (63-84%) suggesting a high degree of confinement while C_{ts} values are small (0.01-1.9 days) suggesting a low degree of confinement. This is because D_{con} reflects the hydraulic diffusivity of an area surrounding the borehole and not just the borehole lithology log, as discussed in section 10.5.

Thus vertical pneumatic and hydraulic diffusivities of the confining layer derived from the barometric response function can be integrated with available information on the thicknesses of unsaturated and saturated zones to estimate the characteristic time scale (C_{ts}). This C_{ts} is a measure of the overall aquifer vulnerability to contaminants moving passively with flow where head gradients are downwards. Over much of the confined part of the Chalk Aquifer head gradients are downwards, either continuously or

seasonally, through glacial sediments to the aquifer, see section 4.5 in Chapter 4. The most common hazard to the Chalk Aquifer in East Yorkshire is nitrate contamination. In literature, it is generally accepted that nitrate is highly mobile in groundwater [*Bolger et. al*, 1999; *Liu and Liptak*, 2000]. Therefore, the characteristic time scale (C_{ts}) may be used as a measure of aquifer vulnerability to nitrate or any other conservative contamination. It has generally been assumed that the confining glacial sediment over much of the area provide an effective protective layer to the aquifer from surface contamination [*Smedley et al.*, 2004]. However, barometric response functions derived in this study give non-zero D_{con} and D_{unsat} and therefore the confining layer is nowhere found to purely confine the aquifer. The range of C_{ts} values together with observation of downward direction of head gradient show that aquifer vulnerability is significant over much of the area.

Table 10.3. Vertical hydraulic diffusivities (D_{con}) derived from barometric response functions, thickness and percentage of clay-rich sediments from lithology logs and characteristic time scales for all boreholes.

Borehole	Total thickness of clay (m)	% clay-rich sediments	D_{con}, (m^2/day)	Characteristic time scale, C_{ts} (days)
Benningholme	6.8	42	10	22.5
Wilfholme	2.7	23	25	4.3
Sunk Island	4.3	12	15	73.4
Park House Farm	16.5	80	224	1.9
Routh Low Farm	7.7	57	34.6	4.2
Routh High Farm	7.7	57	133.2	1.4
Thornholme Moor	16.0	84	310	1.1
West Newton Farm	35.4	93	121.1	10.6
Woodhouse Farm	1.1	25	5×10^4	0.07
Bracy Bridge	6	63	2×10^4	0.01

CHAPTER 11: CONCLUSIONS

11.1. Towards study aim and objectives

The aim of this study, as stated in Chapter 1, is to develop a methodology for assessing groundwater vulnerability of confined/semi-confined aquifers using borehole water level response to barometric pressure and to apply this methodology to the Chalk Aquifer of East Yorkshire. To achieve this aim the following objectives were considered:

1. To collect time series data of water levels from a selected group of monitoring boreholes and barometric pressure using automatic pressure transducers.
2. To apply time series analysis to characterize and remove components other than barometric pressure which contribute to the borehole water level signals.
3. To apply the deconvolution technique to filtered water level signals to estimate barometric response functions.
4. To estimate aquifer and confining layer properties through application of theoretical response models.
5. To assess the use of the barometric response function for characterizing aquifer vulnerability for semi-confined aquifers.

11.2. Major conclusions of the study

The major conclusions from this study are:

1) Time series analysis confirmed that the influences contributing to water level signals from examined boreholes are principally barometric pressure, Earth and ocean tides, recharge and pumping effects.

2) Time series analysis techniques are used to filter influences other than barometric pressure from the borehole water level signals in order to obtain accurate estimates of barometric response functions. The recharge contribution occurs at low frequencies up

to 0.05 cycles/days and induced water level variations due to Earth and ocean tides are up to 4.0 cm.

3) Deconvolution techniques are used to estimate the barometric response function from filtered borehole water level and barometric pressure time series. A wide range of barometric response function shapes is obtained in the frequency range of 0.017-2 cycles/day. These barometric response functions show strong dependence on frequency for most of the borehole time series analyzed.

4) The observed frequency range of barometric response functions contains enough information in most cases to estimate the pneumatic (D_{unsat}) and hydraulic (D_{con}) diffusivities of the confining layer to which the lower frequencies in the barometric response function are most sensitive. The estimated ranges for D_{unsat} and D_{con} diffusivities vary over four orders of magnitude, from 0.9 to 128 m^2/day and from 10 to 5×10^4 m^2/day respectively.

5) The static barometric efficiency (*BE*) derived from the barometric response function are generally greater than short-term ($\propto_S$) and long-term ($\propto_L$) barometric efficiencies computed using linear regression. However, estimates of *BE*, $\propto_S$ and $\propto_L$ were found to be nearly equal for cases which show either highly confined or nearly unconfined behavior.

6) Estimated aquifer transmissivity (T_{aqu}) from the barometric response function is highly sensitive to conditions very close to the borehole and thus to borehole construction. Estimates of T_{aqu} can be one or two orders of magnitude lower than the true value (eg. from pumping tests) and thus should be regarded with caution and used as a lower bound.

7) Simple groundwater flow modeling shows that the high frequencies of the barometric response function reflect the confining layer properties in the immediate vicinity of the borehole while low frequencies reflect confining layer properties over greater distances. Low frequencies of the barometric response function are sensitive to the presence of highly conductive vertical pathways through the confining layer up to

some hundreds of meters from the borehole. Thus barometric response functions give information on confining layer properties that may not be apparent from maps of confining layer lithology due to limited resolution.

8) Data collected from the literature on hydraulic conductivity and specific storage for a range of glacial sediments suggest that hydraulic diffusivities are most sensitive to variations in hydraulic conductivity, which varies over 11 orders of magnitude, than to specific storage, which varies only over 2-3 orders of magnitude. It is therefore thought that hydraulic diffusivity may be used as a measure of aquifer vulnerability.

9) Estimates of pneumatic (D_{unsat}) and hydraulic (D_{con}) diffusivities for the twelve boreholes examined here are significant (non-zero), and thus the aquifer is semi-confined everywhere and nowhere purely confined. This together with the observed downward head gradient over most of the Chalk Aquifer in East Yorkshire implies that the aquifer is potentially vulnerable to surface contamination.

10) The properties of confining layer that can be derived from barometric response functions (vertical pneumatic and hydraulic diffusivities) give valuable information for aquifer vulnerability assessment in contrast to conventional aquifer testing approaches which give horizontal hydraulic parameters rather than the vertical parameters which are the most important for aquifer vulnerability.

11) A characteristic time scale term (C_{ts}) is introduced which is a function of thicknesses and vertical diffusivities of the unsaturated and saturated zones in the confining layer derived from the barometric response function. Since diffusivities from the barometric response function reflect the presence of any highly conductive vertical flow pathways through the confining layer, this term is proposed as a measure of the degree of aquifer confinement and as a quantitative measure of intrinsic aquifer vulnerability.

12) Borehole time series data from which barometric response functions may be derived are cheap and easy to collect using simple pressure transducers. The large network of monitoring boreholes throughout the major aquifers in the UK indicates

that these techniques have a significant potential to improve the assessment of groundwater vulnerability.

13) The use of barometric response functions helps to improve our understanding about the strata which confine aquifers. However, the application of this technique is limited to the availability of time series data and monitoring boreholes and is suggested to cover some hundreds of meters from the borehole. Hence, this technique can be integrated with other methods as a quantitative tool for assessing aquifer vulnerability particularly for local scale problems.

11.3. Recommendations for future research

This research has highlighted some questions in need of further investigation. In this study a high pass filter is used to remove recharge and thus the barometric response function is limited to frequencies above the cut-off of this filter. This suggests that further research might explore a better filter to remove recharge, without removing the response to low frequencies of barometric pressure. This has been beyond the scope of the present study. However it has been possible to characterize and better understand the recharge signal which shows that it is predictable to some degree. It is thought that a time domain technique along the lines of those used to remove Earth tides could be developed to remove recharge. This would permit the barometric response function to be extended to lower frequencies where the barometric pressure has significant energy and may further improve the estimation of confining layer properties. In addition, numerical flow modeling has shown that these lower frequencies reflect the confining layer properties up to some distance from the borehole. Therefore these frequencies contain useful information on the heterogeneity of the confining layer and are thus potentially valuable for the assessment of groundwater vulnerability.

Further work can be done to investigate the high frequency contribution of rainfall recharge to water levels of boreholes located near the confined edge. Low coherence between barometric pressure and borehole water levels was observed at two boreholes

located at 1-3 km from the confined edge. This suggests strong contribution from the rainfall recharge at high frequencies. Coherence and cross-correlation analysis between borehole water level and rainfall recharge could be applied to explore the extent of this contribution. Additional work may be needed to filter this contribution at high frequencies in order to get a better estimate of the barometric response function.

More work is needed to explore the impact of heterogeneity of the confining layer on the barometric response function. The present study has shown a simple 2D flow modeling using MODFLOW. This could be further developed using 3D multi-phase (air/water) flow modeling to fully explore the impact of heterogeneity on the response mechanism through both unsaturated and saturated zones. This would potentially provide further insights into the extent to which the barometric response function reflects the confining layer properties.

The implemented techniques and tools for time series analysis of borehole water level and barometric pressure time series could be potentially applied more widely to other problems in hydrogeology such as the response relationships between rainfall, runoff and stream flow in catchment dynamics and borehole water levels and pumping tests in aquifer testing problems. For example, some initial work has been done by *Weiler et al.* [2003] in catchment dynamics and by *Gringarten* [2008] in application to pumping tests.

List of references

Acworth, R.I. and T. Brain. 2008. Calculation of barometric efficiency in shallow piezometers using water levels, atmospheric and Earth tide data. *Hydrogeology Journal*. **16**(8), pp.1469-1481.

Agnew, D.C. 2007. Earth Tides. *In*: T.A. Herring, ed. *Treatise on Geophysics: Geodesy*. New York: Elsevier, pp.163-195.

Aller, L. et al. 1985. *DRASTIC: a standardized system for evaluating groundwater pollution potential using hydrogeologic settings*. Ada, Oklahoma: US EPA, Robert S. Kerr Environmental Research Laboratory, EPA/600/2-85/0108.

Alsumait, J.S. and J.K. Sykulski. 2009. Solving Economic Dispatch Problem using Hybrid GA-PS-SQP Method. *In: EUROCON 2009, 18 - 23 May 2009, Saint Petersburg, Russia*, pp.351-356.

Barker, J.A. 1993. Modelling groundwater flow and transport in the Chalk. *In:* R.A. Downing, M. Price, G.P. Jones, eds. *The Hydrogeology of the Chalk of north-west Europe*. Oxford: Clarendon Press, pp.59-66.

Batu, V. 1998. *Aquifer Hydraulics; A comprehensive guide to hydrogeologic data analysis*. New York: John Wiley & Sons, Inc.

Beavan, J. et al. 1991. Estimating aquifer parameters from analysis of forced fluctuations in well level: An example from the Nubian formation near Aswan, Egypt. 2. Poroelastic properties. *Journal of Geophysical Research-Solid Earth and Planets.* **96**(B7), pp. 12139-12160.

Bell, F.G., M.G. Culshaw, and J.C. Cripps. 1999. A review of selected engineering geological characteristics of English Chalk. *Engineering Geology*. **54**, pp.237-269.

Bendat, J.S. and A.G. Piersol. 2010. *Random data analysis and measurements procedures*. 4th ed. New Jersey: John Wiley & Sons, Inc.

Bloomfield, P. 2000. *Fourier analysis of time series: An introduction*. New York: Wiley-Interscience.

Boland, M.P. et al. 1999. *Guidelines and Protocols for investigations to assess site specific groundwater vulnerability*. UK Environment Agency report, R&D Project Record P2/042/01.

Bolger, P. et al. 1999. Contamination of Australian groundwater systems with nitrate. *Land and Water Resources Research and Development Corporation*. Canberra, Occasional Paper No 03/99.

Bredehoeft, J.D. 1967. Response of well-aquifer systems to Earth tides. *Journal of Geophysical Research*. **72**(12), pp.3075-3087.

Butler, J.J., Jr. 1998. *The design, performance, and analysis of slug tests.* New York, Lewis Publishers.

Butler, J.J., Jr. et al. 2011. New Insights from Well Responses to Fluctuations in barometric Pressure. *Ground Water*. **49**(4), pp.525-533, doi: 10.1111/j.17456584.2010. 00768.x.

Chapman, S. and R.S. Lindzen. 1970. *Atmospheric Tides, Thermal and Gravitational*. Netherlands: D. Reidel, Dordrecht.

Clark, W.E. 1967. Computing the barometric efficiency of a well. *Journal of Hydraulics Division, Proceedings of the American Society of Civil Engineers*. HY4, pp.93-98.

Cooper, H.H., Jr., et al. 1965. The response of well-aquifer systems to seismic waves. *Journal of Geophysical Research*. **70**(16), pp.3915-3926.

Cooper, H.H., Jr., J.D. Bredehoeft, and I.S. Papadopulos. 1967. Response of a finite-diameter well to an instantaneous charge of water. *Water Resources Research*. **3**(1), pp.263–269.

Costa, L. et al. 2012. A hybrid genetic pattern search augmented Lagrangian method for constrained global optimization. *Applied Mathematics and Computation*. **218**(18), pp.9415-9426.

Davis, D.R. and T.C. Rasmussen. 1993. A comparison of linear regression with Clark's Method for estimating barometric efficiency of confined aquifers. *Water Resources Research*. **29**(6), pp. 1849–1854, doi:10.1029/93WR00560.

Dai, A. and J. Wang. 1999. Diurnal and semidiurnal tides in global surface pressure fields. *Journal of The Atmospheric Sciences*. **56**, pp.3874–3891.

Dehant, V., P. Defraigne, and J.M. Wahr. 1999. Tides for a convective Earth. *Journal of Geophysical Research*. **104(**B1), pp.1035-1058.

Downing, R.A. 1998. *Groundwater: Our hidden asset*. Nottingham, UK Groundwater Forum, BGS.

ED*i*NA. 2008. *"Geological Map Data © NERC 2008"*. [online]. [Accessed 28 July 2010]. Available from: http://digimap.edina.ac.uk/geologyroam/mapper.

ED*i*NA. 2011. *"Geological Map Data © NERC 2011"*. [online]. [Accessed 7 December 2011]. Available from: http://digimap.edina.ac.uk/geologyroam/mapper.

Elliot, T., D.S. Chadha, and P.L. Younger. 2001. Water quality impacts and palaeohydrogeology in the Yorkshire Chalk aquifer, UK. *Quarterly Journal of Engineering Geology and Hydrogeology*. **34**, pp.385-398, doi: 10.1144/qjegh.34.4.385.

Environment Agency. 1998. *Policy and practice for the protection of groundwater*, 2nd ed. London: The Stationery Office.

Evans, K. et al. 1991. Estimating aquifer parameters from analysis of forced fluctuations in well level: An example from the Nubian formation near Aswan, Egypt. 3. Diffusivity estimates for saturated and unsaturated zones. *Journal of Geophysical Research-Solid Earth and Planets*. **96**(B7), pp.12161-12191.

Foster, S.S.D. and R.I. Crease. 1975. Hydraulic behavior of Chalk Aquifer in Yorkshire Wolds. *Proceedings of the Institution of Civil Engineers Part 2-Research and Theory*. **59**(MAR), pp.181-188.

Foster, S.S.D. and V.A. Milton. 1974. The permeability and storage of an unconfined Chalk Aquifer. *Journal of Hydrology.* **23**, pp.299-311.

Foster, S.S.D. and V.A. Milton. 1976. *Hydrological basis for large-scale development of groundwater storage capacity in the East Yorkshire Chalk*. London, UK: Report of the Institute of Geological Sciences, 76/3, Natural Environment Research Council.

Foster, S.S.D. 1993. The Chalk aquifer – its Vulnerability to Pollution. *In:* R.A. Downing, M. Price and G.P. Jones, eds. *The Hydrogeology of the Chalk of north-west Europe*. Oxford: Clarendon Press, pp.93-112.

Frind, E.O., J.W. Molson, and D.L. Rudolph. 2006. Well vulnerability: A quantitative approach for source water protection. *Ground Water*. **44**(5), pp.732–742.

Furbish, D.J. 1991. The response of water level in a well to a time series of atmospheric loading under confined conditions. *Water Resources Research*. **27**(4), pp.557-568.

Gale, I. and H. Rutter. 2006. *The Chalk aquifer of Yorkshire*. Keyworth, Nottingham: British Geological Survey Report (RR/06/04).

Galloway, D. and S. Rojstaczer. 1988. Analysis of the frequency response of water levels in wells to Earth tides and Atmospheric loading. *4th Canadian/American conference*, pp.100-113.

Gonthier, G.J. 2007. *A graphical method for estimation of barometric efficiency from continuous data - concepts and application to a site in the Piedmont, Air Force Plant 6, Marietta, Georgia.* Georgia: USGS, Scientific Investigation Report (2007–5111).

Gringarten, A.C. 2008. From straight lines to deconvolution: The evolution of the state of the art in well test analysis. *SPE Annual Technical Conference and Exhibition, 24-27 September 2006, San Antonio, Texas.* Society of Petroleum Engineers. (SPE 102079), pp.41-62.

Gubbins, D. 2004. *Time series analysis and inverse theory for geophysicists*. Edinburgh, UK: Cambridge University Press.

Hare, P.W. and R.E. Morse. 1997. Water-level fluctuations due to barometric pressure changes in an isolated portion of an unconfined aquifer. *Ground Water*. **35**(4), pp.667-671.

Harrison, D.H. 1971. *New computer programs for the calculation of earth tides*. Report of the Cooperative Institute for Research in Environmental Sciences. Boulder: University of Colorado.

Hartmann, S. 2004. *The nature of flow and transport in the confined chalk aquifer in East Yorkshire*. Ph.D. thesis, School of Earth and Environment, University of Leeds.

Hartmann, S., N.E. Odling and L.J. West. 2007. A multi-directional tracer test in the fractured Chalk aquifer of E. Yorkshire, UK. *Journal of Contaminant Hydrology*. **94**(3-4), pp.315-331, doi: 10.1016/j.jconhyd.2007.07.009.

Healy, R.W., and P.G. Cook. 2002. Using groundwater levels to estimate recharge. *Hydrogeology Journal.* **10**(1), pp.91-109.

Honig, J.A. and J.A. Murphy. 2001. Antecedent water content and air encapsulation effects on physical properties of sand root zone material. *Journal of Turfgrass Science*. **77**.

Hsieh, P.A., J.D. Bredehoeft and J.M. Farr. 1987. Determination of aquifer transmissivity from Earth tide analysis. *Water Resources Research.* **23**(10), pp.1824-1832, doi:10.1029/WR023i010p01824.

Hvorslev, M.J. 1951. *Time lag and soil permeability in groundwater observations*. Waterways Experiment Station: U.S. Army Corps of Engineers, Bulletin No. 36.

Hyder, Z. et al. 1994. Slug tests in partially penetrating wells. *Water Resources Research.* **30**(11), pp.2945-2957.

Hwang, P.A., N.E. Huang and D.W. Wang. 2003. A note on analyzing nonlinear and nonstationary ocean wave data. *Applied Ocean Research*. **25**, pp.187-193.

Inkenbrandt, P.C. et al. 2005. Barometric and Earth-tide induced water-level changes in the Inglefield Sandstone in Southwestern Indiana. *Proceedings of the Indiana Academy of Science*. **114**(1), pp.1–8.

International Center for Earth Tides. 2009. *TSoft and WPARICET software*. [online]. [Accessed 2 November 2009]. Available from:

http://www.upf.pf/ICET/soft/index.html

In-Situ Inc. 2010. *Rugged TROLL® 100 and 200 Operator's Manual, 0091332 rev. 001 06/10*. Fort Collins, CO, USA.

Jacob, C.E. 1940. The flow of water in an elastic artesian aquifer. *Eos Trans, AGU*. **21**, pp.574-586.

Jacob, C.E. 1946. Radial flow in a leaky artesian aquifer. *Eos Trans, AGU*. **27**, pp.198-205.

Kilner, M. 2004. *Pollution vulnerability assessment of an aquifer overlain by glacial sediments using geophysical techniques*. Ph.D. thesis, School of Earth and Environment, University of Leeds.

Kilner, M., L. Jr. West and T. Murray. 2005. Characterization of glacial sediments using geophysical methods for groundwater source protection. *Journal of Applied Geophysics*. **57**, pp.293-305, doi: 10.1016/j.jappgeo.2005.02.002.

Kilpatrick, A. 2008. A high resolution pumping test in the confined Chalk aquifer in East Yorkshire. M.sc. Dissertation, University of Leeds.

Knudby, C. and J. Carrera. 2006. On the use of apparent hydraulic diffusivity as an indicator of connectivity. *Journal of Hydrology*. **329**, pp.377-389.

Kruseman, G.P. and N.A.de Ridder. 2000. *Analysis and evaluation of pumping test data,* 2nd ed. Netherlands: International Institute for Land Reclamation and Improvement/lLRI.

Kümple, H.J. 1997. Tides in Water-Saturated Rock. *In:* H. Wilhelm, W. Zürn and H. Wenzel, eds. *Tidal Phenomena.* Berlin: Springer-Verlag, pp.145-171.

Landmeyer, J.E. 1996. Aquifer response to record low barometric pressures in the Southeastern United States. *Ground Water*. **34**(5), pp.917-924.

Lee J.Y. and K.K. Lee. 1999. Analysis of the quality of parameter estimates from repeated pumping and slug tests in a fractured porous aquifer system in Wonju, Korea. *Ground Water*. **37**(5), pp.692-700.

Liggett J.E. and S. Talwar. 2009. Groundwater vulnerability assessments and integrated water resource management. S*treamline watershed management*, Bulletin Fall 2009, **13/1** (4), pp.18-29.

Liu, D.H.F., and B.G. Liptak. 2000. *Groundwater and surface water pollution*. United States: Lewis publishers, CRC Press LLC.

Liuni, M.P., M. Loddo and D. Schiavone. 2010. Non-linear inversion using a hybrid global search algorithm: applications in gravimetry. *Extended abstract, EGM 2010 International Workshop, Adding new value to Electromagnetic, Gravity and Magnetic Methods for Exploration, April 11-14 2010, Capri, Italy*.

Logan, P. 1964. Estimating transmissibility from routine production tests of water wells. *Ground Water*. **2**, pp.35-37.

Longman, I.M. 1959. Formulas for computing the tidal accelerations due to the Moon and the Sun. *Journal of Geophysical Research.* **64**, pp.2351–2355.

Maréchal, J.C. et al. 2002. Establishment of Earth tide effect on water-level fluctuations in an unconfined hard rock aquifer using spectral analysis. *Journal of Current Science*. **83**(1), pp.61-64.

MATLAB®, version 7.13.0.564. (R2011b). 2011. Natick, Massachusetts: *The MathWorks Inc*.

Martin, P.J. and E.O. Frind. 1998. Modeling a complex multi-aquifer system: The Waterloo Moraine. *Ground Water*. **36**(4), pp.679-690.

Merritt, M.L. 2004. *Estimating hydraulic properties of the Floridan aquifer system by analysis of Earth-tide, ocean-tide, and barometric effects, Collier and Hendry Counties, Florida*. USGS: Water-Resources Investigations, Report (03–4267).

Neuman, S.P., and P.A. Witherspoon. 1969. Applicability of current theories of flow in leaky aquifers. *Water Resources Research*. **5**, pp.817-829.

Moisy, F. 2006. *Homogenize the error bars for X-axis in log scale, errorbarlogx Matlab function* [online]. [Accessed 20 May 2009]. Available from: http://www.fast.u-psud.fr/~moisy/ml/

Papadopulos, S.S., J.D. Bredehoeft, and H.H. Cooper Jr. 1973. On the analysis of 'slug test' data. *Water Resources Research*. **9**(4), pp.1087-1089, doi: 10.1029/WR009i004p0 -1087.

Payne, J.L. and M.J. Eppstein. 2005. A hybrid Genetic Algorithm with Pattern Search for Finding Heavy Atoms in Protein Crystals. *GECCO'05, June 25-29 2005, Washington, DC, USA.*

Parker, A.H. 2009. *The distribution of permeability in the Chalk aquifer of East Yorkshire*. Ph.D. thesis, School of Earth and Environment, University of Leeds.

Parker, A.H. et al. 2010. A forward modeling approach for interpreting impeller flow logs. *Ground Water*. **48**(1), pp.79-91, doi: 10.1111/j.1745-6584.2009.00600.x.

Peck, A.J. 1960. The water table as affected by atmospheric pressure. *Journal of Geophysics Research*. **65**, pp.2383-2388.

Press, W.H. et al. 2007. *Numerical Recipes in FORTRAN*, 3rd ed. UK: Cambridge University Press.

Price, M. 2009. Barometric water-level fluctuations and their measurement using vented and non-vented pressure transducers. *Quarterly Journal of Engineering Geology and Hydrogeology*. **42**, pp.245-250, doi: 10.1144/1470-9236/08-084.

Quilty, E.G. and E.A. Roeloffs. 1991. Removal of barometric-pressure response from water level data. *Journal of Geophysical Research-Solid Earth and Planets*. **96**(B6), pp.10209-10218.

Quinn, J.D. 2009. *The landslides and recession of the Holderness Coast, Yorkshire, UK*. Ph.D. thesis, School of Earth and Environment, University of Leeds.

Rasmussen, T.C. and L.A. Crawford. 1997. Identifying and removing barometric pressure effects in confined and unconfined aquifers. *Ground Water*. **35**(3), pp.502-511.

Rasmussen, T.C. and T.L. Mote. 2007. Monitoring surface and subsurface water storage using confined aquifer water levels at the Savannah River Site, USA. *Vadose Zone Journal*. **6**(2), pp.327-335.

Reed, J.E. 1980. *Type curves for selected problems of flow to wells in confined aquifers*. Book 3, Chapter B3, Applications of Hydraulics, U.S. Geological Survey.

Ritizi, R.W., S. Sorooshian and P.A. Hsieh. 1991. The estimation of fluid flow properties from the response of water levels in wells to the combined atmospheric and Earth tide forces. *Water Resources Research*. **27**(5), pp.883-893.

Rojstaczer, S. 1988a. Determination of fluid-flow properties from the response of water levels in wells to atmospheric loading. *Water Resources Research*. **24**(11), pp.1927-1938.

Rojstaczer, S. 1988b. Intermediate period response of water levels in wells to crustal strain – sensitivity and noise level. *Journal of Geophysical Research-Solid Earth and Planets*. **93**(B11), pp.13619-13634.

Rojstaczer, S. and D.C. Agnew. 1989. The influence of formation material properties on the response of water levels in wells to Earth tides and atmospheric loading. *Journal of Geophysical Research-Solid Earth and Planets*. **94**(B9), pp. 12403-12411.

Rojstaczer, S. and F.S. Riley. 1990. Response of the water level in a well to Earth tides and atmospheric loading under unconfined conditions. *Water Resources Research*. **26**(8), pp.1803-1817.

Roeloffs, E. 1996. Poroelastic techniques in the study of earthquake-related hydrologic phenomena. *Advances in Geophysics*. **37**, pp.135-195, doi:10.1016/s00652687(08)60-2708.

Salmon, S., D. Chadha, and D. Smith. 1996. Development of a groundwater Resource model for the Yorkshire Chalk. *Journal of the Chartered Institution of Water and Environmental Management*. **10**, pp.413–422.

Schlumberger Water Services. 2006. *Mini-Diver Product Manual*. Delft, Netherlands.

Schlumberger Water Services. 2009. *Mini-Diver* [online]. [Accessed 5 July 2009]. Available from: http://www.swstechnology.com

Smedley, P.L., I. Neumann and R. Farrell. 2004. *Baseline report series: 10, The Chalk Aquifer of Yorkshire and North Humberside*. Groundwater Systems and Water Quality, British Geological Survey Commissioned (Report: CR/04/128), Environment Agency Science Group (Report: NC/99/74/10).

Spane, F.A. 2002. Considering barometric pressure in groundwater flow investigations. *Water Resources Research*. **38**(6), pp.1078, doi: 10.1029/2001wr0007-01.

Straughton, G. 2008. *Saline intrusion within the fractured Chalk aquifer of East Yorkshire, UK*. M.Sc. Dissertation, School of Earth and Environment, University of Leeds.

Theis, C.V. 1935. The relation between the lowering of the piezometric surface and the rate and duration of discharge of a well using groundwater storage. *Trans. AGU*. **16**, pp.519-524.

Toll, N.J. and T.C. Rasmussen. 2007. Removal of barometric pressure effects and Earth tides from observed water levels. *Ground Water*. **45**(1), pp.101-105, doi: 10.1111/j.1745-6584.2006.00254.x.

Turk, L.J. 1975. Diurnal fluctuations of water tables induced by atmospheric pressure changes. *Journal of Hydrology*. **26**(1/2), pp.1-16.

United States National Research Council. 1993. *Ground water vulnerability assessment: Predicting relative contamination potential under conditions of uncertainty*. Washington, D.C.: National Academy Press.

United States Environmental Protection Agency. 1993. *A review of methods for assessing aquifer sensitivity and ground water vulnerability to pesticide contamination:* U.S. Environmental Protection Agency, EPA/813/R–93/002.

Urish, D.W. 1981. Electrical resistivity-hydraulic conductivity relationships in glacial outwash aquifers. *Water Resources Research*. **17**(5), pp.1401-1408.

Van Camp, M. and P. Vauterin. 2005. TSoft: graphical and interactive software for the analysis of time series and Earth tides. *Computer & Geosciences*. **31**, pp.631-640.

Volland, H. 1997. Atmospheric tides. *In:* H. Wilhelm, W. Zürn, and H. Wenzel, eds. *Tidal Phenomena, Lecture Notes in Earth Sciences*. Springer Berlin Heidelberg, pp.221-246, doi: 10.1007/BFb0011464.

Vrba, J. and A. Zoporozec. 1994. *Guidebook on mapping groundwater vulnerability*. Hannover, Germany: IAH, International Contribution for Hydrogeology.

Weeks, E.P. 1979. Barometric pressure fluctuations in wells tapping deep unconfined aquifers. *Water Resources Research*. **15**(5), pp.1167-1176.

Weiler, M., et al. 2003. How does rainfall become runoff? A combined tracer and runoff transfer function approach. *Water Resources Research*. **39**(11), p.1315, doi:10.1029/2003WR002331.

Welch, P.D. 1967. The Use of Fast Fourier Transform for the estimation of power spectra: A method based on time averaging over short, modified periodograms. *IEEE Trans. Audio Electroacoustics*. **AU-15**, pp.70-73.

Wellings, S.R. and J.D. Cooper. 1983. The variability of recharge of the English Chalk Aquifer. *Agriculture Water Management*. **6**, pp.243-253.

Younger, P.L. 1993. Simple generalized methods for estimating aquifer storage parameters. *Quarterly Journal of Engineering Geology*. **26**, pp.127-135.

Zhang, B.Y. and D.N. Lerner. 2002. Understanding a complex adit and shaft groundwater source in a Chalk aquifer. *Quarterly Journal of Engineering Geology and Hydrogeology*. **35**, pp.371-379.

Appendix A: List of symbols

Symbol	Parameter	Unit
a_j and b_j	unknown coefficients for each tidal component *j*	cmH_2O
A	amplitude of periodic barometric pressure wave	m
$A^{BRF}(f)$	gain of barometric response function	dimensionless
$A\omega_j$	amplitude of tidal component *j*	cmH_2O
$A\omega_{j\_err}$	standard error of amplitude for tidal component *j*	cmH_2O
b	aquifer thickness	m
b_w	borehole screen length	m
BE	barometric efficiency	dimensionless
B_p	barometric pressure	cmH_2O
BRF(f)	Barometric Response Function	complex
C	number of samples in full record	dimensionless
C_{ts}	characteristic time scale	days
C_{WB}	normalized coherence between water levels and barometric pressure signals	dimensionless
d	depth of the screen of the borehole measured from the top of the aquifer	m
D_{unsat}	vertical pneumatic diffusivity of the unsaturated zone	m^2/day

Symbol	**Parameter**	**Unit**
D_{con}	vertical hydraulic diffusivity of the saturated zone	m^2/day
F_{min}	lowest frequency of interest	cycles/day
FFT_{WL}	Fast Fourier Transform of water level	complex
FFT_{Bp}	Fast Fourier Transform of barometric pressure	complex
g	the gravity acceleration	m/sec^2
h	pneumatic potential	m
H_t	total head	cmH_2O
$H(t)$	head deviation from static at time *t*	m
H_0	initial head displacement at *t=0*	m
i	the imaginary unit ($\sqrt{-1}$)	dimensionless
J_0 and Y_0	zero-order Bessel functions of the first and second kind	dimensionless
J_1 and Y_1	first-order Bessel functions of the first and second kind	dimensionless
k	number of segments from 1 to N	dimensionless
K_0	modified Bessel function of the second kind of order zero	dimensionless
K_{aqu}	hydraulic conductivity of the aquifer	m/day
K_{con}	vertical hydraulic conductivity of confining layer	m/day
K_r	radial component of hydraulic conductivity of the aquifer	m/day

Symbol	**Parameter**	**Unit**
K_z	vertical component of hydraulic conductivity of the aquifer	m/day
L	number of samples in each segment	dimensionless
L_{con}	total thickness of confining layer	m
L_{sat}	thickness of saturated confining layer	m
L_{unsat}	thickness of unsaturated zone	m
M_{SE}	mean squared error	cm^2
n	aquifer porosity	dimensionless
N	total number of segments	dimensionless
p	degrees of freedom	dimensionless
P	pore pressure	m
P_a	air pressure wave	m
$P_{BB}(f)$	auto-spectrum for barometric pressure signal	$cm^2 \cdot day^{-1}$/cycles
$P_{WW}(f)$	auto-spectrum for water level signal	$cm^2 \cdot day^{-1}$/cycles
$P_{WB}(f)$	cross-spectrum between water levels and barometric pressure signals	$cm^2 \cdot day^{-1}$/cycles
Q	dimensionless frequency of saturated confining layer	dimensionless
r	window tapering ratio	dimensionless
r_c	radius of borehole casing	m

Symbol	Parameter	Unit
r_r	radial distance from the borehole	m
r_w	borehole radius	m
R	dimensionless frequency of the unsaturated zone	dimensionless
$R(\tau)$	step response function	dimensionless
R_e	effective radius of the slug test	m
s	drawdown within the aquifer	m
S	storage coefficient of the aquifer in response to slug test	dimensionless
S_s	specific storage of the aquifer in response to slug test	m^{-1}
S_{sa}	specific storage of the aquifer in response to barometric pressure	m^{-1}
S_{sc}	specific storage of the confining layer	m^{-1}
S_{aqu}	storage coefficient of the aquifer	dimensionless
S_{con}	storage coefficient of the confining layer	dimensionless
t	time	days
T	transmissivity of the aquifer in response to slug test	m^2/day
T_0	time at which a normalized head ($H(t)/H_0$) of 0.368 is achieved in Hvorslev model [1951]	sec
T_{aqu}	aquifer transmissivity	m^2/day

Symbol	Parameter	Unit
T_{cf}	capillary fringe attenuation factor	dimensionless
W	dimensionless frequency of flow between the borehole and the aquifer	dimensionless
WL	borehole water level	cmH_2O
x_0	amplitude of fluctuations in borehole water level	m
z	vertical distance from the water table to the ground surface	m
α	dimensionless storage parameter	dimensionless
$\propto_L$	long-term barometric efficiency	dimensionless
$\propto_S$	short-term barometric efficiency	dimensionless
β	dimensionless time parameter	dimensionless
β_f	aquifer compressibility	m^2/N
β_w	water compressibility	m^2/N
δ	percentage of overlap between segments	dimensionless
ε	loading efficiency of aquifer	dimensionless
ε'	loading efficiency of confining layer	dimensionless
$\mu(\tau)$	impulse barometric response function	dimensionless
$\theta\omega_j$	phase of for tidal component *j*	radians
$\theta^{BRF}(f)$	phase of barometric response function	radians

Symbol	**Parameter**	**Unit**
ρ	density of water	Kg/m^3
$\sigma(f)$	normalized standard error of barometric response function	dimensionless
ω	angular frequency	radians/sec
$\xi(t)$	reconstructed sum of Earth tides	cmH_2O
ψ	square root of anisotropy ratio $(K_z/K_r)^{1/2}$	dimensionless
τ	number of lags from 0 to a maximum of m	dimensionless

Appendix B: *SC* Matlab code (pre-processing code)

The *SC* Matlab code has been developed to characterize and separate different components in the borehole water level signal using time series analysis. Then all components in the water level signal other than barometric pressure are removed as a pre-processing step to estimating the barometric response function. This code assumes that data is sampled every 15 minutes but the code also gives an option to re-sample the signals to a time interval which is a multiple of 15 minutes.

The background and methodology for the analysis are described in Chapter 5. In this code, coherence is used to determine the high pass filter cut-off frequency required to remove the recharge signal. A low pass filter is applied to remove the low energy high frequency noise and some pumping effects. Earth and ocean tide components in the borehole water level signal are reconstructed and removed by applying a periodic time domain filter using the method of *Rasmussen and Mote* [2007]. The final filtered signals for both borehole water level and barometric pressure are then exported to text files (A_WL_output.txt and A_Bp_output.txt) which can be then used to estimate barometric efficiency (see Appendix C) and the barometric response function (see Appendix D).

The listing of the *SC* code is provided in the accompanying CD.

B.1. Inputs to the *SC* Matlab code

Input data files:-

Four column vectors are required to run the *SC* code, in (*.txt) format, for theoretical Earth tides (this vector is only used to be compared to data, thus if not available use a dummy vector instead), barometric pressure, total head (data recorded by pressure transducer under water in borehole) and time respectively. Data should be sampled at 15 minutes intervals. Units for barometric pressure and total head should be in cmH_2O. Units of the time vector should be in hours. By default Earth tides are reconstructed using seven tidal frequencies (O_1, P_1, S_1, K_1, N_2, M_2 and S_2), see method in section 5.3.3 after *Rasmussen and Mote* [2007]. However, the *SC* code gives an option to input a chosen column vector (*.txt format) for frequencies to be used to remove Earth tides. These data files should be located in the same folder as the SC.m code.

To run the *SC* code, simply write SC.m in the Matlab command window and press ENTER. Follow the instructions for inputs and press ENTER after each step:

1. Input the name of the theoretical Earth tides vector including extension (*.txt).
2. Input the name of the barometric pressure vector including extension (*.txt).
3. Input the name of the total head vector including extension (*.txt).
4. Input the name of the time vector including extension (*.txt).
5. Option: input (1) to choose to use the full record or input (2) to select the number of points to be used in analysis. Note, if you choose not to use the full record, the code will show you the total number of points and then select the required number of points from the start of the record.
6. Option: input the re-sampling interval (choose between: 15, 30, 45, 60, 90, 120, 240 and 360 minutes).
7. At this point, Figure (1) will pop up showing coherence between barometric pressure and borehole water level and the code will be in a 'pause' mode to give you a chance to decide which type of filter to apply. The chosen filter will be applied to both the water level and barometric pressure signals.
8. Press any key to continue with inputs.
9. Recharge removal: input (1) for high pass zero-phase Butterworth filter, or input (2) for no filters to be applied. Where (1) is chosen, give:
    - The order of the chosen filter.
    - The cut-off frequency in cycles/day.
10. Removal of pumping signal and high frequency noise: input (1) to apply an additional low pass zero-phase Butterworth filter or input (2) for no filter to be applied. Where (1) is chosen, give:
    - The order of the chosen filter.
    - The cut-off frequency in cycles/day.
11. Removal of Earth tides: input (1) for to use default frequencies (O_1, P_1, S_1, K_1, N_2, M_2 and S_2, see Table 5.3) for removing Earth tides or (2) to choose column vector file in (*.txt) format. Where (2) is chosen, give:
    - Input the file name.
12. Input the number of lags for Earth tides removal, see section 5.3.3.

B.2. Outputs of the *SC* Matlab code

Eight output figures will pop up after all inputs are completed, details of these figures are as follows:

1. Figure (1): Coherence between barometric pressure and borehole water level.
2. Figure (2a): Time series of theoretical Earth tides.
3. Figure (2b): Time series of reconstructed Earth tides.
4. Figure (3a): Amplitude spectrum of theoretical Earth tides.
5. Figure (3b): Amplitude spectrum of reconstructed Earth tides.
6. Figure (4a): Time series for barometric pressure (in green), water level input signal (in red), after removing recharge and high frequency noise (in magenta) and after removing Earth tides and ocean tides (in blue).
7. Figure (4b): Time series of removed recharge signal using the applied high pass filter if applied.
8. Figure (5a): coherence between barometric pressure and water level input signal.
9. Figure (5b): coherence between barometric pressure and water level output signal.
10. Figure (6a): Amplitude spectrum of water level input signal.
11. Figure (6b): Amplitude spectrum of barometric pressure.
12. Figure (6c): Superimposed amplitude spectra of barometric pressure (in green), water level input signal (in red) and corrected water level signal (in blue).
13. The Earth tide analysis outputs are shown in the Matlab command window, the first raw of outputs shows the mean-squared-error of the least-squares solution, Equation 5.5b (section 5.3.3). In addition five outputs columns of figures are shown:
    - Column (1): number of frequencies used for Earth tides analysis.
    - Column (2): frequencies used in Earth tides analysis in cycles/day.
    - Column (3): the number of unknowns (coefficients a_j and b_j) in Earth tides analysis.
    - Column (4): estimated values for coefficients, a_j and b_j.
    - Column (5): standard error for each coefficient, a_j and b_j.
14. Two exported text files (A_WL_output.txt and A_Bp_output.txt) will be saved in the same folder as the code to be used for further analysis.

B.3. Validation test of the *SC* Matlab code

This code was validated using a constructed synthetic test. A water level (WL) time series of 60000 data points (625 days at 15 minutes interval) was made up assuming a barometric efficiency of 60%. The water level data were reconstructed by multiplying the barometric pressure data (B_p) by -0.6. Then reconstructed Earth tides (ET_{syn}) for Benningholme borehole were added so that $WL = -0.6 \times B_p + ET_{syn}$. The SC code was then run with the following criteria; a high pass filter of 0.01 cycles/day, a low pass filter of 3 cycles/day and number of lags (m) of 100 used in Equation 5.5 is used for filtering Earth tides.

Results showed a step response function ($R(\tau)$, Equation 5.6) of 0.6 at all lags as anticipated from the synthetic water level signal (i.e. 60% of B_p). The reconstructed Earth tides signal is in good agreement with synthetic Earth tides, correlation of 0.99 and R^2 of 0.99, Figure B.1. In addition, mean squared error (average sum of squares, M_{SE}) value for solving Equation 5.5 is 4×10^{-4}.

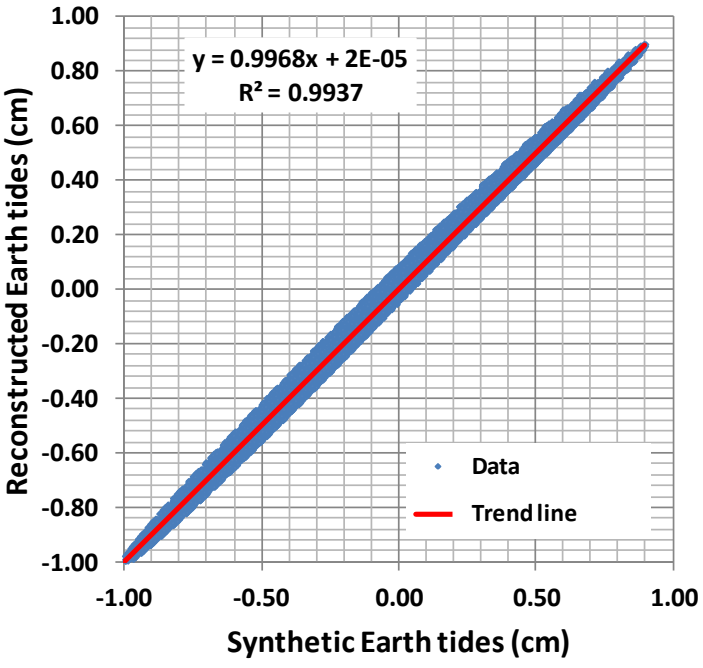

Figure B.1. Synthetic versus reconstructed Earth tide, Correlation of 0.99 and R^2=0.99.

Appendix C: *BE* Matlab code

The *BE* Matlab code has been developed to calculate long-term and short-term barometric efficiencies from time series of borehole water levels and barometric pressure using the linear regression methods described in *Rasmussen and Crawford* [1997]. The background and methodology are described in detail in Chapter 6. This code assumes that data is sampled every 15 minutes but the code also gives an option to re-sample the signals to a time interval which is a multiple of 15 minutes. This code also assumes that both water level and barometric pressure series are expressed as equivalent units of cmH_2O. Equations 6.1 and 6.2 are solved using the '*robustfit*' Matlab function [*MathWorks Inc.,* 2011], which uses an iteratively reweighted linear-least-squares approach to obtain a regression coefficient that is less influenced by outliers than an ordinary linear-least-squares fit. The long-term barometric efficiency is the slope of linear trend of B_p versus WL. The short-term barometric efficiency is the slope of linear trend of ΔB_p versus ΔWL, where ΔWL and ΔB_p are the changes in water level and barometric pressure respectively, for a given time interval Δt. The barometric efficiency is determined together with standard error % and R^2 value.

The listing of the *BE* code is provided in the accompanying CD.

C.1. Inputs to the *BE* Matlab code

To run the *BE* code, simply write BE.m in the Matlab command window, then press ENTER, and follow the instructions below:

1. If you have used the SC code to filter the signals, input the number of lags used in the *SC* code (Appendix B) otherwise input zero.
2. Input names of files containing four column vectors in (*.txt) format, in the order requested in the Matlab command window, for unfiltered and filtered barometric pressure and water level time series. These data files should be located in the same folder as the BE.m code.
3. Input the chosen re-sampling interval in minutes, 30 or 45 or 60 or 90 or 120 or 240 or 360, otherwise input 15 to use the original recording sampling interval of 15 minutes.

C.2. Outputs of the *BE* Matlab code

Following successful execution, one figure with four sub-figures will be displayed:

1. Figure (1a): Long-term barometric efficiency for unfiltered signals. Water level on vertical axis versus barometric pressure on horizontal axis together with the best fit line.
2. Figure (1b): Short-term barometric efficiency for unfiltered signals. First differences of water level on vertical axis versus first differences of barometric pressure on horizontal axis together with the best fit line.
3. Figure (1c): Long-term barometric efficiency for filtered signals. Water level on vertical axis versus barometric pressure on horizontal axis together with the best fit line.
4. Figure (1d): Short-term barometric efficiency for filtered signals. First differences of water level on vertical axis versus first differences of barometric pressure on horizontal axis together with the best fit line.

All figures titles include calculated barometric efficiency, R^2 value and standard error %.

C.3. Validation test of the *BE* Matlab code

This code was validated using a synthetic test. A water level (WL) time series of 60000 data points (625 days at 15 minutes interval) was made up assuming a barometric efficiency of 60%. The water level data were reconstructed by multiplying the barometric pressure data (B_p) by -0.6, so that WL= $-0.6\times B_p$. This essentially assumes a fully confined aquifer were both the long-term ($\propto_L$) and short-term ($\propto_S$) barometric efficiencies are equal (60%). The *BE* Matlab code was used to estimate ($\propto_L$) and ($\propto_S$), and results are shown in Figure C.1. As anticipated, estimated values for both efficiencies are identical and equal to 60% with zero standard error and R^2=1.

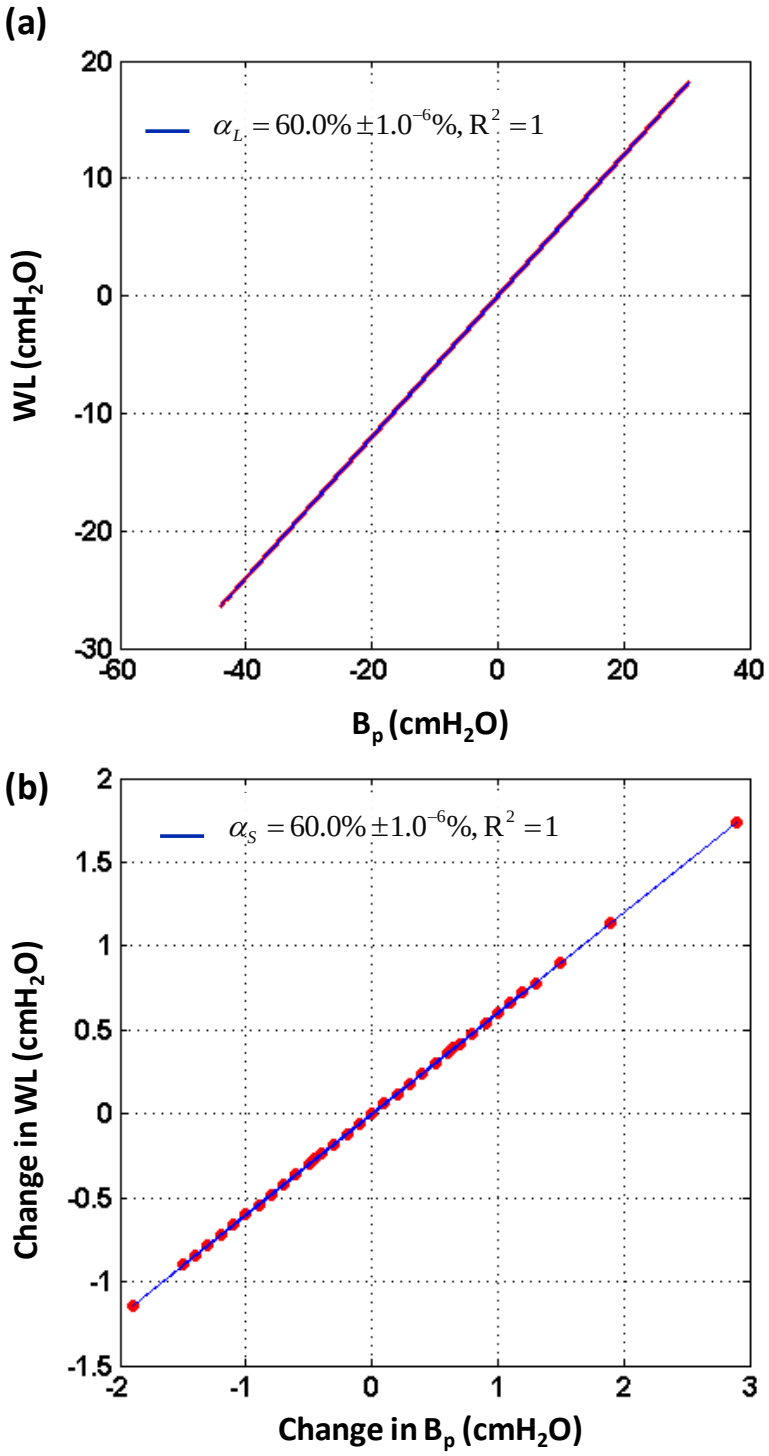

Figure C.1. Validation test for the *BE* Matlab code, As anticipated from the test design, estimated values for both efficiencies ($\propto_L$ and $\propto_S$) are identical and are equal to 60% with zero standard error and R^2=1. Red dots are data points and the line in blue is the fitted linear trend.

Appendix D: *RF* Matlab code

The *RF* Matlab code has been developed to implement the "cross-spectral deconvolution by ensemble averaging" method developed by *Welch* [1967] using the '*tfestimate*' Matlab function [*MathWorks Inc.*, 2011], see section 6.3.3. In this code the Welch's method is integrated with an overlapping frequency band technique, described by *Beavan et al.* [1991], see section 6.3.4. This code is designed to use up to five overlapping frequency bands. For each frequency band, the '*tfestimate*' function uses the Welch method, computing the cross-spectral density between the water level and barometric pressure signals, $P_{WB}(f)$, and the auto-spectral density of the barometric pressure signal, $P_{BB}(f)$, and then computing the quotient to obtain the barometric response function, $BRF(f)$, estimate. Then the code allows selecting the final barometric response function over the five overlapping frequency bands. The barometric response function is estimated along with uncertainty bounds of one standard error bars, section 6.3.4.

The listing of the *RF* code is provided in the accompanying CD.

D.1. Inputs and outputs of the *RF* Matlab code

To use the *RF* code follow the instructions below:

1. Sampling intervals of time series data of water level and barometric pressure should be 15 minutes. These time series should be filtered using the *SC* code (Appendix B) to remove influences other than barometric pressure from the water level signal.
2. Each of the water level and barometric pressure filtered records should be recorded in a column vector format (*.txt) and should be named "A_WL_output.txt" and "A_Bp_output.txt" respectively.
3. Load water level and barometric pressure filtered records to the Matlab workspace by typing:
    - load –ascii A_WL_output.txt
    - load –ascii A_Bp_output.txt
4. Open the RF.m file to input the following:

- Input values for K1, K2, K3, K4 and K5 (lines number 35-39 in *RF* code listing), where each K value controls the number of points to be used for the Fast Fourier Transform (FFT) at each frequency band. This option pads the input signals with zeros at their ends if required, which increases resolution of the barometric response function and avoids artefacts of undesired periodicity. The default number for FFT is the next power of 2 to the total number of samples in each segment (K=0), i.e. K=1 will increase the power of 2 plus one. Example if default value for the number of FFT is 2^13, if K=1 this number will be 2^14.
- Input a lower cut-off frequency for each overlapping frequency band (lines number 44-48 in *RF* code listing).

5. Save changes made to the RF.m file.
6. Run the code by typing RF.m in the Matlab command window, and then press ENTER.
7. Figure (1) will be displayed with two sub figures:
   - Figure (1a): Five coherence estimates between water level and barometric pressure signals, one for each frequency band.
   - Figure (1b): Amplitude spectrum of filtered water level signal.
8. Figure (2) is composed of four sub figures, two of them (a and b) will be displayed at this stage:
   - Figure (2a): Estimated BRF gain for five overlapping frequency bands.
   - Figure (2b): Estimated BRF phase for five overlapping frequency bands.
9. Use coherence and amplitude (output Figure 1) and estimated response function for five overlapping frequency bands (output Figure 2a and 2b) to decide intersections between bands. Intersections are frequencies at which the code will concatenate the final selected BRF out of the five overlapping frequency bands.
10. Input four selected intersections (in cycles/day) between the five overlapping bands, one at a time.
11. Figure (2), c and d will be displayed:
    - Figure (2c): Constructed BRF gain from five overlapping frequency bands.

- Figure (2d): Constructed BRF phase from five overlapping frequency bands.

12. In this code, the frequency range over which the barometric response function is determined is composed of a continuous frequency band, with additional (optional) 15 points and two points at 1 and 2 cycles/day. Input upper frequency limit (in cycles/day) selected for the initial continuous frequency band.
13. Input up to 15 selected frequencies which you want to add to the initial continuous frequency band, otherwise press ENTER to cancel.
14. Input (1) to include data point at 1 cycle/day or (2) to exclude it.
15. Input (1) to include data point at 2 cycles/day or (2) to exclude it.
16. Figure (3): Final determined barometric response function with error bars will be displayed.
17. Number of segments and the length of each segment in days for each overlapping frequency band will be displayed on the Matlab command window.
18. A file named as output_to_fit.txt will be saved in the same folder with the RF.m file. This file includes the final estimated barometric response function in the form of one column vector that is composed of seven concatenated column vectors of equal lengths; gain values, phase values, frequency values, error in gain estimate, error in phase estimate, real part of barometric response function and imaginary part of barometric response function. The output_to_fit.txt will be used for further analysis to fit the theoretical model to the estimated barometric response function.

D.2. Validation test of the *RF* Matlab code

The *RF* was tested using the same synthetic data set used in Appendix C (section C.3). Where the water level signal (WL) was made up to be -60% of the magnitude of the barometric pressure (B_p) signal, i.e. WL= $-0.6\times B_p$, at the Benningholme borehole. As shown in Figure D.1, estimated gain component of the BRF is 0.6 at all frequencies and the phase component is -180˚ at all frequencies, this represents the fully confined aquifer case which is anticipated from the designed synthetic data set. Both gain and

phase components are shown in Figure D.1 together with one standard error bars, however error bars are very small to be observed due to the perfect coherence between synthetic WL and B_p signals.

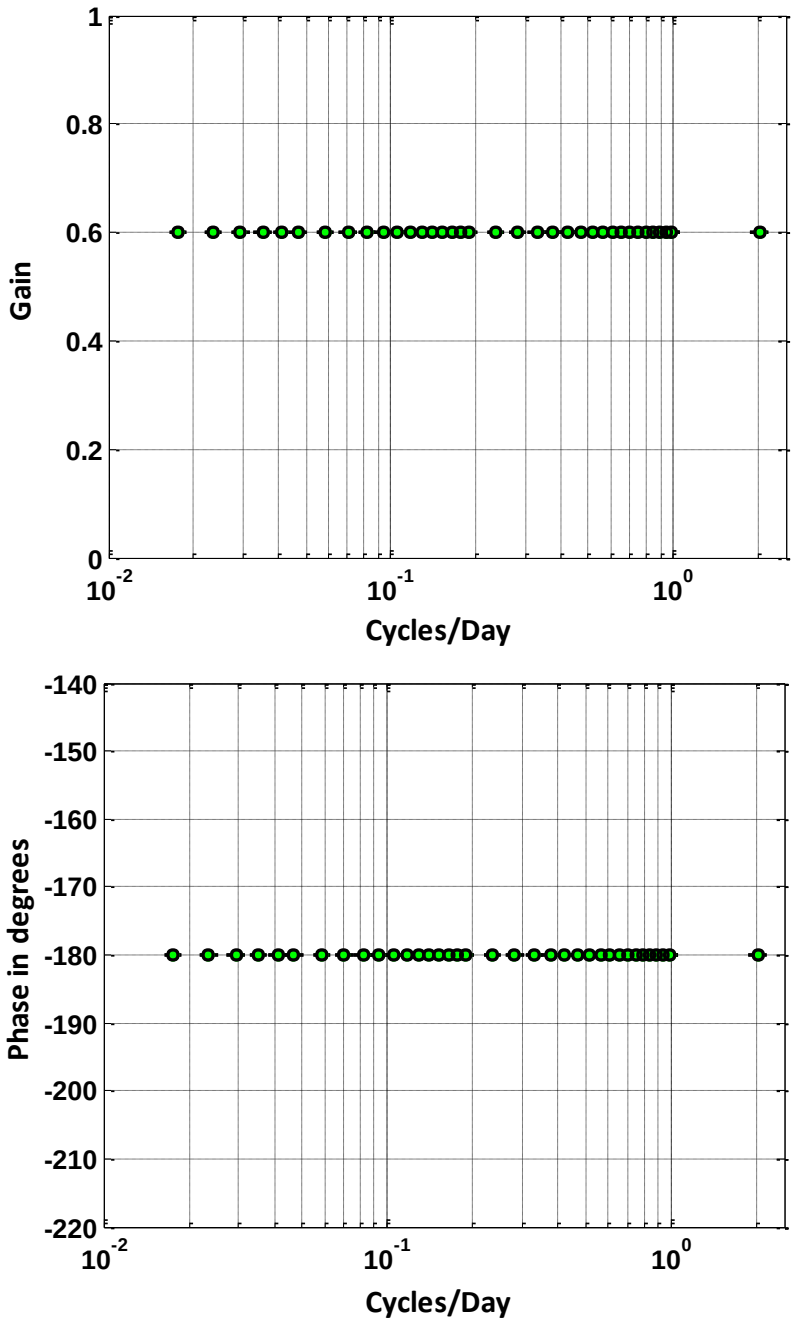

Figure D.1. Validation test for the RF code, estimated gain component of the BRF is 0.6 at all frequencies and the phase component is -180˚ at all frequencies, this represents the fully confined aquifer case which is anticipated from the designed synthetic data set.

Appendix E: *Automatic_Fitting* Matlab code

The *Automatic_Fitting* Matlab code has been developed to obtain the best fit solution of *Rojstaczer* [1988a] model to estimated barometric response functions using the hybrid genetic (GA) and pattern search (PS) algorithms (Chapter 7, section 7.3). The Matlab function '*HybridFcn*' is used to integrate the two Matlab functions '*ga*' and '*patternsearch*' [*MathWorks Inc.*, 2011] to construct the hybrid algorithm. This code is designed to apply lower and upper bounds for each fitting parameter. These are six parameters; barometric efficiency (BE), pneumatic diffusivity of the unsaturated zone (D_{unsat}), hydraulic diffusivity of the saturated zone (D_{con}), aquifer transmissivity (T_{aqu}), capillary fringe attenuation factor (T_{cf}), and the thickness of the unsaturated zone (L_{unsat}). The objective function to be minimized is the sum of square differences in the complex plane between complex forms for estimated and model barometric response functions. The objective function to be minimized has been developed in a Matlab function code (AF_Function.m) which calculate the objective function value (Fvalue) for each solution searched by the GA and for each iteration refined by the PS.

The listings of the *Automatic_Fitting* and AF_Function codes are provided in the accompanying CD.

E.1. Inputs to the *Automatic_Fitting* Matlab code

To run this code, the code file (Automatic_Fitting.m) together with the function file (AF_Function.m) and the output_to_fit.txt (contains estimated barometric response function) which is the output file from *RF* Matlab code (Appendix D) should all be in the same folder.

Open both files Automatic_Fitting.m (line numbers 34-37) and AF_Function.m (line numbers 20-23) in Matlab and manually edit the input values for:

- borehole radius (r_w),
- total thickness of the confining layer (L_{con}),

- storage coefficient of the confining layer (S_{con})**,** and
- storage coefficient of the aquifer (S_{aqu}).

In the Automatic_Fitting.m file (lines number 46 and 47), input lower bounds (lb) and upper bounds (ub) for each fitting parameter to constrain the optimization, and input the population size (line number 71) preferred. Defaults for these parameters are given in section 7.3.

To run the *Automatic_Fitting* code, simply write Automatic_Fitting.m in the Matlab command window and press ENTER.

E.2. Outputs of the *Automatic_Fitting* Matlab code

Two output figures will pop up, after all inputs are completed, including the following:

1. Figure (1a): Shows steps of the Genetic algorithm (GA) with generation number on the horizontal axis versus the objective function best value.
2. Figure (1b): Values of the best fit solution of each fitting parameter plotted as a bar chart.

   In the lower left corner of this figure there is an interactive button labeled 'stop'. If you feel satisfied about the GA results so far and want to switch to the Pattern search algorithm (PS) click the stop button, otherwise leave it and it will switch automatically when the difference between two consecutive solutions is less than a specified threshold (TolFun in the code, default 10^{-6}).

3. Figure (2): This Figure will appear after the best fit solution is found, showing the best fit model curve together with the estimated BRF and one standard deviation error bars (error bars is shown using code by *Moisy* [2006]).

In addition to these two figures, the Matlab command window shows step by step details of the optimization process for both GA and PS. It will also show best fit parameters values, minimum objective function value and the time elapsed during the optimization process.

E.3. Validation test of the *Automatic_Fitting* Matlab code

To test the Automatic_Fitting Matlab code, a synthetic barometric response function was designed using the model of *Rojstaczer* [1988a] within frequency band of 0.017-1.0 cycle/day and parameters estimated at the Benningholme borehole (Tables 7.2). The synthetic BRF together with the best fit curve are shown in Figure E.1. Estimated parameters (Table E.1) using the automatic fit (optimization parameters are listed in Table E.2) are very similar to the synthetic BRF parameters except for the D_{unsat} parameter. The poor fit to this parameter is caused by the lack of sensitivity to this parameter. Thus the fit is not sensitive as described in section 7.3 and Table 7.2. The hybrid automatic search GA-PS algorithm had converged to the best fit solution with a minimum objective function value (Fvalue) of 1.1×10^{-9}.

Table E.1. List of fitting parameters for best automatic (GA-PS algorithm) fit solution for the synthetic BRF.

	BE (-)	$D_{con,}$ (m^2/day)	$D_{unsat,}$ (m^2/day)	$T_{aqu,}$ (m^2/day)	T_{cf} (-)	L_{unsat} (m)
Synthetic BRF	0.49	10.0	10.0	1.50	0.82	1.20
Lower bound	0	0	0	0	0	1.0
Upper bound	1	1000	2000	1000	1	2.5
Automatic fit GA-PS	0.49	10.2	700.2	1.51	0.83	1.22

Table E.2. List of optimization parameters for best automatic (GA-PS algorithm) fit solution for the synthetic BRF.

Number of generations (GA)	6
Population size (solutions in each generation)	10000
Fvalue (GA)	8.5×10^{-5}
Number of iterations (PS)	3167
Fvalue (PS)	1.1×10^{-9}
Total elapsed time (GA-PS) in minutes	5.7
Total number of evaluations of the objective function	120319

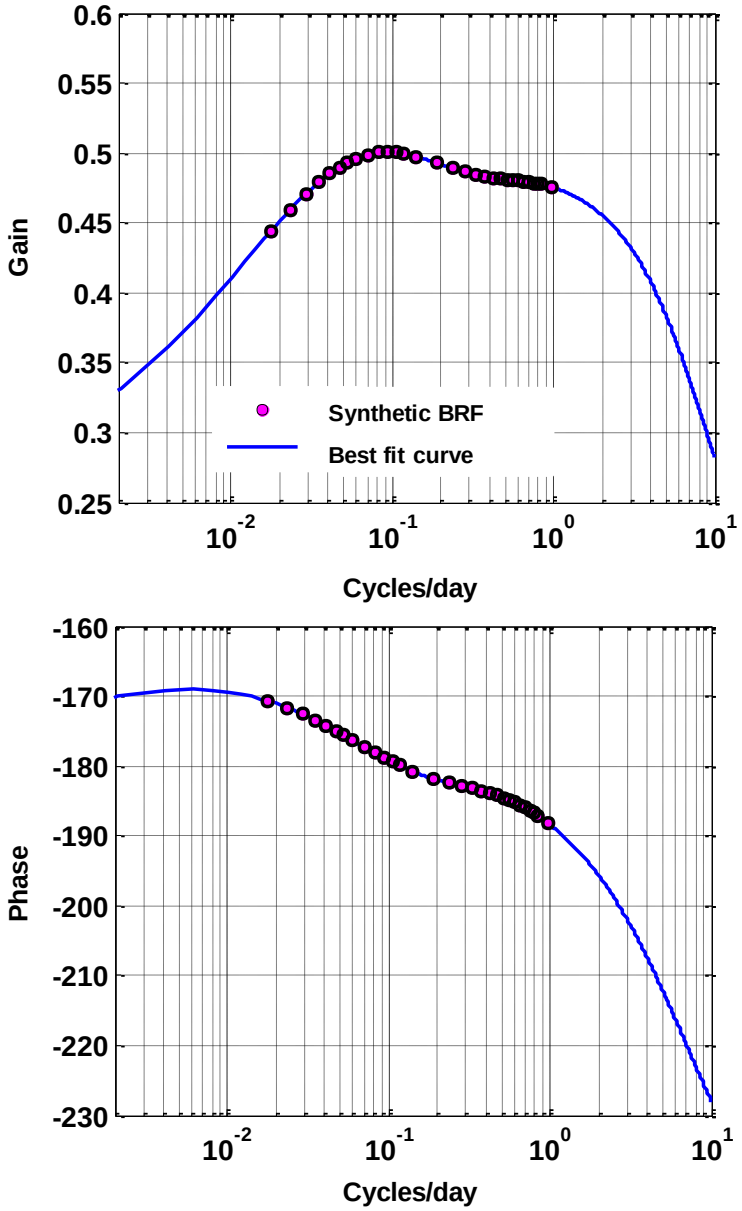

Figure E.1. Synthetic BRF together with the best fit curve [*Rojstaczer*, 1988a] obtained using the hybrid (GA-PS) algorithm.

Appendix F: *Manual_Fitting* Matlab code

This code has been designed to plot the estimated barometric response function with one standard deviation error bars together with three theoretical model curves specified by the user. In this study, this code was used to determine the limits to parameters by finding the upper and lower limits that result in model curves lying within the error bars of the estimated barometric response function. The listing of this code is provided in the accompanying CD.

F.1. Inputs to the *Manual_Fitting* Matlab code

To use this code, the code file (Manual_Fitting.m) together with the output_to_fit.txt (contains estimated barometric response function by the *RF* Matlab code, Appendix D) should all be in the same folder.

Open the Manual_Fitting.m code in Matlab and manually edit the input values for borehole radius (rw, line number 14 in listing) and total thickness of the confining layer (Lcon, line number 15 in listing). Input three values (for each of the theoretical model curves to be plotted) for each parameter (line numbers 25-68 in listing);

- static barometric efficiency (*BE*),
- the aquifer transmissivity (T_{aqu}),
- pneumatic diffusivity of the unsaturated zone (D_{unsat}),
- hydraulic diffusivity of the confining layer (D_{con})
- the unsaturated zone thickness (L_{unsat}),
- storage coefficient of the aquifer (S_{aqu}),
- storage coefficient of the confining layer (S_{con}), and
- capillary fringe attenuation factor (T_{cf}).

To run the Manual_Fitting code, simply write Manual_Fitting.m in the Matlab command window and press ENTER.

F.2. Outputs of the *Manual_Fitting* Matlab code

One output figure will pop up after running the code which shows the three specified theoretical model curves, plotted together with the barometric response function and one standard deviation error bars. In addition to this figure, the Matlab command window will also show the value of objective function for each fitting curve.